

NOTE TO USERS

This reproduction is the best copy available.

UMI®

**PHASE SEPARATION BY SPINODAL
DECOMPOSITION IN POLYMER BLENDS
UNDER A SINGLE AND DOUBLE
QUENCH:
A COMPUTATIONAL STUDY**

by

Tuyet Tran

Bachelor of Engineering - Chemical Engineering

Ryerson University

Toronto, Ontario, Canada, 2001

A thesis

presented to Ryerson University in fulfillment of the

thesis requirement for the degree of

Master of Applied Science

in

Chemical Engineering

Toronto, Ontario, Canada, 2004

©Tuyet Tran, 2004

UMI Number: EC52982

All rights reserved

INFORMATION TO USERS

The quality of this reproduction is dependent upon the quality of the copy submitted. Broken or indistinct print, colored or poor quality illustrations and photographs, print bleed-through, substandard margins, and improper alignment can adversely affect reproduction.

In the unlikely event that the author did not send a complete manuscript and there are missing pages, these will be noted. Also, if unauthorized copyright material had to be removed, a note will indicate the deletion.

UMI[®]

UMI Microform EC52982
Copyright 2008 by ProQuest LLC
All rights reserved. This microform edition is protected against
unauthorized copying under Title 17, United States Code.

ProQuest LLC
789 East Eisenhower Parkway
P.O. Box 1346
Ann Arbor, MI 48106-1346

Borrower's Page

Ryerson University requires the signatures of all persons using or photocopying this thesis. Please sign below, and give address and date.

Sign/Address/Date:

Abstract

PHASE SEPARATION BY SPINODAL DECOMPOSITION IN POLYMER BLENDS UNDER A SINGLE AND DOUBLE QUENCH: A COMPUTATIONAL STUDY

Tuyet Tran

Master of Applied Science in Chemical Engineering, 2004

Ryerson University

A mathematical model and computer simulations were used to describe the dynamics of thermally induced phase separation (TIPS) by spinodal decomposition for polymer blends (single quench and double quench) using the nonlinear Cahn-Hilliard theory and the Flory-Huggins-de Gennes free energy. The importance of TIPS is to enhance material properties such as toughness, impact resistance, and elasticity. Therefore, controlling the morphology is a critical factor in optimizing performance. The numerical results for the single quench are consistent with known characteristics of phase separation by spinodal decomposition observed in polymer blends. The numerical results for double quenching replicate recently published experimental and numerical work. Under a double quench the numerical work shows that a critical quench depth exists before secondary phase separation occurs, the growth rate of the primary and secondary structures are dependent on domain size and early stage dynamics for the secondary structures, after the second jump, appears to follow the linear Cahn-Hilliard theory.

Acknowledgements

I would like to thank Dr. Philip Chan and Dr. D errick Rousseau for giving me the opportunity to work on this project and for their guidance. Furthermore, my gratitude goes out to Dr. Ali Lohi and Dr. Muhammed Fayed for their support and guidance.

My appreciation goes out to the graduate and undergraduate students in the Food lab, my mentors Rick Buchanan and Dr. Rickey Yada and my friends Suying Lai, Elizabeth Lee, Corrine Chan, Patricia Leung, Heidi Chan, Kellie Fong and Han Nguyen for their support and encouragement throughout the course of this thesis. I would like to give special thanks to Danny Lee and Ivan Vecchia for their advice and assistance with troubleshooting.

My thanks goes out to Ryerson University School of Graduate Studies for providing me with a scholarship during my studies. In addition I would also like to express my gratitude to Dr. D errick Rousseau for providing me with a stipend during the extended period of my thesis.

Lastly, I would like to thank my parents, my sisters and my aunt for believing in me and for their patience.

To My Family

Table of Contents

Abstract	iv
Acknowledgements	v
Table of Contents	vii
List of Figures	x
List of Tables	xxix
List of Symbols	xxx
1 Introduction	1
1.1 Mechanism of Phase Separation in Polymer Blends.....	1
1.2 Thermally Induced Phase Separation.....	5
1.3 Two-Step TIPS Methods.....	8
1.4 Thesis Objectives.....	10
1.5 Methodology and Approach.....	11
1.6 Thesis Organization.....	12
2 Literature Review	16
2.1 Single Quench TIPS Studies in Polymer Systems.....	17
2.2 Two-Step TIPS Studies in Polymer Systems.....	23
3 Theoretical Background	42
3.1 Thermodynamics of Phase Separation in Polymer Blends.....	43
3.1.1 The Flory-Huggins Theory.....	44
3.1.2 The Phase Diagram for Polymer Blends.....	45
3.2 Spinodal Decomposition.....	51
3.2.1 Early, Intermediate and Late Stages of Spinodal Decomposition.....	51
3.2.2 The Cahn-Hilliard Theory.....	52
3.2.3 Concentration Dependent Mobility and Mutual Diffusion	55
3.2.4 Reptation Theory and Self-diffusion Coefficient.....	58
3.2.5 Concentration Dependent Gradient Energy.....	61

4	Model Development and Method of Solution.....	64
4.1	Governing Equations for Phase Separation by Spinodal Decomposition in Polymer Blends.....	65
4.2	The One-Dimensional Model.....	68
4.3	The Two-Dimensional Model.....	70
4.4	Initial and Boundary Condition.....	71
4.5	Method of Solution: The Galerkin Finite Element Method.....	73
4.6	Program Summary.....	77
5	Results and Discussion: 1-D TIPS Single Quench.....	78
5.1	Symmetrical Phase Diagram.....	80
5.2	Dimensionless Spatial Concentration Profiles.....	80
5.3	The Evolution of the Dimensionless Structure Factor.....	83
5.3.1	The Growth of the Dimensionless Structure Factor in the Early Stages of SD.....	90
5.4	Dimensionless Diffusion Coefficient	92
5.5	Quench Depth	94
5.6	Change in Dimensionless Spatial Chemical Potential and Second Derivative of Free Energy with Respect to Composition	95
6	Results and Discussion: 1-D TIPS Double Quench.....	106
6.1	Dimensionless Transition Time for the Second Quench.....	110
6.2	Dimensionless Spatial Concentration Profiles.....	113
6.5	The Evolution of the Dimensionless Structure Factor After the Second Temperature Jump.....	121
6.3.1	Second Temperature Jump to $T_2^* = 0.2$	122
6.3.2	Second Deeper Temperature Jump to $T_2^* = 0.1$	126
6.4	Quench Depth and Secondary Phase Separation.....	132
6.5	Change in Dimensionless Spatial Chemical Potential and Second Derivative of Free Energy with Respect to Composition for Double Quenching	135
6.6	Growth of Primary Structures After the Second Jump to $T_2^* = 0.2$	144

6.7 A Comparison of the Growth of Primary and Secondary Structures After the Second Jump to $T_2^* = 0.1$	153
6.8 Remarks on the Early Stages of Phase Separation After the Second Jump to $T_2^* = 0.1$ where Secondary Structures are Observed.....	157
7 Results and Discussion: 2-D TIPS Single and Double Quench	162
7.1 Single TIPS Critical Quench.....	163
7.2 Single TIPS Off-Critical Quench.....	164
7.3 Two-Step TIPS: Critical Quench.....	168
7.4 Two-Step TIPS: Off-Critical Quench.....	173
8 Conclusions.....	179
References.....	185
Appendix A: Hermitian Basis Functions for the 1-D and 2-D Model.....	192
Appendix B: Figures for 1-D Model: Single Quench.....	195
Appendix C: Figures for 1-D Model: Double Quench	215

List of Figures

Figure 1.1 A temperature versus composition phase diagram for a binary polymer mixture showing an UCST. The solid thick black line is the binodal (equilibrium curve) and the thin black line is the spinodal curve separating the metastable region and the unstable region. In the metastable region, phase separation occurs by nucleation and growth (NG) and in the unstable region, phase separation occurs by spinodal decomposition (SD). The critical point is the point at which the first sign of phase separation occurs.....2

Figure 1.2 A temperature versus composition phase diagram for a binary polymer mixture showing the different morphologies that can be obtained depending on the location on the quench at temperature T_1 . If the polymer mixture is quenched into the metastable region, phase separation occurs by NG and the droplet type structure is formed. If the polymer mixture is quenched into the unstable region, phase separation occurs by SD and two morphologies are developed, droplet (off critical quench) and interconnected (critical quench). Depending on the location of the quench, the droplet type structure has a different continuous phase (surrounding matrix) and dispersed phase as indicated by the reversal of the black and white regions as shown in the SD structures.....3

Figure 1.3 A schematic of the evolution of phase separation by the mechanism of nucleation and growth (NG) from the initial fluctuations at time t_1 to the development and growth of domain sizes at time t_2 . The arrows in the initial time period indicate the direction of the diffusion (downward) typical of NG. The upper

and lower equilibrium values are labeled as c_U and c_L respectively. The initial average composition is labeled as c_o6

Figure 1.4 A schematic of the evolution of phase separation by the mechanism of spinodal decomposition (SD) from the initial fluctuations at time t_i to the development and growth of domain sizes at time t_j . The arrows in the initial time period indicate the direction of the diffusion (upward) typical of SD. The upper and lower equilibrium values are labeled as c_U and c_L respectively. The initial average composition is labeled as c_o7

Figure 1.5 Temperature versus composition phase diagram illustrating the method of TIPS. Point A is the initial homogeneous phase subject to a deep quench into the unstable region (at T_1) where phase separation occurs by SD, point B. The tie lines determine the composition of each phase. The horizontal line running across this phase diagram is a tie line that relates the composition of the two phases. c_1^\dagger represents the composition of polymer 1 and $c_1^{\dagger\dagger}$ represents the composition of polymer 29

Figure 1.6 A schematic of the method of double quenching and the morphology that may develop for a critical and an off critical initial composition. The mixture is first quenched to T_1 where it is allowed to phase separated by SD for a certain period of time before it is quenched again to a temperature T_2 (still within the unstable region). The smaller domains represent the secondary structures that form. On the left hand side, the critical quench case shows the interconnected structure as the primary structure and the smaller droplets as the secondary structure. On the right hand side, the off critical quench shows larger droplets being the primary structure and smaller droplets as the secondary structure.....10

Figure 1.7	Flowchart detailing the methods and procedures for the mathematical modeling and computer simulation of TIPS for polymer blends undergoing single and double quenching.....	13
Figure 2.1	A temperature versus composition phase diagrams for binary mixture of PS-PVME showing the different test conditions in the double quench experiment. The first test performed was from point a I to point B (first temperature jump) and then from point B to point C (second temperature jump). The second test was from point I to point A and then point C. The third trial was a reversed from a deeper quench to a shallower quench from point I to C point (first temperature jump) then point C to point B (second temperature jump).....	29
Figure 2.2	Schematic the constructive and destructive interferences that may be occurring between the initial development of the concentration profile at T_1 and that in the second quench at T_2 . [Adapted from reference [Adapted from Ohnaga <i>et al.</i> , 1994].....	32
Figure 2.3	A proposed concentration profile showing the evolution of the concentration fluctuations for an off critical quench under a single quench (dashed lines) and a double quench (solid line). The introduction of multiple little peaks and troughs upon the second quench represent the formation of secondary structures. The picture above the concentration profile illustrates a 2 dimensional picture of the resulting morphology from this concentration profile. [Adapted from Yang <i>et al.</i> , 1998]	36
Figure 3.1	Typical temperature versus composition phase diagrams for binary polymer systems showing a) upper critical solution temperature, b)	

lower critical solution temperature or c) a combination of upper and lower critical solution temperature [Adapted from Tanaka, 2000]47

Figure 3.2 A plot of the relationship between the free energy versus composition and temperature versus composition for a binary polymer mixture. The binodal is the equilibrium curve and is constructed by the tangent line labeled $\beta' - \beta''$ where the change in the chemical potential of the coexisting phases is equal. The spinodal curve is constructed through the use of the inflection points in the free energy diagram. As T decreases, the miscibility decreases, representative of the UCST only.....50

Figure 5.1 A model symmetrical phase diagram for a polymer blend of degree of polymerization $N_1 = N_2 = 1000$. The dimensionless critical composition and temperature for this blend are $c_c = 0.50$ and $T_c^* = 0.33293$ respectively. The binodal (equilibrium curve) is represented by the solid curve and spinodal with the dashed curve. The two circles represent the locations of investigation (a critical $c_o^* = 0.5$ and off critical $c_o^* = 0.6$ quench) at a dimensionless temperature of $T_1^* = 0.25$. The upper and lower equilibrium values at $T_1^* = 0.25$ are 0.91230 and 0.08766 respectively.....81

Figure 5.2 The evolution of the dimensionless spatial concentration profile for a single quench into the unstable region of the phase diagram at the following dimensionless times: (a) $t^* = 3.527$, (b) $t^* = 3.843$, (c) $t^* = 4.014$, and (d) $t^* = 4.57$. The dashed line through the center of the graph represents the initial average concentration $c_o^* = 0.5$.

The dimensionless diffusion coefficient for this case is $D^* = 200\,000$84

Figure 5.3 The evolution of the dimensionless spatial concentration profile for a single quench into the unstable region of the phase diagram at the following dimensionless times: (a) $t^* = 4.898$, (b) $t^* = 5.092$, (c) $t^* = 5.292$, and (d) $t^* = 5.703$. The dashed line through the center of the graph represents the initial average concentration $c_o^* = 0.6$. The dimensionless diffusion coefficient for this case is $D^* = 200\,000$85

Figure 5.4 Typical light scattering profile showing the evolution of phase separation by SD in the early to the beginning of the intermediate stages. Each profile represents the intensity at a certain time t . The increase in time is indication by the arrow in the up direction. The scattering intensity is increasing with time while the position is constant, characteristic of the early stages of SD.....87

Figure 5.5 The evolution of the dimensionless structure factor for a single critical quench ($c_o^* = 0.5$, $D^* = 200\,000$ and $T^* = 0.25$) into the unstable region of the phase diagram at the following dimensionless times: $t^* = 3.527$ (thick grey line), $t^* = 3.843$ (dash with two dots), $t^* = 4.014$ (dash-dot line), $t^* = 4.186$ (dotted line), $t^* = 4.57$ (long dashed line), $t^* = 5.026$ (solid line).....89

Figure 5.6 The evolution of the dimensionless structure factor for a single off critical quench ($c_o^* = 0.6$, $D^* = 200\,000$ and $T^* = 0.25$) into the unstable region of the phase diagram at the following

dimensionless times: $t^* = 4.579$ (thick grey line), $t^* = 4.737$ (dash with two dots), $t^* = 5.898$ (dash-dot line), $t^* = 5.092$ (dotted line), $t^* = 5.292$ (long dashed line), $t^* = 5.703$ (solid line)..... 89

Figure 5.7 The evolution of the dimensionless maximum structure factor with dimensionless time from $t^* = 3.879$ to $t^* = 5.212$ for a single quench ($c_o^* = 0.5$, $D^* = 200\ 000$ and $T_l^* = 0.25$) into the unstable region of the phase diagram. At the early stages of phase separation by SD the initial increase is linear and gradually slows down into the beginning of the intermediate stage where coarsening occurs. The dashed line indicates the linearity for the early stages before it deviates.....91

Figure 5.8 The evolution of the dimensionless maximum structure factor with dimensionless time from $t^* = 5.164$ to $t^* = 5.864$ for a single quench ($c_o^* = 0.6$, $D^* = 200\ 000$ and $T_l^* = 0.25$) into the unstable region of the phase diagram. At the early stages of phase separation by SD the initial increase is linear and gradually slows down into the beginning of the intermediate stage where coarsening occurs. The dashed line indicates the linearity for the early stages before it deviates.....92

Figure 5.9 The evolution of the dimensionless spatial concentration profile for a single quench into the unstable region of the phase diagram at the following dimensionless times: (a) $t^* = 0.2128$, (b) $t^* = 0.2221$, (c) $t^* = 0.2323$, and (d) $t^* = 0.2533$. The dashed line through the center of the graph represents the initial average concentration $c_o^* = 0.6$. The dimensionless diffusion coefficient for this case is $D^* = 500\ 000$ and the dimensionless temperature is $T_l^* = 0.2$96

Figure 5.10 The evolution of the change in the dimensionless spatial chemical potential for a single quench into the unstable region of the phase diagram at the following dimensionless times: (a) $t^* = 3.527$, (b) $t^* = 3.843$, (c) $t^* = 4.014$, and (d) $t^* = 4.57$. The change in the dimensionless chemical potential is defined as the difference between the chemical potential polymer 1 in the mixture to that of its pure phase. The dimensionless initial concentration is $c_0^* = 0.5$ and the dimensionless diffusion coefficient is $D^* = 200\ 000$**99**

Figure 5.11 The evolution of the change in the dimensionless spatial chemical potential for a single quench into the unstable region of the phase diagram at the following dimensionless times: (a) $t^* = 4.898$, (b) $t^* = 5.092$, (c) $t^* = 5.292$, and (d) $t^* = 5.703$. The change in the dimensionless chemical potential is defined as the difference between the chemical potential polymer 1 in the mixture to that of its pure phase. The dimensionless initial concentration is $c_0^* = 0.6$ and the dimensionless diffusion coefficient is $D^* = 200\ 000$**100**

Figure 5.12 A comparison between the dimensionless spatial concentration profile (a) to the change in the dimensionless spatial chemical potential for a single critical quench with $D^* = 800\ 000$ at a dimensionless time of $t^* = 0.273$**101**

Figure 5.13 The evolution of the change in the dimensionless spatial second derivative of the free energy with respect to composition of component 1 for a single quench into the unstable region of the phase diagram at the following dimensionless times: (a) $t^* = 3.527$, (b) $t^* = 3.843$, (c) $t^* = 4.014$, and (d) $t^* = 4.57$. The change in the dimensionless second derivative of free energy is used to determine the conditions of stability ($F^{**} > 0$), meta-stability

($F^{**} > 0$), and instability ($F^{**} < 0$). The dimensionless initial concentration is $c_0^* = 0.5$ and the dimensionless diffusion coefficient is $D^* = 200\,000$104

Figure 5.14 The evolution of the change in the dimensionless spatial second derivative of the free energy with respect to composition of component 1 for a single quench into the unstable region of the phase diagram at the following dimensionless times: (a) $t^* = 4.898$, (b) $t^* = 5.092$, (c) $t^* = 5.292$, and (d) $t^* = 5.703$. The change in the dimensionless second derivative of free energy is used to determine the conditions of stability ($F^{**} > 0$), meta-stability ($F^{**} > 0$), and instability ($F^{**} < 0$). The dimensionless initial concentration is $c_0^* = 0.6$ and the dimensionless diffusion coefficient is $D^* = 200\,000$105

Figure 6.1 The evolution of the dimensionless maximum structure factor with dimensionless time from $t^* = 0.8594$ to $t^* = 1.00$ for a single quench ($c_0^* = 0.5$, $D^* = 200\,000$ and $T_1^* = 0.25$) into the unstable region of the phase diagram. The dimensionless transition time is 4.720. At the early stages of phase separation by SD the initial increase is linear and gradually slows down into the beginning of the intermediate stage where coarsening occurs. The transition point occurs where the two tangent lines intersect.....111

Figure 6.2 The evolution of the dimensionless spatial concentration profile for a double quench from $T_1^* = 0.25$ to $T_2^* = 0.2$ at the transition time of $t_i^* = 4.72$ at the following dimensionless times: (a) $t^* = 4.731$, (b) $t^* = 4.745$, (c) $t^* = 4.798$, and (d) $t^* = 4.861$. The dashed line through the center of the graph represents the initial average

concentration $c_o^* = 0.5$. The dimensionless diffusion coefficient for this case is $D^* = 200\ 000$115

Figure 6.3 The evolution of the dimensionless spatial concentration profile for a double quench from $T_1^* = 0.25$ to $T_2^* = 0.2$ at the transition time of $t_i^* = 5.52$ at the following dimensionless times: (a) $t^* = 5.534$, (b) $t^* = 5.575$, (c) $t^* = 5.625$, and (d) $t^* = 5.671$. The dashed line through the center of the graph represents the initial average concentration $c_o^* = 0.6$. The dimensionless diffusion coefficient for this case is $D^* = 200\ 000$117

Figure 6.4 The evolution of the dimensionless spatial concentration profile for a double quench from $T_1^* = 0.25$ to $T_2^* = 0.1$ at the transition time of $t_i^* = 4.72$ at the following dimensionless times: (a) $t^* = 4.726$, (b) $t^* = 4.740$, (c) $t^* = 4.748$, and (d) $t^* = 4.769$. The dashed line through the center of the graph represents the initial average concentration $c_o^* = 0.5$. The numbers on top of the graph are used to identify the number of peaks for a dimensionless diffusion coefficient $D^* = 200\ 000$119

Figure 6.5 The evolution of the dimensionless spatial concentration profile for a double quench from $T_1^* = 0.25$ to $T_2^* = 0.1$ at the transition time of $t_i^* = 5.52$ at the following dimensionless times: (a) $t^* = 5.526$, (b) $t^* = 5.545$, (c) $t^* = 5.549$, and (d) $t^* = 5.565$. The dashed line through the center of the graph represents the initial average concentration $c_o^* = 0.6$. The dimensionless diffusion coefficient for this case is $D^* = 200\ 000$120

Figure 6.6 The evolution of the dimensionless structure factor for a double quench from $T_1^* = 0.25$ to $T_2^* = 0.2$ (second temperature jump made at transition time of $t_i^* = 4.72$) at the following dimensionless times: $t^* = 4.731$ (light grey solid line), $t^* = 4.745$ (dash-dot line), $t^* = 4.798$ (dashed line), and $t^* = 4.861$ (solid black line). The initial average concentration $c_o^* = 0.5$. The dimensionless diffusion coefficient is $D^* = 200\ 000$125

Figure 6.7 The evolution of the dimensionless structure factor for a double quench from $T_1^* = 0.25$ to $T_2^* = 0.2$ (second temperature jump made at a transition time of $t_i^* = 5.52$) at the following dimensionless times: $t^* = 5.534$ (light grey solid line), $t^* = 5.575$ (dash – two dots line), $t^* = 5.625$ (dotted line), and $t^* = 5.671$ (solid black line). The initial average concentration $c_o^* = 0.6$. The dimensionless diffusion coefficient for this case is $D^* = 200\ 000$127

Figure 6.8 The evolution of the dimensionless spatial concentration profile for a double quench from $T^* = 0.25$ to $T^* = 0.1$ (at the transition time of $t_i^* = 4.72$) at the following dimensionless times: $t^* = 4.726$ (light grey line), $t^* = 4.740$ (dash-dot line), $t^* = 4.748$ (dotted line), and $t^* = 4.769$ (solid line). The initial average concentration $c_o^* = 0.5$. The dimensionless diffusion coefficient is $D^* = 200\ 000$129

Figure 6.9 The evolution of the dimensionless spatial concentration profile for a double quench from $T^* = 0.25$ to $T^* = 0.1$ (at the transition time of $t_i^* = 5.52$) at the following dimensionless times: $t^* = 5.526$ (dash-dot line), $t^* = 5.545$ (light grey line), $t^* = 5.549$ (dotted line), and $t^* = 5.565$ (solid line). The dashed line through the center of the graph represents the initial average concentration $c_o^* = 0.6$. The

dimensionless diffusion coefficient for this case is
 $D^* = 200\,000$ 131

Figure 6.10 A model symmetrical phase diagram for a polymer blend of degree of polymerization $N_1 = N_2 = 1000$. The two open triangles represent the locations of investigation (a critical $c_o^* = 0.5$ and off critical $c_o^* = 0.6$ quench) at the initial dimensionless temperature jump of $T_1^* = 0.25$ with $D^* = 500\,000$. The open circles represent the locations of the phase separating system when it has reached the transition time $t_t^* = 0.65$ (critical quench) and the open squares represent the phase separating system when it has reached the transition time $t_t^* = 0.903$ (off critical quench) where the second temperature jump is made. The filled circles show the location of the system at the start of the second shallower temperature jump ($T^* = 0.2$) and the deeper temperature jump ($T^* = 0.1$) for the critical quench case. The filled squares show the location of the system at the start of the second shallower temperature jump ($T^* = 0.2$) and the deeper temperature jump ($T^* = 0.1$) for the off critical quench case.....133

Figure 6.11 The evolution of the change in the dimensionless spatial chemical potential for a double quench from $T^* = 0.25$ to $T^* = 0.2$ at the transition time of $t_t^* = 4.72$ at the following dimensionless times: (a) $t^* = 4.731$, (b) $t^* = 4.745$, (c) $t^* = 4.798$, and (d) $t^* = 4.861$. The change in the dimensionless chemical potential is defined as the difference between the chemical potential polymer 1 in the mixture to that of its pure phase. The dimensionless initial concentration is $c_o^* = 0.5$ and the dimensionless diffusion coefficient is $D^* = 200\,000$138

Figure 6.12 The evolution of the change in the dimensionless spatial chemical potential for a double quench from $T^* = 0.25$ to $T^* = 0.2$ at the transition time of $t_i^* = 5.52$ at the following dimensionless times: (a) $t^* = 5.534$, (b) $t^* = 5.575$, (c) $t^* = 5.625$, and (d) $t^* = 5.671$. The change in the dimensionless chemical potential is defined as the difference between the chemical potential polymer 1 in the mixture to that of its pure phase. The dimensionless initial concentration is $c_o^* = 0.6$ and the dimensionless diffusion coefficient is $D^* = 200\ 000$139

Figure 6.13 The evolution of the change in the dimensionless spatial chemical potential for a double quench from $T^* = 0.25$ to $T^* = 0.1$ at the transition time of $t_i^* = 4.72$ at the following dimensionless times: (a) $t^* = 4.726$, (b) $t^* = 4.740$, (c) $t^* = 4.748$, and (d) $t^* = 4.769$. The change in the dimensionless chemical potential is defined as the difference between the chemical potential polymer 1 in the mixture to that of its pure phase. The dimensionless initial concentration is $c_o^* = 0.5$ and the dimensionless diffusion coefficient is $D^* = 200\ 000$142

Figure 6.14 The evolution of the change in the dimensionless spatial chemical potential for a double quench from $T^* = 0.25$ to $T^* = 0.1$ at the transition time of $t_i^* = 5.52$ at the following dimensionless times: (a) $t^* = 5.526$, (b) $t^* = 5.545$, (c) $t^* = 5.549$, and (d) $t^* = 5.565$. The change in the dimensionless chemical potential is defined as the difference between the chemical potential polymer 1 in the mixture to that of its pure phase. The dimensionless initial concentration is $c_o^* = 0.6$ and the dimensionless diffusion coefficient is $D^* = 200\ 000$143

Figure 6.15 The evolution of the change in the dimensionless spatial second derivative of the free energy with respect to composition of component 1 for a double quench from $T^* = 0.25$ to $T^* = 0.2$ at the transition time of $t_i^* = 4.72$ at the following dimensionless times: (a) $t^* = 4.731$, (b) $t^* = 4.745$, (c) $t^* = 4.798$, and (d) $t^* = 4.861$. The change in the dimensionless second derivative of free energy is used to determine the conditions of stability ($F^{*''} > 0$), meta-stability ($F^{*''} > 0$), and instability ($F^{*''} < 0$). The dimensionless initial concentration is $c_0^* = 0.5$ and the dimensionless diffusion coefficient is $D^* = 200\,000$146

Figure 6.16 The evolution of the change in the dimensionless spatial second derivative of the free energy with respect to composition of component 1 for a double quench from $T^* = 0.25$ to $T^* = 0.2$ at the transition time of $t_i^* = 5.52$ at the following dimensionless times: (a) $t^* = 5.534$, (b) $t^* = 5.575$, (c) $t^* = 5.625$, and (d) $t^* = 5.671$. The change in the dimensionless second derivative of free energy is used to determine the conditions of stability ($F^{*''} > 0$), meta-stability ($F^{*''} > 0$), and instability ($F^{*''} < 0$). The dimensionless initial concentration is $c_0^* = 0.6$ and the dimensionless diffusion coefficient is $D^* = 200\,000$147

Figure 6.17 The evolution of the change in the dimensionless spatial second derivative of the free energy with respect to composition of component 1 for a double quench from $T^* = 0.25$ to $T^* = 0.1$ at the transition time of $t_i^* = 4.72$ at the following dimensionless times: (a) $t^* = 4.726$, (b) $t^* = 4.740$, (c) $t^* = 4.748$, and (d) $t^* = 4.769$. The change in the dimensionless second derivative of free energy is used to determine the conditions of stability ($F^{*''} > 0$),

meta-stability ($F^{*''} > 0$), and instability ($F^{*''} < 0$). The dimensionless initial concentration is $c_0^* = 0.5$ and the dimensionless diffusion coefficient is $D^* = 200\,000$**148**

Figure 6.18 The evolution of the change in the dimensionless spatial second derivative of the free energy with respect to composition of component 1 for a double quench from $T^* = 0.25$ to $T^* = 0.1$ at the transition time of $t_t^* = 5.52$ at the following dimensionless times: (a) $t^* = 5.526$, (b) $t^* = 5.545$, (c) $t^* = 5.549$, and (d) $t^* = 5.565$. The change in the dimensionless second derivative of free energy is used to determine the conditions of stability ($F^{*''} > 0$), meta-stability ($F^{*''} > 0$), and instability ($F^{*''} < 0$). The dimensionless initial concentration is $c_0^* = 0.6$ and the dimensionless diffusion coefficient is $D^* = 200\,000$**149**

Figure 6.19 The evolution of the dimensionless structure factor of the primary structure formed just after the second temperature jump to $T^* = 0.2$, plotted against dimensionless reduced times for a critical quench case. The second jump was made at a transition time of $t_t^* = 4.72$ with a dimensionless diffusion coefficient $D^* = 200\,000$**150**

Figure 6.20 The evolution of the dimensionless structure factor of the primary structure formed just after the second temperature jump to $T^* = 0.2$, plotted against dimensionless reduced times for an off critical quench case. The second jump was made at a transition time of $t_t^* = 5.52$ with a dimensionless diffusion coefficient $D^* = 200\,000$**154**

Figure 6.21 The evolution of the dimensionless structure factor of the (a) primary and (b) secondary structures formed just after the second

temperature jump to $T^* = 0.1$ plotted against dimensionless reduced times for a critical quench case. The second temperature jump was made at $t_l^* = 4.72$. The dimensionless diffusion coefficient is $D^* = 200\,000$158

Figure 6.22 The evolution of the dimensionless structure factor of the (a) primary and (b) secondary structures formed just after the second temperature jump to $T^* = 0.1$ plotted against dimensionless reduced times for an off critical quench case. The second temperature jump was made at $t_l^* = 5.52$. The dimensionless diffusion coefficient is $D^* = 200\,000$160

Figure 6.23 The evolution of the growth of the dimensionless structure factor of the secondary structure formed at the second temperature jump, $T^* = 0.1$, plotted against dimensionless reduced times for a critical quench with $D^* = 200\,000$161

Figure 6.24 The evolution of the growth of the dimensionless structure factor of the secondary structure formed at the second temperature jump, $T^* = 0.1$, plotted against dimensionless reduced times for an off critical quench with $D^* = 200\,000$161

Figure 7.1 A plot of the 2-D dimensionless spatial concentration profiles, $c^*(x^*, y^*)$, showing the evolution of structure development (left) and the growth of the concentration fluctuations (right) for a single critical ($c_o^* = 0.5$) quench to $T_l^* = 0.25$ with $D^* = 200\,000$ at the following dimensionless times: (a) $t^* = 3.267$, (b) $t^* = 3.633$, (c) $t^* = 3.869$, and (d) $t^* = 4.931$. The grey scale represents the compositions of the phase separating blend on the bottom right.....166

Figure 7.2 A plot of the 2-D dimensionless spatial concentration profiles, $c^*(x^*, y^*)$, showing the evolution of structure development (left) and the growth of the concentration fluctuations (right) for a single critical ($c_o^* = 0.5$) quench to $T_I^* = 0.25$ with $D^* = 500\ 000$ at the following dimensionless times: (a) $t^* = 0.5053$, (b) $t^* = 0.5317$, (c) $t^* = 0.5965$, and (d) $t^* = 0.6552$. The grey scale represents the compositions of the phase separating blend on the bottom right.....167

Figure 7.3 A plot of the 2-D dimensionless spatial concentration profiles, $c^*(x^*, y^*)$, showing the evolution of structure development (left) and the growth of the concentration fluctuations (right) for a single off critical ($c_o^* = 0.6$) quench to $T_I^* = 0.25$ with $D^* = 200\ 000$ at the following dimensionless times: (a) $t^* = 4.416$, (b) $t^* = 4.619$, (c) $t^* = 5.048$, and (d) $t^* = 5.292$. The grey scale represents the compositions of the phase separating blend on the bottom right.....169

Figure 7.4 A plot of the 2-D dimensionless spatial concentration profiles, $c^*(x^*, y^*)$, showing the evolution of structure development (left) and the growth of the concentration fluctuations (right) for a single off critical ($c_o^* = 0.6$) quench to $T_I^* = 0.25$ with $D^* = 500\ 000$ at the following dimensionless times: (a) $t^* = 0.5053$, (b) $t^* = 0.5317$, (c) $t^* = 0.5965$, and (d) $t^* = 0.6552$. The grey scale represents the compositions of the phase separating blend on the bottom right.....170

Figure 7.5 A plot of the 2-D dimensionless spatial concentration profiles, $c^*(x^*, y^*)$, showing the evolution of structure development (left) and the growth of the concentration fluctuations (right) for a single off critical ($c_o^* = 0.6$) quench to $T_l^* = 0.2$ with $D^* = 500\ 000$ at the following dimensionless times: (a) $t^* = 0.1812$, (b) $t^* = 0.2029$, (c) $t^* = 0.2133$, and (d) $t^* = 0.2187$. The grey scale represents the compositions of the phase separating blend on the bottom right.....171

Figure 7.6 A plot of the 2-D dimensionless spatial concentration profiles, $c^*(x^*, y^*)$, showing the evolution of structure development for a double critical ($c_o^* = 0.5$) quench from $T_l^* = 0.25$ to $T_l^* = 0.1$ with $D^* = 200\ 000$. The following dimensionless times correspond to profiles made after the second jump at $t^* = 4.931$: (a) $t^* = 4.935$, (b) $t^* = 4.941$, (c) $t^* = 4.950$, and (d) $t^* = 4.952$ (e) $t^* = 4.953$ and (f) 4.9531. The first sign of secondary phase separation occurs in c) at $t^* = 4.950$. The grey scale represents the compositions of the phase separating blend on the bottom right.....175

Figure 7.7 A plot of the 3-D dimensionless spatial concentration profiles, $c^*(x^*, y^*)$, showing the evolution of structure development for a double critical ($c_o^* = 0.5$) quench from $T_l^* = 0.25$ to $T_l^* = 0.1$ with $D^* = 200\ 000$. The following dimensionless times correspond to profiles made after the second jump at $t^* = 4.931$: (a) $t^* = 4.935$, (b) $t^* = 4.941$, (c) $t^* = 4.950$, and (d) $t^* = 4.952$ (e) $t^* = 4.953$ and (f) 4.9531. The first sign of secondary phase separation occurs in c) at $t^* = 4.950$. The grey scale represents the compositions of the phase separating blend on the bottom right.....176

Figure 7.8 A plot of the 2-D dimensionless spatial concentration profiles, $c^*(x^*, y^*)$, showing the evolution of structure development for a double off critical ($c_o^* = 0.6$) quench from $T_I^* = 0.25$ to $T_I^* = 0.1$ with $D^* = 200\ 000$. The following dimensionless times correspond to profiles made after the second jump at $t^* = 5.292$: (a) $t^* = 5.294$, (b) $t^* = 5.307$, (c) $t^* = 5.313$, and (d) $t^* = 5.315$ (e) $t^* = 5.317$ and (f) 5.320. The first sign of secondary phase separation occurs in c) at $t^* = 5.313$. The grey scale represents the compositions of the phase separating blend on the bottom right.....177

Figure 7.9 A plot of the 3-D dimensionless spatial concentration profiles, $c^*(x^*, y^*)$, showing the evolution of concentration fluctuations for a double off critical ($c_o^* = 0.6$) quench from $T_I^* = 0.25$ to $T_I^* = 0.1$ with $D^* = 200\ 000$. The following dimensionless times correspond to profiles made after the second jump at $t^* = 5.292$: (a) $t^* = 5.294$, (b) $t^* = 5.307$, (c) $t^* = 5.313$, and (d) $t^* = 5.315$ (e) $t^* = 5.317$ and (f) 5.320. The first sign of secondary phase separation occurs in c) at $t^* = 5.313$178

List of Tables

Table 5.1	Summary of the dimensionless parameters used in the 1-D TIPS study for a single quench.....	79
Table 5.2	Dimensionless characteristic lengths in the early stages of SD for the structures formed at $T_1^* = 0.25$ with increasing D^*	90
Table 6.1	Summary of the dimensionless parameters used in the 1-D numerical study for double quenching.....	107
Table 6.2	A summary of the dimensionless transition times (at $T_1^* = 0.25$) determined from plotting the maximum values of the dimensionless structure factor with dimensionless time.	112
Table 6.3	Dimensionless characteristic lengths for the primary structures ($T_1^* = 0.25$) and the secondary peaks ($T_2^* = 0.2$) formed.....	127
Table 6.4	Dimensionless characteristic lengths for the primary structures ($T_1^* = 0.25$) and the secondary structures ($T_2^* = 0.1$) formed upon further quenching from after the determined dimensionless transition times.....	131
Table 7.1	Summary of the dimensionless parameters used in the 2-D numerical study for a single critical and off critical quench.....	163

List of Symbols

Symbols

A	an entropic constant in determining the F-H interaction parameter
$A(k, t)$	Fourier transform of the composition fluctuations
a	statistical segment length
B	an enthalpic constant in determining the F-H interaction parameter
b	bond length
c	concentration of component 1 (polymer 1)
c_c	critical polymer concentration
c_0	initial average polymer concentration
c_U	upper equilibrium value
c_L	low equilibrium value
c_1^\dagger	composition of polymer 1 in coexisting phase 1
$c_1^{\dagger\dagger}$	composition of polymer 1 in coexisting phase 2
D	mutual diffusion coefficient
$D_{\text{Rouse-self}}$	Rouse theory self-diffusion coefficient
$D_{\text{rep-self}}$	reptation theory self-diffusion coefficient
D_i	self-diffusion coefficient of polymer i
$f(c)$	homogeneous free energy of mixing
F	total free energy of mixing
F^{**}	dimensionless second derivative of free energy with respect to composition
I	light scattering intensity
J	interdiffusional flux

k^*	dimensionless wave number
k_m^*	dimensionless maximum wave number
k_B	Boltzmann constant
M	mobility
M_i	mobility of individual components
N_c	critical polymer length
N_e	degree of polymerization between entanglements
N_1	degree of polymerization of polymer 1
N_2	degree of polymerization of polymer 2
q	light scattering wave vector
R	gas constant
R_G	radius of gyration of polymer
S^*	dimensionless structure factor
t^*	dimensionless time
t_R^*	dimensionless reduced time
t_i^*	dimensionless transition time
T	temperature
T_1^*	dimensionless initial temperature jump
T_2^*	dimensionless second temperature jump at transition time
T_c^*	dimensionless critical temperature
T_{Qd}^*	dimensionless quench depth
ΔT_1	the difference between the quench first temperature and the critical temperature
ΔT_2	the difference between the quench second temperature and the critical temperature
X	kinetic term in describing mutual diffusion
x, y	distance of rectangular coordinates

x_i	mole fraction in solution of component i
ΔG_M	change in Gibbs free energy of mixing
ΔH_M	change in enthalpy of mixing
ΔS_M	change in entropy of mixing

Greek Letters

χ	Flory-Huggins interaction parameter
χ_c	critical interaction parameter
δ	Kunh length
κ	gradient energy coefficient
λ	effective interaction distance between monomers
λ^*	dimensionless characteristic length
Λ	Onsager coefficient
μ_1°	dimensionless chemical potential of pure component polymer 1
μ_1	chemical potential of polymer 1
μ_2	chemical potential polymer 2
ν	volume of a cell or segment
Ω	number of possible ways N_1 and N_2 can be arranged in the lattice
ξ	monomer friction coefficient of a polymer
ψ	thermodynamic factor in describing mutual diffusion
$\Delta\mu_1^*$	dimensionless change of the chemical potential of polymer 1

Acronyms

LCST	lower critical solution temperature
NG	nucleation and growth
SD	spinodal decomposition
TIPS	thermally induced phase separation
UCST	upper critical solution temperature

Chapter 1

Introduction

A number of industrial processes use the technique of phase separation to produce materials for everyday use [Leblond, 2002]. Applications include the formation of membranes, for separation processes [Mulder, 1996], the formation of polymer dispersed liquid crystal films for electro optical devices [Doane, 1989; Nwabunma *et al.*, 2000], the production of high impact resistant materials [Chow, 1980; Utracki, 1991] in the plastics industry, coatings of capsules [Leblond, 2002] in the pharmaceutical industry, and the production of low fat spreads [Harding *et al.*, 1995] in the food industry. Therefore, research, both experimental and numerical, in understanding how phase separation occurs in polymer blends to control the morphology for specific applications is important.

1.1 The Mechanisms of Phase Separation in Polymer Blends

The mechanism of phase separation depends on the location of a polymer blend in the phase diagram. Figure 1.1 shows a typical temperature versus composition phase diagram labeling the different regions of interest in studying phase separation kinetics. Figure 1.1 is called an upper critical solution temperature

(UCST) type phase diagram. The filled black circle is the critical point. Above this point, the system is in the homogeneous one-phase region and is stable. The solid thick black curve is the binodal (equilibrium) curve and the thin black line is the spinodal curve. The spinodal curve separates the two known mechanisms of phase separation namely, (i) nucleation and growth (NG), and (ii) spinodal decomposition (SD). The regions between the binodal

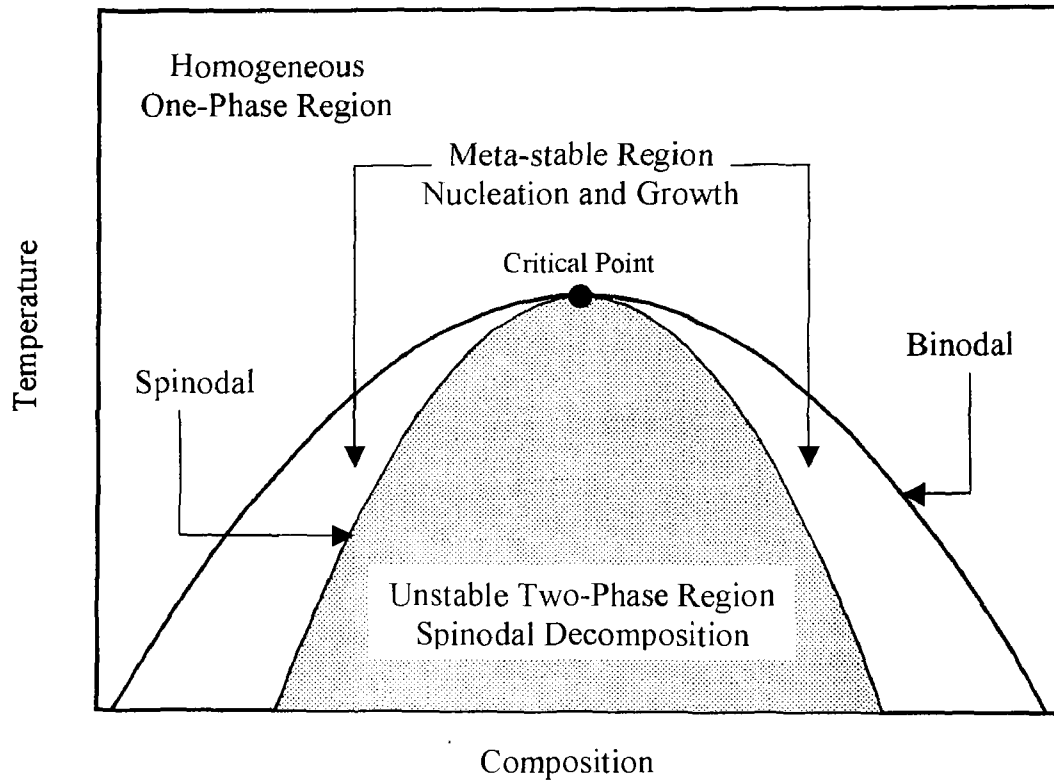


Figure 1.1: A temperature versus composition phase diagram at constant pressure for a binary polymer mixture showing an UCST. The solid thick black line is the binodal (equilibrium curve) and the thin black line is the spinodal curve separating the meta-stable region and the unstable region. In the metastable region, phase separation occurs by nucleation and growth (NG) and in the unstable region, phase separation occurs by spinodal decomposition (SD). The filled black circle represents the critical point.

and spinodal curve are the NG regions and the shaded grey area within the spinodal curve is the unstable region. Different types of morphologies are

developed for NG and SD. Figure 1.2 shows a phase diagram to illustrate these two mechanisms. When a homogeneous polymer mixture is quenched into the meta-stable region, this leads to the onset of nucleation and growth. The formation of nuclei begins and gradually grows in size due to the increase in free energy of the mixture. The resulting structure is the formation of spherical

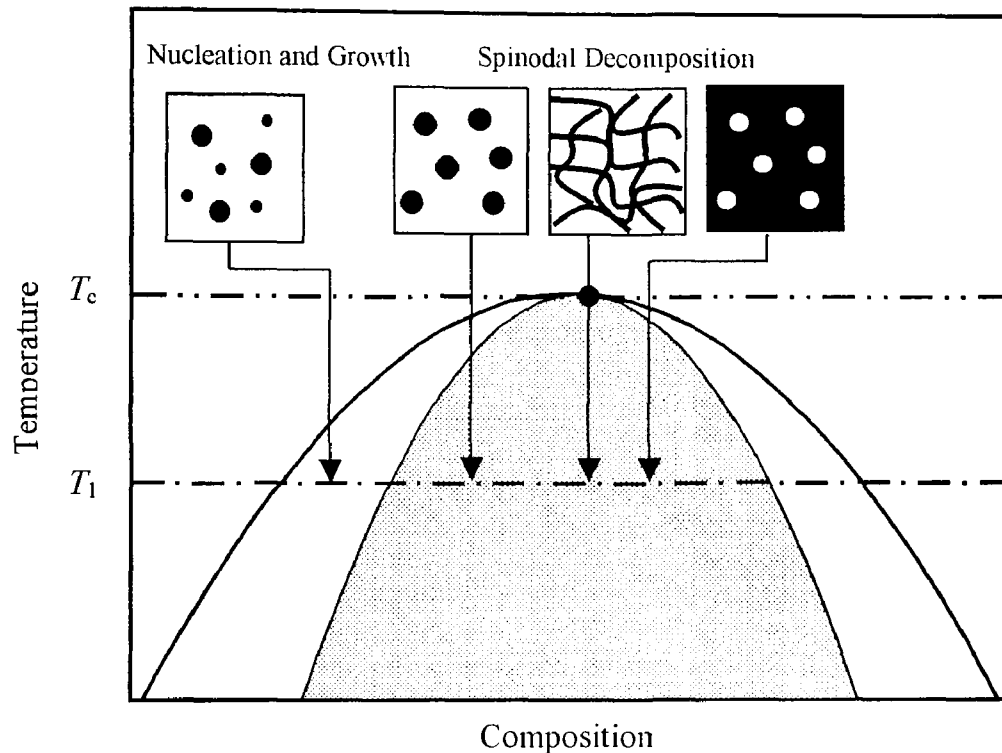


Figure 1.2: A temperature versus composition phase diagram for a binary polymer mixture showing the different morphologies that can be obtained depending on the location of the quench at temperature T_1 . If the polymer mixture is quenched into the meta-stable region, phase separation occurs by NG and the droplet type structure is formed. If the polymer mixture is quenched into the unstable region, phase separation occurs by SD and two morphologies are developed, droplet (off critical quench) and interconnected (critical quench). Depending on the location of the quench, the droplet type structure has a different continuous phase (surrounding matrix) and dispersed phase as indicated by the reversal of the black and white regions as shown in the SD structures. droplets rich in one contained within a continuous phase rich within the other

polymer. These droplets are randomly distributed and vary in size. In the unstable region, spinodal decomposition occurs. This is the result of a quench into the

unstable region where the onset of small concentration fluctuations causes phase separation. Depending on the concentration of the polymer mixture, two types of structures can be obtained. When the concentration of the polymer mixture is equal to the critical concentration, the structure obtained is interconnected. For polymer concentrations not equal to the critical concentration (off-critical quench), a droplet type structure is obtained. Also observed in Figure 1.2 is the difference in the continuous and dispersed phases depending on the location of the quench in the phase diagram as illustrated with the droplet formation by SD. On the left hand side, the droplet type structure has a continuous phase where the surrounding matrix is represented by white and dispersed phase by black droplets. On the right hand side, the continuous and dispersed phases are reversed. Therefore, depending on the desired properties for the blend, the continuous and dispersed phases are obtained accordingly.

Figures 1.3 and 1.4 show the evolution of the one-dimensional concentration profiles for phase separation by NG and SD respectively. In the meta-stable region, a sufficient increase in the composition fluctuations will cause a increase in the free energy of the mixture and cause phase separation by NG. Nuclei are formed and grow where the diffusional flux is inward as indicated in Figure 1.3 by the arrows at time t_i . This process is an activated process in that an energy barrier must be overcome in order for this type of phase separation to occur. The patterns that occur as time increases for NG upon overcoming the energy barrier are shown in Figure 1.3. In the unstable region, infinitely small concentration

fluctuations are enough to drive the mixture to phase separate and therefore, there is no energy barrier to overcome. The composition fluctuations occur by “uphill diffusion” where the gradient in composition moves from low concentration to high concentration as indicated by the arrows in the initial profile of Figure 1.4. The different stages in the evolution of the composition fluctuations for the unstable region shows the initial growth to the coarsening of the mixture where the phase separated regions become larger. A detailed description of the three stages of SD is presented in Chapter 3.

1.2 Thermally Induced Phase Separation (TIPS)

Phase separation of a binary polymer mixture may occur when rapid cooling or heating is applied, shear is applied or the initiation of a reaction occurs. Such methods are called thermally induced phase separation (TIPS), shear induced phase separation (SIPS) and polymerization induced phase separation (PIPS), respectively. The simplest method to induce phase separation is by rapidly decreasing or increasing (depending on the shape of the phase diagram) the temperature of the mixture from the one phase region into the two-phase region of the phase diagram. The temperature is rapidly increased for the lower critical solution temperature (LCST) phase diagram. For the UCST the temperature is rapidly decreased to induce phase separation. Thermally induced phase

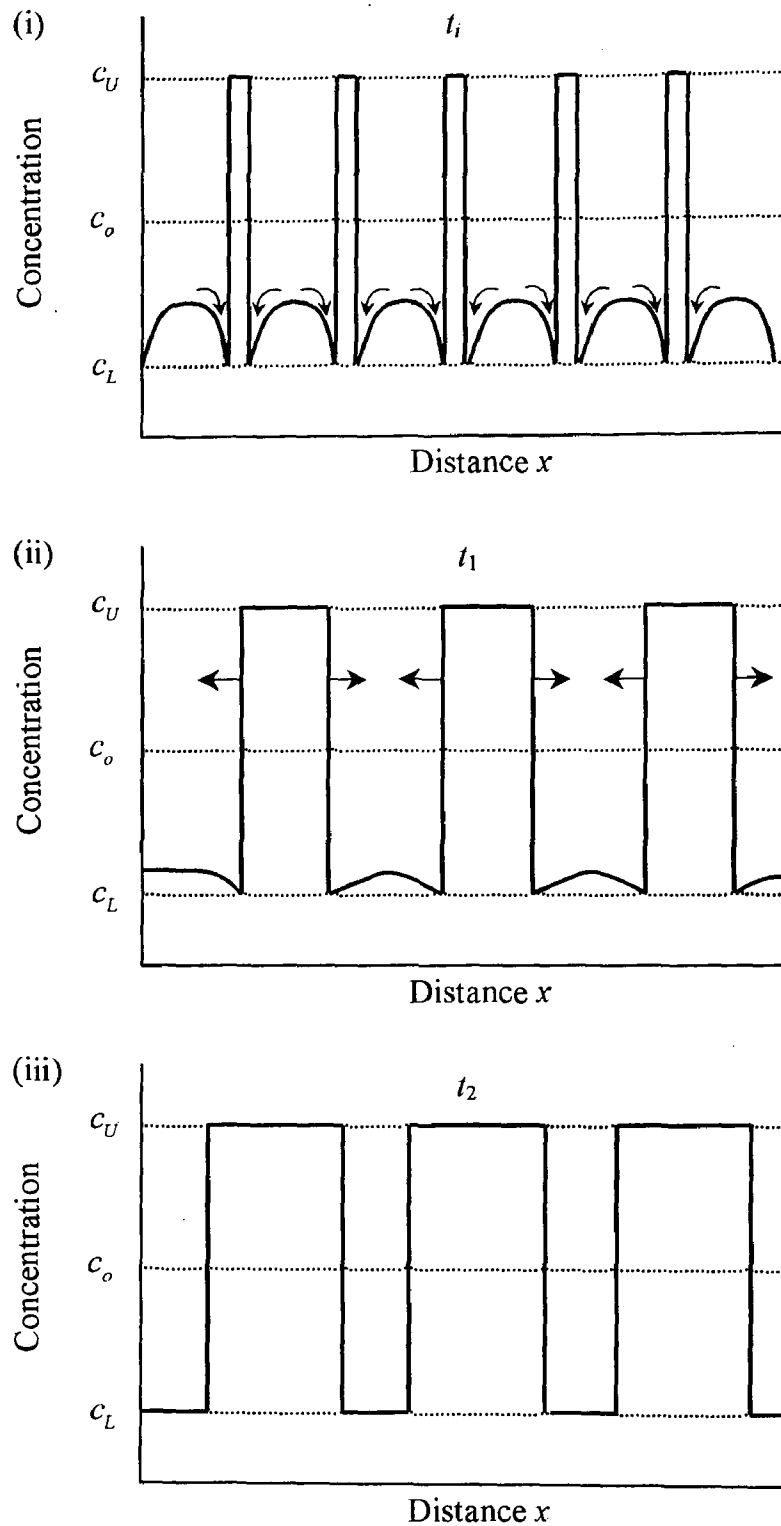


Figure 1.3: A schematic of the evolution of phase separation by the mechanism of nucleation and growth (NG) from the initial fluctuations at time t_i to the development and growth of domain sizes at time t_2 . The arrows in the initial time period indicate the direction of the diffusion (downward) typical of NG. The upper and lower equilibrium values are labeled as c_U and c_L respectively. The initial average composition is labeled as c_o .

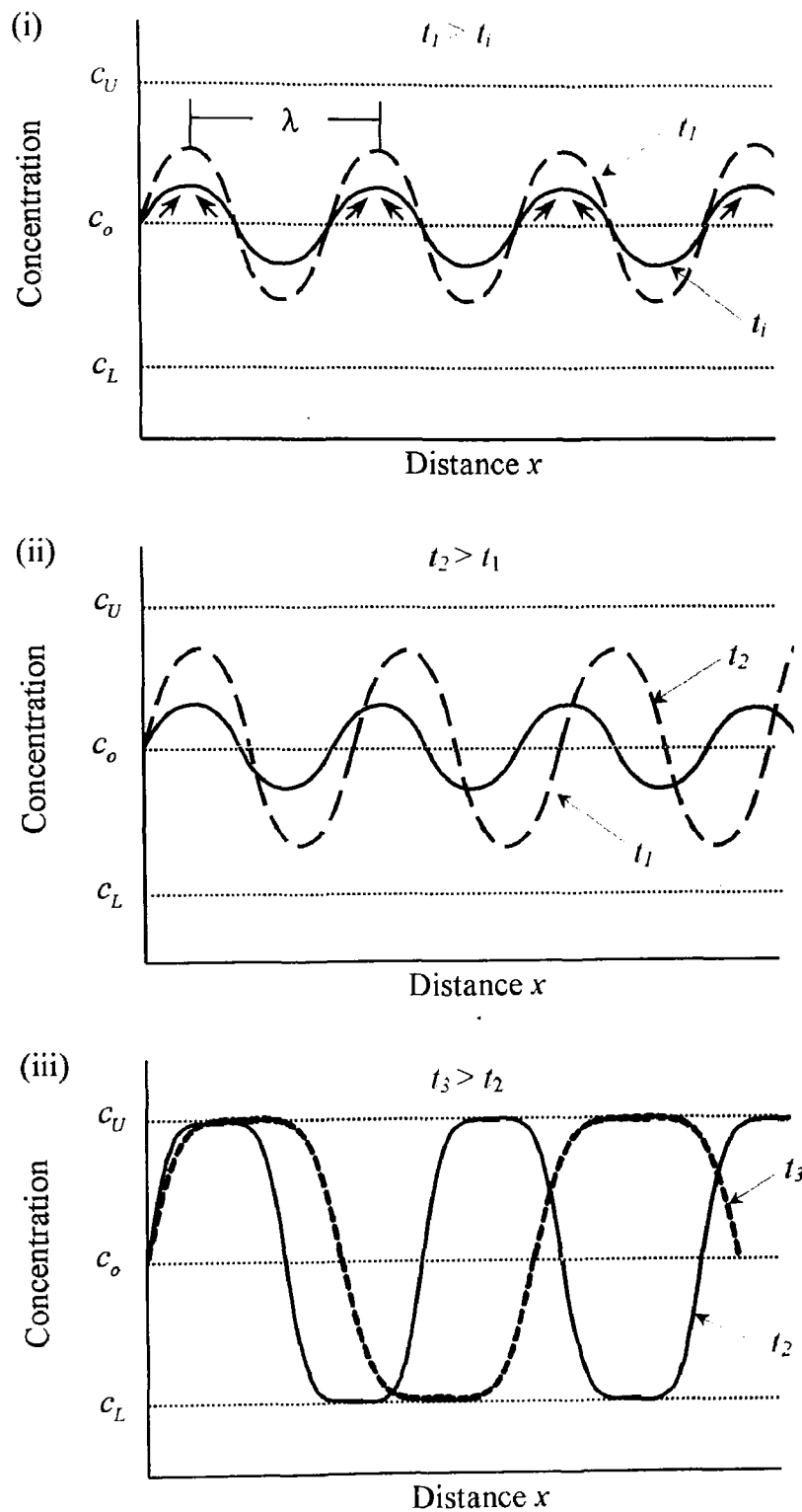


Figure 1.4: A schematic of the evolution of phase separation by the mechanism of spinodal decomposition (SD) from the initial fluctuations at time t_i to the development and growth of domain sizes at time t_3 . The arrows in the initial time period indicate the direction of the diffusion (upward) typical of SD. The upper and lower equilibrium values are labeled as c_U and c_L , respectively. The initial average composition is labeled as c_0 .

separation is commonly used in the study of phase separation in polymer systems [Strobl, 1985; Chakrabarti *et al.*, 1990; Takenaka *et al.*, 1992; Tanaka, 1993; Zhang *et al.*, 1995]. The TIPS method is described according to Figure 1.5. In this method, often a temperature versus composition phase diagram is constructed to determine where the quench conditions should be made in order to form particular microstructures. In Figure 1.5, the system has an UCST, where the T_c is the critical point and is the highest temperature at which phase separation may occur. Initially, a homogeneous mixture of polymer 1 and polymer 2 is obtained at a temperature in region *A*. This mixture is then subjected to a rapid decrease in temperature well into the unstable region of the phase diagram to a temperature T_I (point B). Upon decreasing the temperature, the thermodynamic driving force is increased and in order to minimize the free energy, the mixture separates into two phases. The tie line connects the two phases coexisting phases at equilibrium. The resulting morphology is then a continuous phase made of polymer 1 dispersed in the phase of polymer 2.

1.3 Two-Step TIPS method

Another technique to generate different phase separated morphologies is the two-step or double quenching [Tanaka, 1993; Hashimoto *et al.*, 2000a] TIPS method. The mechanisms of NG and SD are still applicable to this technique. Figure 1.6 shows the phase diagram for a double quench case showing the different morphologies that are possible for the initial critical and initial off-

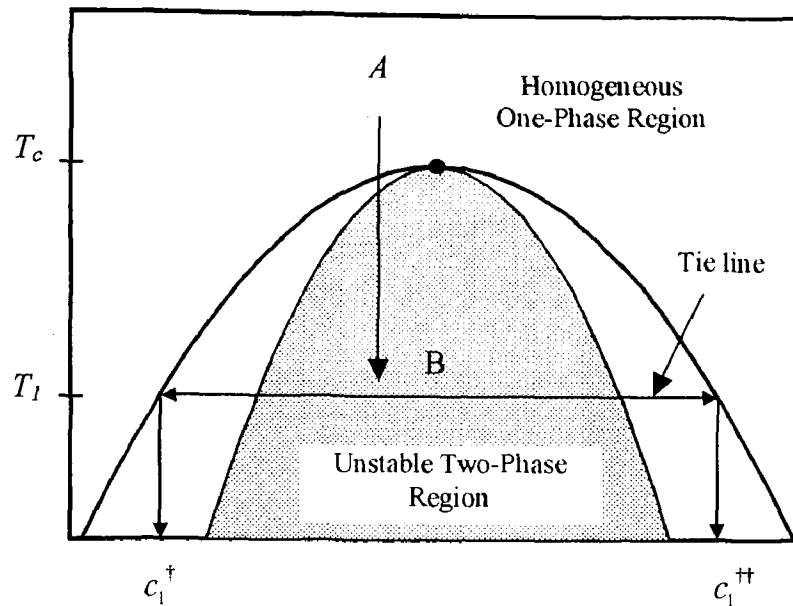


Figure 1.5: Temperature versus composition phase diagram illustrating the TIPS method. Point A is the initial homogeneous phase. A deep quench is made into the unstable region (at T_1) where phase separation occurs by SD as shown at point B. The horizontal line running across this phase diagram is a tie line that relates the composition of polymer 1 in the two coexisting phases. c_1^+ and c_1^{++} represents the equilibrium compositions of polymer 1.

critical quench by SD. In Figure 1.6, there are two types of morphologies that can be obtained by double quenching. For an initial critical quench at temperature T_1 , the interconnected structure is obtained and allowed to phase separate for a period of time. After a time, t , while the mixture is still within the spinodal region, the temperature is dropped again to T_2 and because the mixture is now in the off-critical state, the morphology is of droplet type. Therefore, the resulting structure is interconnected with small droplets dispersed within. For the initial off-critical quench to T_1 , the droplet type structure is obtained and allowed to phase separate for a period of time before quenching to T_2 . At this point the mixture is still off-critical and droplets dispersed within droplets are observed as well as the formation of droplets in the continuous phase. This two-step method is a

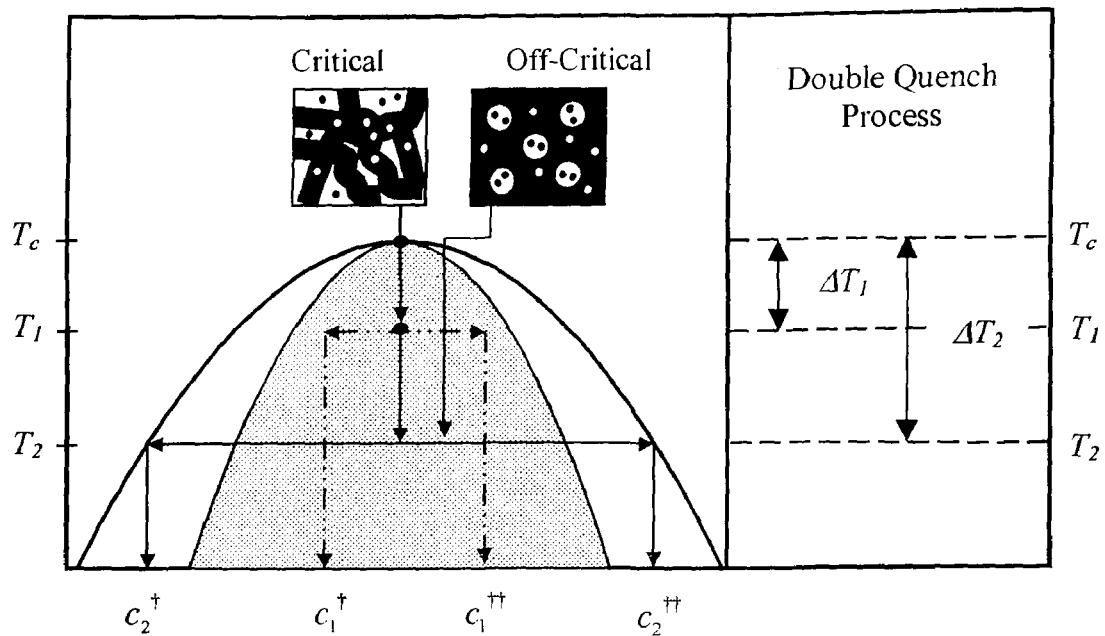


Figure 1.6: A schematic of the method of double quenching and the morphology that may develop for a critical and an off-critical initial composition. The mixture is first quenched to T_1 where it is allowed to phase separate by SD for a certain period of time before it is quenched again to a temperature T_2 (still within the unstable region). The smaller domains represent the secondary structures that form. On the left hand side, the critical quench case shows the interconnected structure as the primary structure and the smaller droplets as the secondary structure. On the right hand side, the off-critical quench shows larger droplets being the primary structure and smaller droplets as the secondary structure.

simplified version of the continuous cooling that is commonly observed in industrial processing and is important as a stepping stone to understand what occurs in more complex situations [Carmesin *et. al.*, 1986].

1.4 Thesis Objectives

The following is a list of the objectives for this thesis where phase separation by SD is studied using mathematical modeling and computer simulations:

1. To study the single quench and two-step quench TIPS method for phase separation by SD in a symmetrical polymer blend by developing a

mathematical model. This model will describe the dynamics of phase separation via spinodal decomposition for polymer blends using the nonlinear Cahn-Hilliard theory and the Flory-Huggins-de Gennes free energy. The mobility and the energy gradient coefficient are assumed to be composition dependent.

2. To solve the mathematical model in one dimension and two dimensions.
3. To present the 1-D and 2-D simulation results for a single quench to verify that this model shows the same known trends associated with spinodal decomposition using the TIPS method.
4. To present the 1-D results for a double quench to better understand the mechanism of secondary phase separation and to verify the results from the 1-D double quench model by comparison with published experimental work on two-step TIPS.
5. To present the pattern formation in two-step quenching to verify the experimental work of Hashimoto [Hashimoto *et al.*, 2000; Hayashi *et al.*, 2000a; Hayashi *et al.*, 2000b].
6. To expand the use of this model to study phase separation in food biopolymers by proposing possible approaches to adapting this model for analyzing food systems.

1.5 Methodology and Approach

This thesis is concerned with mathematical modeling and computer simulation of phase separation for polymer blends by the mechanism of SD. The objectives of

this thesis will be completed according to the method and approach shown in the flow chart in Figure 1.7. The flow chart can be broken down into different tasks. The first stage involves a detailed search of the literature to determine the different models that have been used to describe phase separation by SD for polymer blends. The literature review will also involve reviewing published experimental work for different analytical techniques used for studying phase separation. The next step involves determining what is lacking in the literature and how mathematical modeling and computer simulations can help fill these gaps to further understand phase separation. This leads to the thesis objectives. To answer the objectives, the model is developed and tested with published experimental and numerical work. The model is then refined if the numerical work does not reflect what is known to occur experimentally.

1.6 Thesis Organization

The thesis is broken down into a total of nine chapters and is organized in the following manner:

Chapter 1: This chapter introduces phase separation and the importance of studying it. It details the different mechanism involved in phase separation as well as the different methods to induce phase separation. The focus is on the method of thermally induced phase separation for a single step and a two-step process. This leads to the thesis objectives and the methodology and approach.

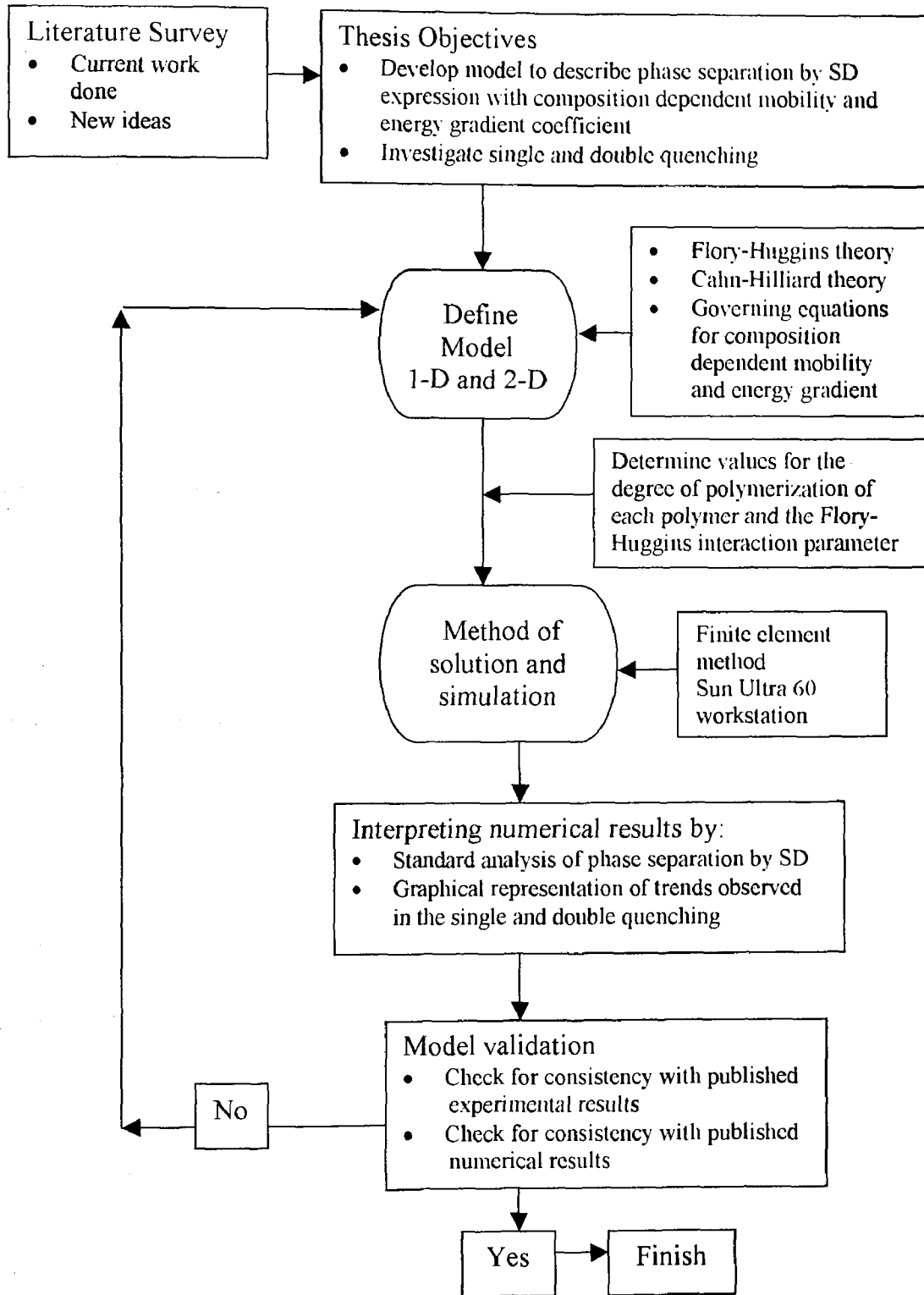


Figure 1.7: Flowchart detailing the methods and procedures for the mathematical modeling and computer simulation of TIPS for polymer blends undergoing single and double quenching.

Chapter 2: This chapter is a literature review of phase separation for the TIPS method detailed in two sections, isothermal quench and double quenching. It outlines the different experimental and numerical work that has been conducted and the important findings.

Chapter 3: This chapter discusses the theoretical background needed to develop the governing equation that describes phase separation by SD. In this chapter the Cahn-Hilliard theory and Flory-Huggins free energy is introduced. Equations for the concentration dependence of mobility and the energy gradient coefficient are also presented.

Chapter 4: This chapter presents the model development and the method of solution. The model is derived in one dimension and in two dimensions. Initial and boundary conditions are presented for solving the model.

Chapter 5: This chapter presents the one-dimensional results for the single quench TIPS method. A critical and an off-critical quench case are evaluated. There are three quench temperatures and three different diffusion coefficients examined. The numerical work is validated through other published experimental and numerical work by standard analysis methods for phase separation by SD.

Chapter 6: This chapter presents the numerical results in one-dimension for two-step quenching. An initial critical and initial off-critical quench are studied. Two quench depths are examined to observe the effects on morphology. The same three different diffusion coefficients are used as in the single quench case to

observe the effect of driving force on double phase separation. The numerical work is then compared with published experimental and numerical work.

Chapter 7: This chapter presents the numerical results in two dimensions where concentration profiles for single and double quenching are discussed. Two cases are examined, a critical and an off-critical case. Two quench depths are used to observe the change in the pattern development. This work is validated with published experimental and numerical work.

Chapter 8: This chapter details the possibility of extending this model developed for studying phase separation in polymer blends to food biopolymer blends. It includes recent literature on the evidence that phase separation in food biopolymers may follow the same mechanism as in polymer blends. Some suggestions are given in search of the literature that might be useful in determining the parameters necessary for inputting into the program.

Chapter 9: This chapter concludes all the findings from the numerical results in one and two dimensions on single and double quenching.

Chapter 2

Literature Review

The importance of phase separation and its application in many industries is introduced in this section. Being able to control the morphology of the phase separating material is a critical factor in optimizing the performance of these materials and therefore, studying the kinetics of phase separation (experimentally and theoretically) is a vital part of the design process. This section summarizes the research that has been conducted to study phase separation by SD under the TIPS method for polymer blends. The first section introduces earlier studies on a single temperature jump process. The second section describes a commonly observed phenomenon in experimental investigations of phase separation, the secondary phase separated structure. The process used to develop this type of structure is what is called double quenching [Tanaka, 1993] or the two-step TIPS process [Hashimoto *et al.*, 2000]. Both numerical and experimental work has been used to investigate this phenomenon to better understand the morphological development in phase separation.

2.1 Single Quench TIPS Studies on Polymer Systems

The interest in studying phase separation by SD is not only due to the large number of applications it has in industry but also in helping to further understand the non-equilibrium thermodynamics of phase separating mixtures [Hashimoto *et al.*, 1986; Ohnaga and Inoue, 1989; Hashimoto *et al.*, 2000]. The simplest method of producing phase-separated microstructures is by single quench TIPS and is used to experimentally study phase separation phenomena in polymer systems. From the single quench condition, the possible morphologies and the control of their formation are well understood with the vast amount of both experimental and numerical work that has been published. Therefore, this section highlights the most important findings for characterizing phase separation by SD in both experimental and numerical work.

Of particular importance to the experimental study of phase separation by SD is the work of Hashimoto *et al.* [Hashimoto *et al.*, 1983; Izumitani *et al.*, 1985; Izumitani and Hashimoto, 1985; Hashimoto *et al.*, 1986a; Hashimoto *et al.*, 1986b; Inaba *et al.*, 1986; Jinnai *et al.*, 1986; Shibayama *et al.*, 1986; Takenaka *et al.*, 1987; Izumitani *et al.*, 1990; Takenaka *et al.*, 1990; Hashimoto *et al.*, 1991; Jinnai *et al.*, 1991; Takenaka *et al.*, 1992; Hashimoto, 1993; Takenaka and Hashimoto, 1994; Hashimoto *et al.*, 1994; Ribbe and Hashimoto, 1997; Yamada *et al.*, 1988; Takeno and Hashimoto, 1998; Vaidya *et al.*, 2001] who used light scattering techniques to characterize the evolution of phase separation by SD for various polymer blends. In their work on a mixture of SBR/PB [Izumitani *et al.*,

1985], they were able to do an in-depth analysis on the kinetics of phase separation in the very early stages of SD because of the slow rate of phase separation of this mixture. They showed that the early stages of phase separation by SD can be described by the linearized Cahn-Hilliard theory [Cahn, 1965] and the growth of the maximum scattering intensity in the early stages is exponential. They also showed the limit of the early stages before nonlinear growth patterns were observed. Following the study on of SBR/PB, they were able to characterize the different stages of phase separation by SD into an early, intermediate and late stage [Hashimoto *et al.*, 1986a] for a mixture of PS/PVME. It has been argued that the stages can be further broken down [Strobl, 1985], however, the three stages are most commonly presented in the literature (see Figure 1.4) and are representative of the evolution of SD for polymer blends. In further studies, after characterizing the three stages, attention was paid to individual stages for various mixtures. In the early stages of phase separation by SD, for a mixture of PS/PVME under critical quench conditions, they were able to show that the linearized Cahn theory [Cahn, 1965] well predicted the early stages of phase separation [Hashimoto *et al.*, 1986a]. A number of other studies they conducted also show that the linearized Cahn-Hilliard theory holds for the early stages of SD for polymer blends [Hashimoto *et al.*, 1983; Hashimoto *et al.*, 1986b; Izumitani *et al.*, 1990; Takenaka and Hashimoto, 1994]. A later study on the early stages of SD and the effects of molecular weight distribution was examined [Takenaka and Hashimoto, 1994]. They found that the linear Cahn-Hilliard theory also reasonably described the early stages of SD. The intermediate stage of phase

separation by SD has been discussed both in the early stage and late stage publications [Hashimoto *et al.*, 1986a; Hashimoto *et al.*, 1986b; Takenaka *et al.*, 1990; Hashimoto, 1993]. Remarks have been made on the composition fluctuations in the intermediate stage as well as the growth of the scaled structure factor. In the intermediate stages, the wavelength and the amplitude of the composition fluctuations continue to grow and are indicated by the new scaling relations introduced for wave number and intensity [Hashimoto *et al.*, 1986b]. The morphology developed in the intermediate stage upon phase separation by SD can be described by the scaled structure factor. The scaled structure factor was found to increase with time and is not universal [Takenaka *et al.*, 1990]. This indicates that phase separation has not reached thermodynamic equilibrium. In the study of the late stages of phase separation by SD, the following results were obtained for understanding the growth patterns [Hashimoto *et al.*, 1986b; Izumitani *et al.*, 1990; Takenaka *et al.*, 1990; Jinnai *et al.*, 1991; Hashimoto *et al.*, 1994]. They introduced reduced variables for the analysis of the late stages of SD, and found scaling laws to fit the late stages of SD. These scaling laws for the reduced wave number and reduced scattering intensity fall onto a master curve when plotted against reduced time at different quench conditions indicating that the late stage coarsening of SD is the same regardless of temperature [Hashimoto *et al.*, 1986b]. The morphology developed upon phase separation by SD was described by the scaled structure factor for late stages. For a mixture of PS/PVME under critical quench conditions, Hashimoto *et al.* [Hashimoto *et al.*, 1986a; Takenaka *et al.*, 1992; Takenaka *et al.*, 1990], were able to show that the

scaled structure factor follows relatively well with the theory of late stage dynamics in metal alloys, small molecular liquids and glasses [Hashimoto *et al.*, 1986a]. Like the scaling laws for reduced scattering intensity, the scaled structure factor also falls onto a master curve indicating that the growth of the pattern in the late stages grow with dynamical self-similarity. Hashimoto *et al.* [Takenaka *et al.*, 1987; Jinnai *et al.*, 1993] also examined different parameters associated with SD, for instance, the temperature dependence of the Onsager kinetic coefficient. The Onsager coefficient is an important parameter that describes the mobility of the blend. The reason for studying the temperature dependence of the Onsager coefficient was to validate the theoretical work by Pincus [1981] and Binder [1983] and the results were within reasonable agreement [Jinnai *et al.*, 1993].

Other experimental work that has been conducted in studying phase separation by SD using the TIPS method [Gelles and Frank, 1983; Okada and Han, 1986; Strobl *et al.*, 1986; Schwahn *et al.*, 1987; Bates and Wiltzius, 1989; Kyu and Saldanha, 1998; Wiltzius *et al.*, 1988; Lee and Kyu, 1990; Schwahn *et al.*, 1990; Kyu and Lim, 1991; Gorga *et al.*, 2002]. The analysis of these mixtures also follows closely to the observations that were made by Hashimoto *et al.* except for the work of Wiltzius *et al.* [1988] who observe a different scaling pattern for the late stages of phase separation by SD in that the evolution of the scaled structure factor does not fall onto a master curve as was observed for Hashimoto's work.

In terms of numerical work, there have been a number of publications on modeling and computer simulation of phase separation by SD for binary polymer blends. The nonlinear Cahn-Hilliard (C-H) equation and the Flory-Huggins-de

Genes (F-H-de Gennes) free energy density are used in the model development to describe the dynamics of phase separation by SD. The parameters contained within the C-H and F-H-de Gennes equations, mobility (containing the transport information of the individual polymers) and the energy gradient coefficient (accounting for the resistance to the phase separation process due to the development of interfaces to try and restore the system to its lowest energy level) have been assumed to be a function of composition [Zhang *et al.*, 1995; Chakrabarti *et al.*, 1990; Glotzer, 1995; Kontis and Muthukumar, 1992; Castellano and Glotzer, 1995; Ariyapadi and Nauman, 1991; Castellano and Corberi, 2000]. Constant mobility has been used for simplicity by various authors in studying the dynamics of phase separation for polymer blends [Brown and Chakrabarti, 1993a; Ohnaga *et al.*, 1989; Brown and Chakrabarti, 1993b; Roth *et al.*, 2002; Chakrabarti *et al.*, 1989]. Other more complex studies carried out using the nonlinear C-H and F-H-de Gennes free energy have been used to model a ternary polymer blend undergoing phase separation by SD in two-dimensions to observe pattern formation [Nauman and Qiwei, 1994] and SD in polydispersed polymer mixtures [Takenaka *et al.*, 1993].

Analysis from the numerical work has focused on a variety of different aspects. A common investigation is in the evolution of the concentration profiles in one-dimension [Ohnaga *et al.*, 1989; Nauman and Qiwei, 2001; Castellano and Glotzer, 1995] to further understand the mechanism of phase separation by SD. In observing pattern formation, a two-dimensional model is used where a critical quench produces an interconnected structure and an off critical quench produces a

droplet type structure [Matsuoka and Yamamoto, 1995; Castellano and Glotzer, 1995; Brown and Chakrabarti, 1993b; Castellano and Corberi, 2000; Nauman and Qiwei, 2001; Ariyapadi and Nauman, 1991]. There has also been modelling in three dimensions to investigate phase separation [Chakrabarti *et al.*, 1989]. Analysis of the structure obtained has been performed by evaluating the evolution of the structure factor for critical [Chakrabarti *et al.*, 1990; Brown and Chakrabarti, 1993b; Kontis and Muthukumar, 1992; Zhang *et al.*, 1995] and off critical quenches [Kontis and Muthukumar, 1992; Zhang *et al.*, 1995; Brown and Chakrabarti, 1993b]. Finally, investigating the pinning of phase separated structures has also been an area of interest for studying polymer blends [Castellano and Corberi, 2000; Castellano and Glotzer, 1995]. The analysis ties in very well with the experimentally observed characteristics of phase separation by SD. For instance, the one-dimensional model [Ohnaga *et al.*, 1989] has shown the evolution of the phase separation by SD according to the three stages describe by Hashimoto *et al.* [Hashimoto *et al.*, 1986a]. In investigating the growth of the initial composition fluctuations in the early stages of SD, a single maximum wave number was observed and the evolution of the structure factor grow exponentially with time [Chakrabarti *et al.*, 1990]. This exponential growth in the structure factor is also consistent with experimental investigations on the evolution of the light scattering data [Okada and Han, 1986]. Also, in terms of the evolution of pattern formation for the critical and off critical quench, the numerical two-dimensional results show the interconnected structure for the off critical quench

and the droplet type structure for the off critical quench case which have been observed in experiment [Hashimoto, 1993].

2.2 Two – Step TIPS Studies in Polymer Systems

The drive for possibly obtaining more diverse morphologies to be used has prompted new techniques to produce phase separated materials. For instance, the introduction of a temperature gradient [Okinaka and Tran-Cong, 1995] and the introduction of a concentration gradient [Lacasta *et al.*, 1994] to develop new morphologies that are anisotropic in nature have found applications in holograms and pharmaceutical products. There is then motivation to consider double [Tanaka, 1993] or two-step phase [Hashimoto *et al.*, 2000] separation as yet another kind of morphology that can perhaps be put to practical use. Referring back to Figure 1.6, the method of double quenching and the types of morphologies that have been observed in experiment for a critical quench [Tao *et al.*, 1995] and an off critical quench [Tanaka, 1993] were shown. In the critical and the off-critical quench case the method of double quenching is the same. The mixture is quenched to T_1 (within the unstable region of the phase diagram) where phase separation by SD is allowed to proceed for a certain period of time before it is quenched again to the second temperature T_2 (the mixture is still within the unstable region). Double quenching [Tanaka, 1993] or two-step phase separation [Hashimoto *et al.*, 2000] for polymer systems has been studied since the late 1980s [Carmesin *et al.*, 1986; Ohnaga *et al.*, 1989] to 1990s [Yang *et al.*, 1998; Tanaka and Araki, 1998; Clarke *et al.*, 1995; Tao *et al.*, 1995; Chen *et al.*, 1994;

Tanaka, 1994; Tanaka, 1993; Kwak *et al.*, 1993; Ohnaga *et al.*, 1994]. The majority of these studies are focused on secondary structures experimentally with little theoretical explanation of the observations. Some numerical work has been done in one-dimension to explore the effects of a double quench [Ohnaga *et al.*, 1989] and even continuous quenching [Ohnaga *et al.*, 1994] on the concentration profiles but again, there was no in-depth analysis based on the fundamentals of phase separation by SD. A 2-dimensional numerical study has been performed on fluid mixtures by Tanaka and Araki [Tanaka and Araki, 1998] but the model development and the finding do not pertain to polymer mixtures. More recently, double quenching was revisited experimentally by Hashimoto *et al.* [Hashimoto *et al.*, 2000; Hayashi *et al.*, 2000a; Hayashi *et al.*, 2000b] who examined at a fundamental level, what was occurring under the quench conditions.

Furthermore, in industrial processing, heating and cooling are involved in a continuous sense and therefore, the simpler two-step quenching can provide a stepping stone for understanding more complex real systems [Carmesin *et al.*, 1986]. It is also worth mentioning that this type of secondary structure has also been observed in polymer solutions (binary and ternary) [Tanaka, 1993; Yamamura *et al.*, 2002; Graca *et al.*, 2002] and biopolymer mixtures related to food studies [Norton and Frith, 2001]. Therefore, an in-depth analysis of secondary phase separation in polymer blends can also provide useful information for explaining the same phenomena that occurs in other systems. Future work, as suggested by Hashimoto *et al.* [Hayashi *et al.*, 2000b], would be to revisit mathematical modeling and computer simulation of double phase separation to

see whether their experimental observations and in depth analysis of secondary phase separation also prevail in the modeling. A recent publication by Henderson and Clarke [2004] followed the method of Hashimoto et al. very closely [Hayashi *et al.*, 2000b] to model double phase separation for polymer blends. Their numerical results on the investigation of double quenching at an initial critical composition were in agreement with the work of Hashimoto. Some important questions about the formation of secondary structures are how it develops, when it develops and what effects it has on the final product formed. To answer some of these questions, a summary of some of the key works in the literature on the study of double quenching and the formation of secondary structures is provided in chronological order. Ohnaga and Inoue [1989] performed the first numerical study of double quenching and their study aimed at providing a framework for designing materials (polymers) that required continuous thermal treatment. They studied polymer mixtures of polystyrene/poly(vinyl methyl ether) and polybutadiene/poly(styrene co-butadiene) undergoing a double quench by mathematical modeling using the nonlinear C-H equation and computer simulations. The numerical results were presented in one-dimension for the polymer mixtures, one exhibiting a lower critical solution temperature (LCST) (polystyrene/poly(vinyl methyl ether)) and the other an UCST (polybutadiene/poly(styrene co-butadiene)) for an off-critical quench. Their investigation was split into two sections. First, the concentration fluctuations for an isothermal quench from the one-phase to the two-phase region were examined. They showed that their model of the time evolution of the concentration

fluctuations was consistent with the observed characteristics of phase separation by SD for the early to late stages [Hashimoto, 1993]. The second test was for a double quench where the first quench was allowed to progress for a certain period of time in the two-phase region before the second quench took place. They investigated the effects of a shallower and deeper quench and concluded from their simulations that when the second quench depth, ΔT_2 is less than half of the first quench depth, $\frac{1}{2}\Delta T_1$, the concentration fluctuations decay from the original concentration fluctuations of ΔT_1 . When ΔT_2 is between ΔT_1 and $\frac{1}{2}\Delta T_1$, there is an initial decay in the concentration fluctuations for a short period of time before it gradually grows and when ΔT_2 is greater than ΔT_1 , the concentration fluctuations originally from the first quench appear to show additional smaller waves (crests) forming in between the troughs. They also found that the smaller waves occurred only when the initial concentration fluctuations were well developed. Ohnaga and Inoue [1989] were able to determine the effects of deeper and shallower quenches for a polymer blend through observations of the concentration profiles and the effects of quenching at an earlier time or later time to see the effects on the phase separation process.

Experimental work is necessary to determine whether observations from simulation hold true for polymer systems as there are still many uncertainties in understanding double phase separation. In terms of equilibrium thermodynamics, experimental work helps to answer many questions. For example, what changes are occurring when double phase separation is observed or when the growths of

the amplitude of the concentration fluctuations are just magnified, is there any relationship that can be made between the growth rates of the initial wavelengths and the secondary wavelengths, how is the development of the initial wavelength affected by the rising of the second wavelengths, and how significant a value for the second wavelength is required before there is a significant change in the pattern formation (i.e. secondary structure forming within already initial phase separating structure)? Some of these questions were qualitatively answered through the experimental investigations of forming secondary structures using both polymer blends and solutions in the work by Tanaka. [1993]. Tanaka experimentally studied a mixture of polystyrene (PS) /poly (vinyl methyl ether) (PVME) and PVME/water undergoing a double quench to examine the evolution of the morphology using phase-contrast microscopy. The composition used in this study for PS-PVME was 50-50 wt% mixture, and that for PVME-water was 5-95 wt% mixture. For both systems, a two-step quench was initiated and the formation of the droplet type secondary structures was observed. Three trials performed on the PS-PVME mixture to observe what occurs at different quench depths. Figure 2.1 shows a schematic representation of the quench sequence used in Tanaka's work. The first case was from point I to point B (first temperature jump) and then from point B to point C (second temperature jump). The second case the PS-PVME mixture was subjected to a shallower quench at A and then a deep quench into the unstable region to observe the pattern formation (point I to point A and then point C). Finally, the third trial was reversed from a deeper

quench to a shallower quench from point I to point C (first temperature jump) and then point C to point B (second temperature jump).

In the first case (I to B to C), double phase separation was observed and small domains appeared within the large domains that were continuously phase separating. After the second temperature jump to T_2 , the secondary droplets appeared after a certain period of time. The small droplets eventually disappeared as they combined and diffused towards the interface of the large domains. In the second case, for the same mixture at the same composition, there was a change in the initial temperature to a higher initial value and then quenched to T_2 (I to A to C). The resulting morphology observed was very different from the first case. Double phase separation was observed at a much earlier time, almost immediately after the second jump. Rather than the large droplets observed in case one, the phase separated structure appeared like long round rods shifting in position before it became of droplet type at a later time. The last case of a deep quench to a shallow quench (I to C to B) showed large droplets in the initial quench and after the second quench interface instability was observed because of the diffusion of PVME through the interface towards the exterior of the droplets causing the interface to deform. One trial was performed for the polymer solution PVME/water and double phase separation was observed much more readily as the diffusion process is much more rapid. From these experimental observations, Tanaka concluded that in all cases, the variables that affect secondary phase formation are the initial and final quench temperatures (ΔT_1 and ΔT_2) and the time taken before the first phase separation process to occur before making the second

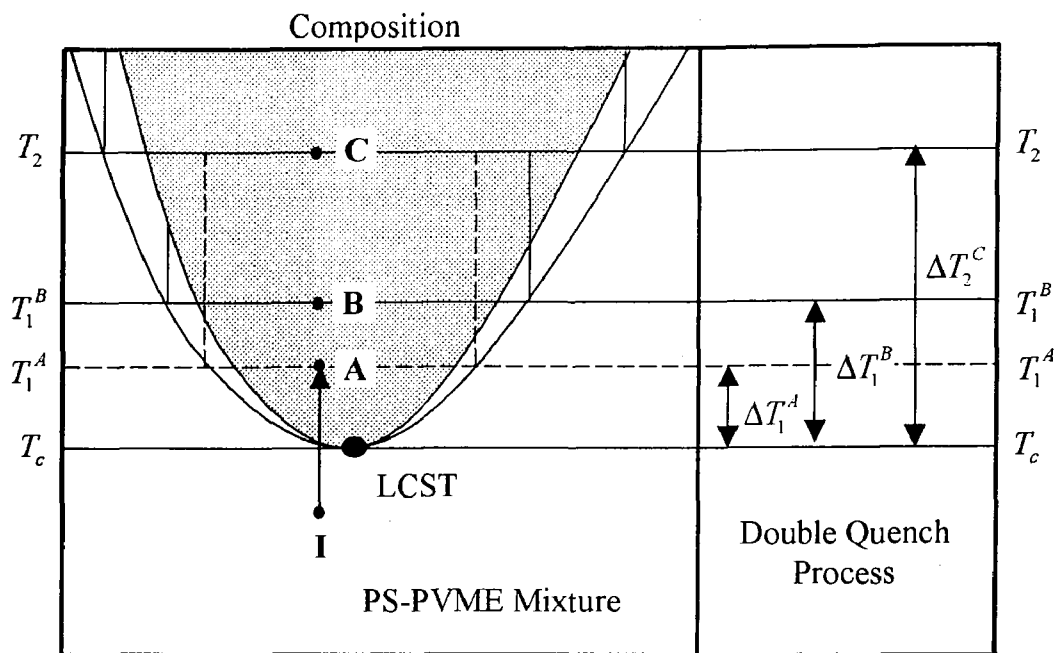


Figure 2.1: A temperature versus composition phase diagrams for a binary mixture of PS-PVME showing the different test conditions in the double-quench experiment. The first test performed was from point I to point B (first temperature jump) and then from point B to point C (second temperature jump). The second test was from point I to point A and then point C. The third trial was a reversed from a deeper quench to a shallower quench from point I to C point (first temperature jump) then point C to point B (second temperature jump). [Adapted from Tanaka, 1993]

temperature jump. A schematic of a phase diagram was constructed by Tanaka to qualitatively explain the possible mechanisms that may be occurring to form secondary structures. Figure 2.4 shows the same asymmetric phase diagram with the possible mechanisms proposed by Tanaka excluding the reverse case from a deeper to a shallower quench [Adapted from Tanaka, 1993]. The location of the initial starting point for the second quench has a large impact on the possible formation of the secondary phase separated regions. In his qualitative analysis, he points out that the growth of the secondary structures may be a result of NG for

both phases, SD for both phases or a combination of NG for one phase and SD for the other.

More experimental work was performed on different polymer mixtures to observe pattern formation by Kwak *et al.* [1993]. They experimentally investigated the emerging morphology during a two-step phase separation process for a mixture of polystyrene/poly(2-chlorostyrene)/n-butyl phthalate blend exhibiting a LCST using an initial off critical composition for the temperature jump. Like Tanaka [1993], Kwak *et al.* examined the effect of increasing the driving force on phase separation. An scanning electron microscope and light scattering apparatus was used to capture images and data of double phase separation and from the time evolution of their images, they were able to observe the same characteristics as Tanaka did for the PS-PVME mixture [Tanaka, 1993]. After the second jump, small domains started to appear and grew within the already existing domains until the small domains eventually stopped growing and gradually decreased in number. Finally, the small domains disappeared and only the large domains continued to grow. Light scattering (which has not yet been used as a method of analysis for double phase separation) was used to determine the change in the characteristic length (defined as $\lambda = \frac{2\pi}{q}$) before and after the second temperature jump. λ is the wavelength or the characteristic length and q is the scattering vector. A plot of the growth rate of the characteristic length with time before and after the second quench showed that the characteristic length of the large domains, after the second quench, continued to grow but at a substantially slower rate than for a single quench. This piece of information provides a deeper insight

into how the growth of the primary phase separating domains is affected by the second quench and by the formation of the secondary domains. An attempt was made by Kwak *et al.* [1993] to formulate an empirical expression to describe the change in the domain size upon making the second temperature jump. Their expression was only good for the early period of the second jump.

Following previous work by Ohnaga and Inoue [1989] on modeling and computer simulation of phase separation at different quench depths, Ohnaga *et al.* [1994] used the same ideas to study reaction induced phase separation in monomer/polymer mixtures, in this case, poly(ether sulfone) (PES)/ diglycidyl ether of bisphenol A (epoxy), by mathematical modeling and computer simulation in one-dimension under continuous quench conditions. A shift of the phase diagram as the molecular weight of the epoxy increased thrust the system into the unstable region of the phase diagram. This continuous quenching process was used to mimic the changes that occurred upon the shift of the phase diagram, towards higher critical solution temperatures, resulting in the mixture moving deeper and deeper into the unstable region. This study provided an analysis of the evolution of the concentration profiles upon a continuous change in temperature. The nonlinear C-H equation was used to describe the effects of polymerization-induced phase separation by SD. The interest in that research was to determine whether reaction-induced phase separation follows the structure formation of the single quench case by SD. The system was allowed to phase separate isothermally for a period of time before an additional quench was made and this was continuous for about four to five successive quenches deeper into the

unstable region (given by β). This profile reflects the observations made by Tanaka [1993] and Kwak *et al.* [1993] where the secondary structures were observed almost instantly after the second quench. Ohnaga *et al.* [1994] proposed a diagram of the constructive and destructive interference that may be occurring between the initial development of the concentration profile with that in the second quench to explain the formation of the concentration profile observed. The following schematic is a reconstruction of the one shown by Ohnaga *et al.* [1994]:

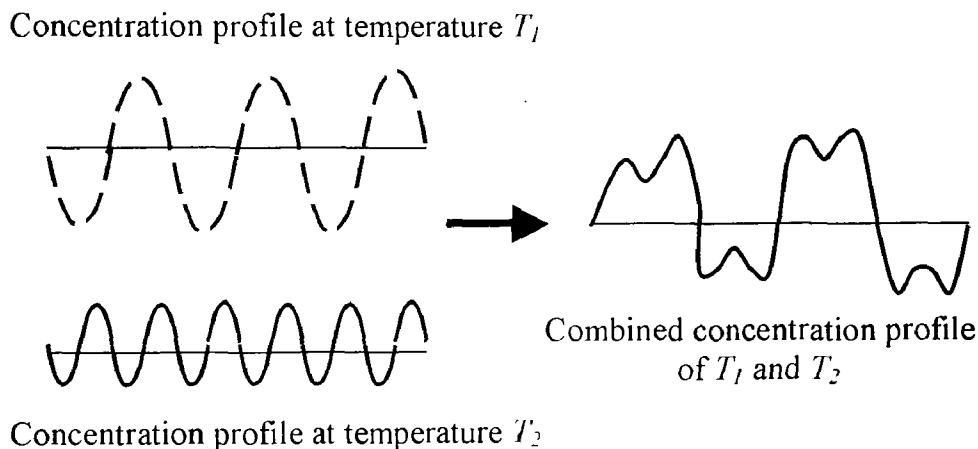


Figure 2.2: Schematics of the constructive and destructive interferences that may be occurring between the initial development of the concentration profile at T_1 and that in the second quench at T_2 . [Adapted from Ohnaga *et al.*, 1994]

Further evidence of double phase separation, after the one-dimensional simulations by Ohnaga *et al.* [1994], was presented by Clarke *et al.* [1995] who studied the phase behaviour of linear/branched polymer blends using the Flory-Huggins (F-H) free energy expression. They presented experimental evidence of double phase separation of an epoxy/polysulfone blend where the interconnected structure was formed by primary phase separation and droplet type structures formed from secondary phase separation, using scanning electron microscopy.

Although they were able to induce secondary phase separating structures, they were only able to give qualitative reasons for the appearance of these structures. They surmised that the secondary domains may be due to the location of the system in the phase diagram (i.e. in the meta-stable region before it proceeds into the unstable region such that nucleation and growth takes place first before spinodal decomposition) or that cross-linking occurs in the coexisting phases during the phase separation process leading to further instability within the coexisting phases (secondary phase separation).

Tao *et al.* [1995] studied two-step phase separation for a mixture of polystyrene/poly(2-chlorostyrene) having a LCST phase diagram using light scattering and scanning electron microscopy. Their images of double phase separation were similar to those presented by [Clarke *et al.*, 1995] with the interconnected structure from primary phase separation and droplet type morphology from secondary phase separation. The purpose of their study of the two-step process was to give a basis for understanding more complex behaviour under continuous quench conditions that are often found in industrial processing. Like Tanaka [1993] and Kwak *et al.*, [1993], they experimentally observed the effect of increasing the thermodynamic driving force on phase separation with the two-step method. However, a new focus in their paper was on the evolution of the emerging morphology after the second jump while making the second jump at the intermediate stages of phase separation. Something to note is that their system was not strictly binary in that they added di-n-butyl phthalate (DBP) to the mixture to extend the experimental temperature range in studying phase

separation. Their analysis looked at the growth of the characteristic length of the primary interconnected structure during the first temperature jump and after the second temperature jump. To investigate this, the characteristic length was calculated using the light scattering data from the secondary quench. They noticed that the growth of the characteristic length increased for the primary interconnected structure when secondary droplets appeared. This observation is consistent with the initial work of Kwak *et al.* [1993]. They then altered the initial quench depth while keeping the second quench temperature constant to observe effects on the characteristic length, and found that droplets observed within the interconnected structure decreased when increasing the initial temperature. In terms of the characteristic length, they saw no obvious changes in the growth rate of the primary structures. An empirical scaling law was developed for determining the evolution of the characteristic length by the addition of a term accounting for the difference in time from the initial temperature jump to the second jump. But that expression was not derived from basic principles [Hashimoto *et al.*, 2000], and was only good up to the end of the early stages before it diverged when comparing with the data they obtained.

Yang *et al.* [1998] looked at a mixture of diallyl phthalate (DAP)/poly (2,6-dimethyl-1,4-phenylene ether) (PPE) having an UCST phase diagram. The focus of their work was on the morphology developed during curing using light scattering, Fourier transform infrared spectroscopy, and transmission electron microscopy for polymerization induced phase separation, where by they found secondary phase separation in the final structure. They showed that the primary

and secondary structure were of the droplet type, and proposed a possible explanation for this phenomenon. Figure 2.3 shows the evolution of the concentration profile for the secondary structure formation they proposed. This development of the concentration profile is similar to the ones observed by Ohnaga and Inoue [1989] in the one-dimensional numerical results of double quenching. However, the amount of interference to the initial concentration profile from the secondary temperature jump was not as dramatic as shown here in the figure. Also, the system under study by Ohnaga and Inoue [1989] was not reaction-induced phase separation.

Up to this point, most of the work done on double phase separation has been based on the formation of secondary structures and image analysis. There has been very little work or in-depth quantitative analysis of the mechanism of double phase separation in the literature [Hayashi *et al.*, 2000a]. The first in a series of papers written by Hashimoto *et al.* [2000; Hayashi *et al.*, 2000a and 2000b] have recently revisited the two-step phase separation phenomena to further understand, on a quantitative level based on light scattering data, the morphological development of secondary phase separated regions within a polymer blend of deuterated polybutadiene (DPB), and protonated polyisoprene (HPI) having an initial composition close to the critical composition for the initial quench. The polymers used in this study have very similar properties (i.e., very narrow molecular weight distributions, nearly symmetrical in terms of density, statistical segment length, monomeric friction coefficient and glass transition temperature). The system has a LCST phase diagram and the mixture was subjected to a critical

Secondary Phase Separated Droplet Formation by SD for an Off-Critical Quench

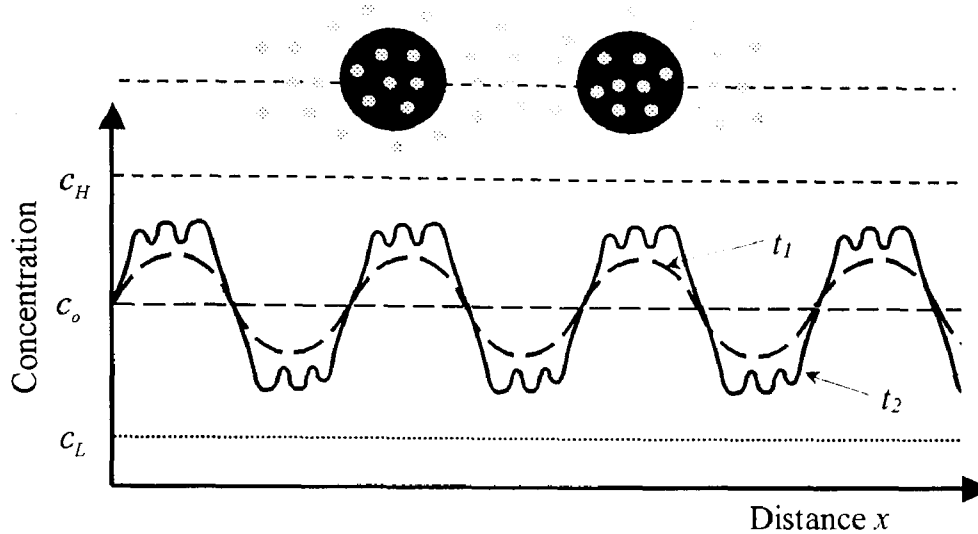


Figure 2.3: A proposed 1-D concentration profile showing the evolution of the concentration fluctuations for an off critical quench under a single quench (dashed lines) and a double quench (solid line). The introduction of multiple little peaks and troughs upon the second quench represents the formation of secondary structures. The picture above the concentration profile illustrates a 2-D picture of the resulting morphology from this concentration profile. [Adapted from Yang *et al.*, 1998].

quench. A number of concerns were posed in trying to gain a better understanding of the mechanism for secondary structure formation within an already phase separated regime. In the attempt to answer these questions, Hashimoto *et al.* [2000] have been able to fill in the gaps between what has been experimentally observed and how the process can be explained at a fundamental level. Their concerns were:

- To determine whether there were scaling laws that could be used as a tool to predict the change from the initial structure (first quench) to the final structure at the second quench.

- If the formation of secondary structures may be limited to a certain conditions (a critical time i.e. the early, intermediate and late stage of development)
- To be able to describe, quantitatively, the evolution of the growth of both primary and secondary structures as described in previous studies
- To determine the theories that best describe the double quenching process (i.e. Is the C-H nonlinear equation applicable for double quenching?)

The procedure taken after the first temperature jump was to allow the system to phase separate until the equilibrium compositions of the two phases were reached before the second quench was made. The second quench was still within the unstable region of the phase diagram and therefore phase separation would be characterized by SD. From a set of experiments the size of the initial structure was varied before making the second quench and the light scattering profiles described the evolution of pattern formation for double quenching distinguishing three regimes [Hashimoto *et al.*, 2000]. The three stages are as follows, first, after the second temperature jump, there was a broad peak (secondary peak) that forms and grows with time. Second, this broad peak increased in intensity with time and third, the peak eventually decreased at longer times but the original peak intensity, from the first quench, continued to grow. The data was then used to develop new scaling laws to describe the spatial and temporal changes that occur in double quenching. An interesting result from the new scaling laws showed that after the second quench, the initial structure was relaxed and transformed into a new

structure and grew according to the scaling laws of a single quench into the unstable region by SD at the second temperature. The next paper written by Hayashi *et al.* [2000a], tackles the other questions regarding the evolution of the structure of the primary and secondary domains by examining the evolution of the structure factor. The same two-step quench process, and the same mixture of deuterated polybutadiene (DPB) and protonated polyisoprene (HPI) was investigated. They examined the effect of the initial domain size on the formation of secondary structures and found that at early stages of the initial quench where the initial domain size is not too large, secondary structures do not occur and the initial structures continued to grow after the second temperature jump. With larger domain sizes for the initial structure, secondary structures were observed. From their light scattering data used to evaluate the evolution of the structure factor, they found that initial domain size played a major role in the development of secondary structures. Also, they were able to characterize the development into three stages like in the single quench case [Hayashi *et al.*, 2000a]. In stage one, the secondary structures formed and grew inside the primary structures. The growth of the secondary structures was similar to that of the early stage in a single quench case at the second temperature jump and was very evident. Also, the peak intensity of the primary structures grew alongside the secondary ones. In stage two, both the primary and secondary structures grew together at relative rates to each other and the secondary structures are still present in the initial structures. Finally, in stage three the secondary structures start to disappear and the time evolution of growth of the structures approach the single quench values in the late

stage at the second temperature. The results suggest that the growth of the secondary structures was affected by the size of the initial structures as was mentioned in their first paper [Hashimoto *et al.*, 2000]. Evaluation of the structure factor then answers the questions they pose on the development of the secondary structure within the primary structure being nonlinear in nature. The final paper was written to investigate the validity of linearized C-H theory for the early stage SD after the second temperature jump on the development the secondary structures [Hayashi *et al.*, 2000b]. For the same mixture studied in their previous two papers and applying the same methods [Hashimoto *et al.*, 2001; Hayashi *et al.*, 2000a] they found that the linear theory for the single quench SD process holds for the early stages in the formation of the secondary structures at the second jump. In this work, Hayashi *et al.* [2000b] also discussed the concept of confinement effect on the early stages of phase separation by SD noting that it has not been addressed by Kwak *et al.* [1993], Tanaka [1993], nor Tao *et al.* [1995] in their experimental work of double phase separation. They introduce the concept of a free-SD process and confined-SD process [Hayashi *et al.*, 2000b]. They define confined-SD as the development of secondary structures in the primary structures where the primary structure acts as a new medium in which the secondary phase separation takes place and free-SD is the typical SD of a regular single quench process. Another idea that was presented was the concept of “superposed SD” [Hayashi *et al.*, 2000b]. This superposed SD is the result of taking the individual composition just before the second temperature jump and quenching them to the second temperature as if they were single quenches. The

result of superposed SD would then be a combination of the two individual cases of free SD to describe the double quenching process of confined SD because in theory, the process may be a linear combination of the individual quenches at the early stages of SD. Early stages of SD on the evolution of the composition fluctuations do not affect the characteristic wave number of the dominant mode of the concentration fluctuations and affect only the values of the diffusion coefficients. They argue that on a qualitative level, these values are reasonable with their assumptions stated earlier about the early stages for the confined and free SD. Comparing confined-SD with superposed-SD they found major differences in the values for the diffusion coefficients. The values of the diffusion coefficient in the confined-SD were roughly half that of the superposed-SD process. This leads them to believe that the differences in the diffusion coefficients stems from the idea of the confinement effect that the large domains have on the growth of the small domains. Therefore, from their analysis of light scattering data for the confined-SD, free-SD and superposed-SD, they conclude that small domains are not spatially affected (the scattering vector remained relatively constant) provided there was enough space for them to be generated. Growth rate of the composition fluctuations of the secondary structures was be coupled with the growth of the interface of the large domains (at a certain characteristic length) and therefore, slowed down compared to its growth rate in a free SD process. Upon analysis using the linear C-H theory, they found that the effect of space confinement in the SD process. This reasoning was used to explain

the discrepancies in the mutual diffusion coefficient for the confined and the superposed SD process.

An important final note made in the paper by Hayashi *et al.* [2000b] was the limitations of the time resolved light scattering apparatus in observing the effects of using smaller domains sizes immediately before the second-step phase separation. To do this, they proposed the use of time resolved neutron scattering [Hayashi *et al.*, 2000b]. In this respect, modeling and computer simulation would be of a powerful means of studying the effects of having small domains sizes developed in the early stages of SD under a single quench before a second quench is made and observing the effects on structure development.

Recently, a publication by Henderson and Clarke [2004] followed the method presented by Hashimoto *et al.* [2000] to model double phase separation for polymer blends. They examined a critical mixture and the second temperature jump was made at the late stages of phase separation by SD. Their model consisted of the nonlinear C-H equation and the F-H-de Gennes free energy expression. The mobility was assumed to be constant. They examined pattern formation for a critical quench in 2-D, the growth of the structure factor and the effect of quench depth on the formation of secondary structures. What they observed was similar to the experimental work of Hashimoto [2000; Hayashi *et al.*, 2000a and 2000b], however, their work was on the early stages of phase separation by SD showed discrepancies in the calculation of amplification factor and maximum wave number.

Chapter 3

Theoretical Background

This section presents the necessary theory in describing phase separation of polymer blends. The nature of phase separation in a two-component system involves changes in energy, namely, Gibbs free energy. This chapter begins with thermodynamics where the process of phase separation from an initially homogeneous mixture is examined. It involves discussing mixing behaviour and the construction of the phase diagram using the Flory-Huggins (F-H) theory. Subsequently, the nonlinear Cahn-Hilliard (C-H) theory is presented which is used to describe the dynamics of phase separation by SD. In early studies of metal alloys using the C-H theory, the mobility and the coefficient of the energy gradient were assumed to be constant [Langer *et al.*, 1975; Copetti and Elliot, 1990]. In some polymer studies, the mobility was assumed to be constant and the energy gradient coefficient was assumed to be a function of composition [Ohnaga *et al.*, 1989; Chakrabarti *et al.*, 1989; Chakrabarti *et al.*, 1990; Brown and Chakrabarti, 1993a; Matsuoka and Yamamoto, 1995, Henderson and Clarke, 2004]. In other polymer blend studies, the mobility was assumed to be a function of composition in the form of $M(c) = NDc(1-c)$ where D is the self-diffusion coefficient, c is composition, and N is the degree of polymerization of the

polymer. The energy gradient was also assumed to be a function of composition [Ariyapadi and Nauman 1991; Kontis and Muthukumar, 1992; Glotzer, 1995; Aksimentiev *et al.*, 2000; Castellano and Glotzer, 1995; Castellano and Corberi, 2000]. Both mobility and the coefficient of the energy gradient are known to be composition dependent for polymer blends. The last section in this chapter will then present the development of the expressions for composition dependent mobility and gradient energy.

3.1 Thermodynamics of Phase Separation in Polymer Blends

The governing equation that describes the thermodynamic stability of a mixture is the change in Gibbs free energy. Under constant temperature and pressure the change in Gibbs free energy is defined as:

$$\Delta G_M = \Delta H_M - T\Delta S_M \quad (3.1)$$

where ΔG_M is the Gibbs free energy of mixing, ΔH_M is the enthalpy of mixing, T is the absolute temperature of mixing and ΔS_M is the entropy of mixing. Stability (i.e. whether or not the system is miscible or immiscible) depends on the value of ΔH_M and ΔS_M . When $\Delta G_M \leq 0$, a homogeneous solution exists. This means that the Gibbs free energy of the mixture is less than the Gibbs free energy of the sum of the pure components. This condition is necessary but not enough to ensure stability of a system [Van Dijk and Wakker, 1997]. To ensure stability, the sign of the second derivative of ΔG_M with respect to the composition must to be evaluated. For ideal mixtures it is assumed that $\Delta H_M = 0$, therefore, only ΔS_M is

left in the free energy expression. However, for polymer mixtures, which are non-ideal, both the ΔH_M and ΔS_M must be considered.

3.1.1 The Flory-Huggins Theory

The F-H theory can be used to describe the free energy of mixing for a polymer mixture. As mentioned earlier, polymer mixtures are non-ideal and therefore, the enthalpy of mixing cannot be ignored. The free energy of mixing for polymer blends contains two parts, an entropic contribution and an enthalpic contribution. The entropic contribution is associated with the configuration of polymers within the mixture and the enthalpic contribution is associated with the interactions between different segments in the mixture. The free energy is determined through the assumption of an athermal polymer mixture (i.e. $\Delta H_M = 0$ and ΔS_M is not ideal) [Van Dijk and Wakker, 1997]. A lattice model is used to describe the possible arrangements that can be obtained for binary polymer mixtures [Cowie, 1998]. Since polymer chains are long segments, the number of arrangements possible is less than that for smaller molecules and therefore, the entropy of mixing is much smaller. The lattice model for polymer mixtures is based on Boltzmann's law of entropy. Boltzmann's law is:

$$\Delta S_M = k_B \ln \Omega \tag{3.2}$$

where k_B is the Boltzmann's constant and Ω is the number of ways that N_1 and N_2 segments can be arranged in the lattice [Van Dijk and Wakker, 1997]. After some mathematical manipulation the change in entropy due to mixing of two polymers is given by:

$$\frac{\Delta S_M}{k_B} = \left[\frac{c}{N_1} \ln c + \frac{(1-c)}{N_2} \ln(1-c) \right] \quad (3.3)$$

c is the volume fraction of polymer 1. This term describes the arrangement of the polymer segments within the mixture and is relatively small for large degree of polymerization. The enthalpy of mixing is given by:

$$\Delta H_M = k_B T \chi c(1-c) \quad (3.4)$$

The χ parameter is a measure of the effective interactions between polymer segments. From this arrangement and through some mathematical manipulation, the F-H free energy for a polymer mixture can be described by the following equation:

$$f(c) = \frac{k_B T}{v} \left(\underbrace{\frac{c}{N_1} \ln c + \frac{(1-c)}{N_2} \ln(1-c)}_{\text{Entropic contribution}} + \underbrace{\chi c(1-c)}_{\text{Enthalpic contribution}} \right) \quad (3.5)$$

where $f(c)$ is the free energy density, χ is the F-H interaction parameter [Flory, 1953], v is the volume of a segment, and c is the composition of one polymer.

3.1.2 The Phase Diagram for Polymer Blends

Polymer blend phase diagrams can be determined experimentally or constructed using the F-H free energy expression. In Figure 3.1, some common phase diagrams for binary polymer mixtures are shown [Tanaka, 2000]. Figure 3.1 a) has an upper critical solution temperature UCST temperature type phase diagram. The UCST is the highest temperature at which first sign of phase separation can

be observed. Figure 3.1 b) shows a lower critical solution temperature (LCST) type phase diagram. This point corresponds to the lowest temperature at which the first sign of phase separation occurs. Finally, in Figure 3.1 c), the temperature versus composition phase diagram shows a mixture where both the UCST and the LCST exist. Graphically, the relationship between the free energy versus composition and temperature versus composition is shown in Figure 3.2. In the free energy phase diagram, as the temperature is decreased from T_3 to T_1 , the free energy changes. T_1 is taken as the example to show how the temperature versus composition phase diagram is constructed using the free energy plot. The binodal is also known as the equilibrium curve and is constructed through the corresponding points of tangency on the free energy diagram. The condition for equilibrium between the two coexisting phases is when the chemical potential of component i , in one phase (1) is equal to the chemical potential of component i in the coexisting phase (2). This leads to the condition that the total change in free energy of component i is zero $\frac{\partial F}{\partial c_i} = (\mu_i^{(1)} - \mu_i^{(2)}) = 0$. The tangent line labelled $\beta' - \beta''$ gives this condition where the chemical potential of the coexisting phases is equal. The spinodal curve is constructed through the use of the inflection points ($\frac{\partial^2 F}{\partial c^2} = 0$) in the free energy diagram. The second derivative of free energy with respect to composition determines the drive for phase separation around the inflection ($\frac{\partial^2 F}{\partial c^2} = 0$) points where $\frac{\partial^2 F}{\partial c^2} > 0$, stability or meta-stability are possible and $\frac{\partial^2 F}{\partial c^2} < 0$ results in instability for the binary

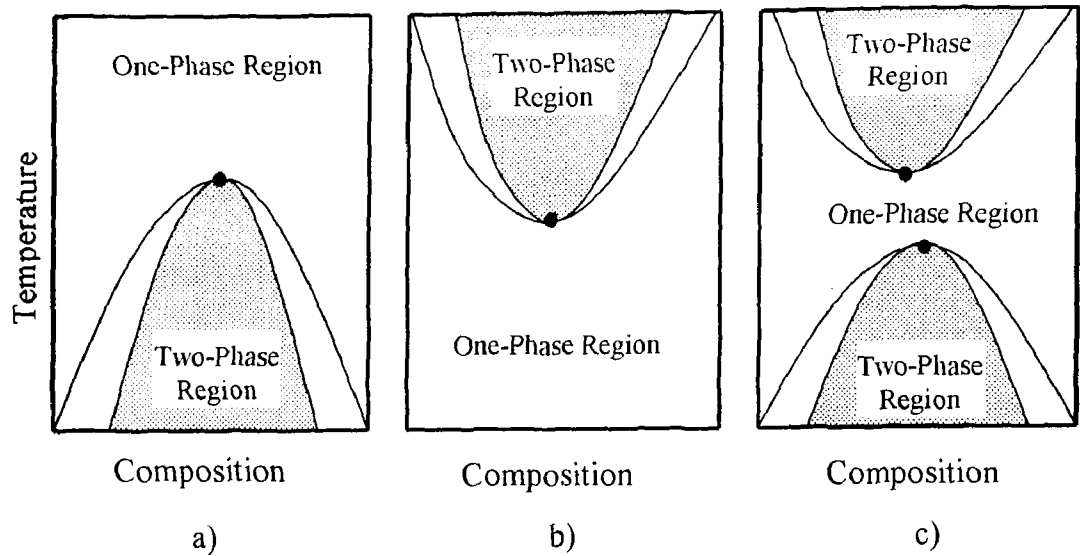


Figure 3.1 Typical temperature versus composition phase diagrams for binary polymer systems showing a) upper critical solution temperature, b) lower critical solution temperature or c) a combination of upper and lower critical solution temperature [Adapted from Tanaka, 2000].

mixture. For meta-stability, the second derivative of free energy with respect to composition is greater than zero and if the composition fluctuations are small, the energy barrier will not be crossed and the blend will be restored to its original composition. For instability, the second derivative of free energy with respect to composition is less than zero and small composition fluctuations are enough to create instability. The curvature of the second derivative of free energy with respect to composition (change in sign) can then detail the degree of stability, alongside the knowledge of the first derivative of free energy with respect to composition, with concave downwards (local maximum) being unstable and concave upwards (local minimum) can be meta-stable or stable. At the spinodal points, there is no thermodynamic driving force to cause the mixture to phase separate or to restore the blend to its original composition upon small fluctuations. The spinodal then separates the meta-stable from the unstable region.

Theoretically, to determine the equilibrium (binodal curve) compositions, the F-H free energy is used to find chemical potential of each component in their respective phases. Equations (3.6 a) through (3.6 d) are the chemical potentials for the two equilibrium phases of components 1 and 2. At equilibrium, the chemical potential is the same everywhere in the two phases of components 1 and 2 (i.e. for component 1 $\mu_{1c^\dagger} = \mu_{1c^{\ddagger}}$). Equating equations (3.6 a) with (3.6 b) and (3.6 c) with (3.6 d) the system of equations can be solved for the values of c^\dagger and c^{\ddagger} [Kurata, 1982] which represent the coexisting phases in equilibrium. The subscripts 1 and 2 for c^\dagger and c^{\ddagger} identify the component in the mixture.

$$\mu_{1c^\dagger} = \mu_{1c^{\ddagger}} \begin{cases} \ln(c_1^\dagger) + \left(1 - \frac{N_1}{N_2}\right)(1 - c_1^\dagger) + \chi N_1 (1 - c_1^\dagger)^2 & (3.6 \text{ a}) \\ \ln(c_1^{\ddagger}) + \left(1 - \frac{N_1}{N_2}\right)(1 - c_1^{\ddagger}) + \chi N_1 (1 - c_1^{\ddagger})^2 & (3.6 \text{ b}) \end{cases}$$

$$\mu_{2c^\dagger} = \mu_{2c^{\ddagger}} \begin{cases} \ln(1 - c_2^\dagger) + \left(1 - \frac{N_1}{N_2}\right)(c_2^\dagger) + \chi N_2 (c_2^\dagger)^2 & (3.6 \text{ c}) \\ \ln(1 - c_2^{\ddagger}) + \left(1 - \frac{N_1}{N_2}\right)(c_2^{\ddagger}) + \chi N_2 (c_2^{\ddagger})^2 & (3.6 \text{ d}) \end{cases}$$

The spinodal curve is obtained by taking the second derivative of the F-H free energy and setting it equal to zero.

$$\frac{\partial^2 f}{\partial c^2} = 1 - \left[1 - \frac{N_1}{N_2}\right]c - 2\chi N_1 c + 2\chi N_1 c^2 = 0 \quad (3.7)$$

Equation (3.7) is a quadratic equation that can be solved to find the compositions at the spinodal.

The F-H interaction parameter is needed in order to evaluate equations (3.6) to (3.7). It is commonly assumed to be a function of temperature and is expressed as a combination of both enthalpic and entropic contributions.

$$\chi = A + \frac{B}{T} \quad (3.8)$$

A and B are determined experimentally and represent the entropic and enthalpic contributions, respectively. The entropic contribution accounts for the segment-segment interactions between the polymers within the mixture. The enthalpic terms accounts for the change in energy upon mixing of the polymers as a result of the interactions between segments.

The critical point in the phase diagram can be calculated by setting the second and third derivatives of the F-H free energy expression to zero $\left(\frac{\partial^2 f}{\partial c^2} = \frac{\partial^3 f}{\partial c^3} = 0 \right)$.

There are several critical values associated with the critical point and they are given below. The critical concentration is given as:

$$c_c = \frac{1}{2} \left[\frac{1}{1 + \left(\frac{N_1}{N_2} \right)^{1/2}} \right] \quad (3.9)$$

The critical F-H interaction parameter is given by:

$$\chi_c = \frac{1}{2} \left[\frac{1}{N_1^{1/2}} + \frac{1}{N_2^{1/2}} \right]^2 \quad (3.10)$$

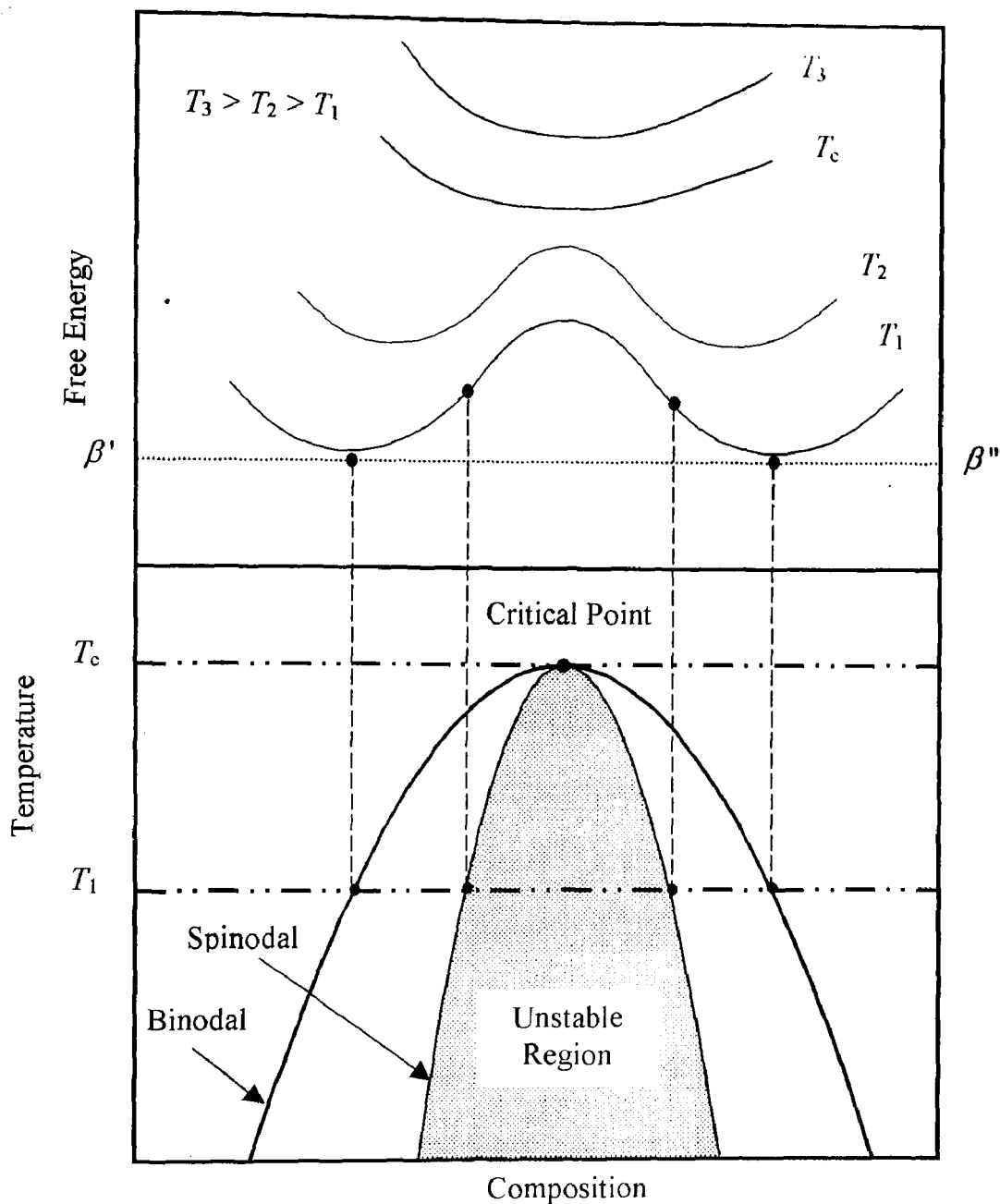


Figure 3.2: A plot of the relationship between the free energy versus composition and temperature versus composition for a binary polymer mixture. The binodal is the equilibrium curve and is constructed by the tangent line labelled $\beta' - \beta''$ where the change in the chemical potential of the coexisting phases is equal. The spinodal curve is constructed through the use of the inflection points in the free energy diagram. As T decreases, the miscibility decreases, representative of the UCST only.

Phase separation occurs for values of the F-H interaction parameter greater than the critical value $\chi > \chi_c$. This increases the value of the enthalpy of mixing such that the change in free energy is now positive and therefore the system is unstable.

For a symmetrical blend, the critical value χ_c reduces to $\frac{2}{N}$. The critical value of χ_c can also be used to determine the critical temperature. The critical temperature is given by:

$$T_c = \frac{B}{\chi_c - A} = \frac{B}{\left[\frac{1}{2} \left(\frac{1}{N_1^{1/2}} + \frac{1}{N_2^{1/2}} \right)^2 \right] - A} \quad (3.11)$$

3.2 Spinodal Decomposition

3.2.1 Early, Intermediate and Late Stages of Spinodal Decomposition

The mechanism of spinodal decomposition can be broken down into three stages, early, intermediate and late. Each stage has distinct characteristics describe by sinusoidal waves of the changes in concentration as a function of position in one dimension. This is shown in Figure 1.4. In the initial stage, the concentration fluctuations are small at t_i and as time increases to t_l , the amplitude of the concentration increases but the wavelength remains constant. The depletion and migration of one of the polymers towards an increasingly rapid growth of the concentration fluctuation is shown with arrows moving from low concentration to high concentration. This is characteristic of the SD process to have uphill

diffusion [Cahn, 1965; Chan, 1998]. The initial stage is usually the most difficult to visualize since it happens at a fast rate. In the intermediate stage, Figure 1.4 (ii), the concentration fluctuations are still increasing with time from t_1 to t_2 , showing an increase in the amplitude of the concentration fluctuations. However, there is an increase in the wavelength of the concentration fluctuation spatially. Finally, in Figure 1.4 (iii), the late stage of SD, the concentration fluctuations increase until they reach their respective equilibrium concentrations (constant amplitude), labelled c_H (upper concentration) and c_L (lower concentration). The wavelength increases with time due coarsening.

3.2.2 The Cahn-Hilliard Theory

Cahn [1965] was the first to describe the kinetics of phase separation by SD for metals and glasses and has since been extended to study phase separation in polymer solutions and blends [de Gennes, 1980]. The nonlinear C-H equation describes the spinodal process as a series of sinusoidal waves that govern the spatial and temporal evolution of the concentration fluctuations. It was developed from the continuity equation of mass where the diffusional flux is related to the driving force for phase separation (the chemical potential).

The continuity equation is given as:

$$\frac{\partial c}{\partial t} = -\nabla \cdot \mathbf{J} \quad (3.12)$$

where c is the composition, and \mathbf{J} is the interdiffusional flux of the components.

\mathbf{J} is related to the gradient in chemical potential by the following expression:

$$\mathbf{J} = -M\nabla(\mu_2 - \mu_1) \quad (3.13)$$

M is a proportionality factor called the mobility and is known to be composition dependent. In the development of the C-H equation, the mobility is assumed to be constant. The composition dependence of mobility will be examined in another section below. μ_1 and μ_2 are the chemical potentials of components 1 and 2. The concentration fluctuations in a polymer mixture are related to the change in the total free energy and can be broken down into two parts, a homogenous free energy term and a term to take into account the increase in free energy due to concentration fluctuations. The total free energy is then given as [Cahn, 1965]:

$$F = \int [f(c) + \kappa(\nabla c)^2] dV \quad (3.14)$$

where $f(c)$ is the free energy of the homogeneous polymer mixture and $\kappa(\nabla c)^2$ takes into account the increase in free energy. κ is a positive constant but is known to be a function of composition. It will be treated as a constant in deriving the C-H equation. The concentration dependence of κ will be discussed in another section. The homogeneous free energy term can be obtained from the F-H theory (equation 3.5). To insert equation (3.14) into the continuity equation the change in the chemical potential needs to be evaluated. The change in chemical potential is defined as:

$$\mu_2 - \mu_1 = \frac{\partial F}{\partial c} = \frac{\partial f}{\partial c} - 2\kappa\nabla^2 c \quad (3.15)$$

The net flux of the binary polymer mixture is related to total free energy in the following expression:

$$\mathbf{J} = -M\nabla(\mu_2 - \mu_1) = -M\nabla\left(\frac{\partial f(c)}{\partial c} - 2\kappa\nabla^2 c\right) \quad (3.16)$$

By inserting equation (3.16) into the continuity equation (3.12) one obtains the nonlinear C-H equation:

$$\frac{\partial c}{\partial t} = \nabla \cdot \left[M\nabla \left(\frac{\partial f(c)}{\partial c} - 2\kappa\nabla^2 c \right) \right] \quad (3.17)$$

For the early stage of SD, the C-H equation is linearized about an average concentration c_0 . The linearized C-H equation is valid for the early stage because the initial concentration fluctuations are small (weakly nonlinear), therefore, the linear C-H equation is:

$$\frac{\partial c}{\partial t} = M \left(\frac{\partial^2 f(c)}{\partial c^2} \Big|_{c_0} \nabla^2 c - 2\kappa\nabla^4 c \right) \quad (3.18)$$

$M \frac{\partial^2 f(c)}{\partial c^2}$ is known as a collective diffusion coefficient [Cahn, 1965]. The collective diffusion coefficient is negative (uphill) when the first term of equation (3.18) is less than zero and this is the case in the unstable SD region. The solution to equation (3.18) uses Fourier series. The general solution for equation (3.18) is given as:

$$c(\mathbf{r}, t) - c_0 = \sum_{\mathbf{k}} A(\mathbf{k}, t) e^{i\mathbf{k} \cdot \mathbf{r}} \quad (3.19 \text{ a})$$

$$A(\mathbf{k}, t) e^{i\mathbf{k} \cdot \mathbf{r}} = A(\mathbf{k}, 0) e^{R(\mathbf{k})t} \quad (3.19 \text{ b})$$

$$R(k) = -Mk^2 \left(\frac{\partial^2 f(c)}{\partial c^2} \Big|_{c_0} + 2\kappa k^2 \right) \quad (3.19 \text{ c})$$

where $k_i = \frac{2\pi}{\lambda_i}$ and λ_i is the wavelength for fluctuation i . $R(k)$ is known as the

amplification factor. For $R(k) > 0$, $\left| \frac{\partial^2 f(c)}{\partial c^2} \Big|_{c_0} \right| > |2\kappa k^2|$ meaning that concentration

fluctuations only occur under this condition from equations (3.19 a) through (3.19

c). This inequality is satisfied for the wave number range of $0 < k < k_c$. k_c is the

critical wave number and is defined as:

$$k_c = \left[\left(-\frac{1}{2\kappa} \right) \frac{\partial^2 f(c)}{\partial c^2} \Big|_{c_0} \right]^{1/2} \quad (3.20)$$

In equation (3.19 b) the exponent contains the amplification factor, therefore, the

concentration fluctuations that grows the fastest is:

$$k_m = \frac{1}{\sqrt{2}} k_c \quad (3.21)$$

3.2.3 Concentration Dependent Mobility and Mutual Diffusion

As mentioned above the mobility is known to be a function of composition. It can

be expressed as a function of the mutual diffusion coefficient, which measures the

rate at which the composition of the mixture is dispersed. According to equation

(3.13) the diffusional flux was given as:

$$\mathbf{J} = -M \frac{\partial^2 f(c)}{\partial c^2} \nabla c = -D \nabla c \quad (3.22)$$

In equation (3.14) the mutual diffusion coefficient is the product of the mobility

and the second derivative of the free energy with respect to composition.

Rearranging equation (3.22), the total mobility as a function of composition is:

$$M(c) = \frac{D(c)}{\frac{\partial^2 f(c)}{\partial c^2}} \quad (3.23)$$

There are two theories used to describe the mobility of polymers upon mixing, the slow mode theory and the fast mode theory [Kramer *et al.*, 1984]. The slow mode theory predicts that mutual diffusion of the binary polymer blend is limited by the slower component in the mixture [Kramer *et al.*, 1984]. On the other hand, the fast mode theory predicts that the diffusion rate is limited by the faster component. The expression for mutual diffusion in the slow and fast mode theories is made up of a thermodynamic term ψ and a kinetic term X [Jilge *et al.*, 1990; Akcasu *et al.*, 1995]:

$$D(c) = \psi X \quad (3.24)$$

The thermodynamic factor is associated with the static arrangement of the polymer segments and the kinetic factor is associated with the self-diffusion of the polymer segments [Akcasu *et al.*, 1995]. The composition dependent total mobility for a polymer system was introduced by de Gennes [de Gennes, 1980] and as a ratio of transport properties to that of the driving force for phase separation (chemical potential). The expression is:

$$\Lambda = \frac{\Lambda_1 \Lambda_2}{\Lambda_1 + \Lambda_2} \quad (3.25)$$

Where $\Lambda_i(c) = \frac{D_i N_i}{c}$ is the Onsager coefficient of the individual component describing the diffusion in a polymer system with D_i and N_i as the self-diffusion coefficient and degree of polymerization for the individual components. The

component Onsager coefficient is related to the individual mobility, $M_i(c)$, of the component by:

$$\Lambda_i(c) = k_B T M_i(c) \quad (3.26)$$

Equation (3.25) can be rewritten in terms of total mobility to give the slow mode theory [Kramer *et al.*, 1984]:

$$\frac{1}{M} = \frac{1}{M_1} + \frac{1}{M_2} \quad (3.27)$$

Where M is the total mobility and M_1 and M_2 are the individual mobilities of components 1 and 2 respectively. The individual mobilities of each component are expressed in terms of a self-diffusion coefficient:

$$M_1(c) = \frac{D_1(c)}{\frac{\partial^2 f_1(c)}{\partial c^2}} = \frac{D_1(c)}{\frac{k_B T}{v} \left(\frac{1}{N_1 c} \right)} \quad (3.28 \text{ a})$$

$$M_2(c) = \frac{D_2(c)}{\frac{\partial^2 f_2(c)}{\partial c^2}} = \frac{D_2(c)}{\frac{k_B T}{v} \left(\frac{1}{N_2 (1-c)} \right)} \quad (3.28 \text{ b})$$

In equation (3.27), if it was assumed that component 2 had a larger mobility ($D_1 \ll D_2$) than component 1, M_2 would be very large and therefore, the total mobility would be controlled by the mobility of component 1 (the slower moving component)

For the fast mode theory, the total mobility of the mixture is written as [Kramer *et al.*, 1984]:

$$M = M_1(1-c) + M_2 c \quad (3.29)$$

Again if it was assumed that the faster component in the mixture was component 2 then M_2 would be much larger in value than M_1 and therefore, the total mobility will be controlled by the faster moving component. Inserting equations (3.28 a) and (3.28 b) into the slow and fast mode theories and rearranging the expression, the total mobility becomes:

$$M(c) = \frac{[N_1 D_1 c][N_2 D_2 (1-c)]}{\frac{k_B T}{v} [N_1 D_1 c + N_2 D_2 (1-c)]} \quad (\text{slow mode}) \quad (3.30)$$

$$M(c) = \left[\frac{N_1 D_1 c (1-c) v + N_2 D_2 c v (1-c)}{k_B T} \right] \quad (\text{fast mode}) \quad (3.31)$$

Whether the slow mode theory or the fast mode theory best describes the interdiffusion of the polymer segments is still a topic of debate amongst researchers. There have been publications that are in favour of using the slow mode theory [de Gennes, 1980; Green *et al.*, 1985; Binder, 1983] while others believe the fast mode theory is a better prediction [Kramer *et al.*, 1984; Composto and Kramer, 1988]. The rest of the derivation for the total mobility will use the slow mode theory following the work of de Gennes [1980] in describing the dynamics of phase separation in polymer blends as it well describes phase separation by SD [Pincus, 1981; Binder, 1983].

3.2.4 Reptation Theory and the Self-Diffusion Coefficient

The self-diffusion coefficients measure the rate at which individual components of the mixture diffuse and are determined experimentally using labeling techniques to identify the components. There are two theories to describe the self-

diffusion coefficient, the Rouse theory [Rouse, 1953] and the reptation theory [de Gennes, 1971]. Both theories describe the self-diffusion coefficient in terms of physical properties of the polymer. The Rouse model describes a polymer chain as a spring and bead model where the chains are considered flexible repeating units moving freely in a medium. There exists a resistance force caused by the interaction between the medium and the coil of the spring called a frictional force and is incorporated into the self-diffusion coefficient of the polymer [Rouse, 1953]. The self-diffusion coefficient using the Rouse model is:

$$D_{\text{Rouse-self}} = \frac{k_B T'}{N\xi} \quad (3.32)$$

Where N is the degree of polymerization and ξ is monomer friction coefficient.

The reptation model describes the motion of a long polymer chain as a snake-like motion traveling through a constrained area [de Gennes, 1971]. The constraints are due to the entangled polymer coils in the mixture (unable to cross over another polymer chain) such that the only motion can be of a sliding or a creeping effect along the contours of the polymer length [de Gennes, 1971]. The self-diffusion coefficient described by the reptation model [Doi and Edwards, 1986] is:

$$D_{\text{reptation-self}} = \frac{k_B T' a^2}{3N^2 \xi b^2} \quad (3.33)$$

Where a is the step length of a primitive chain, and b is the bond length. The difference in both theories lies in the dependence of D_s on N , where in Rouse the dependence is N^{-1} and in reptation it is N^{-2} . Equation (3.33) can be further simplified by the following relationship between a and b [Doi and Edwards, 1986].

$$a^2 = \frac{4N_e b^2}{5N^2} \quad (3.34)$$

Where N_e in equation (3.34) is the degree of polymerization between entanglements. Inserting (3.34) into (3.33), the self-diffusion coefficient becomes:

$$D_{rep-self} = \frac{4k_B T}{15\xi} \left[\frac{N_e}{N^2} \right] \quad (3.35)$$

There exists a crossover between Rouse to reptation dynamics [de Gennes, 1971; Klein, 1978; Brochard *et al.*, 1983]. Experimentally, there is a critical polymer length, N_c , where the physical property (viscosity) of the polymer changes significantly as a function of N . The value of N_c is approximately 300-600 monomer units [Klein, 1978; Brochard *et al.*, 1983]. Brochard *et al.* [1983] used this critical value in their development of an expression for the mutual diffusion coefficient for $N < N_c$ (the non-entanglement regime) and for $N > N_c$ (the entanglement regime). The non-entanglement regime can be well described by the Rouse model and the entanglement regime the reptation model [Klein, 1978]. Therefore, the total mobility for the non-entanglement regime ($N < N_c$) using the slow mode theory is:

$$M(c) = \left[\frac{vc(1-c)}{\xi_2 c + \xi_1 (1-c)} \right] \quad (3.36 a)$$

If we assume that the monomeric friction coefficient is the same for both polymers $\xi = \xi_1 = \xi_2$ then equation (3.36 a) becomes:

$$M(c) = \left[\frac{vc(1-c)}{\xi} \right] \quad (3.36 b)$$

For the entanglement regime ($N > N_c$) again using the slow mode theory, the total mobility is:

$$M(c) = \left[\frac{4\nu N_{e1} N_{e2} c (1-c)}{15(\xi_2 N_{e1} N_2 c + \xi_1 N_{e2} N_1 (1-c))} \right] \quad (3.37 \text{ a})$$

If we assume that $\xi = \xi_1 = \xi_2$ and $N = N_{e1} = N_{e2}$ (degree of polymerization between entanglements of polymer 1 and 2 respectively) equation (3.37 a) becomes:

$$M(c) = \left[\frac{4\nu c (1-c)}{15\xi (N_2 c + N_1 (1-c))} \right] \quad (3.37 \text{ b})$$

In studying phase separation by SD for polymer blends the reptation theory has been used to describe the self-diffusion [de Gennes, 1980; Pincus, 1981].

3.2.5 Concentration-Dependent Gradient Energy

The energy gradient in the nonlinear C-H equation is the contribution to the free energy resulting from concentration fluctuations (non-homogeneous) and is related to the formation of interfaces between the two polymers. κ is assumed to be always greater than zero. de Gennes [1980] proposed that the gradient energy coefficient was made up of both enthalpic and entropic contributions and later discussed in a review paper on phase separation by Nauman and Qiwei [2001]:

$$\kappa = \kappa_H + \kappa_S \quad (3.38)$$

The entropic effect is due to the connectivity of monomer units and therefore is only applicable to polymer systems [Hashimoto *et al.*, 1983]. This additional term into the free energy takes into account the changes in energy upon the spatial

variations in the composition when phase separation occurs [de Gennes, 1980]. It is expressed as a function of composition in a variety of forms:

$$\kappa(c) = \underbrace{\left[\frac{\delta_1^2}{36c} + \frac{\delta_2^2}{36(1-c)} \right]}_{\text{Entropic contribution}} + \underbrace{\lambda\chi}_{\text{Enthalpic contribution}} = \left(\frac{a^2}{36c(1-c)} \right) \quad (3.39 \text{ a})$$

$$\kappa(c) = \frac{1}{18} \left[\frac{\delta_1^2}{c} + \frac{\delta_2^2}{(1-c)} \right] \quad (3.39 \text{ b})$$

$$\kappa(c) = \frac{1}{3} [R_{G1}^2 + R_{G2}^2] \chi + \frac{1}{3} N \left[\frac{R_{G1}^2}{c} + \frac{R_{G2}^2}{(1-c)} \right] \quad (3.39 \text{ c})$$

$$\kappa(c) = \frac{1}{24} \left[\frac{a^2}{(1-c)} \right] \quad (3.39 \text{ d})$$

In equation (3.39 a) [Castellano and Glozter, 1995] under conditions of extreme incompatibility $\lambda\chi$ (χ very small) is approximately zero and $\left(\frac{a^2}{36c(1-c)} \right)$ dominates. a is the statistical length and λ is the effective interaction distance between monomers and is assumed to be equal to the Kuhn length δ . The Kuhn length is related to the radius of gyration R_{Gi} by the following expression:

$$\delta_i^2 = \frac{R_{Gi}^2}{N_i} \quad (3.40)$$

Therefore, from equation (3.40) $a = \delta$. Note that the entropic term is a function of the relative size of the polymer. The different arrangements of the polymer segments in the mixture are limited by the size of the polymer chains and therefore, increase the free energy and opposing phase separation. Therefore, the

value coefficient of the energy gradient, κ , renders a resistance to the phase separation process due to the development of interfaces to try and restore the system to its lowest energy level. Equations (3.39 b) [Lee *et al.*, 1999], (3.39 c) [Ariyapadi and Nauman, 1991] and (3.39 d) [Jones and Richards, 1999] can also be simplified in the following manner. The difference in the coefficients comes from using the random phase approximation (RPA), the Debye function and placing restrictions on the range where the expression is valid (Equation (3.39 d)) [Jones and Richards, 1999]. Equation (3.39 a) is often used in computer simulations for studying phase separation by SD as it is assumed that the polymer mixture undergoing phase separation is highly incompatible [Zhang *et al.*, 1995; Chakrabarti *et al.*, 1990; Glotzer, 1995; Matsuoka and Yamamoto, 1995].

Chapter 4

Model Development and Method of Solution

This section presents the model development and the method of solution for the one-dimensional and two-dimensional study of phase separation by SD for a single quench and a double quench. The governing equations used in the model development will be presented to obtain a general spatial, time dependent, differential equation. From this, through algebraic simplification and rearrangement, the dimensionless equation describing the dynamics of phase separation by SD will be presented. The following conditions and assumptions have been applied in the model developed to describe phase separation of chemically identical polymer blends [de Gennes, 1980; Glotzer, 1995]:

- Phase separation occurs by the method of TIPS
- Polymer blend is of identical chemical structure ($N_1 = N_2 = N = 1000$)
- Entanglement properties are also identical ($\xi = \xi_1 = \xi_2$, $N = N_{e1} = N_{e2}$, $\lambda = \delta$)
- χ is a function of temperature only
- κ and M are a function of composition

The method used to solve the model is the Galerkin finite element (GFE) method with Hermitian basis functions. The following procedure was used for the GFE method in solving the dimensionless differential equation [Huebner *et al.*, 1995]:

1. Choose elements, basis functions and mesh
2. Write equation in Galerkin form
3. Lower the order of the differential equation
4. Apply conditions
5. Write out equation set
6. Assemble matrix and residual vector
7. Solve resulting system

Only the implemented GFE method, the nondimensionalized equations, the initial and boundary conditions will be discussed.

4.1 Governing Equations Used to Describe Phase Separation by Spinodal Decomposition for a Polymer Blend

The model development is based on the fundamental equations introduced in Chapter 3. The concentration fluctuations in a polymer mixture are related to the change in total free energy in the form [Cahn, 1965]:

$$F = \int \left[f(c) + \kappa (\nabla c)^2 \right] dV \quad (4.1)$$

The total free energy is broken down into two parts, a homogenous free energy of mixing term and a term to take into account the increase in free energy due to concentration fluctuations. The homogeneous free energy of mixing can be

described by the F-H free energy expression containing the enthalpic and entropic contributions of mixing in polymer blends described below [Flory, 1953]:

$$f(c) = \frac{k_B T}{v} \left(\frac{c}{N_1} \ln c + \frac{(1-c)}{N_2} \ln(1-c) + \chi c(1-c) \right) \quad (4.2)$$

The term that takes into account the increase in free energy due to composition fluctuations and formation of interfaces between the two polymers has a composition dependent term κ described by [de Gennes, 1980]:

$$\kappa(c) = \left(\frac{a^2}{36c(1-c)} \right) \quad (4.3)$$

The dynamics of the concentration fluctuations is represented by the continuity equation containing the driving force for phase separation (the chemical potential) within the diffusional flux:

$$\frac{\partial c}{\partial t} = -\nabla \cdot \mathbf{J} \quad (4.5)$$

The gradient in chemical potential is defined as the change in the total free energy with respect to composition and therefore, taking the derivative of equation (4.1) arrives at:

$$\mathbf{J} = -M \nabla (\mu_2 - \mu_1) = -M \nabla \left(\frac{\partial f(c)}{\partial c} - 2\kappa \nabla^2 c \right) \quad (4.6)$$

M is a proportionality factor called mobility and is known to be composition-dependent. To determine an expression for the total mobility, the slow mode theory is applied [de Gennes, 1980]:

$$\frac{1}{M} = \frac{1}{M_1} + \frac{1}{M_2} \quad (4.7)$$

This expression for total mobility relates the individual mobilities of the polymers and states that the slowest moving component is rate-controlling. To express the mobility in terms of diffusive transport properties, the reptation theory [Doi and Edwards, 1986] was applied to describe the self-diffusion of the polymers in the blend and the total mobility becomes:

$$M(c) = \left[\frac{4vc(1-c)}{15\xi(N_2c + N_1(1-c))} \right] \quad (4.8)$$

Inserting equations (4.1) to (4.8) into the continuity equation, the following expression is used to describe the dynamics of phase separation by SD:

$$\frac{\partial c}{\partial t} = \nabla \cdot \left[M \nabla \left(\frac{\partial f(c)}{\partial c} - 2\kappa \nabla^2 c \right) \right] \quad (4.10)$$

Substituting equations (4.5) to (4.6), rearranging and collecting like terms equation (4.10) is then transformed into the following fourth order partial differential equation for the further development of 1-D and 2-D models:

$$\begin{aligned}
 \frac{\partial c}{\partial t} = & \left[\frac{4N_2 k_B T}{15\xi} \right] \left\{ \left[\frac{1}{cN_2 + (1-c)N_1} \right] \left[(1-2c) - \frac{c(1-c)(N_2 - N_1)}{cN_2 + (1-c)N_1} \right] \left[\frac{1}{cN_1} + \frac{1}{(1-c)N_2} - 2\chi \right] (\nabla c)^2 \right. \\
 & + \left[\frac{1}{cN_2 + (1-c)N_1} \right] \left[\frac{c-1}{cN_1} + \frac{c}{(1-c)N_2} \right] (\nabla c)^2 \\
 & \left. + \left[\frac{1}{cN_2 + (1-c)N_1} \right] \left[\frac{1-c}{N_1} + \frac{c}{N_2} - 2c(1-c)\chi \right] (\nabla^2 c) \right\} \\
 & - \left[\frac{4N_2 c^2 k_B T}{15\xi} \right] \left\{ \left[\frac{1}{cN_2 + (1-c)N_1} \right] \left[(1-2c) - \frac{c(1-c)(N_2 - N_1)}{cN_2 + (1-c)N_1} \right] \left[\frac{2c-1}{2(c-c^2)^2} \right] (\nabla c)^2 (\nabla^2 c) \right. \\
 & + \left[\frac{1}{cN_2 + (1-c)N_1} \right] \left[\frac{(c-c^2) + (1-2c)}{(c-c^2)^2} \right] (\nabla c)^2 (\nabla^2 c) \\
 & + \left[\frac{1}{cN_2 + (1-c)N_1} \right] \left[\frac{(2c-1)}{2(c-c^2)} \right] (\nabla^2 c)^2 \\
 & + \left[\frac{1}{cN_2 + (1-c)N_1} \right] \left[\frac{(2c-1)}{(c-c^2)} \right] (\nabla c) (\nabla^2 c) \\
 & + \left[\frac{1}{cN_2 + (1-c)N_1} \right] \left[(1-2c) - \frac{c(1-c)(N_2 - N_1)}{cN_2 + (1-c)N_1} \right] \left[\frac{1}{2c(1-c)} \right] (\nabla c) (\nabla^2 c) \\
 & \left. + \left[\frac{1}{cN_2 + (1-c)N_1} \right] \left[\frac{1}{2} \right] (\nabla^4 c) \right\} \quad (4.11)
 \end{aligned}$$

4.2 The One -Dimensional Model

In the 1-D model, 256 elements were used. The governing equation, transformed from equation (4.11) into dimensionless form in one dimension is:

$$\begin{aligned}
 \frac{\partial^*}{\partial^*} = DT^* & \left\{ \begin{aligned} & \left[\frac{1}{c^*N_2 + (1-c^*)N_1} \left[(1-2c^*) - \frac{c^*(1-c^*)(N_2-N_1)}{c^*N_2 + (1-c^*)N_1} \left[\frac{1}{c^*N_1} + \frac{1}{(1-c^*)N_2} - 2\chi^* \right] \left(\frac{\partial^*}{\partial^*} \right)^2 \right] \right. \\ & + \left[\frac{1}{c^*N_2 + (1-c^*)N_1} \left[\frac{c^*-1}{c^*N_1} + \frac{c^*}{(1-c^*)N_2} \right] \left(\frac{\partial^*}{\partial^*} \right)^2 \right. \\ & \left. \left. + \left[\frac{1}{c^*N_2 + (1-c^*)N_1} \left[\frac{1-c^*}{N_1} + \frac{c^*}{N_2} - 2c^*(1-c^*)\chi^* \right] \left(\frac{\partial^2 c^*}{\partial^*{}^2} \right) \right] \right\} \\ \\ \\
 \frac{T^*}{9} & \left\{ \begin{aligned} & \left[\frac{1}{c^*N_2 + (1-c^*)N_1} \left[(1-2c^*) - \frac{c^*(1-c^*)(N_2-N_1)}{c^*N_2 + (1-c^*)N_1} \left[\frac{2c^*-1}{2(c^*-c^{*2})} \right] \left(\frac{\partial^*}{\partial^*} \right)^2 \left(\frac{\partial^2 c^*}{\partial^*{}^2} \right) \right] \right. \\ & + \left[\frac{1}{c^*N_2 + (1-c^*)N_1} \left[\frac{(c^*-c^{*2}) + (1-2c^*)}{(c^*-c^{*2})^2} \right] \left(\frac{\partial^*}{\partial^*} \right)^2 \left(\frac{\partial^2 c^*}{\partial^*{}^2} \right) \right. \\ & + \left[\frac{1}{c^*N_2 + (1-c^*)N_1} \left[\frac{(2c^*-1)}{2(c^*-c^{*2})} \right] \left(\frac{\partial^2 c^*}{\partial^*{}^2} \right)^2 \right. \\ & + \left[\frac{1}{c^*N_2 + (1-c^*)N_1} \left[\frac{(2c^*-1)}{(c^*-c^{*2})} \right] \left(\frac{\partial^*}{\partial^*} \right) \left(\frac{\partial^3 c^*}{\partial^*{}^3} \right) \right. \\ & + \left[\frac{1}{c^*N_2 + (1-c^*)N_1} \left[(1-2c^*) - \frac{c^*(1-c^*)(N_2-N_1)}{c^*N_2 + (1-c^*)N_1} \left[\frac{1}{2c^*(1-c^*)} \right] \left(\frac{\partial^*}{\partial^*} \right) \left(\frac{\partial^3 c^*}{\partial^*{}^3} \right) \right] \right. \\ & \left. \left. + \left[\frac{1}{c^*N_2 + (1-c^*)N_1} \left[\frac{1}{2} \right] \left(\frac{\partial^4 c^*}{\partial^*{}^4} \right) \right] \right\} \quad (4.12)
 \end{aligned}
 \right.
 \end{aligned}$$

The dimensionless terms in equation (4.12) are dimensionless time, temperature, space and diffusion coefficient. The dimensionless terms are expressed in the order stated above as:

$$t^* = \left[\frac{4N_e \left(\frac{k_B T_c}{\nu} \right) a^2 \nu}{15\xi L^4} \right] t \quad (4.13 a)$$

$$T^* = \frac{T}{T_c} \quad (4.13 b)$$

$$c^* = c \quad (4.13 c)$$

$$\nabla^* = \nabla L \quad (4.13 d)$$

$$D^* = \left[\frac{k_B T_c L^2}{\nu \left(\frac{k_B T_c}{\nu} \right) a^2} \right] \quad (4.13 e)$$

4.3 Two-Dimensional Model

In the 2-D model, 20 by 20 elements mesh was used. The governing equation, transformed from equation (4.14) into dimensionless form in the two-dimension model is:

$$\begin{aligned}
 \frac{\partial \bar{c}}{\partial \bar{t}} = D \bar{T} & \left\{ \left[\frac{1-2c^*}{c^* N_2 + (1-c^*) N_1} \frac{c^*(1-c^*)(N_2 - N_1)}{(c^* N_2 + (1-c^*) N_1)^2} \left[\frac{1}{c^* N_1} + \frac{1}{(1-c^*) N_2} - 2\chi^* \right] \left[\frac{\partial \bar{c}}{\partial \bar{x}} + \frac{\partial \bar{c}}{\partial \bar{y}} \right] \left[\frac{\partial \bar{c}}{\partial \bar{x}} + \frac{\partial \bar{c}}{\partial \bar{y}} \right] \right. \right. \\
 & + \left. \left[\frac{1}{c^* N_2 + (1-c^*) N_1} \left[\frac{c^*-1}{c^* N_1} + \frac{c^*}{(1-c^*) N_2} \right] \left[\frac{\partial \bar{c}}{\partial \bar{x}} + \frac{\partial \bar{c}}{\partial \bar{y}} \right] \left[\frac{\partial \bar{c}}{\partial \bar{x}} + \frac{\partial \bar{c}}{\partial \bar{y}} \right] \right. \right. \\
 & \left. \left. + \left[\frac{1}{c^* N_2 + (1-c^*) N_1} \left[\frac{1-c^*}{N_1} + \frac{c^*}{N_2} - 2c^*(1-c^*) \chi^* \right] \left[\frac{\partial^2 \bar{c}}{\partial \bar{x}^2} + \frac{\partial^2 \bar{c}}{\partial \bar{y}^2} \right] \right] \right\} \\
 \bar{T} & \left\{ \left[\frac{1-2c^*}{c^* N_2 + (1-c^*) N_1} \frac{c^*(1-c^*)(N_2 - N_1)}{(c^* N_2 + (1-c^*) N_1)^2} \left[\frac{1}{2} \left(\frac{-1}{c^{*2}(1-c^*)} + \frac{1}{c^*(1-c^*)^2} \right) \right] \left[\frac{\partial \bar{c}}{\partial \bar{x}} + \frac{\partial \bar{c}}{\partial \bar{y}} \right] \left[\frac{\partial \bar{c}}{\partial \bar{x}} + \frac{\partial \bar{c}}{\partial \bar{y}} \right] \left[\frac{\partial^2 \bar{c}}{\partial \bar{x}^2} + \frac{\partial^2 \bar{c}}{\partial \bar{y}^2} \right] \right. \right. \\
 & + \left[\frac{1}{c^* N_2 + (1-c^*) N_1} \left[\frac{1}{c^{*2}} - \frac{1}{c^*(1-c^*)} + \frac{1}{(1-c^*)^2} \right] \left[\frac{\partial \bar{c}}{\partial \bar{x}} + \frac{\partial \bar{c}}{\partial \bar{y}} \right] \left[\frac{\partial \bar{c}}{\partial \bar{x}} + \frac{\partial \bar{c}}{\partial \bar{y}} \right] \left[\frac{\partial^2 \bar{c}}{\partial \bar{x}^2} + \frac{\partial^2 \bar{c}}{\partial \bar{y}^2} \right] \right. \\
 & + \left[\frac{1}{c^* N_2 + (1-c^*) N_1} \left[\frac{1}{2} \left(\frac{-1}{c^*} + \frac{1}{(1-c^*)} \right) \right] \left[\frac{\partial^2 \bar{c}}{\partial \bar{x}^2} + \frac{\partial^2 \bar{c}}{\partial \bar{y}^2} \right] \left[\frac{\partial^2 \bar{c}}{\partial \bar{x}^2} + \frac{\partial^2 \bar{c}}{\partial \bar{y}^2} \right] \right. \\
 & + \left[\frac{1}{c^* N_2 + (1-c^*) N_1} \left[\frac{-1}{c^*} + \frac{1}{(1-c^*)} \right] \left[\frac{\partial^2 \bar{c}}{\partial \bar{x}^2} + \frac{\partial^2 \bar{c}}{\partial \bar{y}^2} \right] \left[\frac{\partial \bar{c}}{\partial \bar{x}} + \frac{\partial \bar{c}}{\partial \bar{y}} \right] \right. \\
 & + \left[\frac{1}{c^*(1-c^*)} \left[\frac{1-2c^*}{c^* N_2 + (1-c^*) N_1} \frac{c^*(1-c^*)(N_2 - N_1)}{(c^* N_2 + (1-c^*) N_1)^2} \left[\frac{\partial^2 \bar{c}}{\partial \bar{x}^2} + \frac{\partial^2 \bar{c}}{\partial \bar{y}^2} \right] \left[\frac{\partial \bar{c}}{\partial \bar{x}} + \frac{\partial \bar{c}}{\partial \bar{y}} \right] \right. \right. \\
 & \left. \left. + \left[\frac{1}{c^* N_2 + (1-c^*) N_1} \left[\frac{\partial^2 \bar{c}}{\partial \bar{x}^2} + \frac{\partial^2 \bar{c}}{\partial \bar{y}^2} \right] \right] \right\}
 \end{aligned}
 \tag{4.14}$$

The dimensionless terms in the 2-D model are the same as those presented in the 1-D model.

4.4 Initial and Boundary Conditions

To solve the one-dimensional and two-dimensional model, initial and boundary conditions are applied. The development of the program for the initial condition is detailed in a paper by Chan and Rey who looked at phase separation in polymer solutions [Chan and Rey, 1995a]. The homophase thermal fluctuations are used

as an initial condition because the concentration is not uniform even in the homogeneous one phase region. There exists infinitesimal deviations from the average concentration called homophase thermal fluctuations so that the initial condition is an average concentration plus a very small value, δ , where the Monte Carlo scheme is employed to determine the value of δ . Mathematically, the initial condition expressed in dimensionless form is [Chan and Rey, 1995a]:

$$c^*(t^* = 0) = c_o^* + \delta \quad (4.15)$$

The boundary conditions in this model are the zero mass flux and the natural boundary conditions. Zero mass flux is applied to the system where no mass is exchanged with its surroundings [Novick-Cohen and Segel, 1984; Elliot and Songmu, 1986]:

$$\mathbf{J} = -M(c) \nabla(\mu_2 - \mu_1) = 0 \quad (4.16)$$

The natural boundary condition [Novick-Cohen and Segel, 1984] states that there is no spatial variation of concentration at the boundaries:

$$(\nabla c) \cdot \mathbf{n} = 0 \quad (4.17)$$

The zero mass flux boundary condition in dimensionless form for the 1-D and 2-D study is [Chan and Rey, 1995a]:

In the one one-dimensional study

$$\frac{\partial^3 c^*}{\partial x^{*3}} = 0 \quad \text{at} \quad t^* > 0, \quad \text{and} \quad x^* = 0 \quad \text{and} \quad x^* = 1 \quad (4.18)$$

In the two-dimensional study

$$\frac{\partial^3 c^*}{\partial x^{*3}} + \frac{\partial^3 c^*}{\partial x^* \partial y^{*2}} = 0 \quad \text{at} \quad t^* > 0, \quad \text{and} \quad x^* = 0 \quad \text{and} \quad x^* = 1 \quad (4.19 a)$$

$$\frac{\partial^3 c^*}{\partial y^{*3}} + \frac{\partial^3 c^*}{\partial x^{*2} \partial y^*} = 0 \quad \text{at } t^* > 0, \quad \text{and } y^* = 0 \quad \text{and } y^* = 1 \quad (4.19 \text{ b})$$

Natural boundary conditions in dimensionless form for the 1-D model contain equation (4.20) and the 2-D model contain equation (4.20) and (4.21) [Chan and Rey, 1995a]:

$$\frac{\partial c^*}{\partial x^*} = 0 \quad \text{at } t^* > 0, \quad \text{and } x^* = 0 \quad \text{and } x^* = 1 \quad (4.20)$$

$$\frac{\partial c^*}{\partial y^*} = 0 \quad \text{at } t^* > 0, \quad \text{and } y^* = 0 \quad \text{and } y^* = 1 \quad (4.21)$$

4.5 Method of Solution: The Galerkin Finite Element

Method

The Galerkin finite element (GFE) method is a method of weighted residuals. It is a useful technique in solving equations whether they are partial differential equations, ordinary differential equations or integral equations by approximating it at discrete points [Huebner *et al.*, 1995]. This technique is advantageous because it can be used to solve systems of any geometry and complexity by dividing the system into subunits called elements, and allowing computational approximations to the solution at nodal points that link the elements. The divided solution region is called the element mesh and in the case of a one-dimensional study the mesh is a line and in a two-dimensional study the mesh is a plane. The following development of the general procedure to solving partial differential equations in two-dimensions is based on the developments given in finite element

texts [Lapidus and Pinder, 1982; Chung, 1978]. To obtain the solution for the one-dimensional case, the two-dimensional case can be simplified to x space and will not be presented.

Consider the following equation in two dimensions with the following boundaries:

$$L(u) = f(x, y, t) = 0 \quad a \leq x \leq b \quad a \leq y \leq b \quad (4.22)$$

In the Galerkin method, the solution to the equation above assumes that u can be represented by an approximation of the form:

$$u_a(x, y, t) = \sum_{j=1}^N u_j(t) \phi^j(x, y) \quad (4.23)$$

The approximate solution, $u_a(x, y, t)$, is then a finite series approximation where $\phi^j(x, y)$ are the basis functions (weighted residuals) and $u_j(t)$ are the unknown coefficients. Placing equation (4.23) into equation (4.22) yields:

$$R = L(u_a) \neq 0 \quad (4.24)$$

The residual, R , is nonzero. If the approximate solution u_a was zero (having a zero residual) then it would be the true analytic solution to $L(u)$. The objective then is to find a set of $u_j(t)$ such that the approximate solution is forced to zero and this will provide the best fit to the exact solution:

$$L(u_a) = 0 \quad (4.25)$$

To do this, the residual is multiplied by a weighting function (equal to the basis functions in the GFE method), set to zero and integrated over the element:

$$F_i = \iint R w_i(x, y) dx dy = \iint L(u_a) \phi^i(x, y) dx dy = 0$$

for $i = 1, 2, \dots, N$ (4.26)

where F_i is the residual vector, w_i is the weighting function and N is the number of nodal points in the mesh. From equation (4.26), a system of N non-linear equations is obtained and the 3-point Gauss quadrature method is used to evaluate the integrals. The system of equations can be arranged in the form:

$$[J]\{u\} = [F] \tag{4.27}$$

where $[J]$ is the Jacobian matrix defined by $J_{i,j} = \frac{\partial F_i}{\partial u_j}$, u_j are the unknown coefficients of interest and $[F]$ is the residual vector. The Newton-Raphson iteration scheme is used to solve the set of equations obtained from equation (4.27) simultaneously and the convergence criterion is such that the difference of the length of the solution vector between two successive vectors is computed to be less than 10^{-6} .

So far, the development of the system of equations used a general expression for the basis function $\phi^j(x, y)$. The choice of basis functions to be inserted into equation (4.26) is Hermitian bicubic basis functions. These basis functions interpolate values of the function and the derivative at the nodes and are useful for solving the fourth order partial differential equation because the lowering of the order of the partial differential equation can be minimized [Lapidus and Pinder, 1982]. For detailed development of the Hermitian basis functions other sources can be referred to [Chung, 1978]. The Hermitian basis functions take the form:

$$\begin{aligned}
 \phi_1 &= a_1 + b_1\xi + c_1\xi^2 + d_1\xi^3 && \text{function} \\
 \phi_2 &= a_2 + b_2\xi + c_2\xi^2 + d_2\xi^3 && \text{slope} \\
 \phi_3 &= a_3 + b_3\xi + c_3\xi^2 + d_3\xi^3 && \text{function} \\
 \phi_4 &= a_4 + b_4\xi + c_4\xi^2 + d_4\xi^3 && \text{slope}
 \end{aligned}
 \tag{4.28}$$

In a one-dimensional study each element has 2 double nodes (one for the function and one for the slope) and four basis functions. In the two-dimensional case, each element has nodes 4 double nodes and 16 basis functions. The two-dimensional case is a product of the one-dimensional basis functions. See Appendix A for the list of Hermitian basis functions.

To lower the order of the partial differential (in this case the model equation being fourth order) the divergence theorem can be used:

$$\iint_{\Omega} \alpha \nabla \cdot \nabla \mathbf{v} dA = \int_{\Gamma} \alpha \mathbf{n} \cdot \mathbf{v} d\Gamma - \iint_{\Omega} \nabla \alpha \cdot \mathbf{v} d\Omega
 \tag{4.29}$$

where α is any scalar, \mathbf{v} is any vector, Γ is the boundary of domain Ω and \mathbf{n} is the unit normal vector. The terms in residual vector containing $\iint \nabla^3 c \phi^i dx dy$ and

$\iint \nabla^4 c \phi^i dx dy$ can be broken down to:

$$\iint \nabla^4 c \phi^i dx dy = \int_{\Gamma} \phi^i \mathbf{n} \cdot \nabla^3 c d\Gamma - \int_{\Gamma} \phi^i \mathbf{n} \cdot (\nabla^2 c \nabla \phi^i) d\Gamma + \iint_{\Omega} \nabla^2 c \nabla^2 \phi^i d\Omega
 \tag{4.30}$$

$$\iint \nabla^3 c \phi^i dx dy = \int_{\Gamma} \phi^i \mathbf{n} \cdot \nabla^2 c d\Gamma - \iint_{\Omega} \nabla \phi^i \cdot \nabla^2 c d\Omega
 \tag{4.31}$$

4.6 Program Summary

The program developed for solving the 1-D and 2-D models was based Chan's program [Chan, 1997] for studying phase separation by SD in polymer solutions where the mobility and interfacial parameters were kept constant. In the 1-D study, 256 elements were used to form the mesh size and in the 2-D model a 20 by 20 element mesh was used. After employing the GFE method and setting up the set of equations in matrix form, the set of equations were solved using the Newton-Raphson iteration scheme. For time integration, the finite difference method and the Euler predictor corrector method was used [Chan, 1997]. An adaptive step size controller was also used to save on computing time [Chan, 1997]. When there is little variation in the function a large time step it taken and when there is more variation small time steps are used.

Chapter 5

Results and Discussion: 1-D TIPS Single Quench

This section presents the numerical results from the one-dimensional TIPS study with a single quench. The focus is in the formation of phase-separated structures and therefore studying the early and beginning of the intermediate stages is sufficient. The model parameters are listed in Table 5.1. The model is based on a symmetrical blend with degree of polymerization of $N_1 = N_2 = 1000$. There are two initial average compositions that will be investigated, a critical quench ($c_o^* = 0.5$) and an off-critical quench ($c_o^* = 0.6$). The study also uses three different values for the dimensionless diffusion coefficient. The order of magnitude for the dimensionless diffusion coefficient directly reflects the parameters taken from experimental studies on the properties of polymers [Daould *et al.*, 1975]. Key features are examined for a critical and an off-critical quench case to ensure that the one-dimensional model exhibits the same known trends for the early to the beginning of the intermediate stage typical of phase separation by SD:

- (i) The evolution of the concentration fluctuations
- (ii) The evolution of the dimensionless structure factor
- (iii) The effect of a shallow and deeper quench

Additional analysis will be to investigate the effect of increasing the dimensionless diffusion coefficient D^* , the change in the chemical potential and the change in the second derivative of free energy with respect to composition upon phase separation by SD.

Table 5.1: Summary of the dimensionless parameters used in the 1-D TIPS study for a single quench.

Parameter	Value
c_o^*	0.5, 0.6
N_1, N_2	1000
D^*	200 000, 500 000, 800 000
T_1^*	0.25 (quench temperature)
T_2^*	0.2 (deeper quench)

The results presented in this chapter for the critical and off-critical quench case are for a value of the dimensionless diffusion coefficient $D^* = 200\ 000$ unless otherwise specified. The results for $D^* = 500\ 000$ and $800\ 000$ are shown in Appendix B

Note in a 1-D study, it is not possible to determine the type of structure that is obtained (interconnected or droplet type). The 1-D study can only well describe the characteristics pertaining to the kinetics of SD. Generally, a 1-D model can be used to fully describe the mechanism of phase separation by SD and a 2-D model is used to determine the type of microstructure obtained.

5.1 Symmetrical Phase Diagram

The temperature versus composition phase diagram for a symmetrical polymer blend used in this study is shown in Figure 5.1. The solid curve represents the binodal (equilibrium curve) and the dashed curve is the spinodal curve. The two filled circles represent the two test conditions for a critical and an off-critical quench with composition of $c_o^* = 0.5$ and $c_o^* = 0.6$, respectively. The composition shown in the phase diagram represents polymer 1. The degree of polymerization for the symmetric blend is $N_1 = N_2 = 1000$ with a critical temperature of $T_c^* = 0.333$, a critical composition of $c_c^* = 0.5$, and a critical value for the F-H interaction parameter of $\chi_c^* = 0.002$. The expression for the F-H interaction parameter used in this study originally came from a mixture of deuterated polybutadiene/protonated polybutadiene [Jinnai *et al.*, 1993]. It was then nondimensionalized to the following form:

$$\chi^* = -5.34 \times 10^{-4} + \frac{0.000844}{T^*} \quad (5.1)$$

For the single quench a dimensionless temperature of $T_1^* = 0.25$ was chosen and will be used as the reference point for the double quenching to be discussed in the next chapter.

5.2 Spatial Concentration Profiles

Figure 5.2 shows the evolution of the dimensionless spatial concentration profiles for a single quench at the critical composition of $c_c = 0.5$, a dimensionless

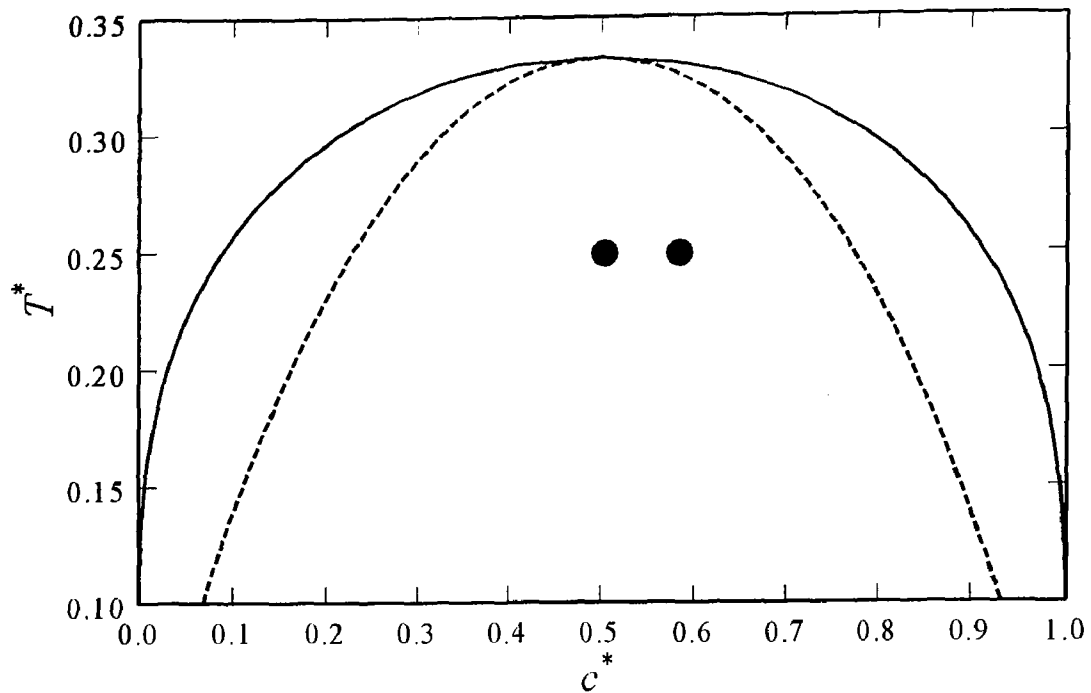


Figure 5.1: A model symmetrical phase diagram for a polymer blend of degree of polymerization $N_1 = N_2 = 1000$. The dimensionless critical composition and temperature for this blend are $c_c^* = 0.50$ and $T_c^* = 0.333$ respectively. The binodal (equilibrium curve) is represented by the solid curve and spinodal with the dashed curve. The two circles represent the locations of investigation (a critical $c_o^* = 0.5$ and off-critical $c_o^* = 0.6$ quench) at a dimensionless temperature of $T_1^* = 0.25$. The upper and lower equilibrium values at $T_1^* = 0.25$ are 0.912 and 0.0877 respectively.

diffusion coefficient of $D^* = 200\,000$ and a dimensionless temperature of $T_1^* = 0.25$. Recall that in Chapter 3, the evolution of concentration profiles were explained in terms of waves. In the early stage, the initial concentration fluctuations appear due to the growth of the most dominant wavelength and are weakly nonlinear. The wavelength remains constant while the amplitude changes. In the beginning of the intermediate stage, the concentration fluctuations continue to increase and into the intermediate stage the wavelength starts to change. All three figures for the critical quench are consistent with the known evolution of the

concentration fluctuations that are typical of phase separation by SD for the early to beginning of the intermediate stages [Hashimoto *et al.*, 1986a]. The dimensionless spatial concentration fluctuations increase with increasing dimensionless time as they approach the equilibrium values while maintaining constant position. Numerically, the results shown here are also consistent with other 1-D studies conducted for polymer blends [Ohnaga and Inoue, 1989; Takenaka *et al.*, 1995]. However, the model and the method of solution differ from the numerical work in this thesis. Figures 5.3 shows the evolution of the dimensionless spatial concentration profiles for a single off-critical quench with an initial average composition of $c_o = 0.6$ at a dimensionless quench temperature of $T_l^* = 0.25$ and a dimensionless diffusion coefficient of $D^* = 200\ 000$. These concentration profiles are also consistent with the trends typical of phase separation by SD for the early to beginning of the intermediate stages [Hashimoto *et al.*, 1986a]. A comparison between the dimensionless times for the critical and off-critical quench shows that for the critical quench ($t^* = 3.527$ to 0.220 for $D^* = 200\ 000$ to $800\ 000$), phase separation occurs at earlier times than the off-critical case ($t^* = 4.898$ to 0.22878 for $D^* = 200\ 000$ to $800\ 000$). This can be explained by referring back to the phase diagram in Figure 5.1. The two filled circles indicate the locations of the quench at $T_l^* = 0.25$ for the critical and off-critical quench case. It is known that the driving force for phase separation is directly related to the distance of the temperature within the confines of the spinodal line [Tao *et al.*, 1995]. It can be observed that the distance from the spinodal curve at $T_l^* = 0.25$ for the critical case is much farther inward than for the off-critical

quench case. Recall from Chapter 3 that the location of the spinodal points are at the inflection points ($\frac{\partial^2 F}{\partial c^2} = 0$) in the change in free energy curve. At these points, there is no influence on the composition fluctuations to overcome energy barriers or to drive phase separation by SD therefore, there will be a smaller driving force for phase separation for the off-critical quench case since it is located closer to the spinodal curve. This explains the reason for the time differences in the critical and off-critical quench and was also observed in the a numerical study for polymer solutions [Chan, 1997].

5.3 The Evolution of the Dimensionless Structure Factor

The structure factor is an important parameter that is often used to characterize the shape of phase-separated domains by SD and relates numerical and experimental studies [Glotzer, 1995]. The numerical data of the computed composition fluctuations are used to calculate the structure factor by taking the fast Fourier transform [Glotzer, 1995]. The relationship between experimental (the scattering intensity from light scattering experiments) and numerical work (the structure factor) is of the following form [Strobl, 1985; Copetti and Elliot, 1990; Skripov and Skripov, 1979]:

$$I(q, t) \propto S(k, t) = \left\langle |A(k, t)|^2 \right\rangle \quad \text{for } k = q \quad (5.2)$$

I is the scattering intensity, q , is the scattering wave vector, S is the structure factor, k is the wave number in Fourier space and $A(k, t)$ is the fast Fourier

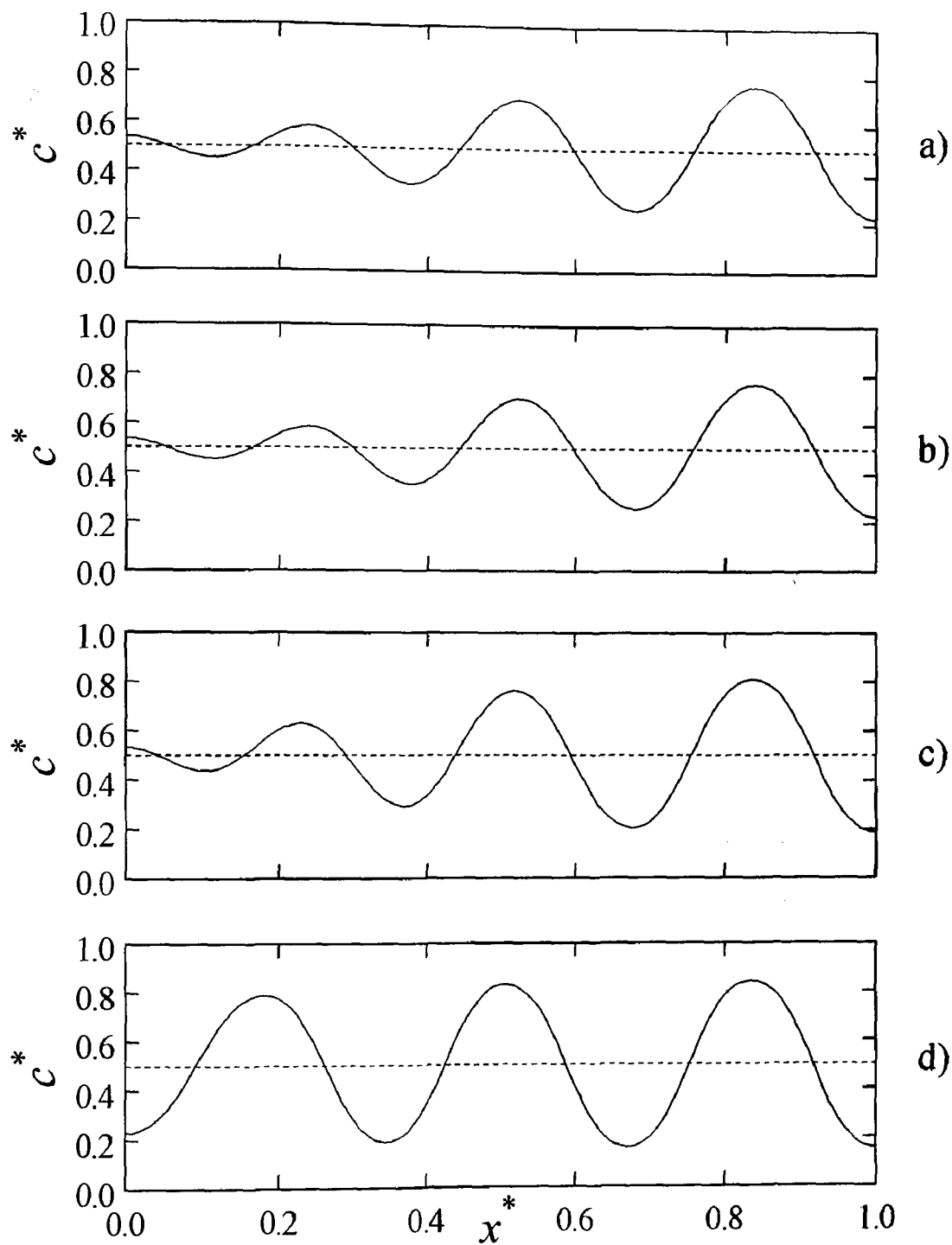


Figure 5.2: The evolution of the dimensionless spatial concentration profile for a single quench into the unstable region of the phase diagram at the following dimensionless times: (a) $t^* = 3.527$, (b) $t^* = 3.843$, (c) $t^* = 4.014$, and (d) $t^* = 4.57$. The dashed line through the center of the graph represents the initial average concentration $c_0^* = 0.5$. The dimensionless diffusion coefficient for this case is $D^* = 200\,000$.

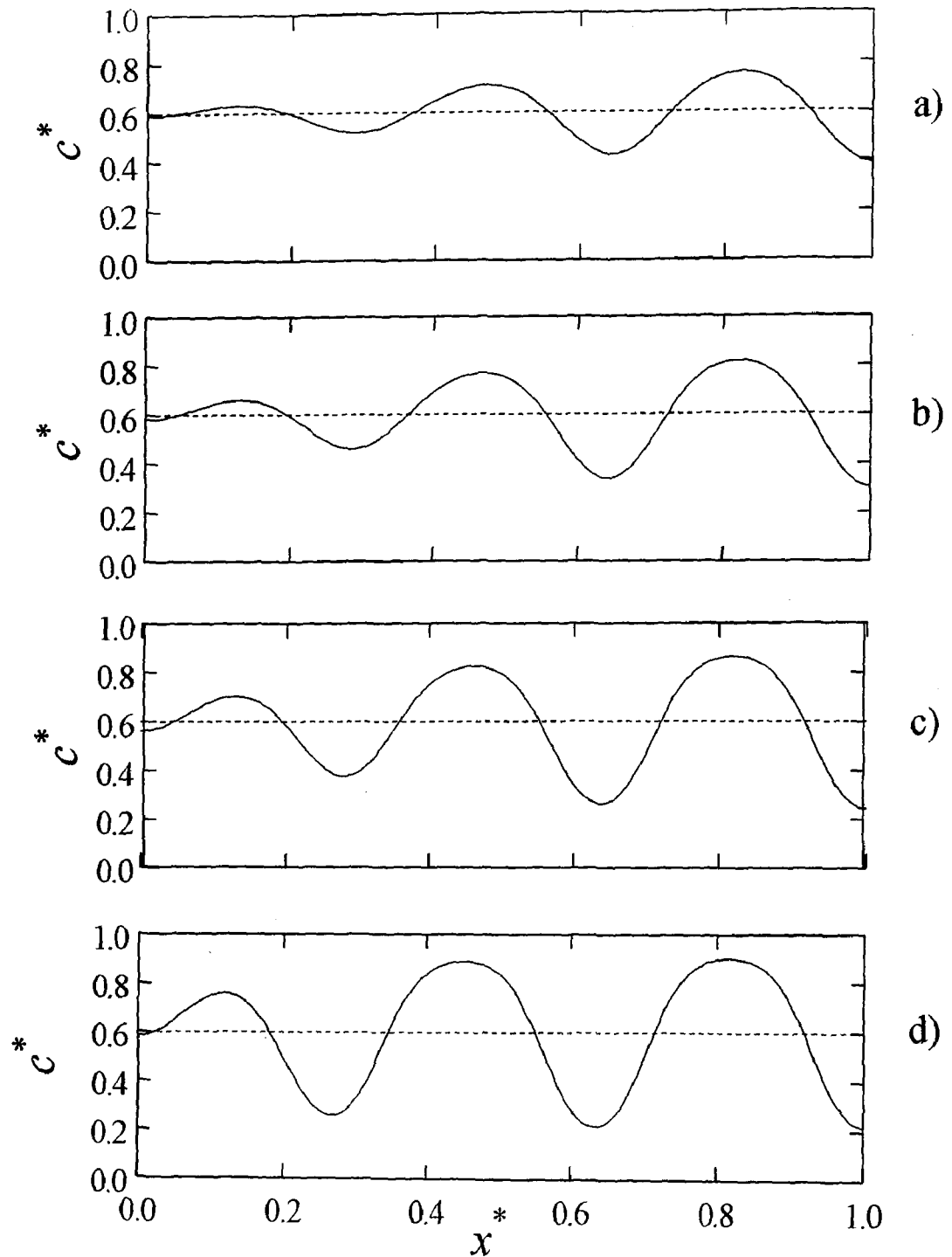


Figure 5.3: The evolution of the dimensionless spatial concentration profile for a single quench into the unstable region of the phase diagram at the following dimensionless times: (a) $t^* = 4.898$, (b) $t^* = 5.092$, (c) $t^* = 5.292$, and (d) $t^* = 5.703$. The dashed line through the center of the graph represents the initial average concentration $c_0^* = 0.6$. The dimensionless diffusion coefficient for this case is $D^* = 200\,000$.

transform of the composition fluctuations $c(r,t)$. The experimental light scattering data is then directly proportional to the structure factor and a detailed discussion of the development of this expression can be found elsewhere [Skripov and Skripov, 1979]. The following summarizes characteristics of the early to the intermediate stages of phase separation by SD from light scattering data [Hashimoto, 1993]:

- i. Early Stages: The scattering intensity grows exponentially and the scattering vector, q , is independent of time. The growth of the composition fluctuations is weakly nonlinear and the plotting the natural log of the evolution of the scattering intensity $I(q,t) = I(q,t=0)\exp(2R(q)t)$ should produce a straight line for the early stages of SD.
- ii. Intermediate Stages: The scattering intensity continues to increase but at a slower rate than in the early stages of phase separation by SD and q decreases and λ (wavelength) increases. The relation between q and λ is

$$q = \frac{2\pi}{\lambda}.$$

A typical plot of the scattering intensity in the early to the beginning of the intermediate stages for phase separation by SD is shown in Figure 5.4. Recall $A(k,t)$ is the Fourier transform of the composition fluctuations, $c(r,t)$. Following Equation (5.2), at the early and intermediate stages of phase separation by SD, the concentration fluctuations in Fourier space, $A(k,t)$, should then also describe the same characteristics as discussed above regarding the development of

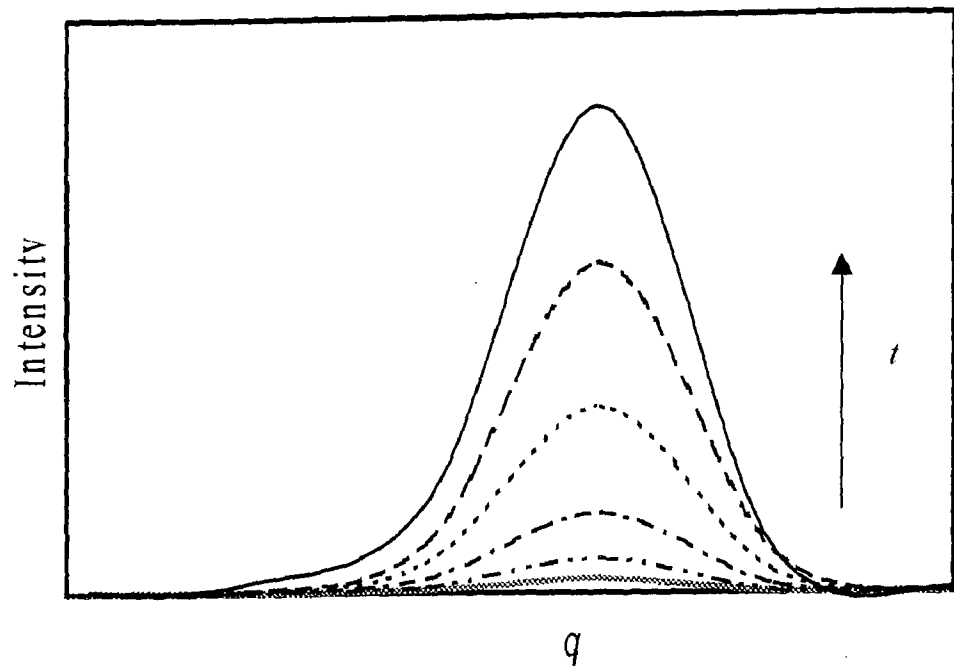


Figure 5.4: Typical light scattering profile showing the evolution of phase separation by SD in the early to the beginning of the intermediate stages. Each profile represents the intensity at a certain time t . The increase in time is indicated by the arrow in the up direction. The scattering intensity is increasing with time while the position is constant, characteristic of the early stages of SD.

the scattering data (the visual representation is shown in Figure 5.4). To ensure that the numerical work in this study is in agreement with the known evolution of scattering profiles as related to the structure factor, the dimensionless structure factor was calculated at different dimensionless times. MATLAB was used to calculate the dimensionless structure factor where a small algorithm was written to determine the fast Fourier transform of the sample data at a specific time and the square of the magnitude of this result to determine the value of the structure factor. Figures 5.5 and 5.6 show the evolution of the dimensionless structure factor as a function of dimensionless wave number, k^* , and dimensionless time for the critical quench case and the off-critical quench case with $D^* = 200\,000$. It can be observed that the value of the dimensionless structure factor increases

exponentially with time in the early stages of phase separation by SD and begins to slow down as it approaches the beginning of the intermediate stages where nonlinear effects come into play. Also, during the early to the beginning of the intermediate stages, the wave number is constant and this is typical of what should be observed [Hashimoto, 1993]. Therefore, the evolution of the dimensionless structure factor (exponential growth and fixed wave number) for the critical quench and the off-critical quench case show the same trends that have been reported both in experiment [Okada and Han, 1986; Wiltzius *et al.*, 1988; Hashimoto *et al.*, 1986a] and numerical work [Chan, 1998; Chakrabarti *et al.*, 1990; Zhang *et al.*, 1995]. Recall that the wave number is related to the wavelength by $k_i = \frac{2\pi}{\lambda_i}$. From this, the maximum value of the wavelength (the dominant wavelength of the concentration fluctuations) or the characteristic length for the early stages of phase separation by SD can be determined. The characteristic length is a common definition used to express the domain size of the phase-separated regions by SD, λ [Hashimoto, 1993]. It is defined as the inverse of the wave number and in dimensionless form the expression is:

$$\lambda^* = \frac{2\pi}{k_i^*} \quad (5.3)$$

For the critical and off-critical quench case, it can be observed that as the dimensionless diffusion coefficient increases, the value of the maximum wave number also increases ($k_m^* = 4$ to 7 refer to appendix B for $D^* = 500\,000$ and $800\,000$) meaning a decrease in the characteristic length (smaller domain size)

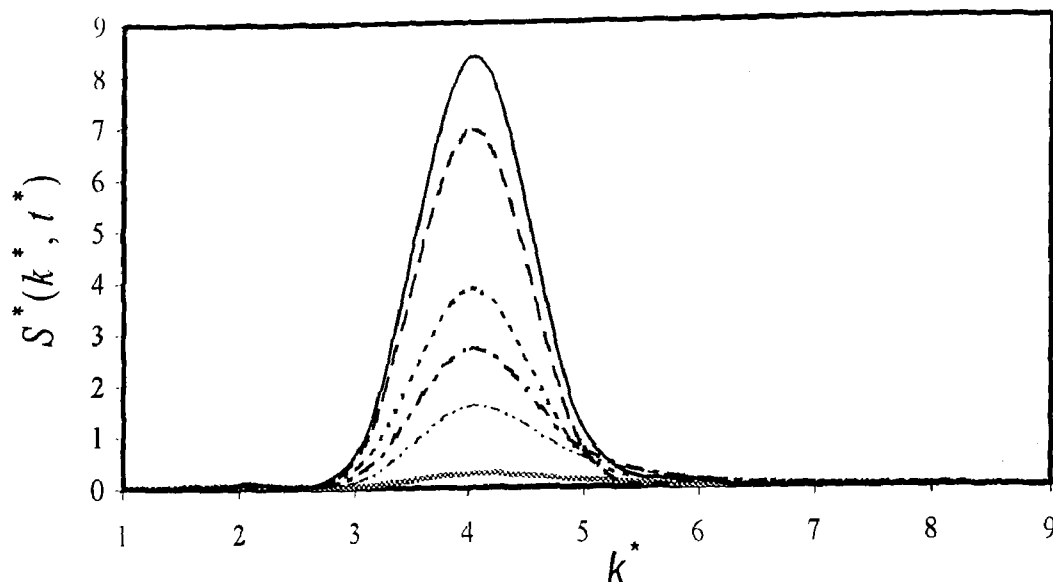


Figure 5.5: The evolution of the dimensionless structure factor for a single critical quench ($c_o^* = 0.5$, $D^* = 200\,000$ and $T^* = 0.25$) into the unstable region of the phase diagram at the following dimensionless times: $t^* = 3.527$ (thick grey line), $t^* = 3.843$ (dash with two dots), $t^* = 4.014$ (dash-dot line), $t^* = 4.186$ (dotted line), $t^* = 4.57$ (long dashed line), $t^* = 5.026$ (solid line).

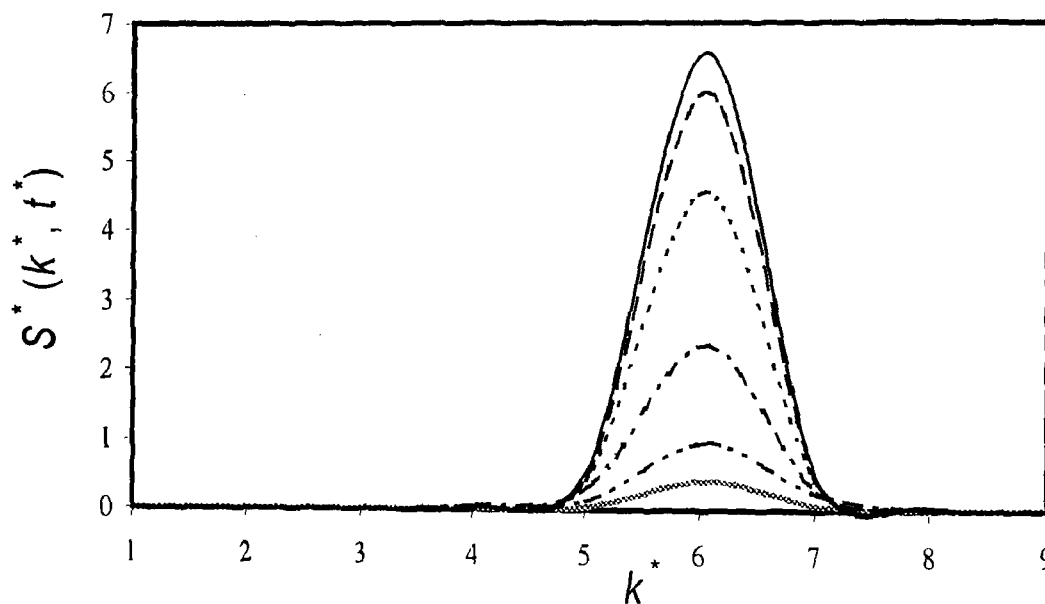


Figure 5.6: The evolution of the dimensionless structure factor for a single off-critical quench ($c_o^* = 0.6$, $D^* = 200\,000$ and $T^* = 0.25$) into the unstable region of the phase diagram at the following dimensionless times: $t^* = 4.579$ (thick grey line), $t^* = 4.737$ (dash with two dots), $t^* = 5.898$ (dash-dot line), $t^* = 5.092$ (dotted line), $t^* = 5.292$ (long dashed line), $t^* = 5.703$ (solid line).

since it has an inverse relationship. Table 5.2 summarizes the calculated values of the dimensionless characteristic lengths for the critical and off-critical quench case. λ_1^* denotes the dimensionless characteristic length for the single quench case. Later, for the double quench case the subscript 2 will be used to identify the secondary characteristic length that forms.

Table 5.2: Dimensionless characteristic lengths in the early stages of SD for the structures formed at $T_1^* = 0.25$ with increasing D^*

Quench	Temperature $T_1^* = 0.25$	λ_1^*
Critical	$c_o^* = 0.5, D^* = 200\ 000$	1.570
	$c_o^* = 0.5, D^* = 500\ 000$	1.047
	$c_o^* = 0.5, D^* = 800\ 000$	0.897
Off-critical	$c_o^* = 0.6, D^* = 200\ 000$	1.570
	$c_o^* = 0.6, D^* = 500\ 000$	1.256
	$c_o^* = 0.6, D^* = 800\ 000$	0.897

5.3.1 The Growth of the Dimensionless Structure Factor in the Early Stages of SD

From experimental observation of the early stages of phase separation by SD in the work of Hashimoto *et al.* [1983; 1986b], the growth of the scattering intensity is exponential in the early stage and taking the natural log of these values should produce a straight line. Into the later stages of phase separation by SD, the growth rate slows down and nonlinear effects take place. This was thought to be due to the coarsening of the mixture [Hashimoto *et al.*, 1986b]. For the early stages from the linear theory, the following relation can be obtained to describe the light scattering data [Hashimoto *et al.*, 1983]:

$$I(q, t) = I(q, t = 0) \exp(2R(q)t) \quad (5.4)$$

Taking the natural log of equation (5.4) gives:

$$\ln I(q, t) = 2R(q)t + \ln I(q, t = 0) \quad (5.5)$$

Equation (5.5) is the equation of a line in the form $y = mx + b$ where m is the slope and b is the intercept. The slope is $2R(q)$. Since $I(q, t) \propto S(k, t) = \langle |A(k, t)|^2 \rangle$

for $k = q$ [Okada and Han, 1986], the evolution of the structure factor also follows the form of equation (5.4) and (5.5) and taking the natural log of the dimensionless structure factor should also show the same trends as the scattering intensity. Figure 5.7 and 5.8 show the plots of the natural log of the maximum value of the dimensionless structure factor versus dimensionless time for the critical and off-critical quench case with $D^* = 200\,000$, respectively.

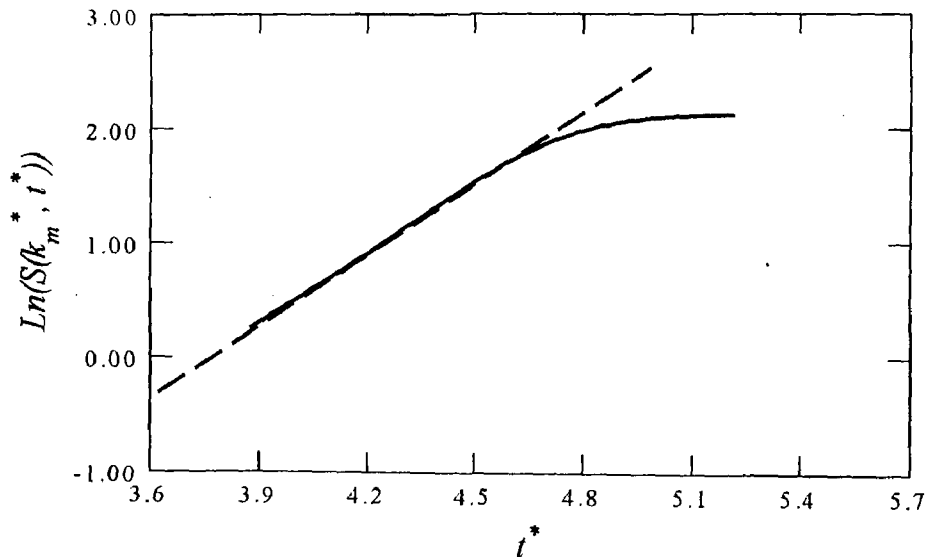


Figure 5.7: The evolution of the dimensionless maximum structure factor with dimensionless time from $t^* = 3.879$ to $t^* = 5.212$ for a single quench ($c_o^* = 0.5$, $D^* = 200\,000$ and $T_1^* = 0.25$) into the unstable region of the phase diagram. At the early stages of phase separation by SD, the initial increase is linear and gradually slows down into the beginning of the intermediate stage where coarsening occurs. The dashed line indicates the linearity for the early stages before it deviates.

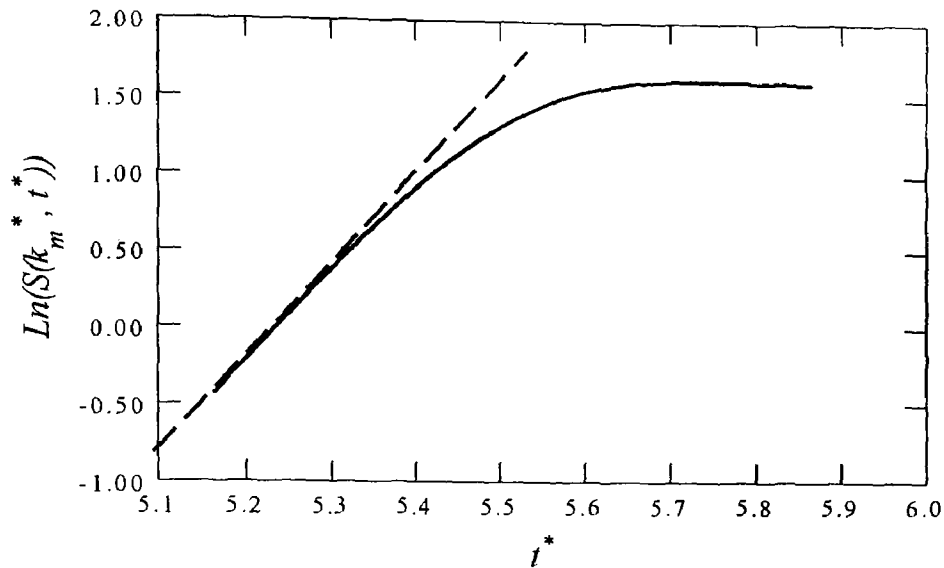


Figure 5.8: The evolution of the dimensionless maximum structure factor with dimensionless time from $t^* = 5.164$ to $t^* = 5.864$ for a single quench ($c_o^* = 0.6$, $D^* = 200\ 000$ and $T_1^* = 0.25$) into the unstable region of the phase diagram. At the early stages of phase separation by SD, the initial increase is linear and gradually slows down into the beginning of the intermediate stage where coarsening occurs. The dashed line indicates the linearity for the early stages before it deviates.

From Figure 5.7 to 5.8, it can be observed that the evolution of the natural log of the dimensionless structure factor at the maximum wave number is linear for the early stages before nonlinear effects begin. The trends observed in experimental work [Hashimoto *et al.*, 1986b; and 1983] and numerical work by Henderson and Clarke [2004].

5.4 The Dimensionless Diffusion Coefficient

The extent of phase separation observed for the critical quench in Figures 5.2, B.1 and B.2 and for the off-critical quench in Figures 5.3, B.4 and B.5 show a gradual increase with increasing dimensionless diffusion coefficient, D^* . This increase in the amount of phase separation can be explained in terms of the definition of the

dimensionless diffusion coefficient, D^* . The dimensionless diffusion coefficient is defined as the ratio of the driving force for phase separation versus the resisting force and is expressed as:

$$D^* = \frac{k_B T_c L^2}{a^2 \nu \left(\frac{k_B T_c}{\nu} \right)} = \frac{\text{driving force for phase separation}}{\text{resisting force}} \quad (5.6)$$

The term in the numerator comes from the change in the free energy density (the chemical potential) which is the driving force for phase separation (refer back to equation 3.16) and the term in the denominator is attributed to the square gradient energy (the interfacial energy) that acts to minimize the total free energy of the phase separating mixture by creating interfaces. As the value of D^* (200 000, 500 000, 800 000) increases, the driving force for phase separation is larger and therefore, more phase separated regions will develop. The increase in the number of crests and troughs in the concentration profile for the critical quench from Figures 5.2, B.1 and B.2 and the off-critical quench from Figures 5.3, B.3 and B.4 show this observation. For instance, in the critical quench case, Figure 5.2 shows three crests evident at a dimensionless diffusion coefficient of $D^* = 200\,000$ and in Figure B.1 there are five crests at a dimensionless diffusion coefficient of $D^* = 500\,000$. Also, note that the dimensionless time at which the first sign of phase separation occurs decreases for the critical quench case from $t^* = 3.527$ to 0.220 and for the off-critical quench case from $t^* = 4.898$ to 0.22878 with increasing D^* . Therefore, by increasing the driving force for phase separation, the amount and the rate of phase separation increases.

5.5 Quench Depth

From the theory of phase separation for the early to the beginning of the intermediate stages of phase separation by SD, it is known that as the temperature is decreased (for the case of a system exhibiting an UCST type phase diagram), the system becomes increasingly unstable due to the increase in the free energy and therefore more phase separated regions should appear [Ohnaga *et al*, 1989; Izumitani *et al*, 1990].

In this section, results will be shown for the off-critical quench case at two values of dimensionless temperature $T_1^* = 0.25$ and $T_2^* = 0.1$ and a dimensionless diffusion coefficient of $D^* = 500\,000$. The trends for the critical quench case are the same and therefore are not shown. The quench depth can be used to determine how deep a quench is relative to another. It is defined with reference to the critical temperature in the following dimensionless form:

$$T_{Q_d}^* = T_c^* - T^* \quad (5.7)$$

For the shallow quench case, at $T_1^* = 0.25$, the value of the quench depth is $T_{Q_d}^* = 0.08293$ and for the deeper quench, at $T_2^* = 0.1$, the quench depth is $T_{Q_d}^* = 0.13293$. Figure B.3 and Figure 5.9 shows the evolution of the concentration fluctuations for the shallow off-critical quench and the deeper off-critical quench, respectively. By comparing the number of crests that are present in Figure B.3 and Figure 5.9, it can be observed that there are more phase-separated regions. In the shallower quench, there are four crests and for the deeper quench there are 14 crests. This has been observed in experiment by Izumitani *et al*. [1990] for a

mixture of polybutadiene (PB)/poly(styrene-r-butadiene) (SBR), where the amount of phase separated regions increased with increasing quench depth.

5.6 The Change in the Dimensionless Spatial Chemical Potential

The chemical potential, μ_i , is used to describe chemical equilibrium involving the diffusive transport of matter [Van Dijk and Wakker, 1997]. $\Delta\mu$ for a polymer mixture in mathematical form for component i is defined as:

$$\Delta\mu_i = \mu_{i_{mix}} - \mu_{i_{pure}} \quad (5.8)$$

From the development of the general equation to describe phase separation by SD

($\frac{\partial c}{\partial t} + \nabla \mathbf{j} = 0$), the diffusional flux contains the thermodynamic driving force, the

change in the chemical potential, for the binary polymer mixture. Therefore, the

plots of the change in the chemical potential will provide useful information about

the mixture in terms of equilibrium thermodynamics. The change in the chemical

potential of polymer 1, μ_1 , in a mixture relative to its pure component, μ_1^o , written

in terms of enthalpic and entropic contributions [Kurata, 1982; Van Dijk and

Wakker, 1997]:

$$\Delta\mu_1 = \mu_1 - \mu_1^o = \ln(c) + \left(1 - \frac{N_1}{N_2}\right)(1-c) + \chi N_1 (1-c)^2 \quad (5.9)$$

The above equation can be written in dimensionless form as follows:

$$\Delta\mu_1^* = \mu_1^* - \mu_1^{o*} = T^* \left[\ln(c^*) + \left(1 - \frac{N_1}{N_2}\right)(1-c^*) + \chi^* N_1 (1-c^*)^2 \right] \quad (5.10)$$

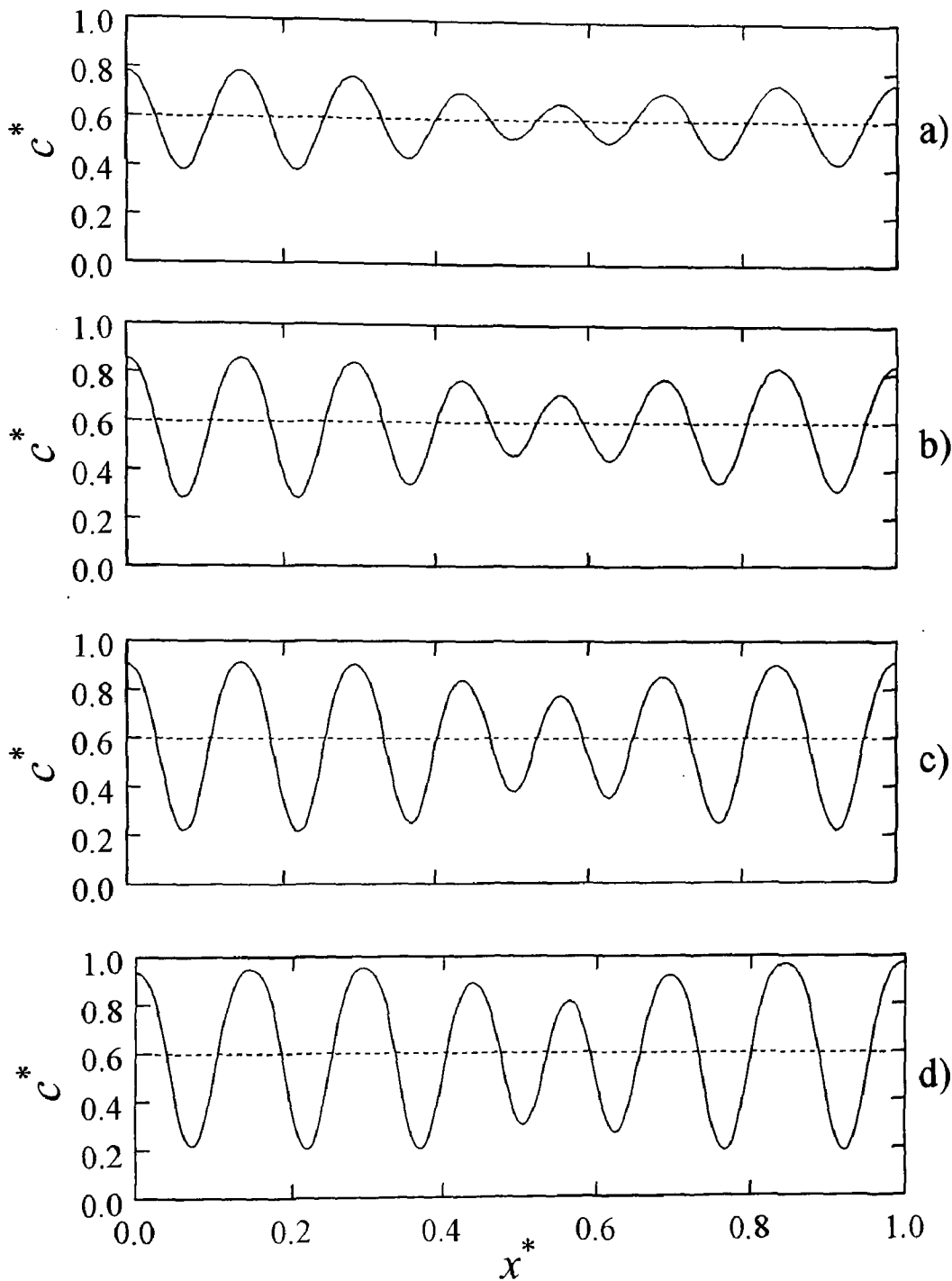


Figure 5.9: The evolution of the dimensionless spatial concentration profile for a single quench into the unstable region of the phase diagram at the following dimensionless times: (a) $t^* = 0.2128$, (b) $t^* = 0.2221$, (c) $t^* = 0.2323$, and (d) $t^* = 0.2533$. The dashed line through the center of the graph represents the initial average concentration $c_o^* = 0.6$. The dimensionless diffusion coefficient for this case is $D^* = 500\,000$ and the dimensionless temperature is $T_I^* = 0.2$.

Equation 5.10 is used to calculate the change in the dimensionless spatial chemical potential of polymer 1 at different dimensionless times. Figure 5.10 and 5.11 show the plots of the evolution of the change in the dimensionless spatial chemical potential for a single critical quench and a single off-critical quench at $D^* = 200\ 000$. The discussion is divided into two aspects, one being the discussion of evolution of the spatial chemical potential at a fixed D^* and the other in discussing how the increase in D^* affects the change in the chemical potential.

Figure B.14 for the critical quench case ($D^* = 800\ 000$) will be used as an example for the discussion of the change in the dimensionless spatial chemical potential of polymer 1. The same general trends are observed for the off-critical quench case at the same value of D^* . From the profiles in Figure 5.10, B.13 and B.14, it can be observed that there are regions where $\Delta\mu_1^*$ increases with increasing dimensionless time to reach a local maximum and regions where $\Delta\mu_1^*$ decreases with increasing dimensionless time to reach a local minimum. This can be explained by combining the spatial chemical potential with the spatial concentration profile at a given dimensionless time. In Figure 5.12, a combined plot is shown for a dimensionless time of $t^* = 0.2733$, which corresponds to the last profile in Figure B.2 of the dimensionless spatial concentration profile and the dimensionless spatial chemical potential. In Figure 5.12, as the composition fluctuations approach the upper equilibrium value, the change in the dimensionless chemical potential decreases to a minimum (local minimum). In other words, the chemical potential of polymer 1 in the mixture is less than that of

its pure phase, $\mu_{1\text{ mix}}^* < \mu_{1\text{ pure}}^*$ and the change in free energy is being minimized. At the limit when c^* approaches 1 (rich in polymer 1), $\Delta\mu_1^* = 0$, meaning the chemical potential of polymer 1 in the mixture, $\mu_{1\text{ mix}}^*$, equals the value of the pure component, $\mu_{1\text{ pure}}^*$. At the positions of the local maxima in Figure 5.12 b), the composition of polymer 1 approaches the lower equilibrium value and these regions are rich in polymer 2. Eventually, the local maximum values will decrease and $\Delta\mu_1^*$ will approach zero. This being the condition for equilibrium where the change in the chemical potential of the coexisting phases becomes equal [Van Dijk and Wakker, 1997]. Going back to Figures 5.10, B.13 and B.14, the effect of increasing the value of the dimensionless diffusion coefficient on the evolution of the change in the dimensionless spatial chemical potential for a single critical quench and a single off-critical quench can be observed. Notice as D^* increases from 200 000 to 800 000, the rate of change in the dimensionless chemical potential also increases. At $D^* = 200\ 000$ to $500\ 000$, for the critical quench, the evolution of the dimensionless spatial chemical potentials reach the local maximum and local minimum values and approach equilibrium, $\Delta\mu_1^* = 0$, at times of $t^* = 4.57$ and $t^* = 0.6946$ respectively. At $D^* = 800\ 000$, towards the end of the profile, the local maximum areas start to decrease towards lower values of $\Delta\mu_1^*$ and similarly, the local minimum values increase towards zero at a much faster rate ($t^* = 0.2733$). Therefore, the increase of D^* can be interpreted as stimulating a faster rate of separation and move towards stabilization of the

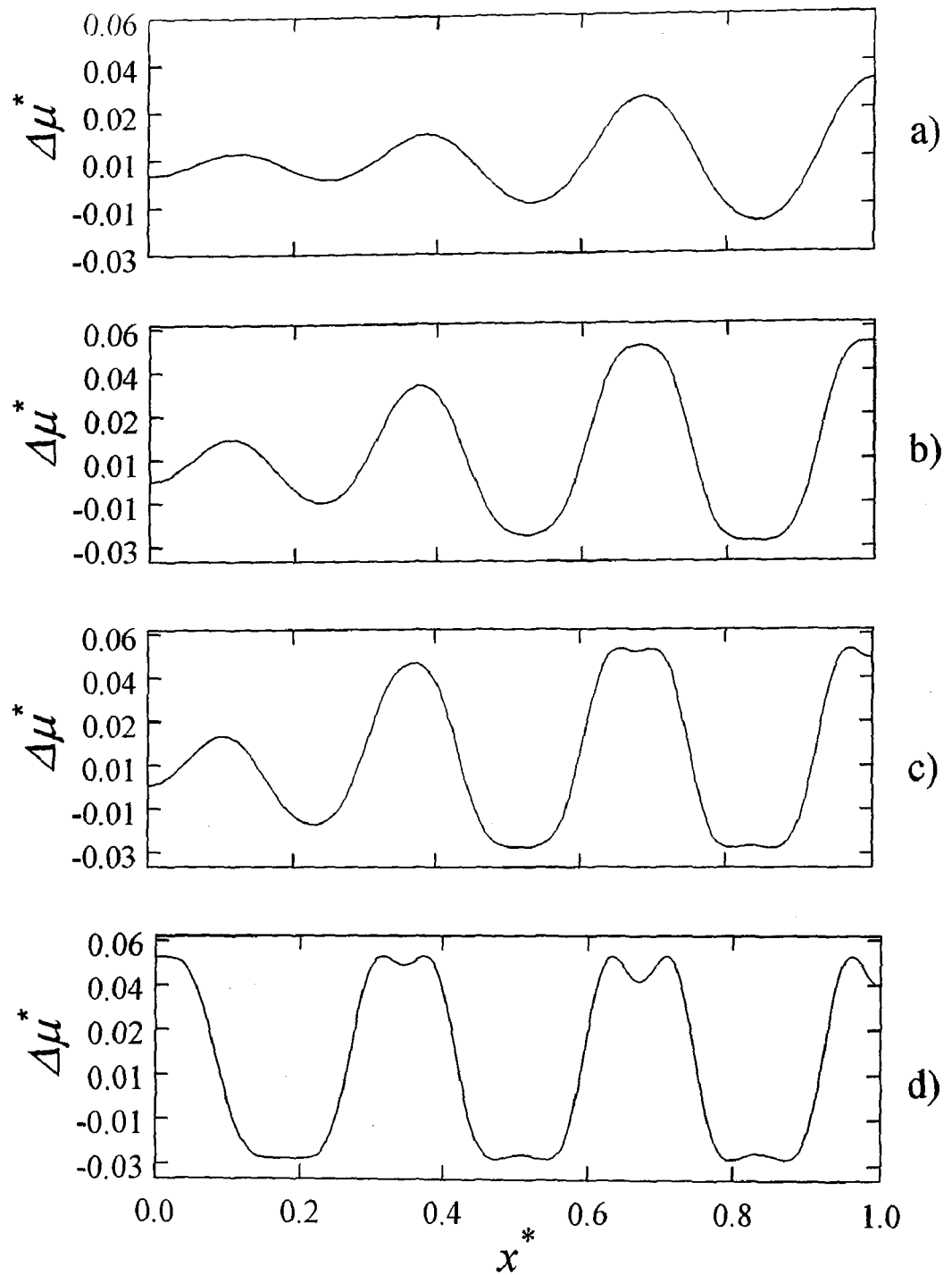


Figure 5.10: The evolution of the change in the dimensionless spatial chemical potential for a single quench into the unstable region of the phase diagram at the following dimensionless times: (a) $t^* = 3.527$, (b) $t^* = 3.843$, (c) $t^* = 4.014$, and (d) $t^* = 4.57$. The change in the dimensionless chemical potential is defined as the difference between the chemical potential polymer 1 in the mixture to that of its pure phase. The dimensionless initial concentration is $c_0^* = 0.5$ and the dimensionless diffusion coefficient is $D^* = 200\,000$.

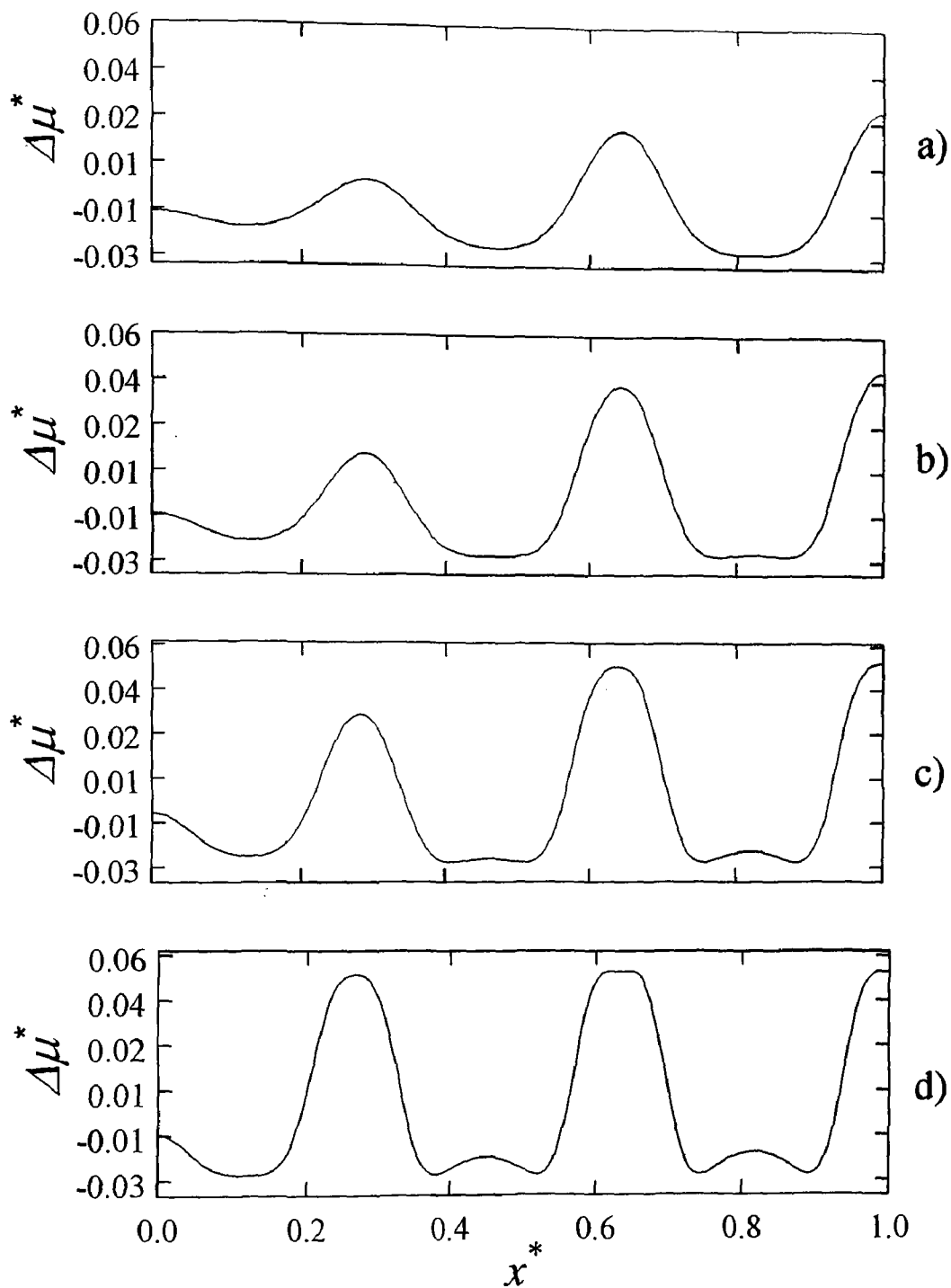


Figure 5.11: The evolution of the change in the dimensionless spatial chemical potential for a single quench into the unstable region of the phase diagram at the following dimensionless times: (a) $t^* = 4.898$, (b) $t^* = 5.092$, (c) $t^* = 5.292$, and (d) $t^* = 5.703$. The change in the dimensionless chemical potential is defined as the difference between the chemical potential polymer 1 in the mixture to that of its pure phase. The dimensionless initial concentration is $c_0^* = 0.6$ and the dimensionless diffusion coefficient is $D^* = 200\,000$.

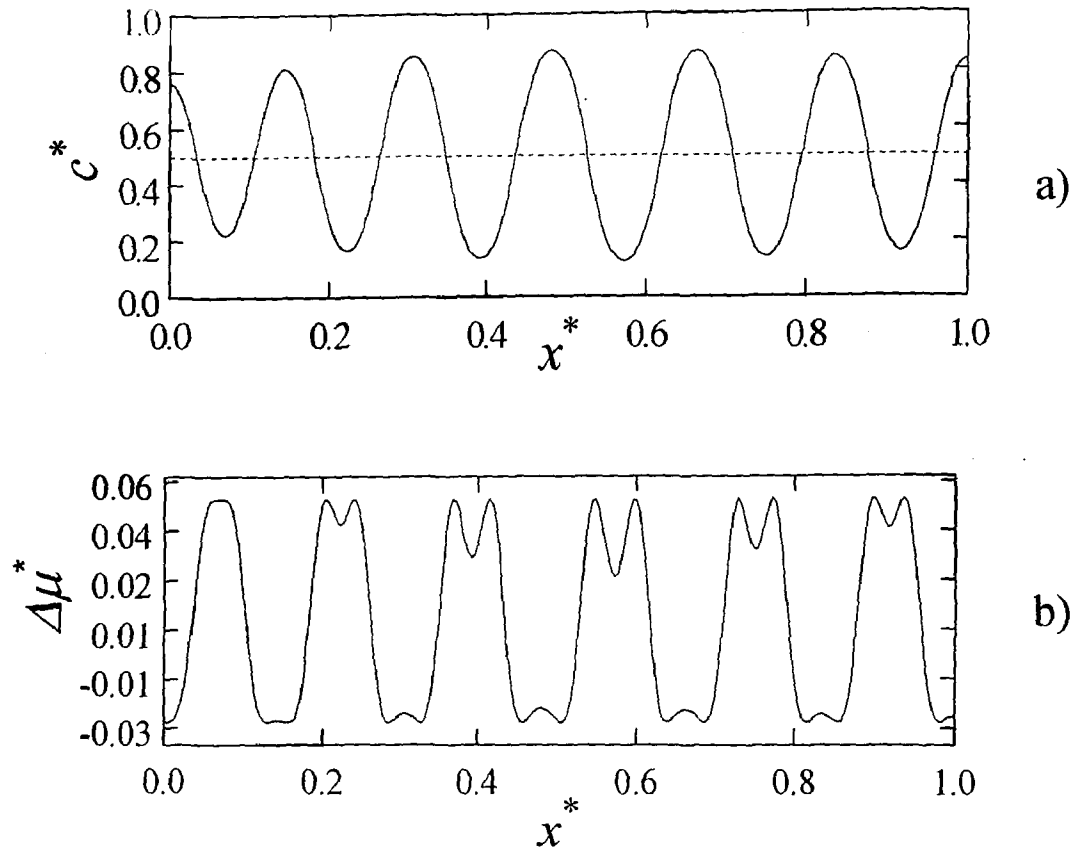


Figure 5.12: A comparison between the dimensionless spatial concentration profile (a) to the change in the dimensionless spatial chemical potential (b) for a single critical quench with $D^* = 800\,000$ at a dimensionless time of $t^* \approx 0.2733$.

polymer blend. The same can be said for the off-critical quench case. Lee *et al.* [2002] showed the same trends in their numerical work for polymer solutions on the investigation of the change in the dimensionless spatial chemical potential. The second derivative of free energy with respect to composition of polymer 1 in dimensionless form is:

$$F^* = T^* \left[\frac{1}{c^*} - 2\chi^* N_1 (1 - c^*) \right] \quad (5.11)$$

The second derivative of free energy with respect to composition determines the drive of the composition fluctuations around the inflection ($\frac{\partial^2 F}{\partial c^2} = 0$) points where $\frac{\partial^2 F}{\partial c^2} > 0$ stability or meta-stability are possible and $\frac{\partial^2 F}{\partial c^2} < 0$ results in instability for the binary mixture. Recall that for instability, the second derivative of free energy with respect to composition must be less than zero and small composition fluctuations are enough to create instability. The curvature of the second derivative of free energy with respect to composition (change in sign) details the degree of stability, alongside the knowledge of the first derivative of free energy with respect to composition, with concave downwards (local maximum) being unstable and concave upwards (local minimum) can be meta-stable or stable. Figures 5.13 and 5.14 show the evolution of the second derivative of the free energy with respect to composition spatially. The critical and off-critical quench are at $T_l^* = 0.25$ with $D^* = 200\ 000$, respectively. From the plots for the critical and off-critical quench case for the change in the second derivative with respect to composition, it can be observed that the steepness in the rate of change increases with time and with increasing D^* (see Figures B.17 to B.20 in Appendix B). This indicates an increase in the instability with time as the system phase separates [Hashimoto *et al.*, 1983]. The values at which second derivative of free energy with respect to composition is zero, $F^{**} = 0$, reflect the points of inflection in the free energy curve at the positions where the curvature changes sign and also at the critical point (Chapter 3). Therefore, the observations of the profiles for the second derivative with respect to composition

match the thermodynamic in describing instability of phase separating mixtures [Van Dijk and Wakker, 1997].

Also referring back to the explanation given for the time discrepancy for the occurrence of phase separation by SD for the critical and off-critical quench, it can be observed that this explanation is valid. By comparing the plots of the second derivative of free energy with respect to composition for the case where $D^* = 200\,000$, it can be observed that the rate of change in the free energy is much faster for the critical quench than for the off-critical quench case. This indicates higher instability for the critical quench case.

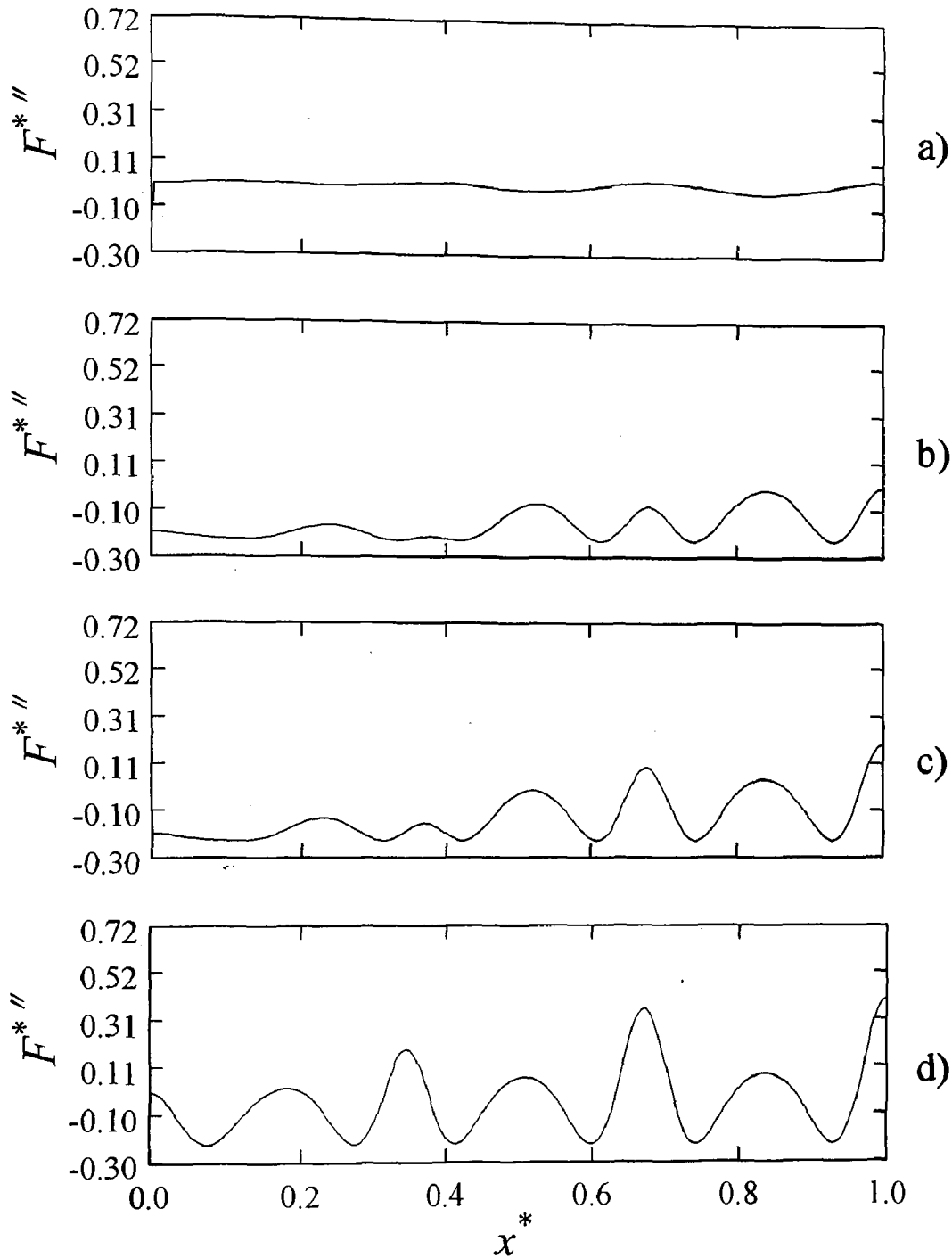


Figure 5.13: The evolution of the change in the dimensionless spatial second derivative of the free energy with respect to composition of component 1 for a single quench into the unstable region of the phase diagram at the following dimensionless times: (a) $t^* = 3.527$, (b) $t^* = 3.843$, (c) $t^* = 4.014$, and (d) $t^* = 4.57$. The change in the dimensionless second derivative of free energy is used to determine the conditions of stability ($F^{*''} > 0$), meta-stability ($F^{*''} > 0$), and instability ($F^{*''} < 0$). The dimensionless initial concentration is $c_0^* = 0.5$ and the dimensionless diffusion coefficient is $D^* = 200\,000$.

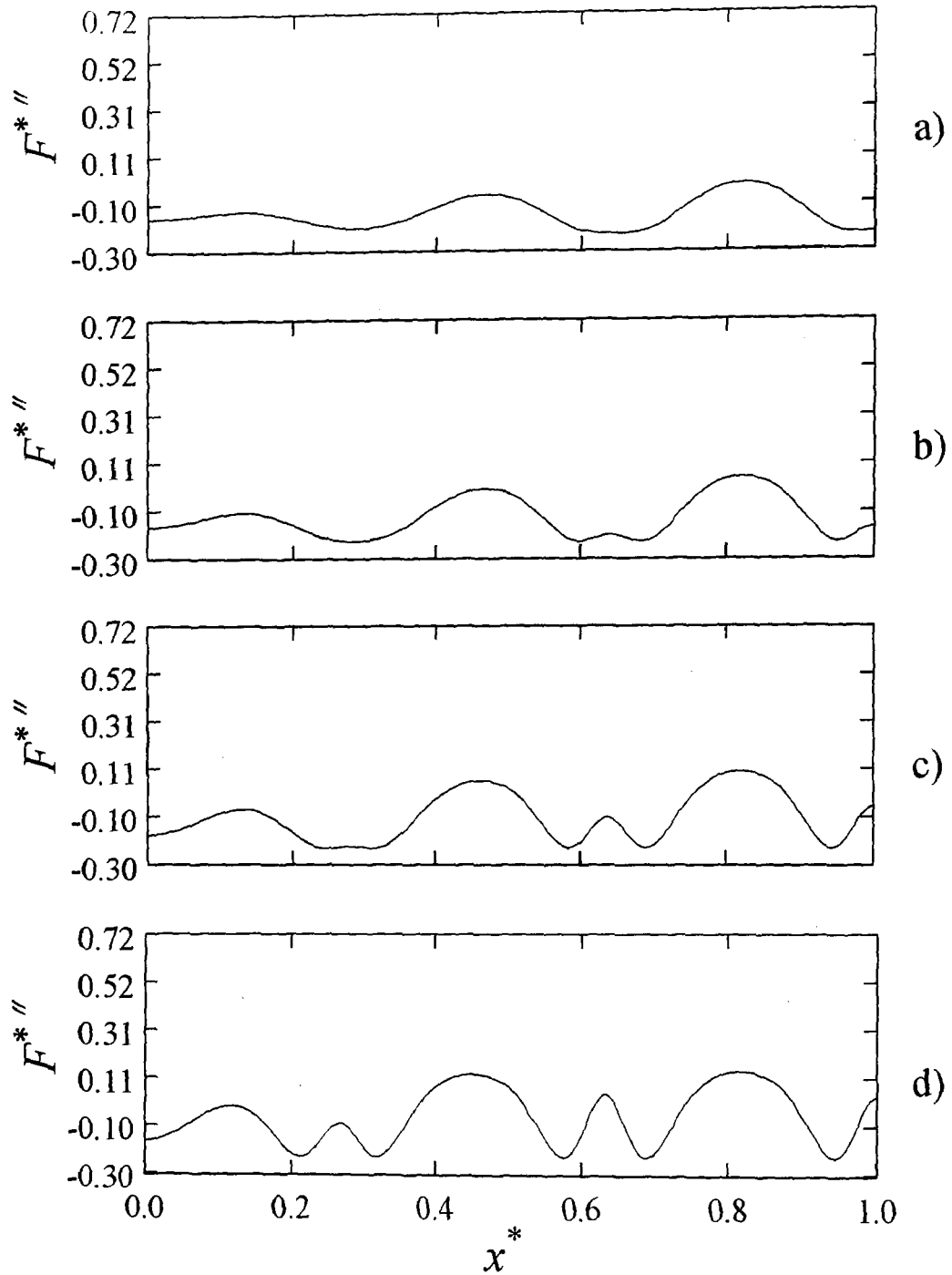


Figure 5.14: The evolution of the change in the dimensionless spatial second derivative of the free energy with respect to composition of component 1 for a single quench into the unstable region of the phase diagram at the following dimensionless times: (a) $t^* = 4.898$, (b) $t^* = 5.092$, (c) $t^* = 5.292$, and (d) $t^* = 5.703$. The change in the dimensionless second derivative of free energy is used to determine the conditions of stability ($F^{*''} > 0$), meta-stability ($F^{*''} > 0$), and instability ($F^{*''} < 0$). The dimensionless initial concentration is $c_0^* = 0.6$ and the dimensionless diffusion coefficient is $D^* = 200\,000$.

Chapter 6

Results and Discussion: 1-D TIPS Double Quench

This chapter presents the 1-D numerical results of phase separation by double quenching (within the unstable region of the phase diagram) of a polymer mixture to observe whether secondary phase separated regions are produced inside the already phase separating regions from the initial quench. Double quenching involves a two-step process whereby the initial quench is allowed to phase separate for a certain period of time before the next quench takes place. In experimental work, the second quench has been made at the intermediate stages [Tanaka, 1993; Tao *et al.*, 1995] and the late stages [Tanaka, 1993; Tao *et al.*, 1995; Hashimoto *et al.*, 2000] of phase separation after the first quench. In the method used by Hashimoto *et al.* the second quench was restricted to the unstable region such that the blend still phase separated by SD [Hashimoto *et al.*, 2000]. In numerical studies Ohnaga *et al.* [1989], made the second quench at different specifications. There are three distinct time periods they quenched at, the early stages of phase separation by SD, when the concentration fluctuations were well-developed and when the concentration fluctuations reached their respective equilibrium values [Ohnaga *et al.*, 1994]. Henderson and Clarke [2004] made

their second jump at the late stage of phase separation by SD following the work of Hashimoto *et al.* very closely [2000]. In this study, the second jump is made at the beginning of the intermediate stages and the technique to determine the time for the temperature jump is based on the results presented by Hashimoto [1986b] in their experimental work on the different stages of phase separation by SD. The second quench will still remain in the unstable region so that phase separation is still occurring by SD. The parameters used in this section are summarized in Table 6.1.

Table 6.1: Summary of the dimensionless parameters used in the 1-D numerical study for double quenching

Parameter	Value
c_o^*	0.5 (critical), 0.6 (off-critical)
N_1, N_2	1000
D^*	200 000, 500 000, 800 000
T_1^*	0.25 (initial quench temperature)
T_2^* (temperature jump)	0.2 (shallow quench)
T_2^* (temperature jump)	0.1 (deeper quench)

An initial critical and an initial off-critical quench case are studied with different values of the driving force, D^* . The dimensionless temperature chosen for the initial quench is $T_1^* = 0.25$ and two dimensionless temperatures are chosen for the second temperature jump $T_2^* = 0.2$ (shallow quench) and $T_2^* = 0.1$ (deeper

quench). In order to be able to mimic real systems that have been studied for double quenching in experiments, the values chosen for this study reflect the order of magnitude of the parameters used in experiment. In Hashimoto's work [2000], for a critical quench, the dimensionless quench depth for the initial temperature jump was calculated to be $T_{Q_1}^* = 0.1667$ and at the second temperature jump, the dimensionless quench depth was $T_{Q_2}^* = 0.9444$. In Tanaka's work [1993], a shallow and a deeper quench were examined. The shallow dimensionless quench depth for the initial temperature jump was calculated to be $T_{Q_1}^* = 0.01667$ and at the second temperature jump, the dimensionless quench depth was $T_{Q_2}^* = 0.1298$. For a deeper quench, the initial dimensionless quench depth was calculated to be $T_{Q_1}^* = 0.040476$ and at the second temperature jump, the dimensionless quench depth was $T_{Q_2}^* = 0.1274$. The reason that the quench depth for the second jump is roughly the same in Tanaka's work is because he examined the effect of making the initial quench depth larger (i.e. a deeper initial quench). The values used in this study are comparable to the experimental values. In this study, for the shallow quench from an initial quench temperature of $T_1^* = 0.25$ to the second quench at $T_2^* = 0.2$, the quench depth for the initial temperature jump is $T_{Q_1}^* = 0.08295$ and at the second quench $T_{Q_2}^* = 0.13295$. For the deeper quench to $T_2^* = 0.1$ the quench depth is $T_{Q_1}^* = 0.2330$.

The method used for double phase separation was shown in Figure 1.6. The double quenching process takes place within the unstable region of the phase diagram so as to ensure that the system is still phase separating by SD. The initial quench is made and the system is allowed to phase separate for a certain period of time, t_i^* , before the second quench. The time t_i^* is the dimensionless transition time which corresponds the transition from the early to the beginning of the intermediate stages of phase separation. In the literature, the criterion for the second quench is based on the stage of SD (i.e. early, intermediate and late stage) [Tanaka, 1993; Tao *et al.*, 1995; Hashimoto *et al.*, 2000].

The overall direction of the numerical work presented in this section will examine the following points to provide a better understanding of the mechanism behind double phase separation by SD:

- (i) Does the evolution of the concentration fluctuations follow the same trends that are observed for a single quench?
- (ii) How is the structure factor affected by the double quench and how can it be used to describe the appearance of secondary structures?
- (iii) How does the driving force (increase in the dimensionless diffusion coefficient D^*) affect the formation of secondary structures?
- (iv) How does quench depth affect the formation of secondary structures (shallow and deeper quench)?
- (v) Are there any significant differences that appear between a critical and an off-critical quench in terms of growth dynamics for secondary phase separation?

- (vi) At what point after the second temperature jump do the secondary structures start to form?
- (vii) How does the growth of the primary and secondary structures evolve during the second temperature jump?
- (viii) Does the secondary phase separation follow the linear C-H theory in the early stages of phase separation?

The interest of this thesis still lies in the formation of the phase-separated structures and therefore only the early to the intermediate stages will be examined. The results presented in this chapter for the critical and off-critical quench case are for a value of the dimensionless diffusion coefficient $D^* = 200\ 000$ unless otherwise specified. The results for $D^* = 500\ 000$ and $800\ 000$ are shown in Appendix C.

6.1 Dimensionless Transition Time (t_t^*) for the Second Quench

Before the second quench is applied, it is necessary to use a consistent method for determining at what point a second temperature jump should be applied in all the simulations. From the dimensionless spatial concentration profiles, the composition fluctuations represented the early to intermediate stages of phase separation by SD. The transition point from the early to the intermediate stages can be determined through the evolution of the dimensionless structure factor at the maximum wave number, k_m , with time. In the work by the Hashimoto *et al.* [1986b] the growth of the scattering intensity is exponential in the early stage and

taking the natural log of these values should produce a straight line. Into the later stages of phase separation by SD, the growth rate slows down where nonlinear effects take place. This was thought to be due to the coarsening of the mixture [Hashimoto *et al.*, 1986b]. The dimensionless transition time, t^* , is defined as the time at which phase separation moves away from the early stage dynamics and enters into the beginning of the intermediate stages. How this time is determined is shown in Figure 6.1 for the critical quench case.

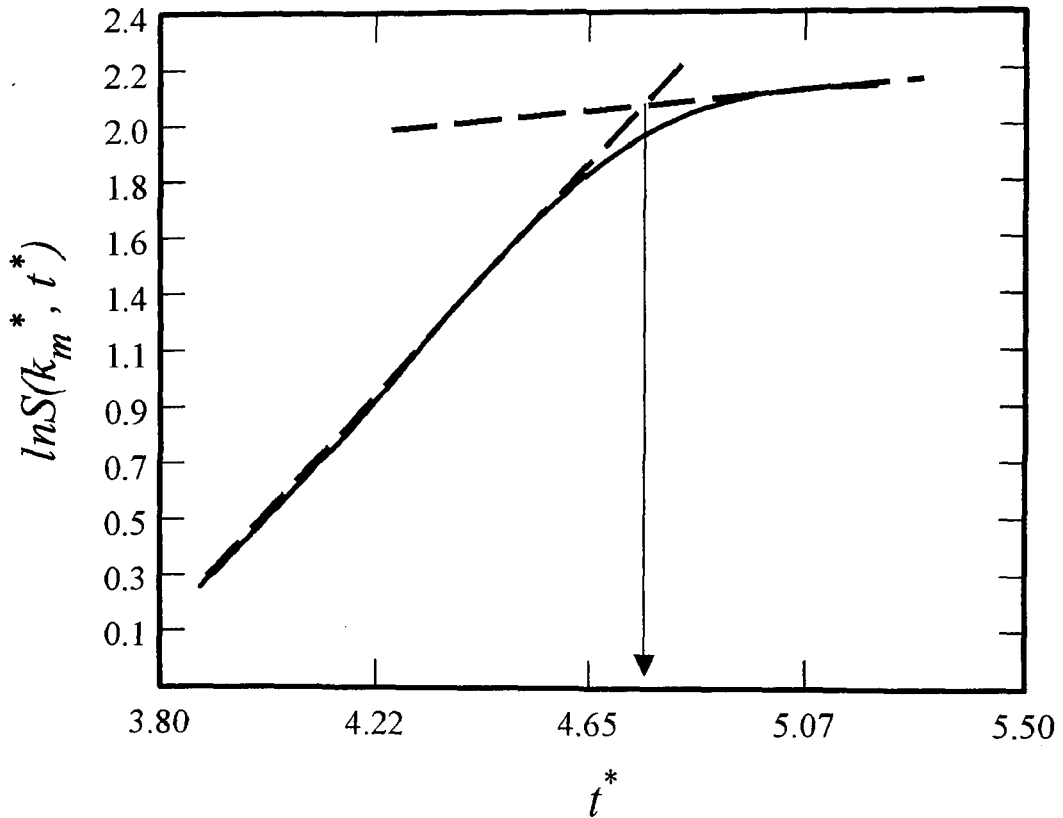


Figure 6.1: The evolution of the dimensionless maximum structure factor with dimensionless time from $t^* = 0.8594$ to $t^* = 1.00$ for a single quench ($c_o^* = 0.5$, $D^* = 200\ 000$ and $T_1^* = 0.25$) into the unstable region of the phase diagram. The dimensionless transition time is 4.720. At the early stages of phase separation by SD the initial increase is linear and gradually slows down into the beginning of the intermediate stage where coarsening occurs. The transition point occurs where the two tangent lines intersect.

From the plot of the maximum values of the dimensionless structure factor at given dimensionless times for the single quench, the dimensionless transition time can be obtained by making two tangent lines where the change in the growth rate is obvious. In Figure 6.1, the two tangent lines are drawn and the point of intersection is where the transition time is located. Figure 6.1 is an actual plot for the critical quench case at $c_o^* = 0.5$, $D^* = 200\ 000$ and $T_1^* = 0.25$. The values correspond to the plot of the structure factor shown in Chapter 5 (Figure 5.3.). Since one of the interests in this section is to determine how driving force affects the formation of secondary structures, a summary of the transitions times at each given condition to be tested is summarized in Table 6.2.

Table 6.2: A summary of the dimensionless transition times (at $T_1^* = 0.25$) determined from plotting the maximum values of the dimensionless structure factor with dimensionless time.

Quench	Parameters	Dimensionless Transition Time t_r^*
Critical	$c_o^* = 0.5, D^* = 200\ 000$	4.720
	$c_o^* = 0.5, D^* = 500\ 000$	0.650
	$c_o^* = 0.5, D^* = 800\ 000$	0.256
Off-critical	$c_o^* = 0.6, D^* = 200\ 000$	5.520
	$c_o^* = 0.6, D^* = 500\ 000$	0.903
	$c_o^* = 0.6, D^* = 800\ 000$	0.323

From Table 6.2, the trend observed with the increase in the dimensionless diffusion coefficient is a decrease in the dimensionless transition time. This should be expected since phase separation occurs at a much faster rate with

increasing D^* and therefore, should reach the beginning of the intermediate stage much faster.

The plots to determine the dimensionless transition time for all other cases will not be shown since the evolution of the maximum value of the dimensionless structure factor with dimensionless time show the same general trend.

There is now a consistent method of determining when the second temperature jump should take place and in the analysis, the jump will be made at the transition time.

6.2 Dimensionless 1-D Spatial Concentration Profiles

Figure 6.2 shows the evolution of the dimensionless spatial concentration profile (for an initial critical) quench after the second temperature jump. The initial phase separation temperature is $T_1^* = 0.25$ and the second temperature jump is $T_2^* = 0.2$ at the transition time. The transition times is $t_t^* = 4.72$ for $D^* = 200\ 000$. For each case (also referring also to Figures C.1 and C.2 in appendix C), after the second temperature jump, there is no evidence of double phase separation. What is observed in the evolution of the spatial concentration profiles is a continuous growth of the already growing initial profiles presented in Figures 5.2, B.1 and B.2 for $D^* = 200\ 000$ to $800\ 000$. Hashimoto *et al.* [2000; Hayashi *et al.*, 2000a] have observed this continuous growth in their experimental work when investigating the effect of initial domain size on secondary phase separation. Numerically, Henderson and Clarke [2004] have also observed this in their 2-D

study on double quenching in the late stages of phase separation by SD at a shallower quench depth. After the second temperature jump, there is a lag time that exists before a significant increase is observed in the growth of the concentration profiles approaching the new upper ($c_U^* = 0.9695$) and lower ($c_L^* = 0.03049$) equilibrium composition values at $T_2^* = 0.2$. This lag time appears because the mixture, upon subjection to a change in conditions, requires time to adjust to the new environment and therefore, experiences a lag or a transition period before reaching the new state. For the initial critical quench case, the lag times decrease from 0.014 to 0.0006 as D^* increases. The decrease in the lag time as D^* increases is expected since D^* increases the rate of phase separation.

Figure 6.3 shows the evolution of the dimensionless spatial concentration profiles (for an initial off-critical quench) after the second temperature jump. Again the initial temperature jump is at a temperature of $T_1^* = 0.25$ and the second temperature jump is $T_2^* = 0.2$ at the transition times. The transition time in this case for $D^* = 200\ 000$ is $t_i^* = 5.52$. The observations made for the critical quench case can also be applied to the off-critical quench case in that the growth of the concentration fluctuations from the initial quench are amplified by the second temperature jump with no sign of double phase separation present. However, there is a slight difference in the concentration profile at $D^* = 500\ 000$ and $800\ 000$ (See Figures C.3 and C.4 in Appendix C). In Figures C.3 and C.4 there is a slight destructive interference that can be observed in peak 3

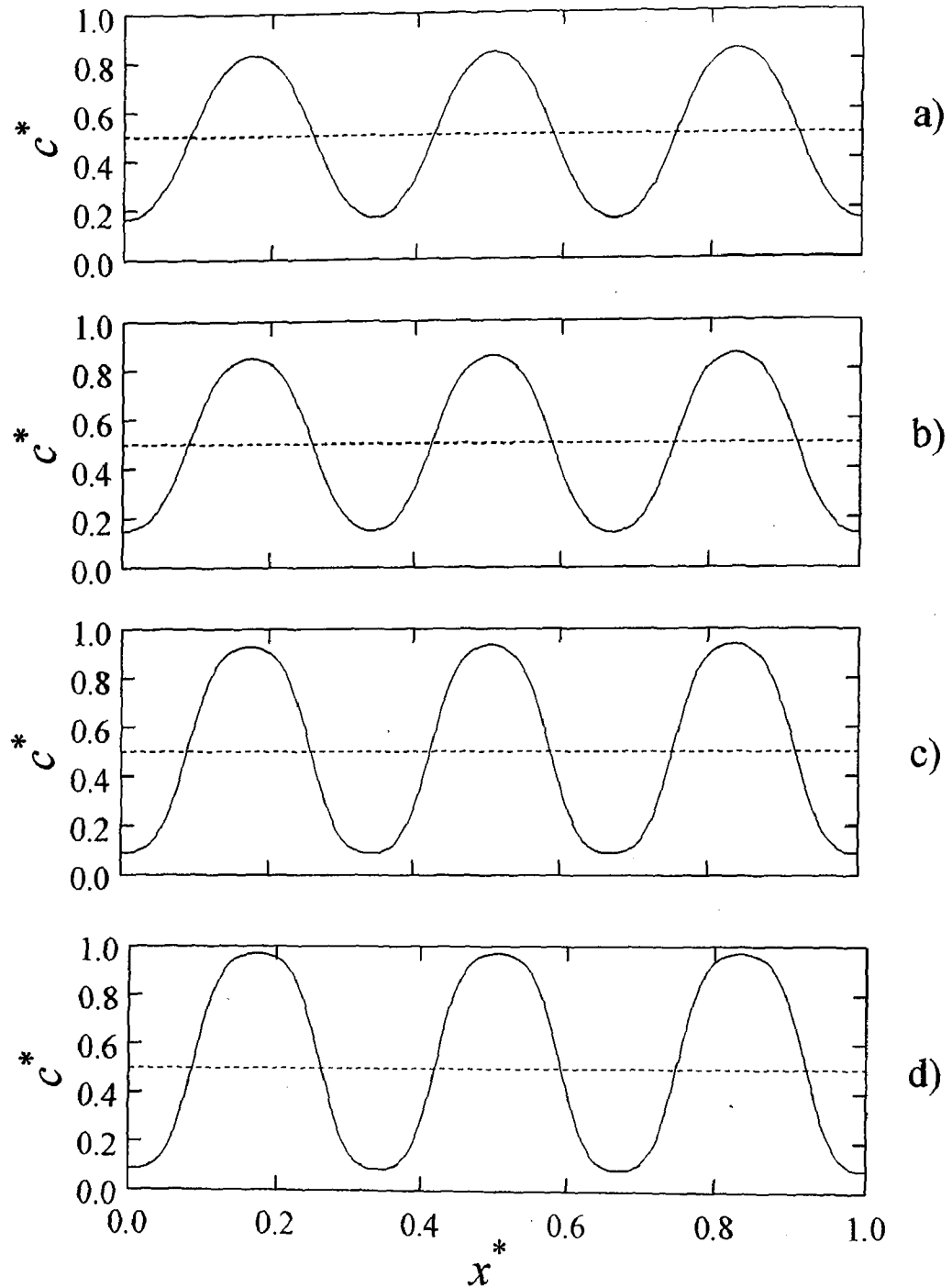


Figure 6.2: The evolution of the dimensionless spatial concentration profile for a double quench from $T_1^* = 0.25$ to $T_2^* = 0.2$ at the transition time of $t_t^* = 4.72$ at the following dimensionless times: (a) $t^* = 4.731$, (b) $t^* = 4.745$, (c) $t^* = 4.798$, and (d) $t^* = 4.861$. The dashed line through the center of the graph represents the initial average concentration $c_o^* = 0.5$. The dimensionless diffusion coefficient for this case is $D^* = 200\,000$.

(Figure C.3) and peak 1 (Figure C.4). However, this increase in D^* is not sufficient to cause the mixture to reach a new instability as it appears to restore itself to match the evolution of the other peaks in the profile. A lag time also exists for the off-critical quench case after the second quench before a significant growth of the concentration fluctuations is observed. The lag times decrease from 0.041 to 0.0063 as D^* increases.

Figure 6.4 shows the evolution of the dimensionless spatial concentration profiles (for the initial critical quench) after the second temperature jump at a deeper quench depth of $T_2^* = 0.1$. The second quench is made at the same transition times shown in Table 6.2. The initial temperature was kept constant at $T_1^* = 0.25$ to be consistent with the shallower quench to observe the effect of making a deeper second quench. The concentration profiles in this case look different from the single quench and the shallower quench at $T_2^* = 0.2$. In Figure 6.4, at $t^* = 4.748$, there are noticeable obstructions in the peaks and troughs of the concentration profile. The obstructions gradually increase with time as the primary peaks approach the new equilibrium values at the second temperature and they decrease at the troughs as the lower equilibrium values are approached. These profiles are similar to the ones generated by Ohnaga *et al.* [1994], in their investigation of reaction induced phase separation (see Chapter 2 for details). A lag time exists after the second quench before the first sign of double phase separation is observed. The lag times are 0.02, 0.0041 and 0.0011 and decreases with increasing D^* . This is consistent the increase in the rate and

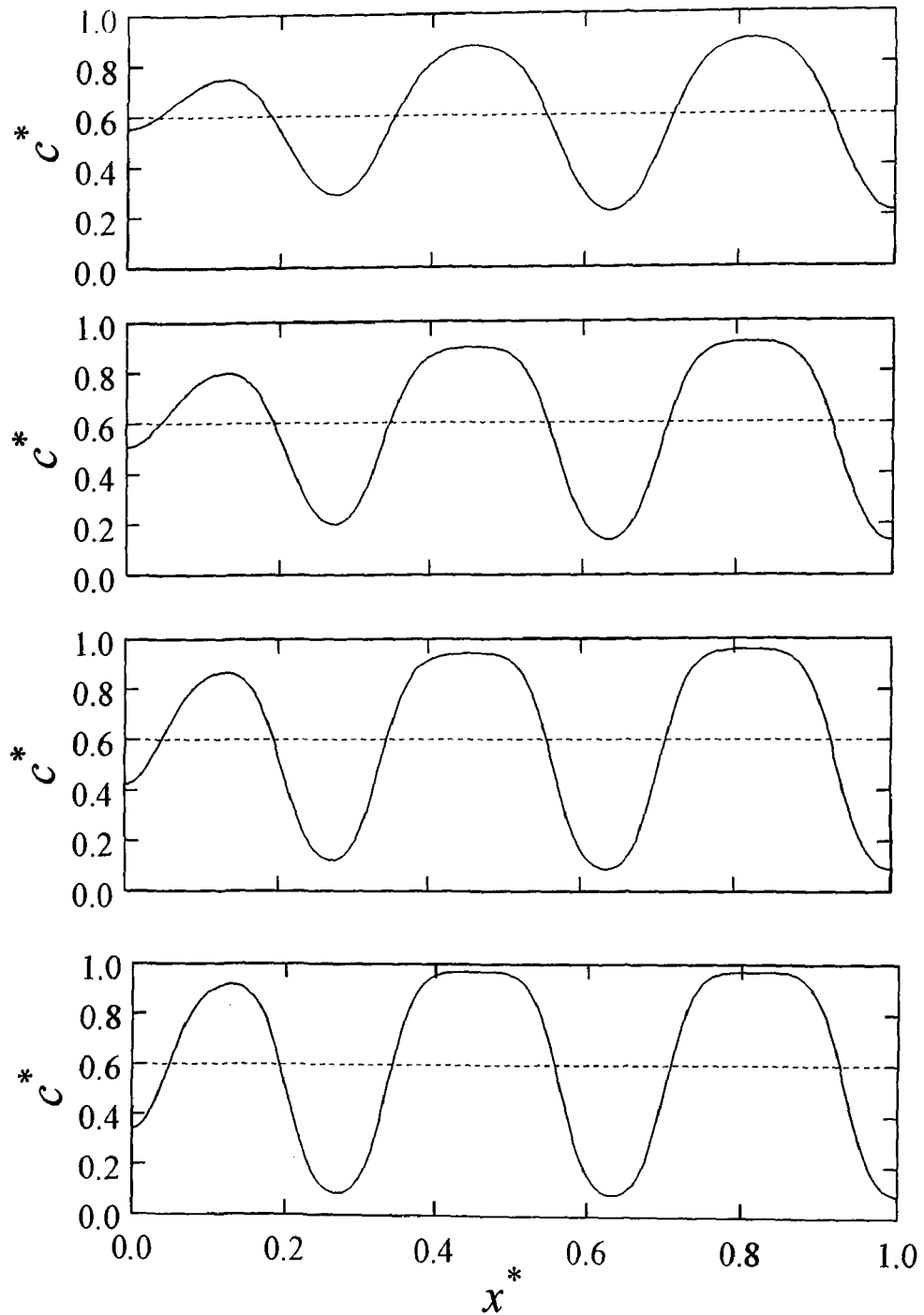


Figure 6.3: The evolution of the dimensionless spatial concentration profile for a double quench from $T_1^* = 0.25$ to $T_2^* = 0.2$ at the transition time of $t_t^* = 5.52$ at the following dimensionless times: (a) $t^* = 5.534$, (b) $t^* = 5.575$, (c) $t^* = 5.625$, and (d) $t^* = 5.671$. The dashed line through the center of the graph represents the initial average concentration $c_0^* = 0.6$. The dimensionless diffusion coefficient for this case is $D^* = 200\,000$.

amount of phase separation with increasing D^* . The same trends hold for D^* 500 000 and 800 000 shown in Appendix C.

Figure 6.5 shows the evolution of the dimensionless spatial concentration profiles (for the initial off-critical quench) after the second temperature jump to a deeper quench depth of $T_2^* = 0.1$ for the same transition times in Table 6.2. The initial temperature was kept constant at $T_1^* = 0.25$. The effect of making a deeper second quench showed noticeable obstructions on the concentration profiles in the peaks and troughs as in the case of the critical quench similar to the ones generated by Ohnaga *et al.* [1994]. The obstructions to the peaks of the composition fluctuations are larger compared to the critical quench case. The troughs in the composition profiles show almost no secondary obstructions. This is attributed to the location of the compositions in the phase diagram before the second quench is made and will be discussed later on. The lag times before the appearance of double phase separation after the second quench are 0.025, 0.0047, and 0.0017 for increasing D^* . This lag time decreases with increasing D^* . The lag times are larger for the initial off-critical quench than for the critical quench. This observation made for the single quench case and was shown to be dependent on the location of the quench as compared to the spinodal curve.

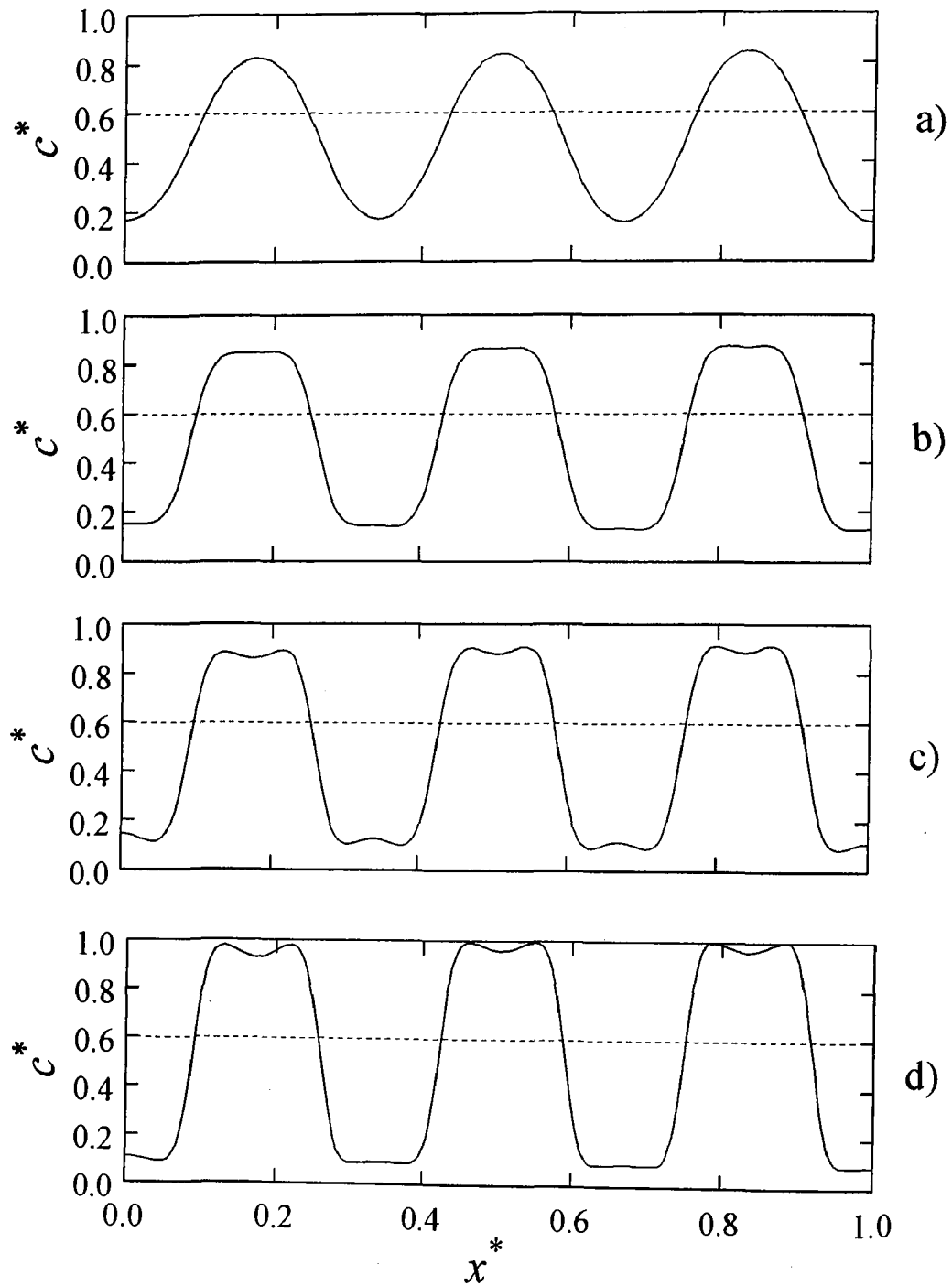


Figure 6.4: The evolution of the dimensionless spatial concentration profile for a double quench from $T_1^* = 0.25$ to $T_2^* = 0.1$ at the transition time of $t_i^* = 4.72$ at the following dimensionless times: (a) $t^* = 4.726$, (b) $t^* = 4.740$, (c) $t^* = 4.748$, and (d) $t^* = 4.769$. The dashed line through the center of the graph represents the initial average concentration $c_o^* = 0.5$. The numbers on top of the graph are used to identify the number of peaks for a dimensionless diffusion coefficient $D^* = 200\,000$.

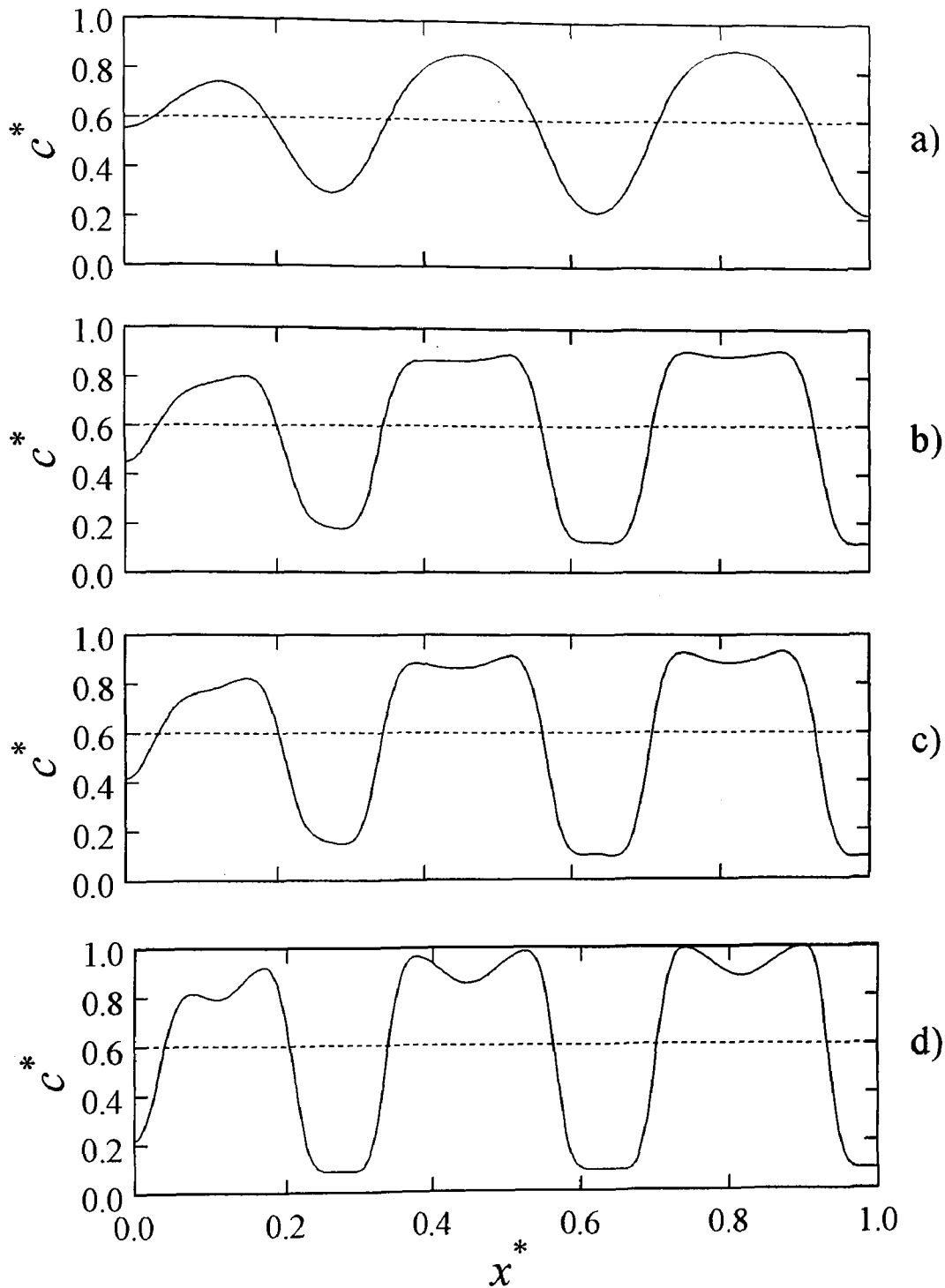


Figure 6.5: The evolution of the dimensionless spatial concentration profile for a double quench from $T_1^* = 0.25$ to $T_2^* = 0.1$ at the transition time of $t_t^* = 5.52$ at the following dimensionless times: (a) $t^* = 5.526$, (b) $t^* = 5.545$, (c) $t^* = 5.549$, and (d) $t^* = 5.565$. The dashed line through the center of the graph represents the initial average concentration $c_0^* = 0.6$. The dimensionless diffusion coefficient for this case is $D^* = 200\,000$.

6.3 The Evolution of the Dimensionless Structure Factor After the Second Temperature Jump

This section is split into two parts to describe the observations of the evolution of the dimensionless structure factor after the second quench to $T_2^* = 0.2$ and $T_2^* = 0.1$ for the initial critical and initial off-critical quench case. Analysis of the growth rates of the primary and secondary peaks (if they form) will be discussed in a later section. Here, the focus is on physical observations and relating what is observed here to the observations made for the evolution of the dimensionless spatial concentration profiles. The dimensionless structure factor is calculated in the same way as described in Chapter 5 for the single quench case. The evolution of the dimensionless structure factor for each case is shown right after the second quench is made at the specified dimensionless transition times in Table 6.2. Unfortunately, it was not possible to examine the entire process of the growth and decay of the secondary structures (when they occurred), which has been done experimentally, due to numerical problems encountered as the mixture reached the equilibrium compositions at T_2^* . Referring to Chapter 4, in the 1-D model, as $c^* \rightarrow 0$ and $c^* \rightarrow 1$ the terms in the model with $\frac{1}{c}$ and $\frac{1}{(1-c)}$ approached infinity respectively.

To relate the numerical results to experimental results, the numerical work should reflect the same evolution in pattern formation detailed in the structure factor as in the work of Hashimoto *et al.* [Hayashi *et al.*, 2000a] and in the 2-D numerical study by Henderson and Clarke [2004]. In the experimental work after the second

quench at a certain domain size formed from the first quench, there appeared a second broad peak that grew with time in the light scattering profile. This observation from the light scattering data was a result of the formation of secondary domains. The structure factor from the numerical work should also show the emergence and growth of a broad peak. Henderson and Clarke [2004] have observed the appearance and growth of a second broad peak in the evolution of the structure factor after a second quench at the late stages of phase separation by SD in their numerical study. This is the basis of comparison for the numerical work presented in the next two sections.

6.3.1 Second Temperature Jump to $T_2^* = 0.2$

Figure 6.6 shows the evolution of the dimensionless structure factor after the second quench to $T_2^* = 0.2$ from the initial critical quench at $T_1^* = 0.25$ for $D^* = 200\ 000$. Recall from the evolution of the concentration profiles for the initial critical quench, (Figures 6.2), after the second quench, the concentration profiles were amplified from the initial single quench profiles. There was no sign of double phase separation present and therefore, the growth of the structure factor should also show an increase in the intensity of the primary peak but no occurrence of a secondary peak forming. This result is in accordance to the definition of the structure factor (Chapter 5) and is observed in the evolution of the dimensionless structure factor for the initial critical quench case at all values of D^* investigated. A similar trend was observed experimentally in Hashimoto's work, where there was no appearance of the second broad peak in at the condition

of a smaller domain size before making the second temperature jump [Hayashi *et al.*, 2000a]. However, the difference in their work and the work presented here is that the dependent variable is the value of the second temperature jump that takes place and not the different domain sizes. Numerically, Henderson and Clarke [2004] also observed the same continuous growth for a shallow quench following Hashimoto's work. The reason that there is no occurrence of a second peak is because the quench depth at $T_2^* = 0.2$ was not significant enough to cause the mixture to destabilize in a secondary sense. This will be explained through the investigation of the change in the chemical potential and the second derivative of the free energy with respect to composition in a later section. A comparison of the structure factor presented here and for the single quench at $T_1^* = 0.25$ show the same values for k_{max}^* for each case, indicating that there is no change in the maximum value of the wave number which encompasses the dominant mode of the composition fluctuations, for the primary structures, in the early period of the second quench. The second quench does not have an effect on the maximum wave number of the primary structure, just the intensity of the phase separation process in the early period after the second quench. This is consistent with the work by Hayashi *et al.* [2000a] and Henderson and Clarke [2004]. In terms of the relative size of the phase-separated regions after the second quench, the information of constant k_{max}^* signifies that the primary structure does not change in size in the early period. Recall the relationship between k_{max}^* and dimensionless characteristic length which measures the relative size of the phase-separated domains, $\lambda^* = \frac{2\pi}{k_{max}^*}$. This observation is consistent with the

experimentally observed evolution of the light scattering data in the work by Hashimoto *et al.* [2000] when investigating the growth of the primary structure after the second quench. Furthermore, the growth of the dimensionless structure factor with time looks the same as for a single quench case in the early stages of SD. After the second quench, the growth of the dimensionless structure factor continues as if in the early stages of SD and proceeds to take the same course as a single quench into the intermediate stages (composition reaching the upper and lower equilibrium values). Hashimoto *et al.* [2000] also confirmed this experimentally for the case where no broad secondary peak was observed and only the primary peak continued to grow. Table 6.3 summarizes the values for the characteristic length for the critical quench at a second temperature jump of $T_2^* = 0.2$.

Figure 6.7 shows the evolution of the dimensionless structure factor after the second quench to $T_2^* = 0.2$ from the initial off-critical quench at $T_1^* = 0.25$ for $D^* = 200\,000$. In the off-critical quench case, the results are different from the evolution of the dimensionless structure factor observed for the critical quench case. There appears to be a secondary broad peak forming in the evolution of the dimensionless structure factor. In Figure 6.7, the peak is extremely small and broad. This small broad peak does not reflect in the evolution of the dimensionless spatial concentration profile in Figure 6.7 and a continuous increase of the original growth of the concentration fluctuations is observed. This secondary peak is more obvious and increases as D^* increases (see Figure C.11 and C.12 in Appendix C). The effect of increasing the dimensionless

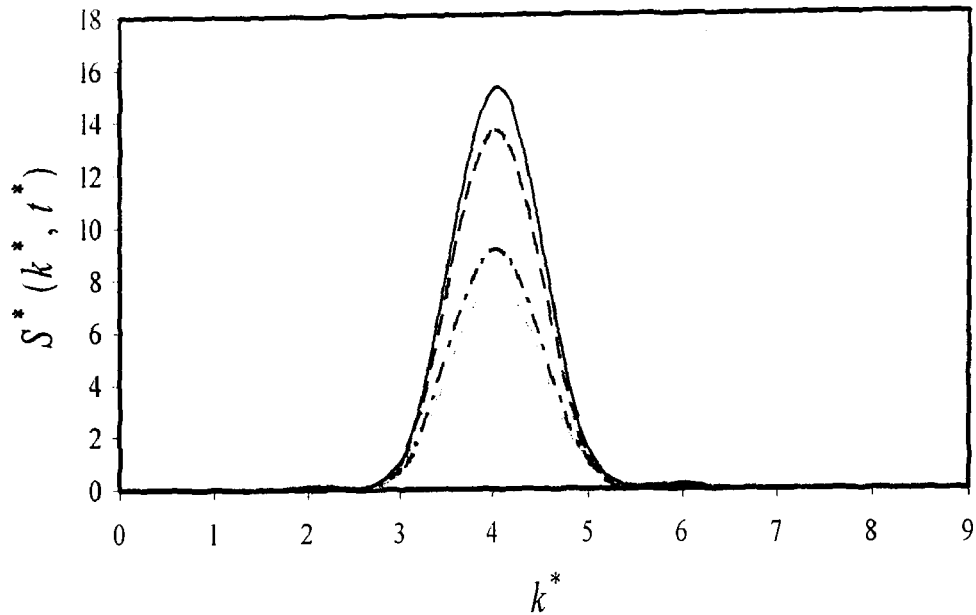


Figure 6.6: The evolution of the dimensionless structure factor for a double quench from $T_1^* = 0.25$ to $T_2^* = 0.2$ (second temperature jump made at transition time of $t_i^* = 4.72$) at the following dimensionless times: $t^* = 4.731$ (light grey solid line), $t^* = 4.745$ (dash-dot line), $t^* = 4.798$ (dashed line), and $t^* = 4.861$ (solid black line). The initial average concentration $c_o^* = 0.5$. The dimensionless diffusion coefficient is $D^* = 200\,000$.

diffusion coefficient (increasing the driving force for phase separation) with the second temperature jump causes the formation of the secondary peak for the initial off-critical quench case and will be discussed in a later section. The growth rate of the primary and secondary peaks is consistently increasing with time. How they grow relative to each other will be explored in a later section. Note that the appearance of a secondary peak was not sufficient enough to cause the mixture to develop secondary structures. However, small destructive interference was observed in the concentration profiles (see Figure C.3 and Figure C.4 in Appendix C). The structure factor for the double and single quench show the same values for k_{max}^* for each case, indicating that there is no change in the

maximum value of the wave number in the early period of the second quench. The second quench does not have an effect on the maximum wave number for the initial off-critical quench case either, just the intensity of the phase separation process in the early period after the second quench. The relative size of the primary phase-separated regions after the second quench does not change in size in the early period. The characteristic lengths of the primary and secondary peaks after a second quench to $T_2^* = 0.2$ for initial off-critical case are summarized below in Table 6.3.

In summary, the shallower second quench does not show secondary phase separation in the initial critical or off-critical quench case. There is only an amplification of the dimensionless structure factor. The maximum wave number remains constant with the same value as the initial quench case in the early period after the second quench.

6.3.2 Second Deeper Temperature Jump to $T_2^* = 0.1$

A deeper quench was made to test for secondary structure formation. Figure 6.8 shows the evolution of the dimensionless structure factor after the second quench to $T_2^* = 0.1$ from the initial critical quench at $T_1^* = 0.25$ for $D^* = 200\,000$. Recall that in the dimensionless spatial concentration profiles (Figures 6.4) for the initial critical quench at $T_1^* = 0.25$ and then to a second quench at $T_2^* = 0.1$, there was the appearance of constructive and destructive interferences. The interference patterns were more obvious in the evolution of the dimensionless spatial concentration profiles as the value of D^* increased (see Figures C.5 and C.6).

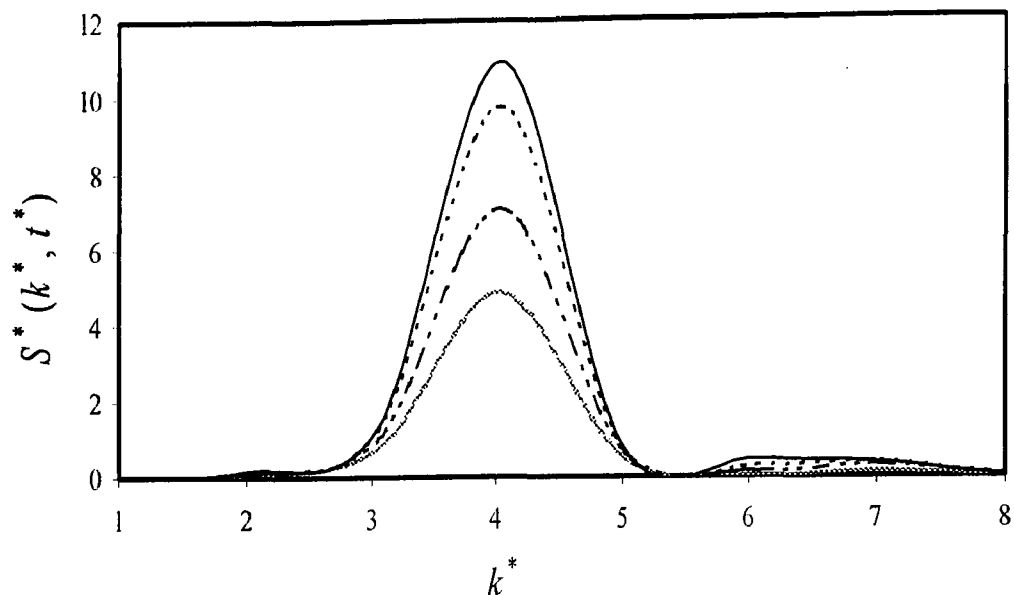


Figure 6.7: The evolution of the dimensionless structure factor for a double quench from $T_1^* = 0.25$ to $T_2^* = 0.2$ (second temperature jump made at a transition time of $t_i^* = 5.52$) at the following dimensionless times: $t^* = 5.534$ (light grey solid line), $t^* = 5.575$ (dash – two dots line), $t^* = 5.625$ (dotted line), and $t^* = 5.671$ (solid black line). The initial average concentration $c_o^* = 0.6$. The dimensionless diffusion coefficient for this case is $D^* = 200\,000$.

Table 6.3: Dimensionless characteristic lengths for the primary structures ($T_1^* = 0.25$) and the secondary peaks ($T_2^* = 0.2$) formed

Initial Quench	Parameter Temperature Jump from $T_1^* = 0.25$ to $T_2^* = 0.2$	λ_1^*	λ_2^*
Critical	$c_o^* = 0.5, D^* = 200\,000$	1.57	NA
	$c_o^* = 0.5, D^* = 500\,000$	1.047	NA
	$c_o^* = 0.5, D^* = 800\,000$	0.897	NA
Off-critical	$c_o^* = 0.6, D^* = 200\,000$	1.57	NA
	$c_o^* = 0.6, D^* = 500\,000$	1.256	0.698
	$c_o^* = 0.6, D^* = 800\,000$	0.897	0.523

These observations are in agreement with the evolution of the dimensionless structure factor. There are obvious secondary peaks that form right after the second quench at $T_2^* = 0.1$. In the profile, both the primary and the secondary peak grow with time. This reflects in the growth of the concentration fluctuations with time as the primary peaks and troughs start to approach the upper and lower equilibrium values and the secondary peaks and troughs start to increase in value as well at $T_2^* = 0.1$. Hayashi *et al.* [2000a] and Henderson and Clarke [2004] have observed the same effects to the growth of the structure factor when secondary structures form. Note that the intensity of the primary peak decreases with increasing D^* when comparing Figure 6.8 to Figure C.13 and C.14. This may be due to the fact that the formation and the increase in growth rate of the secondary peaks is affecting the growth of the primary peaks with time as it approaches the new equilibrium values at $T_2^* = 0.1$. Also, the value of the maximum wave number for the primary peak does not shift when the quench depth is lowered. There is only an increase in the intensity of the primary peak and the appearance and growth of a secondary peak. The interferences observed in the dimensionless spatial concentration profiles where secondary phase separation is observed can be explained by evaluating the dimensionless characteristic length, $\lambda^* = \frac{2\pi}{k_{\max}^*}$, which is equal to the wavelength of the dominant wave in SD. As k_{\max}^* gets larger (smaller), λ^* gets smaller (larger) and therefore, the result of adding the two wavelengths together from the initial quench and the second quench will cause the interferences in the concentration profiles. This explanation was also given by Ohnaga *et al.* [1989] and Yang *et*

al. [1998]. The characteristic lengths of the primary and secondary structures after a second quench to $T_2^* = 0.1$ for the critical case are summarized in Table 6.4. As the dimensionless diffusion coefficient increases, both the primary and secondary characteristic lengths decrease. This should be expected since D^* increases the amount of phase separation.

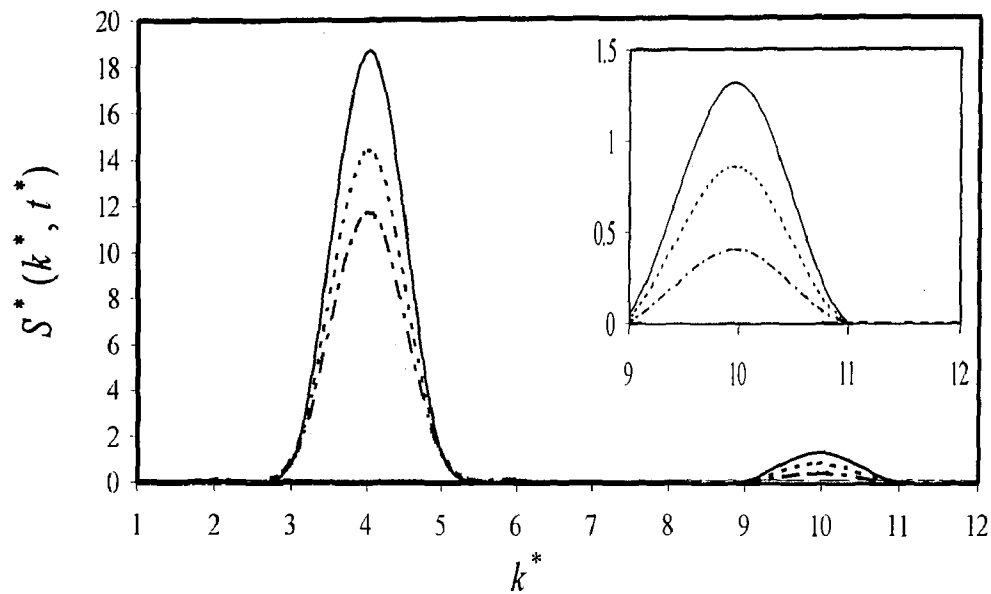


Figure 6.8: The evolution of the dimensionless spatial concentration profile for a double quench from $T^* = 0.25$ to $T^* = 0.1$ (at the transition time of $t_i^* = 4.72$) at the following dimensionless times: $t^* = 4.726$ (light grey line), $t^* = 4.740$ (dash-dot line), $t^* = 4.748$ (dotted line), and $t^* = 4.769$ (solid line). The initial average concentration $c_0^* = 0.5$. The dimensionless diffusion coefficient is $D^* = 200\,000$.

Figure 6.9 shows the evolution of the dimensionless structure factor after the second quench to $T_2^* = 0.1$ from the initial off-critical quench at $T_1^* = 0.25$ for $D^* = 200\,000$. Like the initial critical quench case, the dimensionless spatial concentration profiles in Figures 6.5 shows an increasing amount of constructive and destructive interferences for the initial off-critical quench case. These interferences increase as D^* increases (see Figures C.7 and C.8 in Appendix C).

In the evolution of the dimensionless structure factor, this is reflected in the formation of secondary peaks which can be observed to increase in intensity as D^* increases (see Figures C.15 and C.16). Comparing back to the case where the second quench was to $T_2^* = 0.2$, the intensity of the secondary peak is higher here for all three plots. This can be explained by comparing the location of the quench with respect to the spinodal at $T_2^* = 0.2$ as opposed to $T_2^* = 0.1$ and will be examined in the next section on quench depth and double phase separation. The value of the maximum wave number for the off-critical initial quench and for the second quench does not change for the primary peak in the structure factor plots even with a deeper quench. The characteristic lengths of the primary and secondary structures after a second quench to $T_2^* = 0.1$ for the off-critical case are summarized in Table 6.4. The characteristic lengths also decrease with increasing D^* as in the critical quench case.

Overall, the same trends hold for the initial critical and off-critical quench case in the evolution of the dimensionless structure factor after the second deeper quench. The deeper second quench shows secondary phase separation with the formation and growth of a secondary peak. The primary peak also grows after the second quench in intensity but the maximum wave number remains constant in the early period after the second temperature jump.

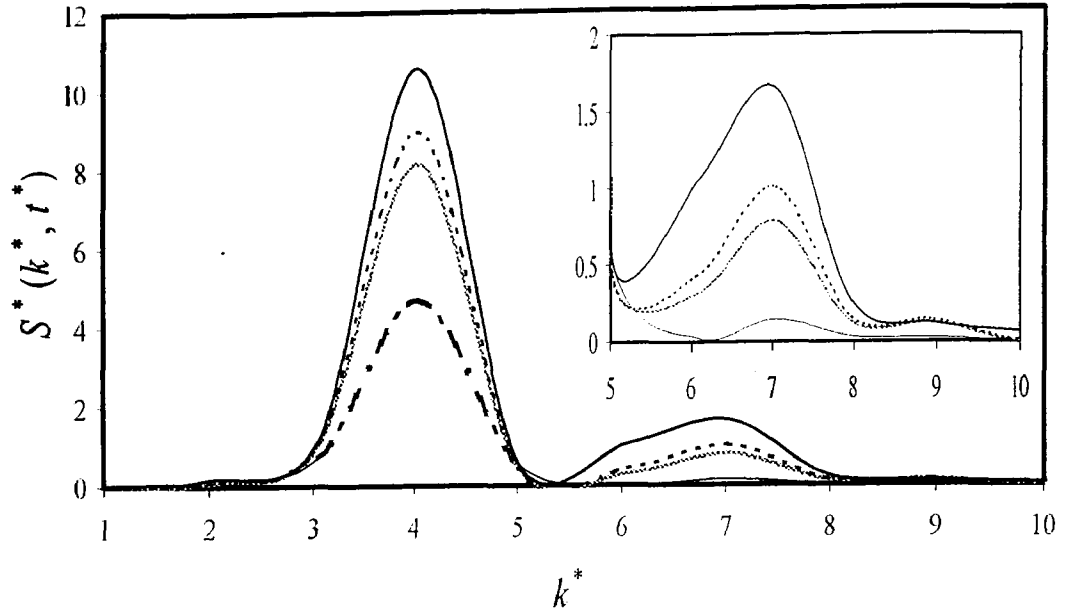


Figure 6.9: The evolution of the dimensionless spatial concentration profile for a double quench from $T_1^* = 0.25$ to $T_2^* = 0.1$ (at the transition time of $t_t^* = 5.52$) at the following dimensionless times: $t^* = 5.526$ (dash-dot line), $t^* = 5.545$ (light grey line), $t^* = 5.549$ (dotted line), and $t^* = 5.565$ (solid line). The dashed line through the center of the graph represents the initial average concentration $c_o^* = 0.6$. The dimensionless diffusion coefficient for this case is $D^* = 200\,000$.

Table 6.4: Dimensionless characteristic lengths for the primary structures ($T_1^* = 0.25$) and the secondary structures ($T_2^* = 0.1$) formed upon further quenching from after the determined dimensionless transition times.

Initial quench	Parameter Temperature jump from $T_1^* = 0.25$ to $T_2^* = 0.1$	λ_1^*	λ_2^*
Critical	$c_o^* = 0.5, D^* = 200\,000$	1.57	0.628
	$c_o^* = 0.5, D^* = 500\,000$	1.047	0.393
	$c_o^* = 0.5, D^* = 800\,000$	0.897	0.349
Off-critical	$c_o^* = 0.6, D^* = 200\,000$	1.57	0.897
	$c_o^* = 0.6, D^* = 500\,000$	1.256	0.698
	$c_o^* = 0.6, D^* = 800\,000$	0.897	0.523

6.4 Quench Depth and Secondary Phase Separation

The dimensionless spatial concentration profiles for the shallower and deeper second quench showed a difference in the evolution of phase separation. At the second jump of $T_2^* = 0.2$, the evolution of the spatial concentration profiles were amplified from the original quench at $T_1^* = 0.25$, eventually approaching the new equilibrium values at the second temperature. At the second jump of $T_2^* = 0.1$, the evolution of the spatial concentration profiles showed the formation of troughs (crests) within the crests (troughs) of the original phase separating profile. This change in the concentration profile can be attributed to the formation of the secondary phase separated regions. Also, for the initial off-critical quench, after the second jump to $T_2^* = 0.1$, the obstructions were more evident in the peaks of the composition fluctuations rather than at the troughs. To examine why these differences occur in the dynamics of phase separation between the two quench depths requires examining the phase diagram. The quench depths are $T_{q,c}^* = 0.13295$ for the shallower quench and $T_{q,c}^* = 0.2330$ for the deeper quench. Figure 6.10 shows the phase diagram for the symmetrical blend studied showing the specific regions of interest for the two quench depths at the critical and the off-critical quench case using the case where $D^* = 500\,000$ to explain the observations (see Figure B.1 and Figure B.3 in Appendix B). The same trends hold for the other values of D^* . This provides information about the mechanism of phase separation. Tanaka [1993] proposed similar mechanisms where by the

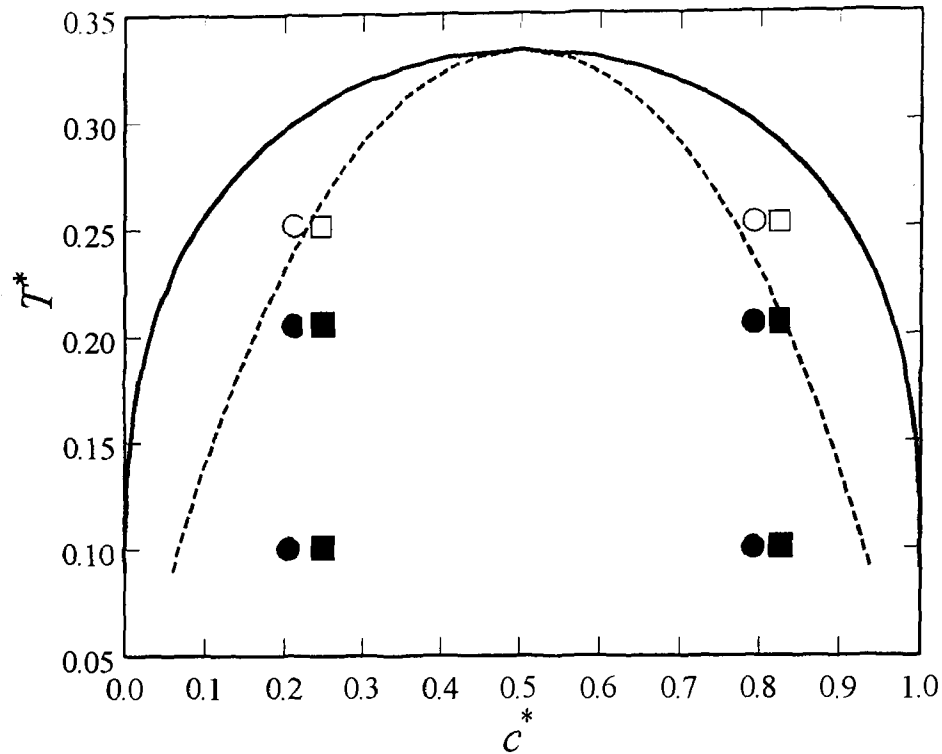


Figure 6.10: A model symmetrical phase diagram for a polymer blend of degree of polymerization $N_1 = N_2 = 1000$. The two open triangles represent the locations of investigation (a critical $c_o^* = 0.5$ and off-critical $c_o^* = 0.6$ quench) at the initial dimensionless temperature jump of $T_1^* = 0.25$ with $D^* = 500\,000$. The open circles represent the locations of the phase separating system when it has reached the transition time $t_i^* = 0.65$ (critical quench) and the open squares represent the phase separating system when it has reached the transition time $t_i^* = 0.903$ (off-critical quench) where the second temperature jump is made. The filled circles show the location of the system at the start of the second shallower temperature jump ($T^* = 0.2$) and the deeper temperature jump ($T^* = 0.1$) for the critical quench case. The filled squares show the location of the system at the start of the second shallower temperature jump ($T^* = 0.2$) and the deeper temperature jump ($T^* = 0.1$) for the off-critical quench case.

location of the compositions before and after the second quench made a significant impact on the formation of secondary phase-separated regions.

In Figure 6.10, the unfilled triangles denote the locations of the initial critical and off-critical quench compositions at $T_1^* = 0.25$. The unfilled circles represent the

compositions of polymer 1 right before the second quench is made to $T_2^* = 0.2$ and $T_2^* = 0.1$ for the initial critical quench. The unfilled squares represent the compositions of polymer 1 right before the second quench is made to $T_2^* = 0.2$ and $T_2^* = 0.1$ for the initial off-critical quench. The filled circles and squares then represent the position of the initial composition for the second quench within the phase diagram for each temperature jump ($T_2^* = 0.2$ and $T_2^* = 0.1$). From the phase diagram, two distinct observations can be made. First, the locations of the compositions for the critical and the off-critical quench at the transition times are slightly different. For the critical quench, the two phase-separated compositions are equidistant from the initial value of 0.5 and are located at approximately the same locations on opposite ends close to the spinodal line. For the off-critical quench case, the two phase-separated compositions are shifted in that one is still located within the spinodal while the other is located beyond the spinodal into the meta-stable region. The second observation is the new location of the composition in the phase diagram after the jump to the second temperature in relation to the position of the spinodal curve (filled circles and squares). For the shallower second quench ($T_{Q_2}^* = 0.13295$), the location of the initial starting point at $T_2^* = 0.2$ is much closer to the spinodal curve for both the critical and the off-critical quench case than compared to the quench at $T_2^* = 0.1$. Recall from Chapter 3 that the location of the spinodal points are at the inflection points ($\frac{\partial^2 F}{\partial c^2} = 0$) in the change in free energy curve. At these points, there is no influence on the composition fluctuations to overcome energy barriers or to drive

phase separation by SD. These two observations can be used to explain differences in the interferences in the spatial concentration profiles for the initial off-critical quench case, at a second temperature jump of $T_2^* = 0.1$, where the peak positions have more obstructions than at the trough positions. Because there is this difference in the locations of the composition for the second quench, the instability at each composition is different and therefore, the difference in the intensity of the obstructions observed. In terms of the two quench depths, it is known that the driving force for phase separation is directly related to the distance of the temperature within the confines of the spinodal curve [Tao *et al.*, 1995]. For the second quench made not too far from the spinodal curve at $T_2^* = 0.2$ there will be a smaller driving force for phase separation. A deeper quench to $T_2^* = 0.1$ has a larger driving force (further inward into the unstable region) where a new instability is observed and double phase separation occurs. Therefore, the deeper the quench depth and the further inward it is into the unstable region, the more likely a new instability will occur and cause double phase separation. Perhaps there is a critical quench depth that must be attained before a new instability will form and cause double phase separation. To investigate this, more simulations will have to be performed and is beyond the scope of this thesis.

6.5 Change in the Dimensionless Spatial Chemical Potential and the Second Derivative of Free Energy For Double Quenching

Figure 6.11 and Figure 6.12 show the evolution of the dimensionless spatial chemical potential after the second quench to $T_2^* = 0.2$ at the transition time

corresponding to $D^* = 200\,000$ for the initial critical and initial off-critical quench case, respectively. Recall, the diffusional flux within the governing equation that describes phase separation by SD contains the thermodynamic driving force, the change in the chemical potential, for the binary polymer mixture. Diffusion occurs to minimize the free energy and therefore, as the mixture separates and approaches equilibrium, the gradient in the free energy (change in the chemical potential) should eventually approach zero, as defined in Chapter 3,

$$\frac{\partial F}{\partial c_i} = (\mu_i^{(1)} - \mu_i^{(2)}) = 0. \quad \text{In Figure 6.11 and Figure 6.12, after the second}$$

temperature jump, the same trends are observed. The only difference is the rate at which the blend approaches stability because of the difference in the values of D^* (see Figures C.17 and C.20 in Appendix C). The profiles look the same as the ones observed for a single quench. However, the rate of change in the chemical potential is much faster than in the single quench case because of the increased quench depth. There are regions where $\Delta\mu_1^*$ increases with increasing dimensionless time to a local maximum and regions where $\Delta\mu_1^*$ decreases with increasing dimensionless time to a local minimum. As the composition fluctuations approach the new upper and lower equilibrium values after the second quench, the change in the dimensionless chemical potential plateaus before it starts to move towards equilibrium. At the local minimum positions, when the blend is stabilizing and at the limit when c^* approaches 1 (rich in polymer 1), $\Delta\mu_1^* = 0$, meaning the chemical potential of polymer 1 in the mixture, $\mu_{1\,mix}^*$, equals the value of the pure component, $\mu_{1\,pure}^*$. At the positions of

the local maximums, the composition of polymer 1 approaches the lower equilibrium value and these regions are rich in polymer 2. Eventually, the local maximum values will decrease and $\Delta\mu_1^*$ will approach zero. This being the condition for equilibrium where the change in the chemical potential of the coexisting phases becomes equal [Van Dijk and Wakker, 1997].

Figures 6.13 and Figure 6.14 show the evolution of the dimensionless spatial chemical potential after the second deeper quench to $T_2^* = 0.1$ (at the transition times corresponding to $D^* = 200\ 000$) for the initial critical and initial off-critical quench case, respectively. For $D^* = 500\ 000$ and $800\ 000$ refer to Figures C.21 to C.24. The profiles after the second temperature jump show the same trends but are slightly different than the shallower second quench case. $\Delta\mu_1^*$ shows a plateau after the second quench and flattens out at the local maxima and minima. The flattening of the local maxima and minima can be attributed to the adjusting of the blend to the change in quench conditions. The introduction of the smaller obstructions that are occurring within the peaks and troughs of the concentration profiles are new instabilities and create a small change in the chemical potential around the local maxima and minima, hence, the flattening at these areas. If allowed to proceed further, until the secondary phase separation disappears (merging with the primary structures), the change in the dimensionless spatial chemical potential should follow the same trend as observed for the shallower second quench case. As the secondary phase separation occurs, the primary peaks and troughs approach the new equilibrium values and the chemical

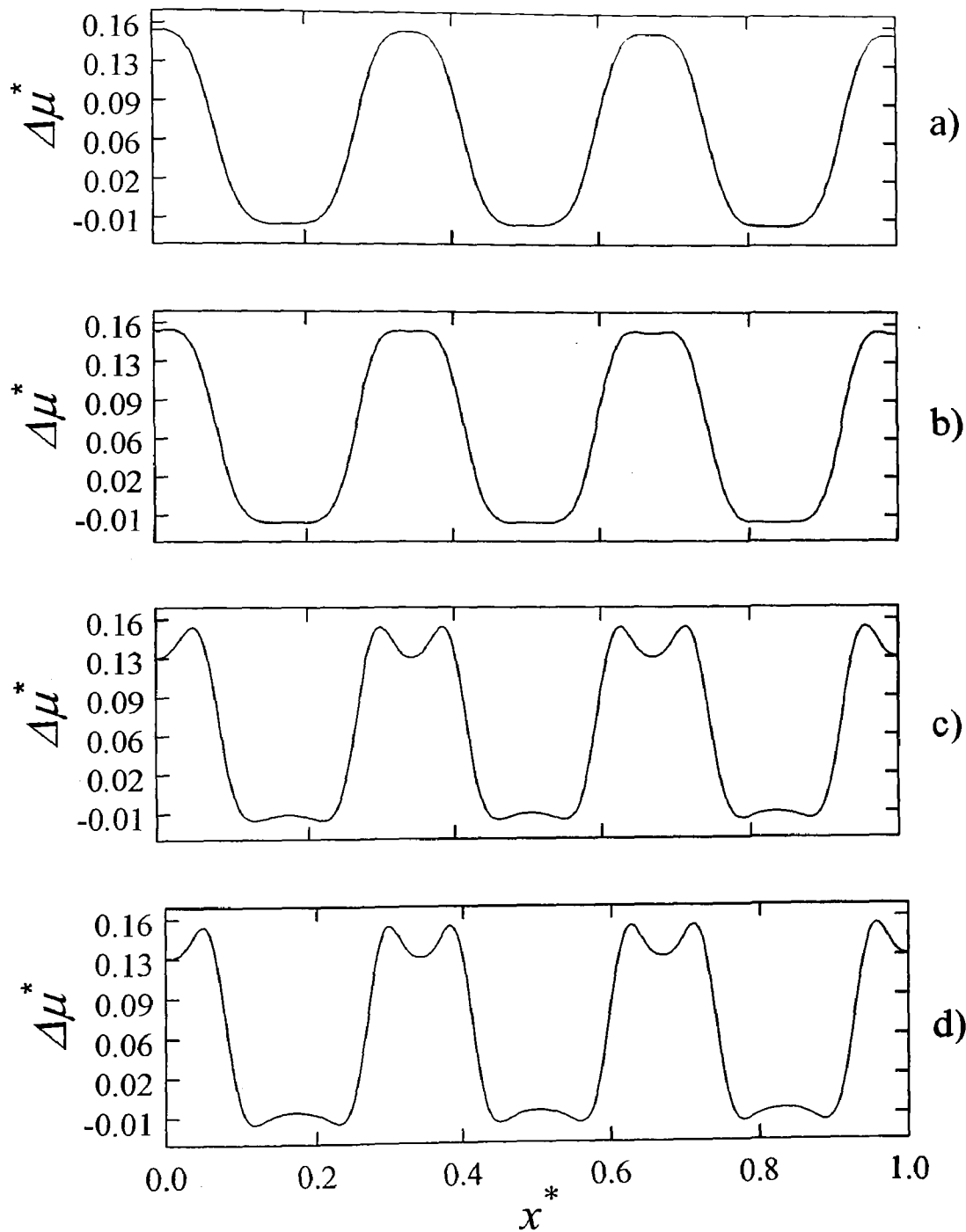


Figure 6.11: The evolution of the change in the dimensionless spatial chemical potential for a double quench from $T_1^* = 0.25$ to $T_2^* = 0.2$ at the transition time of $t_i^* = 4.72$ at the following dimensionless times: (a) $t^* = 4.731$, (b) $t^* = 4.745$, (c) $t^* = 4.798$, and (d) $t^* = 4.861$. The change in the dimensionless chemical potential is defined as the difference between the chemical potential polymer 1 in the mixture to that of its pure phase. The dimensionless initial concentration is $c_o^* = 0.5$ and the dimensionless diffusion coefficient is $D^* = 200\,000$.

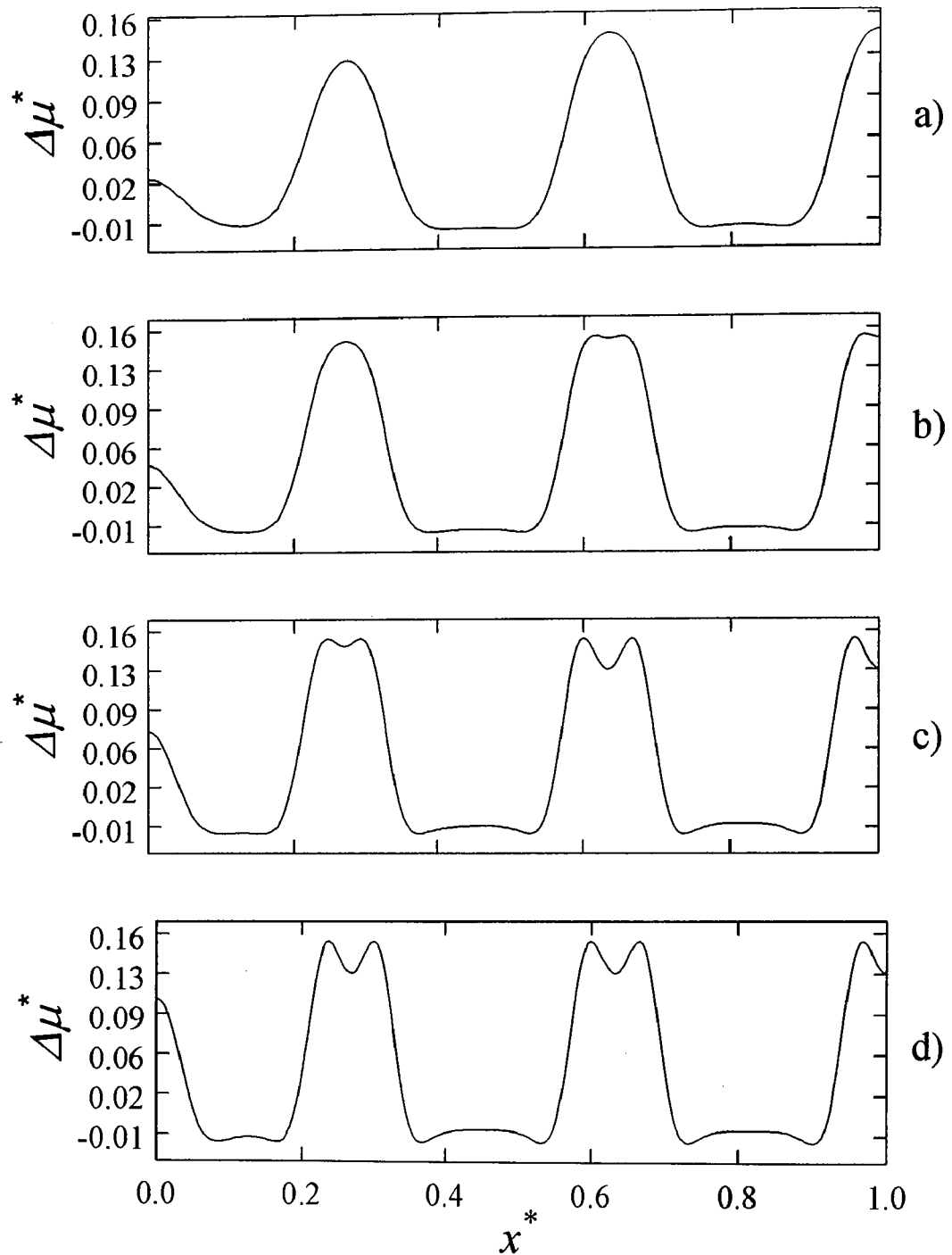


Figure 6.12: The evolution of the change in the dimensionless spatial chemical potential for a double quench from $T_1^* = 0.25$ to $T_2^* = 0.2$ at the transition time of $t_i^* = 5.52$ at the following dimensionless times: (a) $t^* = 5.534$, (b) $t^* = 5.575$, (c) $t^* = 5.625$, and (d) $t^* = 5.671$. The change in the dimensionless chemical potential is defined as the difference between the chemical potential polymer 1 in the mixture to that of its pure phase. The dimensionless initial concentration is $c_0^* = 0.6$ and the dimensionless diffusion coefficient is $D^* = 200\,000$.

potential of polymer 1 in the mixture, μ_1^* approaches the value of the pure component, $\mu_1^*_{pure}$ and $\Delta\mu_1^*$ approaches zero.

Figures 6.15 and 6.16 show the evolution of the second derivative of the free energy with respect to composition spatially after the second quench to $T_2^* = 0.2$ from the initial critical and off-critical quench, respectively. Recall in the unstable region, infinitesimally small composition fluctuations are enough to create instability. The second derivative of free energy with respect to composition determines the drive of the composition fluctuations around the inflection ($\frac{\partial^2 F}{\partial c^2} = 0$) points where $\frac{\partial^2 F}{\partial c^2} > 0$ stability or meta-stability are possible and $\frac{\partial^2 F}{\partial c^2} < 0$ results in instability for the binary mixture. The curvature of the second derivative of free energy with respect to composition can then detail the degree of stability, alongside the knowledge of the first derivative of free energy with respect to composition, with concave downwards (local maximum) being unstable and concave upwards (local minimum) can be meta-stable or stable. The additional increase in the free energy and thus the amount of instability will depend on how far away the system is from the spinodal curve. From the plots of the second derivative of the free energy with respect to composition for the initial critical and initial off-critical quench case, second quench where the impact of the second quench has not fully affected the phase separation rate of the mixture (adjustments to new conditions take into effect). There is a significant increase in the steepness of the curve after the second temperature jump and this increase in

the steepness (increasing the thermodynamic driving force Figures C.25 to C.28) then results in the amplification of the phase separation occurring in the composition profiles where the initial primary fluctuations are amplified and approach the new equilibrium values at the second temperature.

Figures 6.17 and Figures 6.18 show the evolution of the second derivative of the free energy with respect to composition spatially after the second deeper quench to $T_2^* = 0.1$ from the initial critical and off-critical quench, respectively. For the deeper quench, the profiles show the same trend for the second derivative of the free energy with respect to composition for the initial critical and initial off-critical quench case. The second derivative of free energy with respect to composition in this case looks much different than the plots for the shallower quench case. Notice that shortly after the second deeper jump there is a dip in the local maximums and gradually grows. In the local minimums, shortly after the second jump, the emergence and growth of a peak occurs and further divides into a double well shape. The formation of this new double well within the already existing double well becomes more defined as D^* is increased (see Figures C.29 to C.32). This new double well can account for the new instability that occurs when secondary phase separated regions form. The steepness of the curve after the second temperature jump increases (increasing the thermodynamic driving force) in both double well-shaped instabilities. This reflects in the shorter time periods taken for the primary composition fluctuations from $T_1^* = 0.25$ to reach the new equilibrium values at $T_2^* = 0.1$ and for the growing of the new secondary structures. This additional increase in the free energy relating to distance

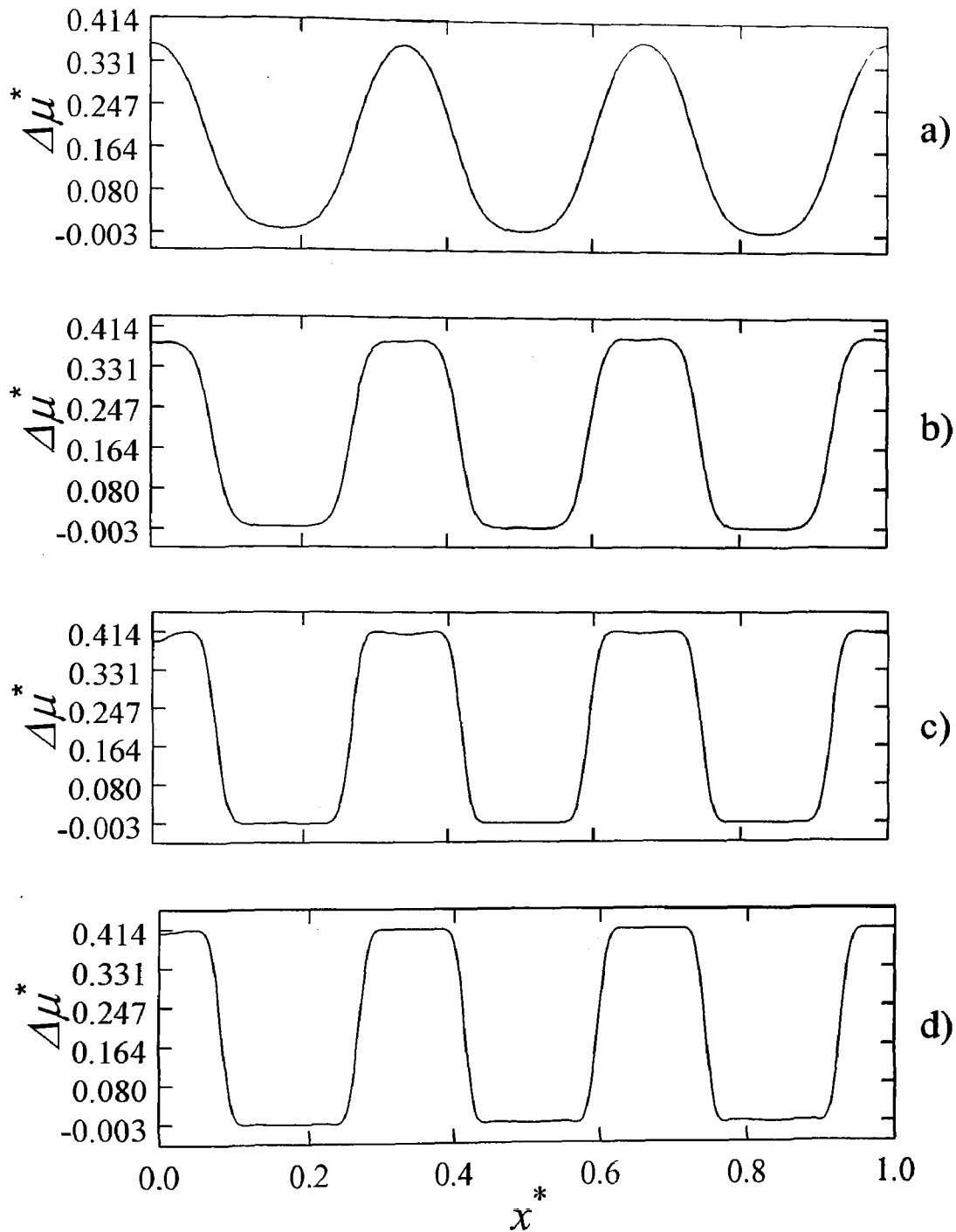


Figure 6.13: The evolution of the change in the dimensionless spatial chemical potential for a double quench from $T_1^* = 0.25$ to $T_2^* = 0.1$ at the transition time of $t_i^* = 4.72$ at the following dimensionless times: (a) $t^* = 4.726$, (b) $t^* = 4.740$, (c) $t^* = 4.748$, and (d) $t^* = 4.769$. The change in the dimensionless chemical potential is defined as the difference between the chemical potential polymer 1 in the mixture to that of its pure phase. The dimensionless initial concentration is $c_o^* = 0.5$ and the dimensionless diffusion coefficient is $D^* = 200\,000$.

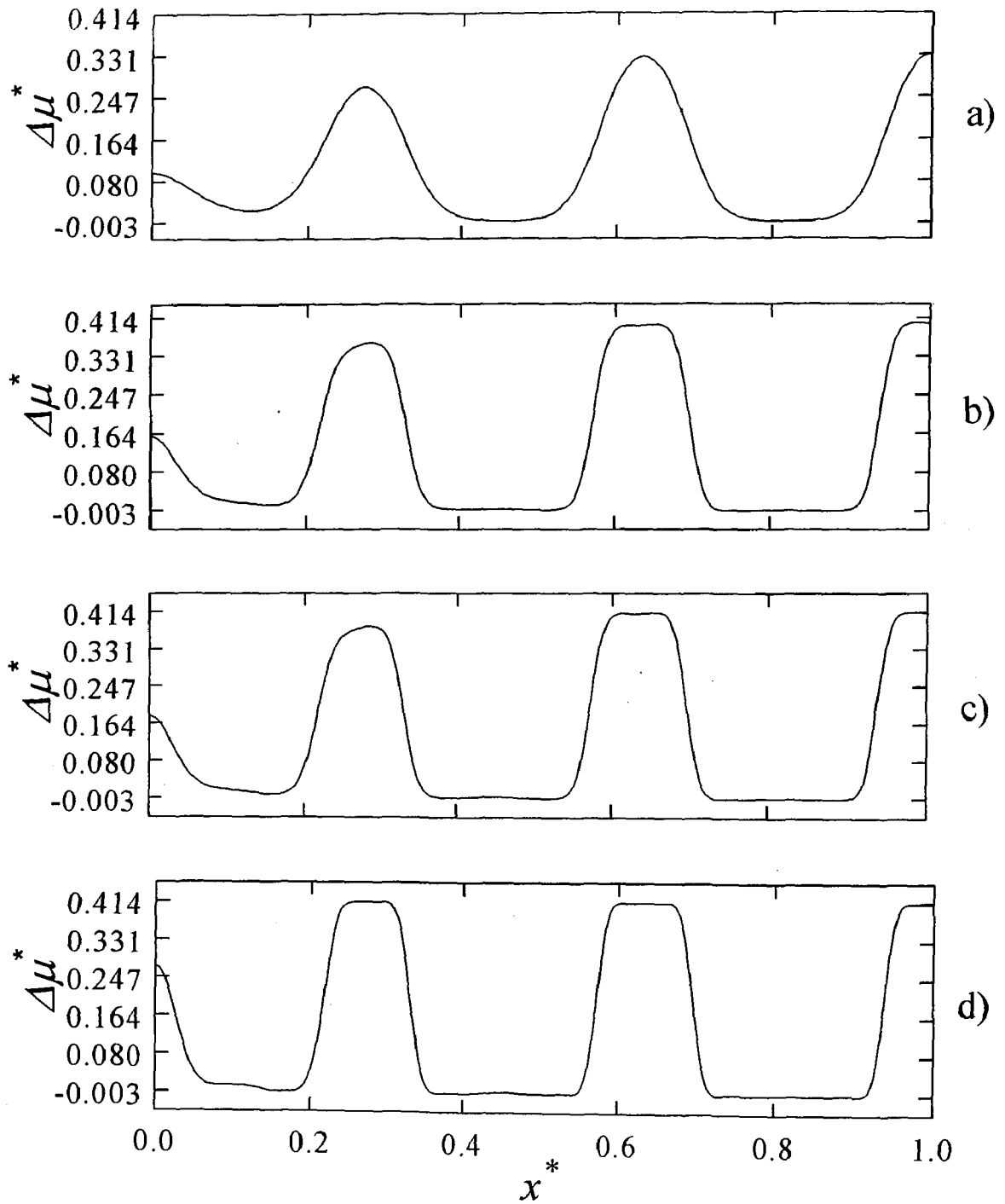


Figure 6.14: The evolution of the change in the dimensionless spatial chemical potential for a double quench from $T_1^* = 0.25$ to $T_2^* = 0.1$ at the transition time of $t_i^* = 5.52$ at the following dimensionless times: (a) $t^* = 5.526$, (b) $t^* = 5.545$, (c) $t^* = 5.549$, and (d) $t^* = 5.565$. The change in the dimensionless chemical potential is defined as the difference between the chemical potential polymer 1 in the mixture to that of its pure phase. The dimensionless initial concentration is $c_0^* = 0.6$ and the dimensionless diffusion coefficient is $D^* = 200\,000$.

from the spinodal curve shows that there exists a point where the instability crosses over from just a further amplification of the composition fluctuations to creating a new instability that renders new fluctuation patterns.

6.6 Growth of Primary Structures After the Second Temperature Jump to $T_2^* = 0.2$

Earlier on in the discussion of the shallower quench from $T_1^* = 0.25$ to $T_2^* = 0.2$, the dimensionless structure factor from the original quench grew with time and at the same constant wave number as at $T_1^* = 0.25$. How the second quench affected the growth rate of the primary and the secondary structures (if formed) was not discussed. In this section the analysis will be on the affect of the second quench on the growth rates of the maximum values of the primary and secondary structure factors (peak values) formed during phase separation by SD. The growth rate of the maximum value of the structure factor after the second quench is plotted against a reduced time, t_R^* , which is defined as [Hashimoto *et al.*, 1986a; Chan, 1998]:

$$t_R^* = \frac{t^*}{t_i^*} \tag{6.1}$$

The reduced time is used so that a general analysis can be made over all the different transition times used from Table 6.2. The maximum values of the dimensionless structure factors remain unchanged. Figure 6.19 shows the growth of the maximum value of the dimensionless structure factor with dimensionless reduced time after the second shallower quench for the initial critical quench case.

The values plotted are taken right after the second quench is made and there are three regions that can be identified for the growth of the primary structure. In the stage I, right after the second quench, there is a steady increase in the growth rate, meaning that the primary structures are further separating as the new conditions are imposed, $T_2^* = 0.2$. Stage I can also be considered the early stages of SD at the primary structure is slowing down and there is a slight dip in the growth rate before it starts to increase again into stage III. The growth rate is nonlinear and can be attributed to the change in the composition fluctuations towards the new equilibrium values at $T_2^* = 0.2$. In this stage, the blend is adjusting to the new conditions while still phase separating. Finally, in stage III the growth rate increases again and plateaus as the blend has reached the new equilibrium values at the new conditions. The evolution of the growth of the dimensionless structure factor is very similar to the plot for the single critical quench case shown in Figure 6.1 where the dimensionless transition time was determined. The difference in the profiles lies in stage II where the composition starts to adjust to the new conditions of the second quench before further separating into their respective phases. The late stages of phase separation was not examined for the single quench case because the interest was in forming the phase separated morphology and not to examine the coarsening dynamics. Overall, the three stages in the growth rate of the maximum value of the dimensionless structure factor after the second quench takes roughly the same form as a single quench case when there is no appearance of the secondary peak and only an amplification of the primary peak from the initial critical quench. As D^* increase, the same

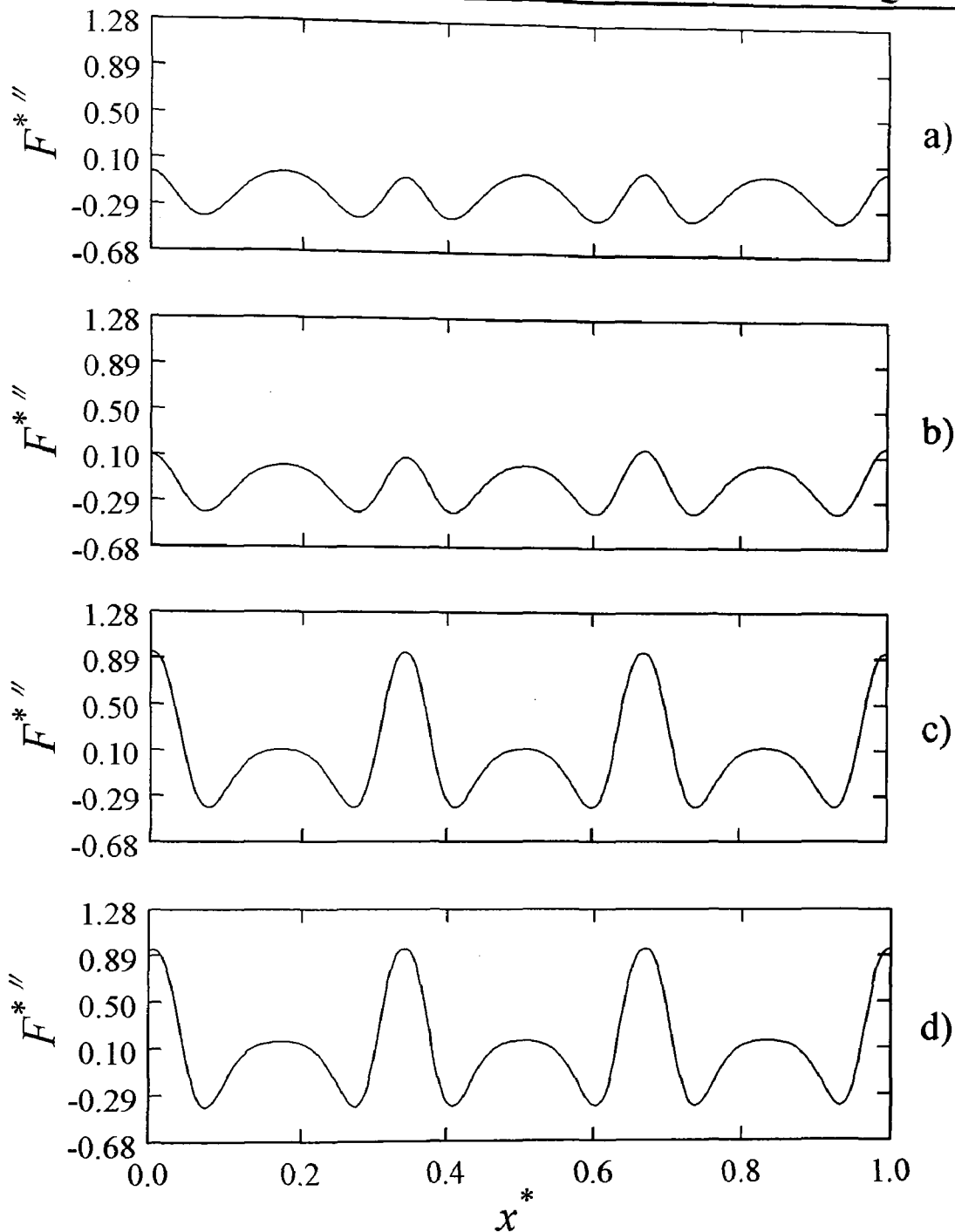


Figure 6.15: The evolution of the change in the dimensionless spatial second derivative of the free energy with respect to composition of component 1 for a double quench from $T_1^* = 0.25$ to $T_2^* = 0.2$ at the transition time of $t_i^* = 4.72$ at the following dimensionless times: (a) $t^* = 4.731$, (b) $t^* = 4.745$, (c) $t^* = 4.798$, and (d) $t^* = 4.861$. The change in the dimensionless second derivative of free energy is used to determine the conditions of stability ($F^{*''} > 0$), meta-stability ($F^{*''} > 0$), and instability ($F^{*''} < 0$). The dimensionless initial concentration is $c_0^* = 0.5$ and the dimensionless diffusion coefficient is $D^* = 200\,000$.

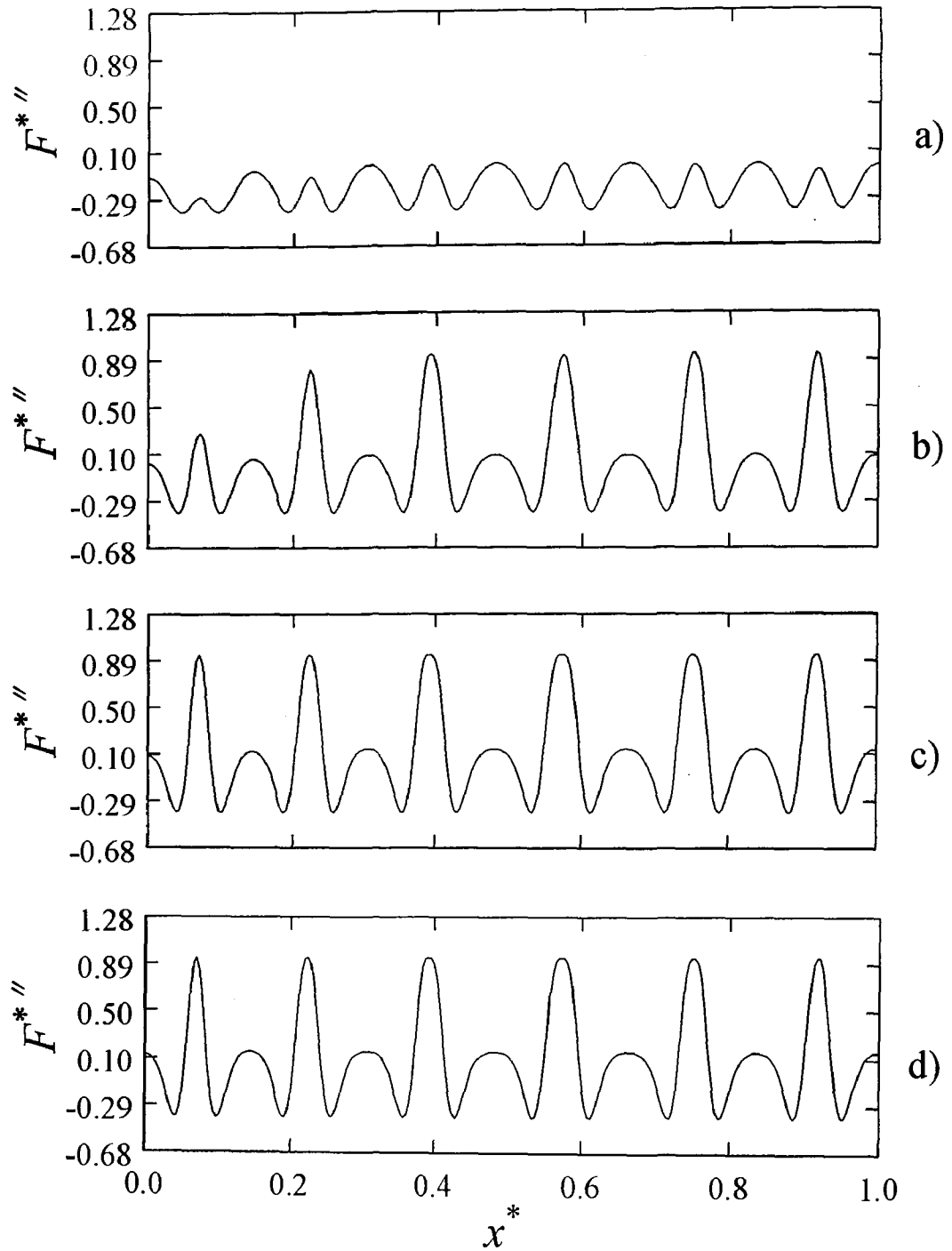


Figure 6.16: The evolution of the change in the dimensionless spatial second derivative of the free energy with respect to composition of component 1 for a double quench from $T_1^* = 0.25$ to $T_2^* = 0.2$ at the transition time of $t_t^* = 5.52$ at the following dimensionless times: (a) $t^* = 5.534$, (b) $t^* = 5.575$, (c) $t^* = 5.625$, and (d) $t^* = 5.671$. The change in the dimensionless second derivative of free energy is used to determine the conditions of stability ($F^{**} > 0$), meta-stability ($F^{**} > 0$), and instability ($F^{**} < 0$). The dimensionless initial concentration is $c_0^* = 0.6$ and the dimensionless diffusion coefficient is $D^* = 200\,000$.

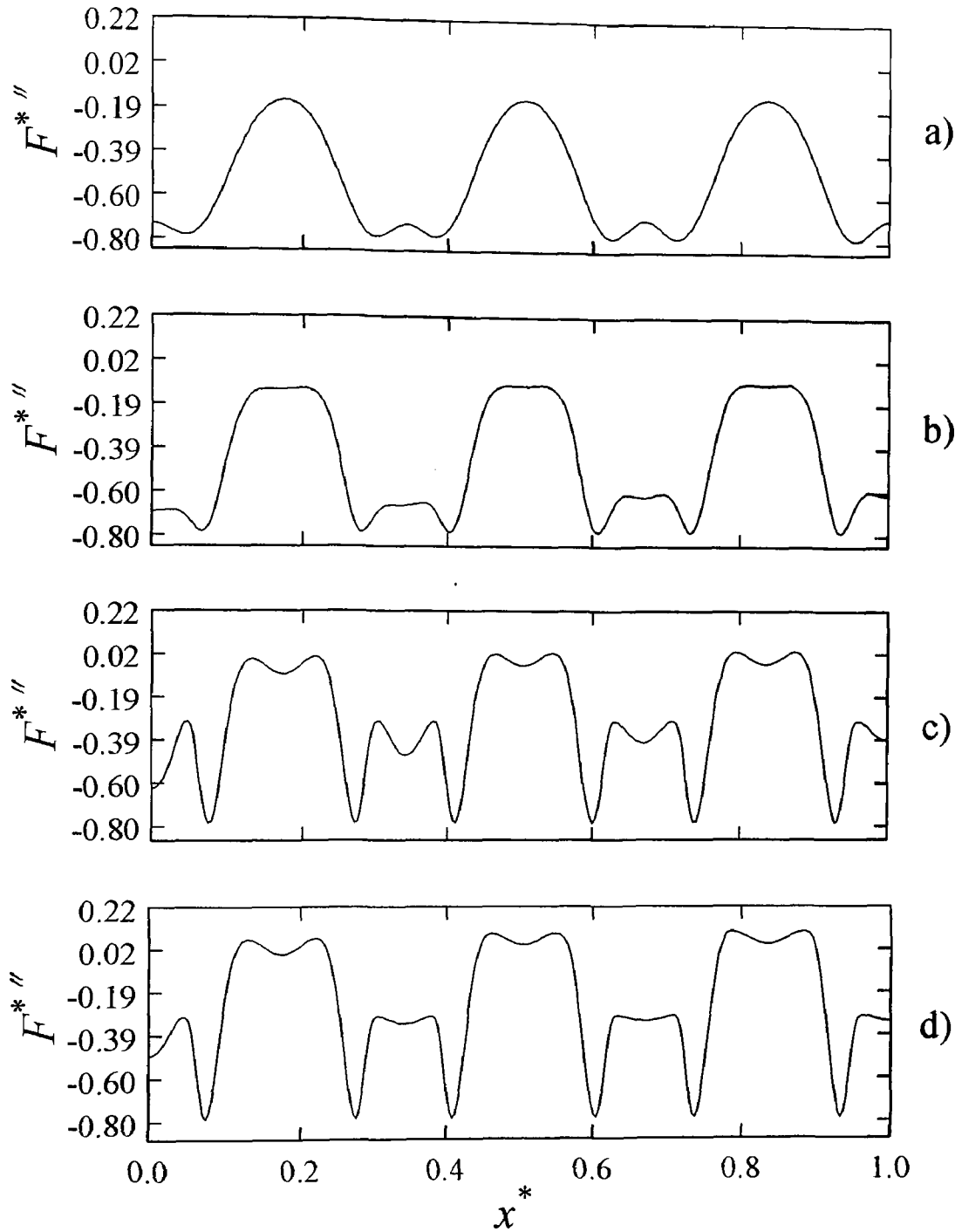


Figure 6.17: The evolution of the change in the dimensionless spatial second derivative of the free energy with respect to composition of component 1 for a double quench from $T_1^* = 0.25$ to $T_2^* = 0.1$ at the transition time of $t_t^* = 4.72$ at the following dimensionless times: (a) $t^* = 4.726$, (b) $t^* = 4.740$, (c) $t^* = 4.748$, and (d) $t^* = 4.769$. The change in the dimensionless second derivative of free energy is used to determine the conditions of stability ($F^{*''} > 0$), meta-stability ($F^{*''} > 0$), and instability ($F^{*''} < 0$). The dimensionless initial concentration is $c_0^* = 0.5$ and the dimensionless diffusion coefficient is $D^* = 200\,000$.

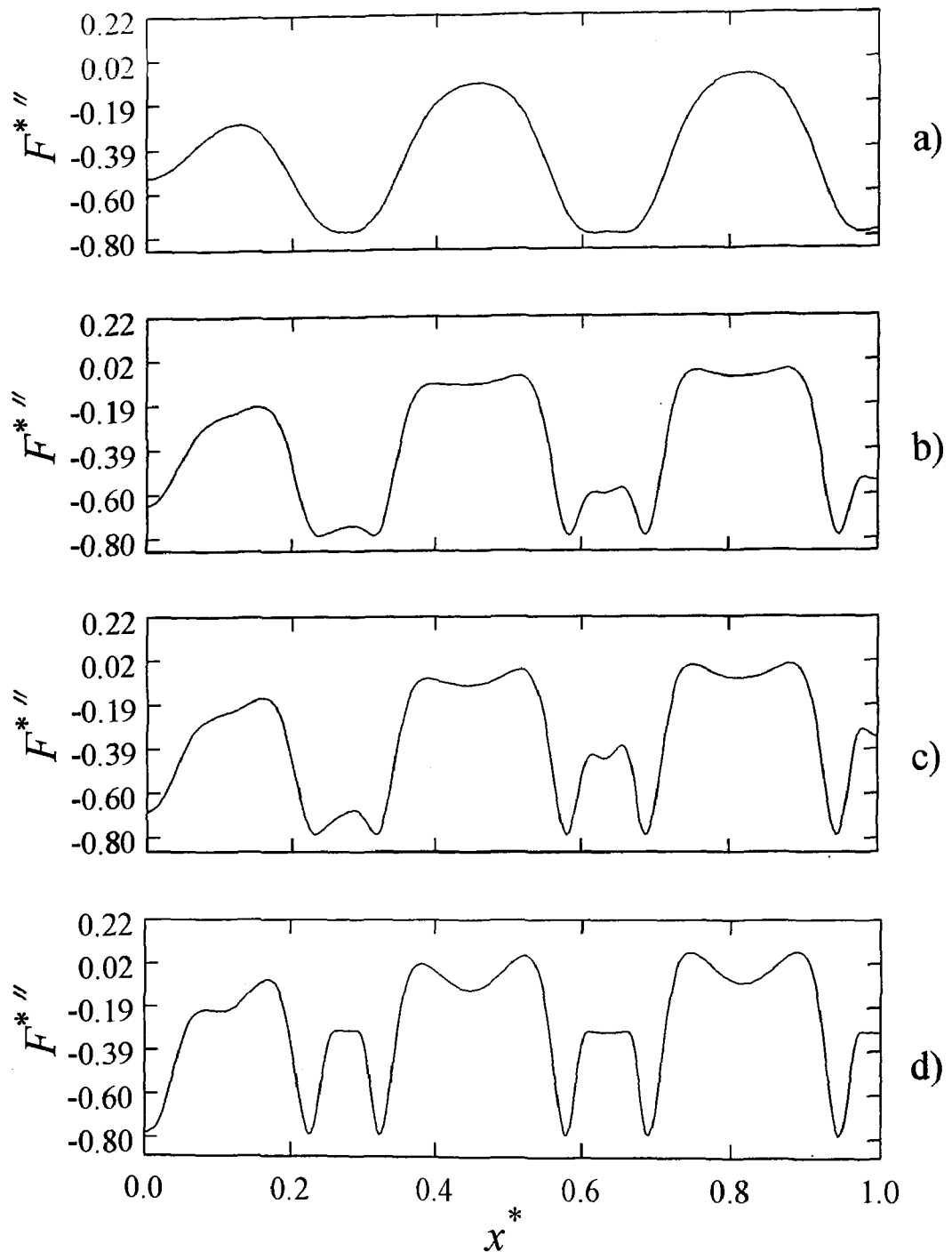


Figure 6.18: The evolution of the change in the dimensionless spatial second derivative of the free energy with respect to composition of component 1 for a double quench from $T_1^* = 0.25$ to $T_2^* = 0.1$ at the transition time of $t_i^* = 5.52$ at the following dimensionless times: (a) $t^* = 5.526$, (b) $t^* = 5.545$, (c) $t^* = 5.549$, and (d) $t^* = 5.565$. The change in the dimensionless second derivative of free energy is used to determine the conditions of stability ($F^{*''} > 0$), meta-stability ($F^{*''} > 0$), and instability ($F^{*''} < 0$). The dimensionless initial concentration is $c_0^* = 0.6$ and the dimensionless diffusion coefficient is $D^* = 200\,000$.

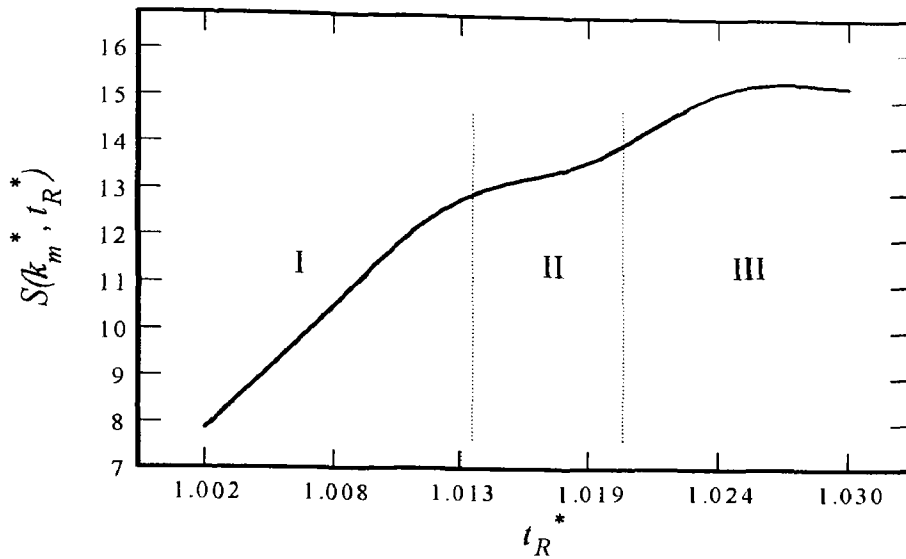


Figure 6.19: The evolution of the maximum value of the dimensionless structure factor of the primary structure formed just after the second temperature jump to $T_2^* = 0.2$, plotted against dimensionless reduced times for a critical quench case. The second jump was made at a transition time of $t_i^* = 4.72$ with a dimensionless diffusion coefficient $D^* = 200\,000$.

trends as those observed (see Figures C.33 and C.34). The only difference being the steepness of the growth rate as the value of D^* increases.

Figure 6.20 shows the growth of the dimensionless structure factor with dimensionless reduced time after the second shallower quench for the initial off-critical quench case. The values plotted are taken right after the second quench is made and as in the case of the initial critical quench, there are three regions that can be identified for the growth of the primary structure. For $D^* = 500\,000$ and $80\,000$, Figures C.35 and C.36 in Appendix C, there is the emergence of secondary peaks (refer back to Figures C.11 and C.12) in the growth of the maximum value of the dimensionless structure factor that have a very small impact on the evolution of the original composition fluctuations as discussed previously in section 6.2. The trends in Figure 6.20 will be discussed separately

from those in Figures C.35 and C.36. In Figure 6.20, the three different growth regions are similar to those observed for the initial critical quench case. In the stage I, right after the second quench, there is a steady increase in the growth rate and the primary structures are further separating as the new conditions are imposed, $T_2^* = 0.2$. In stage II, the growth of the primary structure is slowing down and again there is a slight dip in the growth rate before it starts to pick up again into stage III. The nonlinear growth rate is a result of the adjustments in the composition fluctuations from the initial quench condition at $T_1^* = 0.25$ towards the new equilibrium values at $T_2^* = 0.2$. Finally, in stage III the growth rate increases again and starts to level off as the blend reaches the new equilibrium compositions. In Figures C.35 and C.36 there are two graphs plotted, one for the growth of the primary peak (top graph) and one for the secondary peak observed in the plot of the dimensionless structure factor (bottom). Both are plotted against reduced times so that a comparison can be made between the growth rates of the two peaks simultaneously. As D^* increases, the growth of the secondary peak was more obvious and its effect on the growth rate of the primary structure should have a larger impact. This can be observed when comparing Figures C.35 and C.36 where D^* increases from 500 000 to 800 000 respectively. In Figure C.35, the introduction and the growth of the secondary peak does not seem to have much impact on the growth of the primary peak as can be observed from the profile of the primary peak growth rate. The growth of the primary peak seems to be identical to the growth of the dimensionless structure factor for a single quench case. There are still three distinct regions that can be observed for both the

primary and secondary peak growth. Initially in stage I, the growth of both primary and secondary peak increases steadily and the blend is still phase separating under the new conditions. In stage II, the growth of the primary peak slows down as the composition fluctuations are approaching the new equilibrium values and the secondary peak still continues to grow but at a slower rate. The growth of the primary peak is dominating and therefore, the growth of the secondary peak has little effect on the composition fluctuations. In stage III, the primary peak plateaus in growth rate and the secondary peak continues to grow steadily. To determine the full evolution of the secondary peak growth, the late stages need to be evaluated and does not fall into the scope of this thesis. In Figure C.36, the effect of the growth of the secondary peak is more obvious. Again, the profile has been broken down into three regions. The top graph represents the growth of the dimensionless structure factor of the primary peak and the bottom graph for the growth of the secondary peak at the same reduced times. In stage I, there is only a short period of steady increase in growth of both the primary and secondary peaks. This is because as D^* is increased, the rate of phase separation increases and therefore, the blend is quick to respond to the change of conditions to the new temperature. In stage II, there is a steeper increase in the growth rate for both the primary and secondary peaks as the blend approaches the new equilibrium values at T_2^* . However, the growth of the secondary peak has only a slight effect on the growth of the primary peak and this is reflected in the dimensionless spatial concentration profiles shown in section 6.2. In stage III, the growth of the primary peak levels off while the secondary

peak continues to grow. There is a slight dip in the growth of the secondary peak before it starts to increase again. The reason for this in stage III is not certain. At this point for the off-critical quench case, although there is the appearance of a secondary peak growing and forming, its growth does not significantly affect the growth of the primary structures that form.

6.7 A Comparison of the Growth of Primary and Secondary Structures After the Second Temperature Jump to $T_2^* = 0.1$

A deeper second quench from $T_1^* = 0.25$ to $T_2^* = 0.1$ shows secondary phase separation as observed in the dimensionless spatial concentration profiles. The dimensionless structure factor from the original quench grew with time and at the same constant wave number as at $T_1^* = 0.25$. The emergence and growth of a secondary peak after the second temperature jump was observed in the evolution of the dimensionless structure factor. The second deeper quench and its effects on the growth rate of the primary and the secondary structures can be broken down into three regions as in the shallower quench case. The growth rate of the maximum value of the dimensionless structure factor after the second quench is plotted against a reduced time, t_R^* . Figure 6.21 shows the growth rate of the primary (top) and secondary (bottom) peaks of the maximum structure factor after the second deeper quench at the transition times for the initial critical quench case for $D^* = 200\ 000$. Figure 6.21 shows slightly different evolutions in the growth rate of the primary and secondary peaks due the increase in value of the

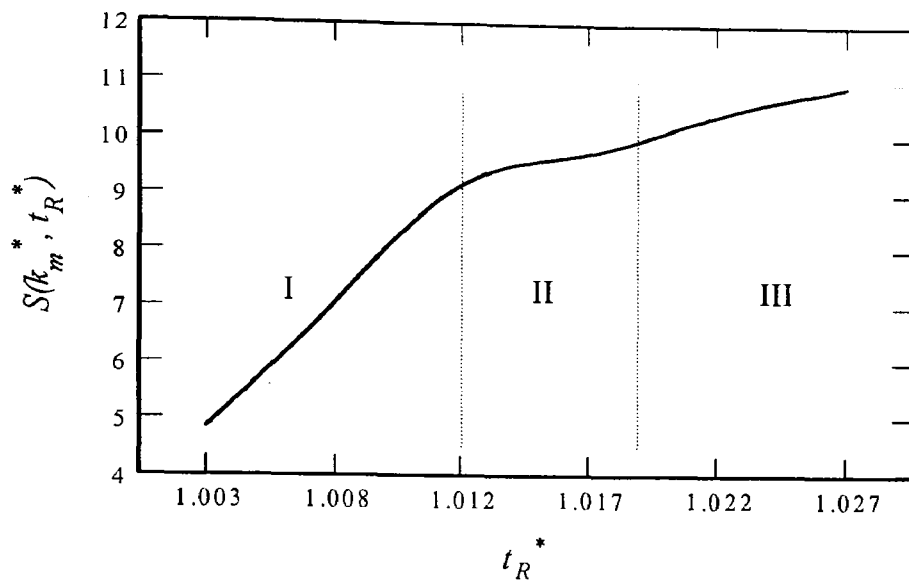


Figure 6.20: The evolution of the maximum value of the dimensionless structure factor of the primary structure formed just after the second temperature jump to $T_2^* = 0.2$, plotted against dimensionless reduced times for an off-critical quench case. The second jump was made at a transition time of $t_i^* = 5.52$ with a dimensionless diffusion coefficient $D^* = 200\,000$.

dimensionless diffusion coefficient (see Figures C.37 and C.38 in Appendix C for $D^* = 500\,000$ and $800\,000$, respectively). Generally, the trends seem to be pretty consistent for the three stages in all cases of D^* studied. In the stage I, right after the second quench, there is a steady increase in the growth rate of the primary peak. The emergence and the growth of the secondary peak starts out at a slower rate than the primary peak in stage I. In stage II, the growth of the primary peak increases slightly and steadily and the growth of the secondary peak increase at a much faster rate having a steeper slope. In stage III, both the growth of the primary and secondary peaks slow down and are roughly at the same rate. At this point, the primary structures have reached the equilibrium compositions at the new temperature while the secondary phase is still developing. These observations are different from those observed experimentally by Hayashi *et al.*

[2000a] for the growth of the maximum scattering intensity with time. Their three stages differ from the one in this study. In stage I, they observe a faster increase in the secondary peak intensity than the primary peak intensity. In stage II, both the growth of the primary and secondary peaks intensities grow at the same rate and in stage III, the growth of the primary peak intensity becomes larger than the secondary peak intensity. The reason for the discrepancy between the observations in this study and in Hashimoto's work maybe due to the time that the second jump was made. Also, stage III describes the late stages in Hashimoto's work and is omitted from this numerical work. Perhaps the evolution of the secondary structures is dependent on the domain size. Hayashi *et al.* [2000a] have suggested this possibility and also introduced the confinement effect where the size of the primary structure acts as a new medium for the growth of the secondary structures. The smaller the domain size of the primary structures, the less room for growth of the secondary structures to form and therefore, different growth rates will be observed for the primary and secondary structures. By comparing the two different observations from making a temperature jump at the beginning of the intermediate stages (in the numerical work of this thesis) and the late stages (experimental work by Hashimoto) shows that the domain size has an effect on the growth patterns.

Figure 6.22 shows the growth rate of the primary (top) and secondary (bottom) peaks of the structure factor after the second deeper quench at the transition times for the initial off-critical quench case for $D^* = 200\ 000$. In the dimensionless maximum structure factor profiles after the second quench, the peak from the

original initial quench grew with time and at the same constant wave number as at $T_1^* = 0.25$ and there is the emergence and growth of the secondary peak at a larger wave number. The second deeper quench for the initial off-critical quench case and its effects on the growth rate of the primary and the secondary structures can be broken down into three regions. The growth rate of the maximum structure factor after the second quench is plotted against a reduced time, t_R^* . Figure 6.22 and Figure C. 39 ($D^* = 500\ 000$) show similar evolutions in the growth rate of the primary and secondary peaks and Figure C.40 ($D^* = 800\ 000$) shows the same trend as Figures C.37 and C.38 in stages I, II and III. In the stage I, right after the second quench, there is a steady increase in the growth rate of the primary peak for all values of D^* investigated. The emergence and the growth of the secondary peak starts out at a slower rate than the primary peak in stage I with a smaller slope. In stage II, the growth of the primary peak increases slightly and steadily and the growth of the secondary peak increase at a much faster rate having a steeper slope. There is slight curvature in all three plots of stage II. This may possible be due to the reorganizing of the phase separating mixture to the new composition fluctuations present. In stage III, for Figure 6.22 and C.39, both the growth of the primary and secondary peaks continue to increase with the secondary peak increasing at a much faster rate. At this point, the primary and secondary structures are still developing. In stage III for Figure C.40, both the growth of the primary and secondary peak starts to level off, indicating that the primary structures have reached their equilibrium values while the secondary peaks have grown to a sufficient size. Perhaps, further investigation would lead

to the decrease in the growth of the secondary peak when the composition fluctuations from the primary and secondary structures merge together at later stages. This has been observed experimentally by Hayashi *et al.* [2000a] and numerically by Henderson and Clarke [2004] for an initial critical quench and a second jump at the late stages of phase separation by SD and not at the beginning of the intermediate stages as described here.

6.8 Remarks on the Early Stages of Phase Separation After the Second Temperature Jump to $T_2^* = 0.1$ where Secondary Structures are Observed

In the experimental work by Hashimoto *et al.* [2000] and numerical work by Henderson and Clarke [2004] the evolution of the secondary phase separation, after the second quench, was found to reasonably follow the linear theory in the early stages of phase separation by SD for a single quench case. To determine if the numerical work presented in this section on the formation of secondary structures also follows the linear theory in the early stages right after the second quench to $T_2^* = 0.1$, the plots of the natural log of the dimensionless structure factor versus dimensionless reduced time is presented in Figures 6.23 and 6.24 for the initial critical and initial off-critical quench case for $D^* = 200\ 000$, respectively. Recall that the plot of the natural log of the dimensionless maximum structure factor versus dimensionless time should have a linear region in the early stages of phase separation by SD. As observed for all the profiles, there exists a small linear region after the second quench when the secondary structures are

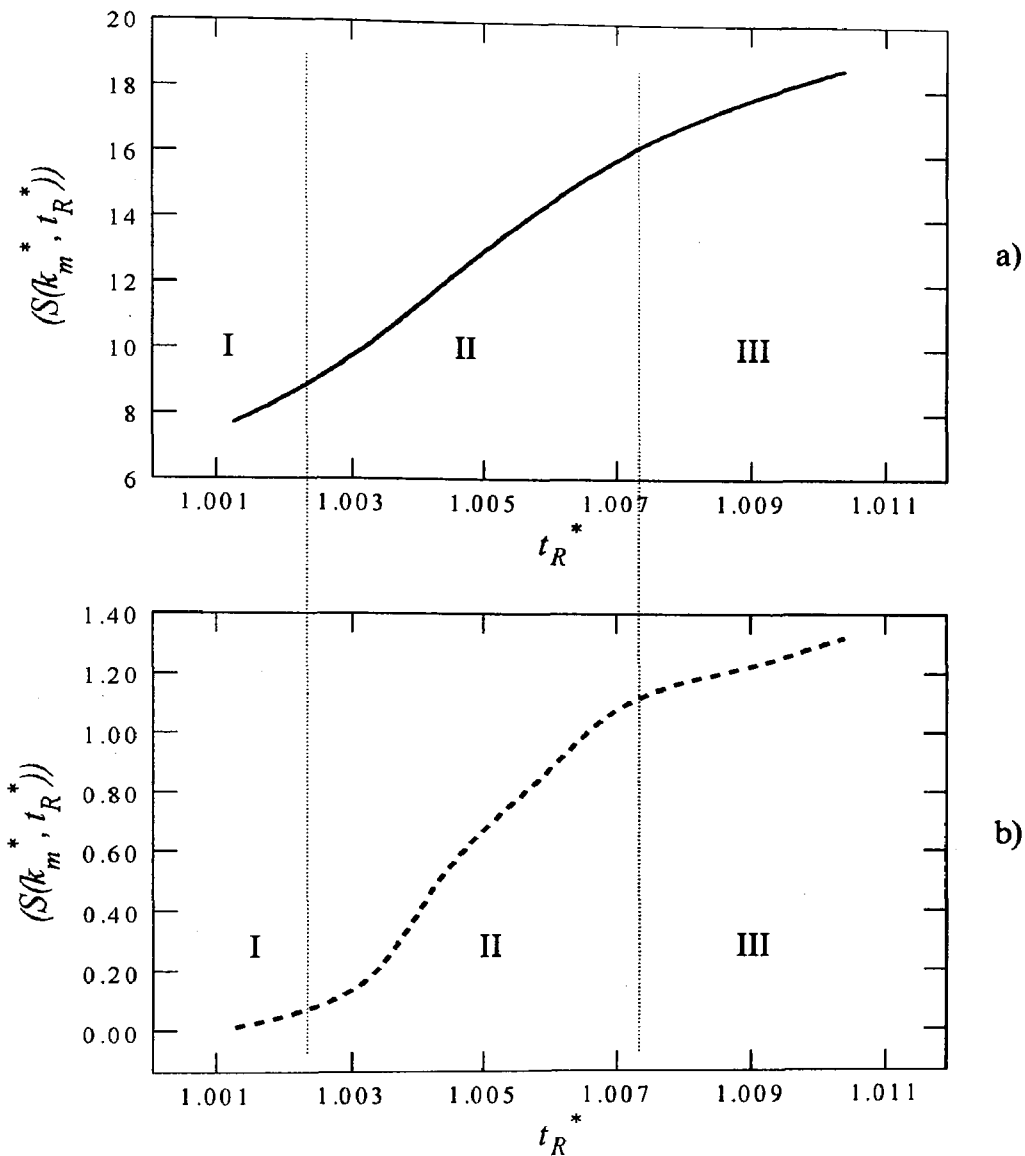


Figure 6.21: The evolution of the dimensionless structure factor of the (a) primary and (b) secondary structures formed just after the second temperature jump to $T_2^* = 0.1$ plotted against dimensionless reduced times for a critical quench case. The second temperature jump was made at $t_i^* = 4.72$. The dimensionless diffusion coefficient is $D^* = 200\,000$.

forming. Therefore, the numerical work presented here is consistent with what has been observed by Hashimoto *et al.* [2000] in experiment and by Henderson and Clarke [2004] in their numerical study on double quenching. Furthermore, it can be observed that in the early stages, the growth of the secondary structures appears to be steeper for $D^* = 200\ 000$ than $500\ 000$ and $800\ 000$ (refer to Figures C.41 to C.44 in Appendix C). Perhaps, the larger domain size provides a better medium to create new instabilities for phase separation for the secondary structures to form more readily. It has been suggested that the primary structure acts as an individual phase where phase separation occurs as if in a single quench, but within the already separating initial structures [Norton and Frith, 2001]. The observations presented here are consistent with the work by Hayashi *et al.* [2000a and 2000b], when investigating the initial domain size and its effects on double phase separation. They observed that if the size of the initial structure is large, then the growth rate of the secondary structure is faster than for an initial smaller domain size. The critical size to which double phase separation is observed is not known and further analysis both experimentally and numerically is required [Hayashi *et al.*, 2000a].

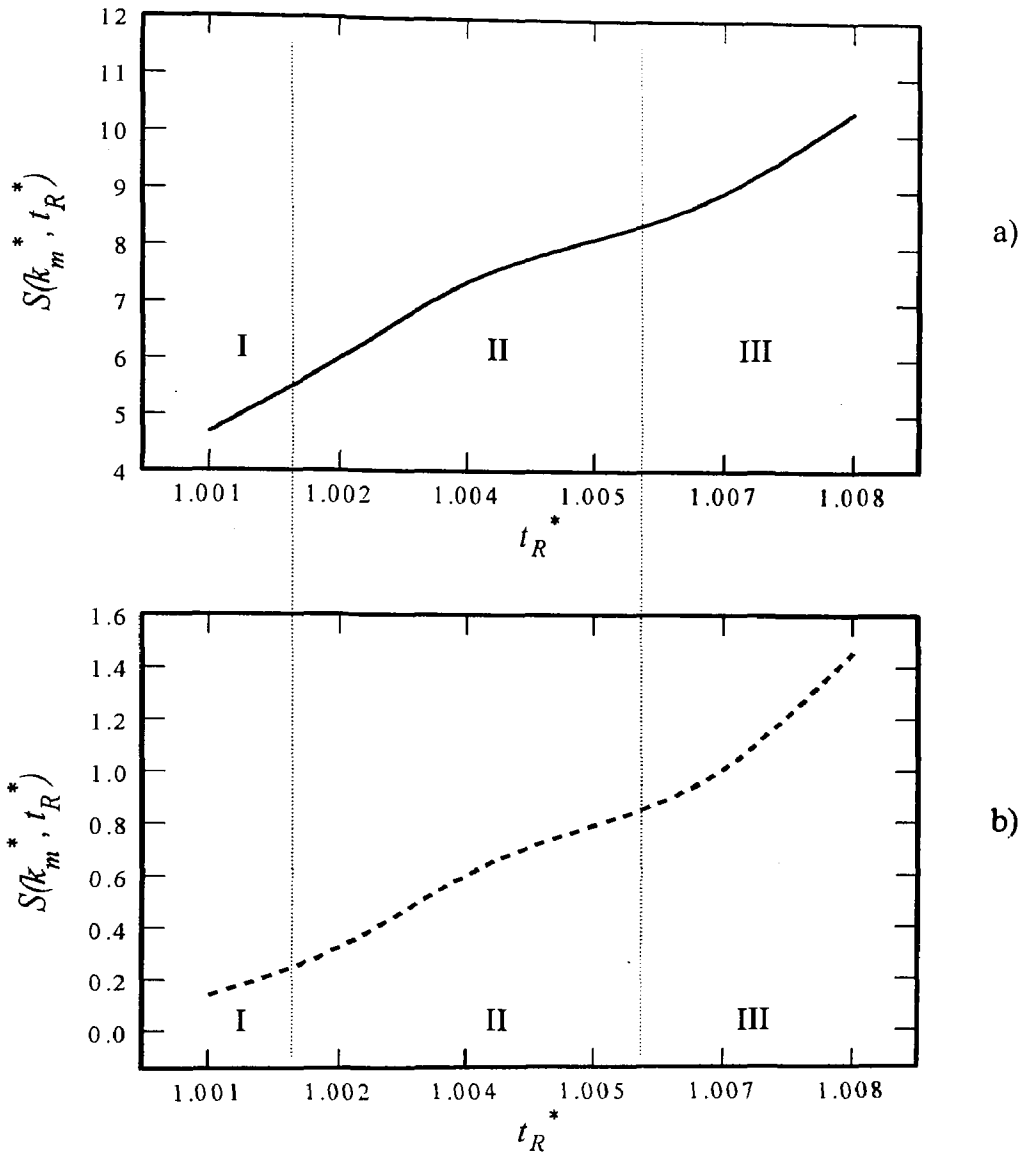


Figure 6.22: The evolution of the dimensionless structure factor of the (a) primary and (b) secondary structures formed just after the second temperature jump to $T_2^* = 0.1$ plotted against dimensionless reduced times for an off-critical quench case. The second temperature jump was made at $t_i^* = 5.52$. The dimensionless diffusion coefficient is $D^* = 200\,000$.

Chapter 7

Results and Discussion: 2-D TIPS Single and Double Quench

In Chapter 5 and 6, the results from the one-dimensional model was presented and discussed based on the nonlinear C-H theory and the F-H-de Gennes free energy for a single and a double quench respectively. The results replicated frequently observed trends of phase separation by SD in experimental and numerical work. Recall that in analyzing SD, the one-dimensional model provides the detail necessary to describe the dynamics of phase separation with the exception of detailing the type of structure formed. This section presents the results of pattern formation for a critical and off-critical quench and a brief discussion on the 2-D numerical work. The patterns formed are typical of those formed by SD for the single and double quench. For the single quench, the dimensionless temperature and diffusion coefficient are adjusted to observe the effects on pattern formation and its consistency with the predictions from the 1-D model. For double quenching, the patterns formed from an initial critical and an initial off-critical quench are presented. With the double quench, in order to verify the pattern formation predicted from experimental work by Hayashi *et al.* [2000a], the second quench was made at the late stages and not at the beginning of the

intermediate stage as in the 1-D study. Because of the amount of time required to run the 2-D simulations, only selected runs were made for the analysis. Table 7.1 summarizes the dimensionless parameters used in this 2-D study.

Table 7.1: Summary of the dimensionless parameters used in the 2-D numerical study for a single critical and off-critical quench

Parameter	Value
c_0^*	0.5, 0.6
N_1, N_2	1000
D^*	200 000, 500 000
T_1^*	0.25 and 0.2

7.1 Single TIPS Critical Quench

Figure 7.1 shows a 2-D structure development (left) and a profile of the concentration fluctuations (right) for a critical quench, $c_0^* = 0.5$, at a single temperature jump of $T_1^* = 0.25$, with a dimensionless diffusion coefficient of $D^* = 200\,000$. The grey scale at the bottom right hand corner of Figure 7.1 shows the different levels of the concentration ranging from $c^* = 0.0$ to $c^* = 1.0$. It has been determined in experiments that the critical quench produces the interconnected structure and the off-critical quench produces the droplet type structure [Hashimoto, 1993]. The structure development on the left shows that the model in this thesis is able to predict the same interconnected structure known for critical quench conditions. Note the change in the color intensity of the structure

development as the concentration fluctuations increase upon phase separation (right).

In order to test the effect of D^* on the critical quench, the value of D^* was increased from 200 000 to 500 000. Figure 7.2 shows the evolution of pattern formation at $D^* = 500\,000$ for the critical quench while maintaining all other parameters the same as in Figure 7.1. From the 1-D model, it was observed that increasing the dimensionless diffusion coefficient increased the rate as well as the amount of phase separation that occurred. Therefore, this trend should also be observed in the 2-D structure development. When comparing the results of Figure 7.1 and Figure 7.2 it is clear that the rate as well as the amount of phase separation increased with increasing dimensionless diffusion coefficient. The 1-D and 2-D models are in agreement with each other for the critical quench case in examining the properties of interest.

7.2 Single TIPS Off-Critical Quench

Figure 7.3 shows a 2-D structure development (left) and a profile of the concentration fluctuations (right) for an off-critical quench, $c_o^* = 0.6$, at a single temperature jump of $T_I^* = 0.25$, with a dimensionless diffusion coefficient of $D^* = 200\,000$. The grey scale in the bottom right hand corner in Figure 7.3 shows the different levels of the concentration ranging from $c^* = 0.0$ to $c^* = 1.0$. The off-critical quench produces the droplet type structure from experimental observations. The evolution of structure development on the left shows the same droplet structure known for an off-critical quench conditions indicating that the

model developed is in good agreement with experimental work. Notice that as the concentration fluctuations increase (right) the structure development profile shows a range of shades, indicating the change in concentration, as the mixture is phase separating. One more feature that is captured in the 2-D structure evolution is the spatial distribution of the composition fluctuations are fairly uniform, which is expected in phase separation by SD. In order to test the effect of D^* on the off-critical quench, the value of D^* was increased from 200 000 to 500 000. Figure 7.4 shows the evolution of pattern formation at $D^* = 500\,000$ for the critical quench while maintaining all other the same as in Figure 7.3. From the 1-D model, it was observed that increasing the dimensionless diffusion coefficient increases the rate as well as the amount of phase separation that occurs. Therefore, this trend should also be observed in the 2-D structure development. When comparing the results of Figure 7.3 and Figure 7.4 it is clear that the rate as well as the amount of phase separation increased with increasing dimensionless diffusion coefficient. In the formation of the droplet type structure, another parameter was tested to verify the agreement of the results from the 1-D study and the 2-D study. The dimensionless temperature was decreased from $T_l^* = 0.25$ to $T_l^* = 0.2$ keeping all other parameters the same as in Figure 7.4. By comparing both profiles generated in Figure 7.4 and Figure 7.5, it can be observed that the amount of phase-separated regions increased with time. This was consistent with the observations in the 1-D model when tested for an off-critical quench case. 1-D and 2-D models are in agreement with each other for the off-critical quench case in examining the properties that were of interest.

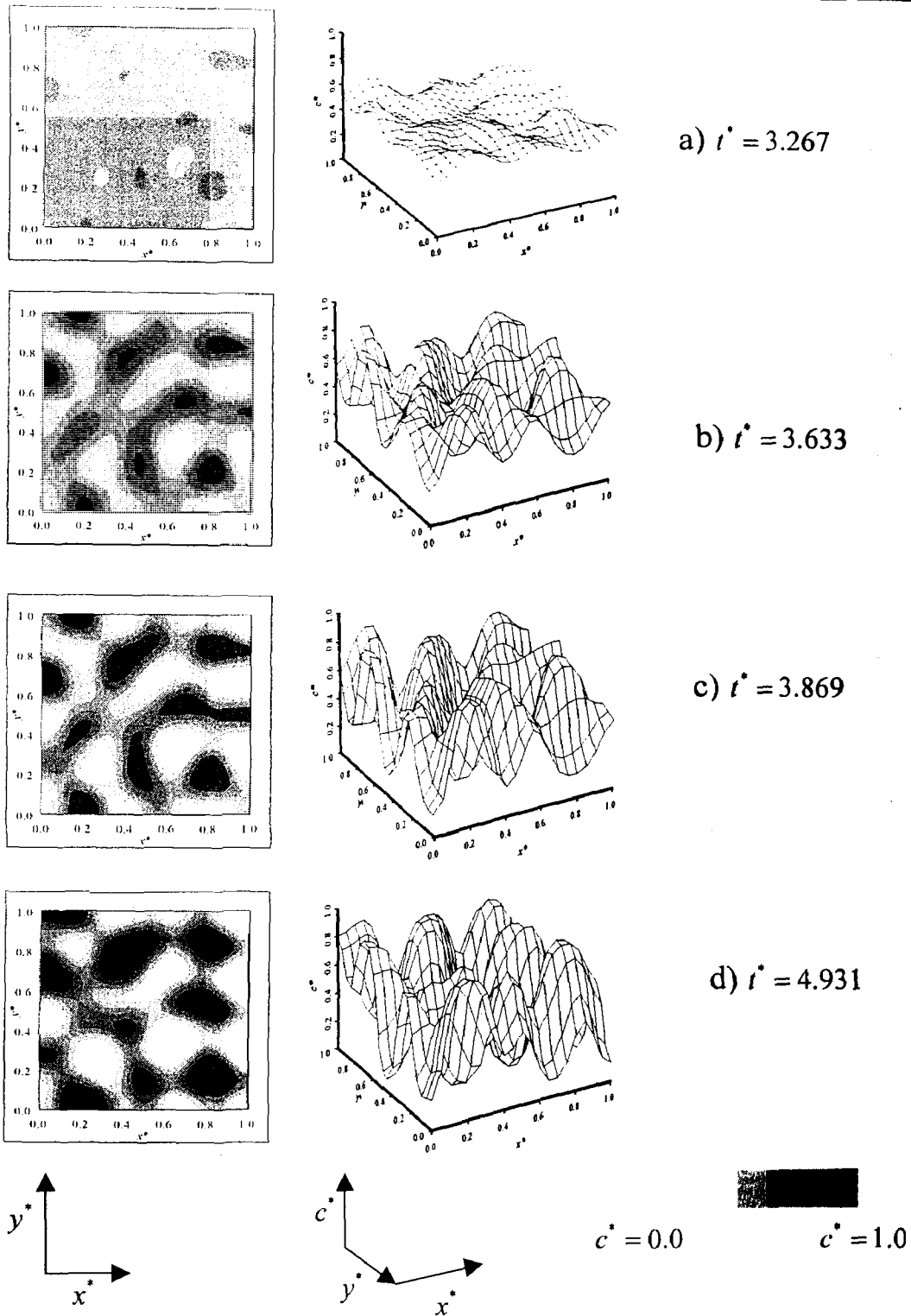


Figure 7.1: A plot of the 2-D dimensionless spatial concentration profiles, $c^*(x^*, y^*)$, showing the evolution of structure development (left) and the growth of the concentration fluctuations (right) for a single critical ($c_o^* = 0.5$) quench to $T_l^* = 0.25$ with $D^* = 200\,000$ at the following dimensionless times: (a) $t^* = 3.267$, (b) $t^* = 3.633$, (c) $t^* = 3.869$, and (d) $t^* = 4.931$. The grey scale represents the compositions of the phase separating blend on the bottom right.

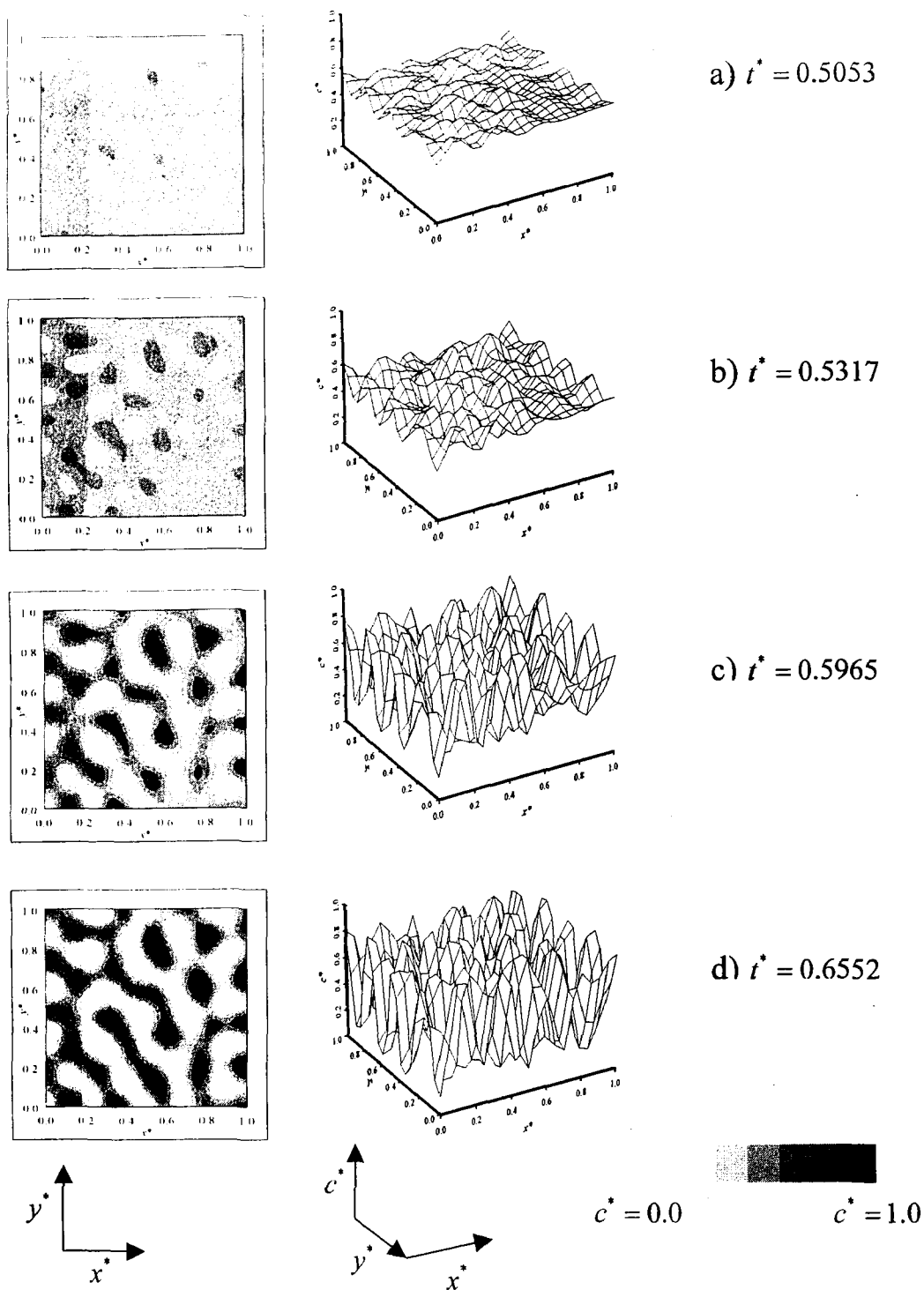


Figure 7.2: A plot of the 2-D dimensionless spatial concentration profiles, $c^*(x^*, y^*)$, showing the evolution of structure development (left) and the growth of the concentration fluctuations (right) for a single critical ($c_o^* = 0.5$) quench to $T_I^* = 0.25$ with $D^* = 500\,000$ at the following dimensionless times: (a) $t^* = 0.5053$, (b) $t^* = 0.5317$, (c) $t^* = 0.5965$, and (d) $t^* = 0.6552$. The grey scale represents the compositions of the phase separating blend on the bottom right.

7.3 Two-Step Phase Separation: Critical Quench

The two-step process used for the 2-D study is different from that used in the 1-D analysis. The 2-D analysis here was done to observe pattern formation as predicted from the experimental work by Hashimoto *et al.* [2000] and Hayashi *et al.* [2000a and 2000b] in their 2-step phase separation process to see whether the secondary structures can be observed numerically under the same quenching methods. Recall in the 1-D study, the second temperature jump was made at a dimensionless transition time, which characterized the end of the early stages and the beginning of the intermediate stages of SD for the single quench. In this section, the second temperature jump was made in the late stages of phase separation by SD where the mixture has reached their respective equilibrium compositions. This method was also used by Tanaka [1993] and Tao *et al.*, [1995] in their experimental study of double quenching. Furthermore, to follow closely to Hashimoto's work [2000], the second quench was made such that the mixture was still within the unstable region and therefore, was still phase separating by SD. As mentioned in the previous section on the single quench conditions, due the amount of computing time required for one 2-D simulation, the results shown here are restricted to certain values of T^* and D^* that best reflect the objectives of this thesis. In Figure 7.6 the dimensionless spatial concentration profiles, $c^*(x^*, y^*)$, show the evolution of structure development for a double critical ($c_o^* = 0.5$) quench from $T_I^* = 0.25$ to $T_I^* = 0.1$ with $D^* = 200\ 000$.

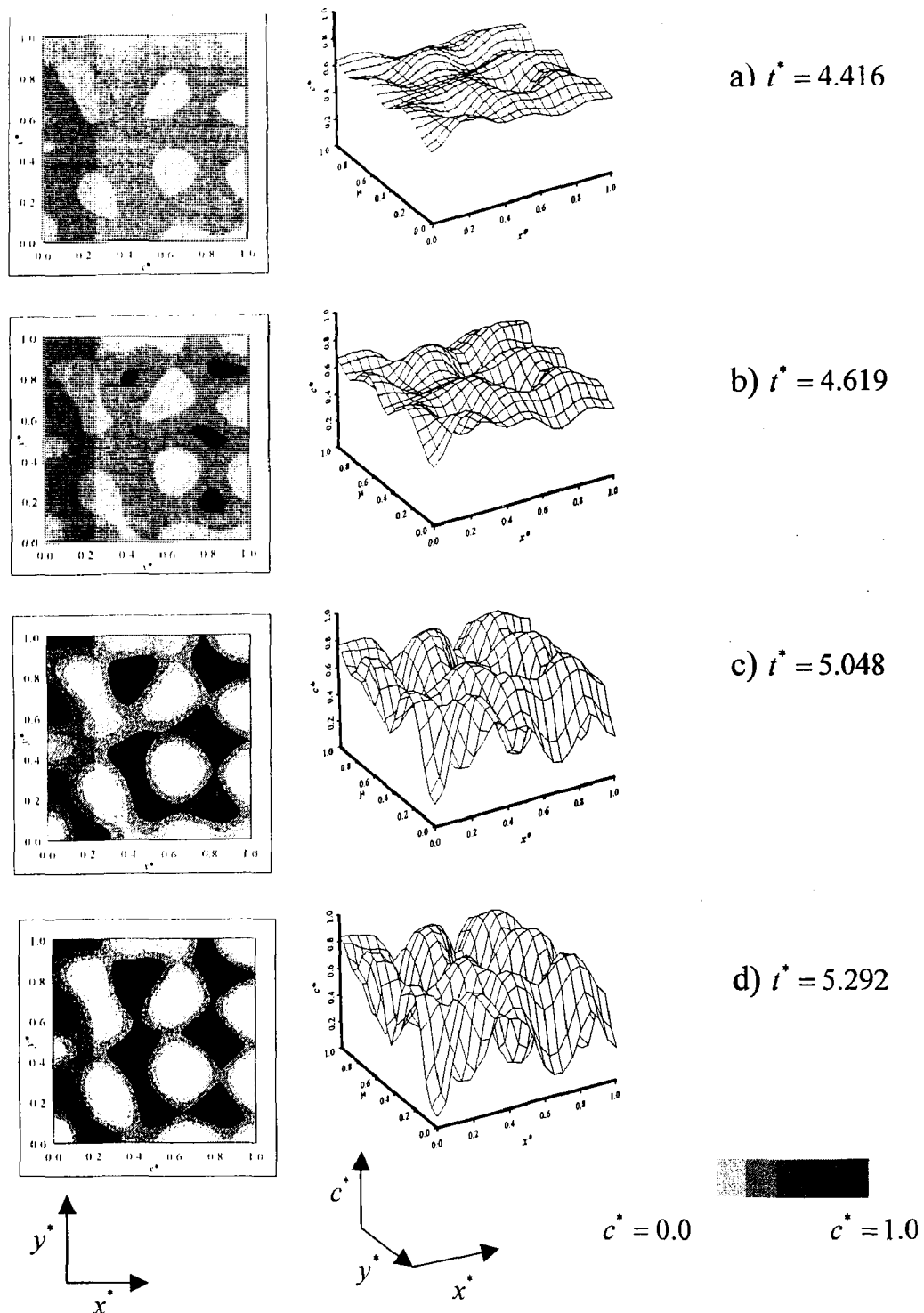


Figure 7.3: A plot of the 2-D dimensionless spatial concentration profiles, $c^*(x^*, y^*)$, showing the evolution of structure development (left) and the growth of the concentration fluctuations (right) for a single off-critical ($c_o^* = 0.6$) quench to $T_l^* = 0.25$ with $D^* = 200\,000$ at the following dimensionless times: (a) $t^* = 4.416$, (b) $t^* = 4.619$, (c) $t^* = 5.048$, and (d) $t^* = 5.292$. The grey scale represents the compositions of the phase separating blend on the bottom right.

Chapter 7: 2-D TIPS Pattern Formation (1 & 2 Step)

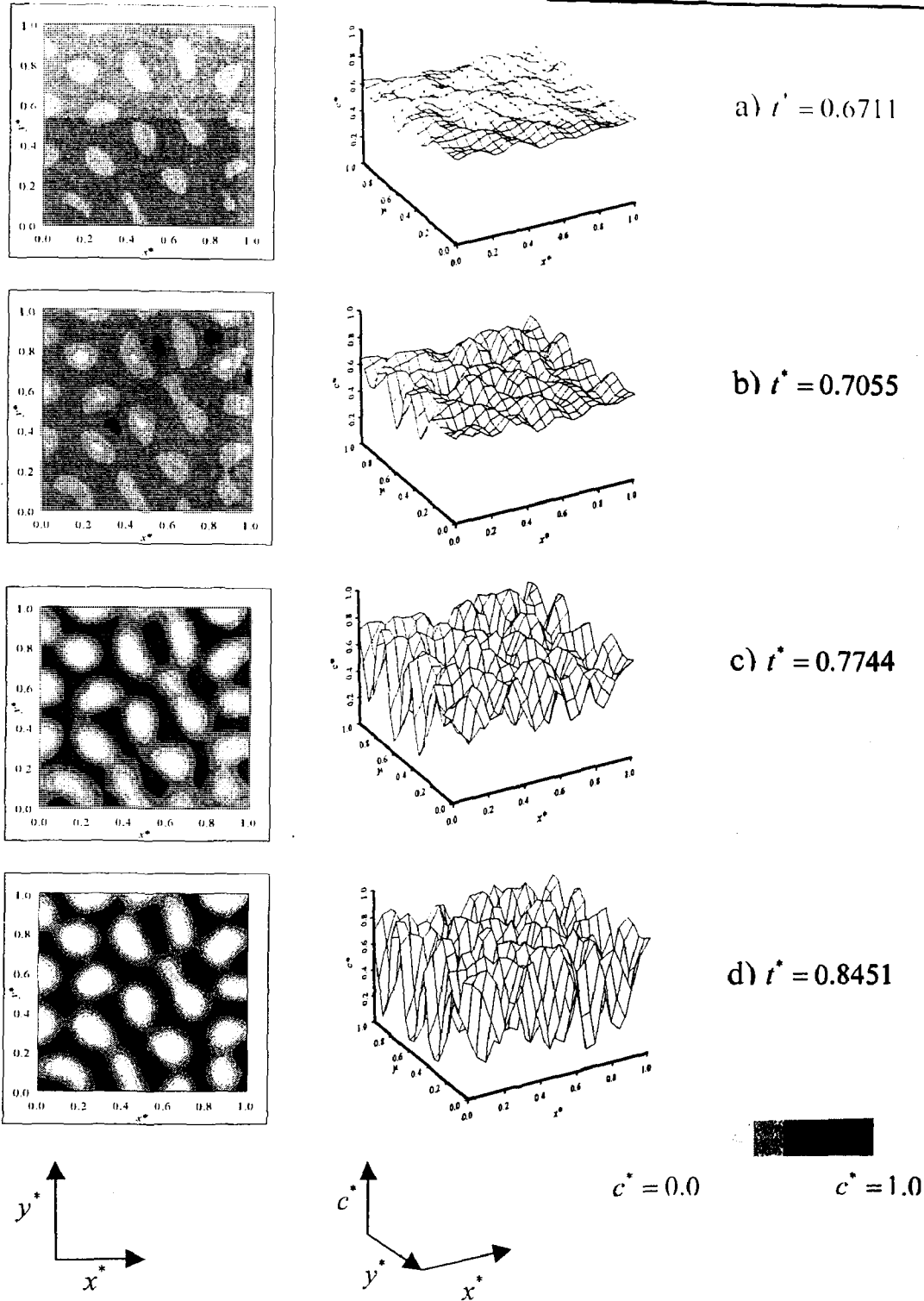


Figure 7.4: A plot of the 2-D dimensionless spatial concentration profiles, $c^*(x^*, y^*)$, showing the evolution of structure development (left) and the growth of the concentration fluctuations (right) for a single off-critical ($c_o^* = 0.6$) quench to $T_l^* = 0.25$ with $D^* = 500\,000$ at the following dimensionless times: (a) $t^* = 0.5053$, (b) $t^* = 0.5317$, (c) $t^* = 0.5965$, and (d) $t^* = 0.6552$. The grey scale represents the compositions of the phase separating blend on the bottom right.

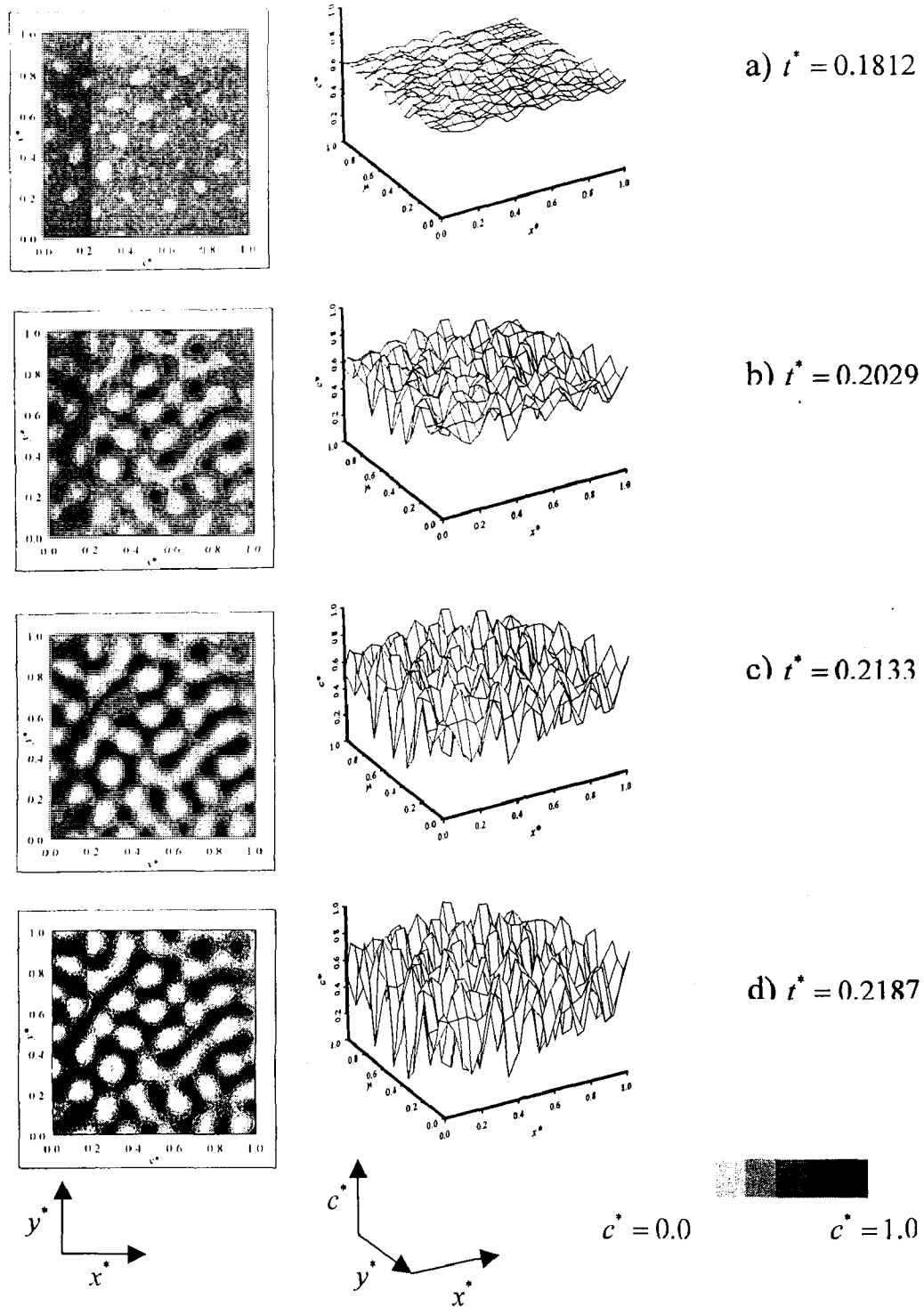


Figure 7.5: A plot of the 2-D dimensionless spatial concentration profiles, $c^*(x^*, y^*)$, showing the evolution of structure development (left) and the growth of the concentration fluctuations (right) for a single off-critical ($c_o^* = 0.6$) quench to $T_l^* = 0.2$ with $D^* = 500\,000$ at the following dimensionless times: (a) $t^* = 0.1812$, (b) $t^* = 0.2029$, (c) $t^* = 0.2133$, and (d) $t^* = 0.2187$. The grey scale represents the compositions of the phase separating blend on the bottom right.

The dimensionless times correspond to profiles made after the second jump at a dimensionless time of $t^* = 4.931$ (a) $t^* = 4.935$, (b) $t^* = 4.941$, (c) $t^* = 4.950$, and (d) $t^* = 4.952$ (e) $t^* = 4.953$ and (f) 4.9531. For a critical quench, the interconnected structure is formed. Upon making the second quench, at the late stage of SD, the initial composition for the second quench corresponds to the values just before the second quench and are off-critical. Off-critical quenches result in droplet type morphologies. In Figure 7.6 this interconnected structure is the result of the primary quench and the droplet type structure is the result of the secondary quench. This pattern formation is consistent with the patterns formed experimentally by Tao *et al.* [1995] and Tanaka [1993] and numerically with the work of Henderson and Clarke [2004]. In Figure 7.6 b), shortly after the second quench, the phase separating regions are shifting and changing in shape as well as concentration (color intensity). This is consistent with what has been observed by Tanaka in his experimental work where the initial phase separated structure was reorganized when the second quench was made [Tanaka, 1993]. This reorganizing of the primary structures continues with time and is not so obvious to the naked eye once the secondary structures start to appear. The first sign of secondary phase separated regions occurs in Figure 7.6 c) at $t^* = 4.950$ and gradually increases in number as shown through Figures 7.6 d) to f). The amount of secondary droplets formed after the second quench were few in number which can be explained by the location of the second temperature jump relative to the spinodal curve. The second quench made in this study was not too far from the spinodal curve, and since the driving force for phase separation is directly related

to the distance of the temperature within the confines of the spinodal curve [Tao *et al.*, 1995], there will be a smaller driving phase separation force. Figure 7.7 shows the evolution of the concentration fluctuations for the same conditions as in Figure 7.6. After the second quench, the composition fluctuations are still rather smooth until $t^* = 4.950$, where the first sign of secondary phase separated regions occur. The profile becomes rough and continues to develop this way for the rest of the structure development. From these profiles, especially from a bird's eye view, the dipping of the crests in certain regions are very noticeable, indicating the occurrence of the constructive and destructive interferences that are occurring from the second quench.

7.4 Two-Step Phase Separation: Off-critical Quench

In the off-critical double quench case, the method for double phase separation is the same as described for the critical quench case. The second quench is made in the late stages of phase separation by SD and lies within the unstable region to ensure phase separation still occurs by SD. Figure 7.8 shows the 2-D dimensionless spatial concentration profiles, $c^*(x^*, y^*)$, of the evolution of structure development for a double off-critical ($c_o^* = 0.6$) quench from $T_l^* = 0.25$ to $T_l^* = 0.1$ with $D^* = 200\ 000$. The dimensionless times correspond to profiles made after the second jump at $t^* = 5.292$: (a) $t^* = 5.294$, (b) $t^* = 5.307$, (c) $t^* = 5.313$, and (d) $t^* = 5.315$ (e) $t^* = 5.317$ and (f) 5.320. For an off-critical double quench, both the primary and secondary structures developed should be of droplet type and this can be observed in Figure 7.8. Tanaka [1993] and Tao *et al.* [1995]

have also observed this pattern formation for the off- critical double quench experimentally. Shortly after the second quench in Figure 7.8 b), there is a noticeable change in the pattern and concentration of the primary structures. Again, like in the critical double quench case, the contours seem to be rougher as the blend adjusts to the new conditions. There is also a noticeable increase in the contrast as the blend evolves with time indicating that the blend is approaching the new equilibrium conditions of the second quench. The first sign of secondary phase separation occurs in Figure 7.8 c) at $t^* = 5.313$ and the amount of secondary droplet type structures gradually increases with time. Again, the amount of secondary droplets formed after the second quench is related to location of the temperature for phase separation within the confines of the spinodal curve [Tao *et al.*, 1995]. Figure 7.9 shows the evolution of the concentration fluctuations for the same conditions as in Figure 7.8. After the second quench, the composition fluctuations are still rather smooth until $t^* = 5.313$, where the first sign of secondary phase separated regions occur. The profile becomes rough and continues to develop this way for the rest of the structure development. From these profiles, after $t^* = 5.313$, there is noticeable occurrence of constructive and destructive interferences that are occurring from the second quench.

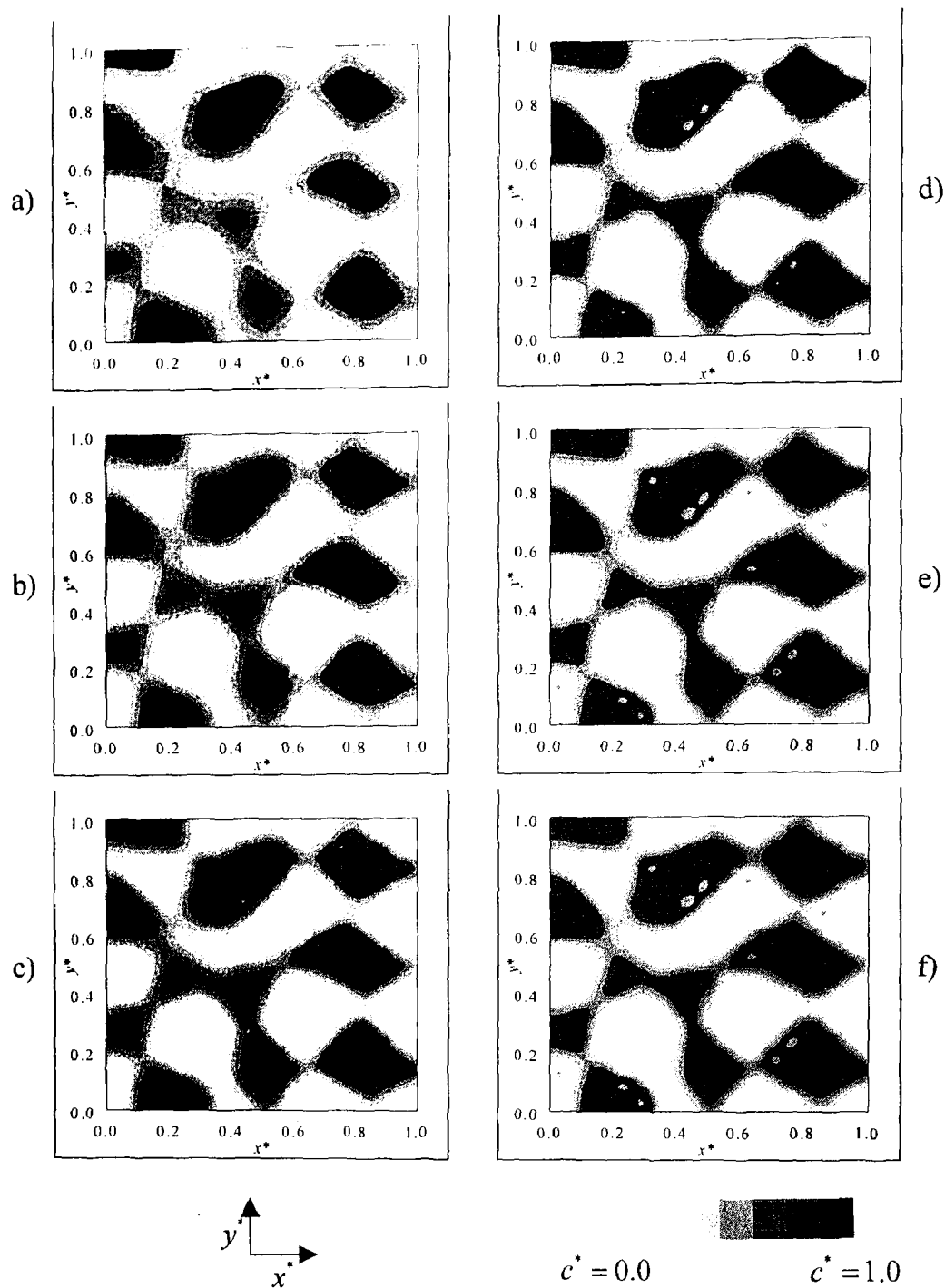


Figure 7.6: A plot of the 2-D dimensionless spatial concentration profiles, $c^*(x^*, y^*)$, showing the evolution of structure development for a double critical ($c_o^* = 0.5$) quench from $T_1^* = 0.25$ to $T_1^* = 0.1$ with $D^* = 200\ 000$. The following dimensionless times correspond to profiles made after the second jump at $t^* = 4.931$: (a) $t^* = 4.935$, (b) $t^* = 4.941$, (c) $t^* = 4.950$, and (d) $t^* = 4.952$ (e) $t^* = 4.953$ and (f) 4.9531. The first sign of secondary phase separation occurs in c) at $t^* = 4.950$. The grey scale represents the compositions of the phase separating blend on the bottom right.

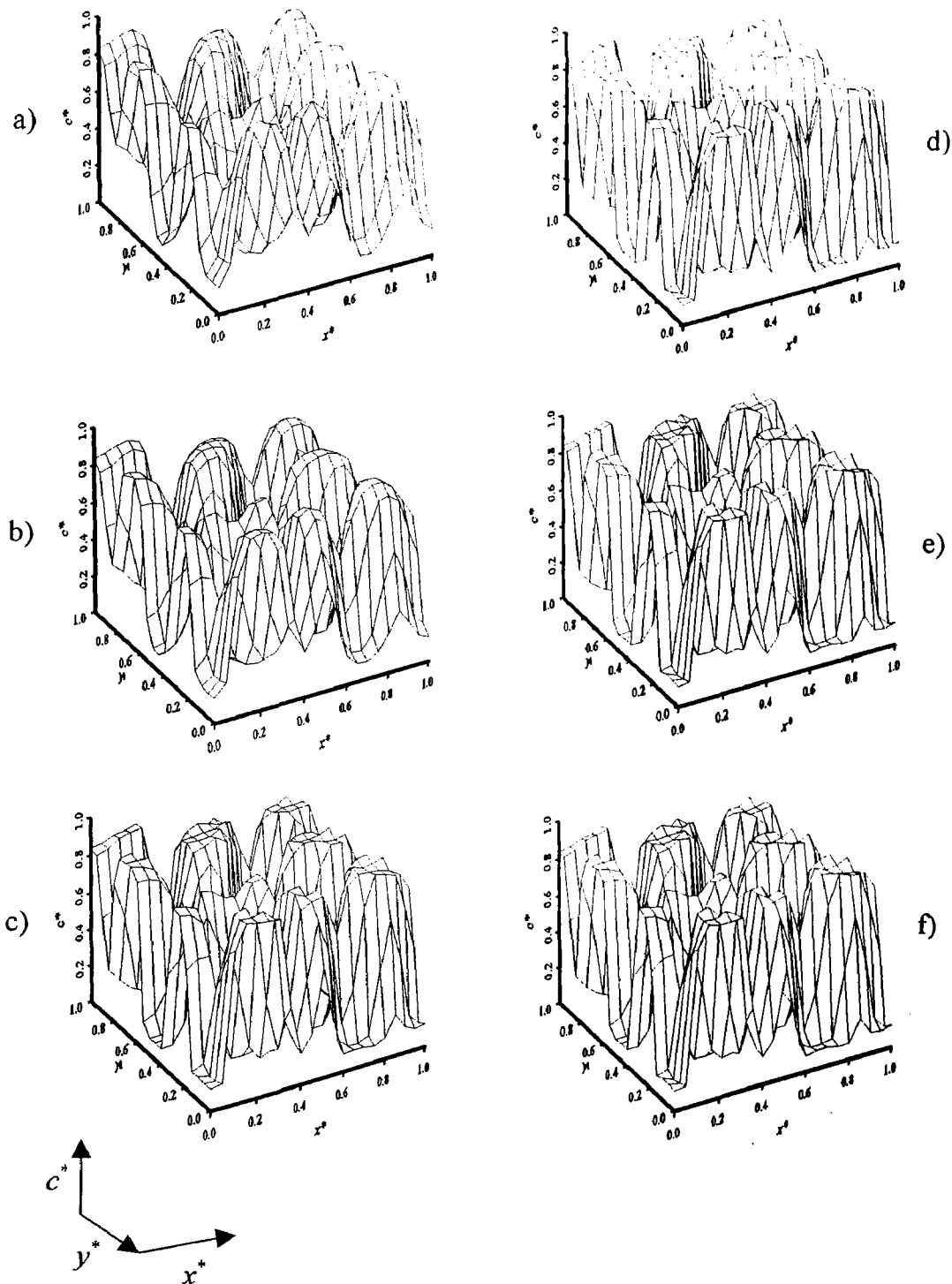


Figure 7.7: A plot of the 3-D dimensionless spatial concentration profiles, $c^*(x^*, y^*)$, showing the evolution of concentration fluctuations for a double critical ($c_o^* = 0.5$) quench from $T_1^* = 0.25$ to $T_1^* = 0.1$ with $D^* = 200\,000$. The following dimensionless times correspond to profiles made after the second jump at $t^* = 4.931$: (a) $t^* = 4.935$, (b) $t^* = 4.941$, (c) $t^* = 4.950$, and (d) $t^* = 4.952$ (e) $t^* = 4.953$ and (f) 4.9531 . The first sign of secondary phase separation occurs in c) at $t^* = 4.950$.

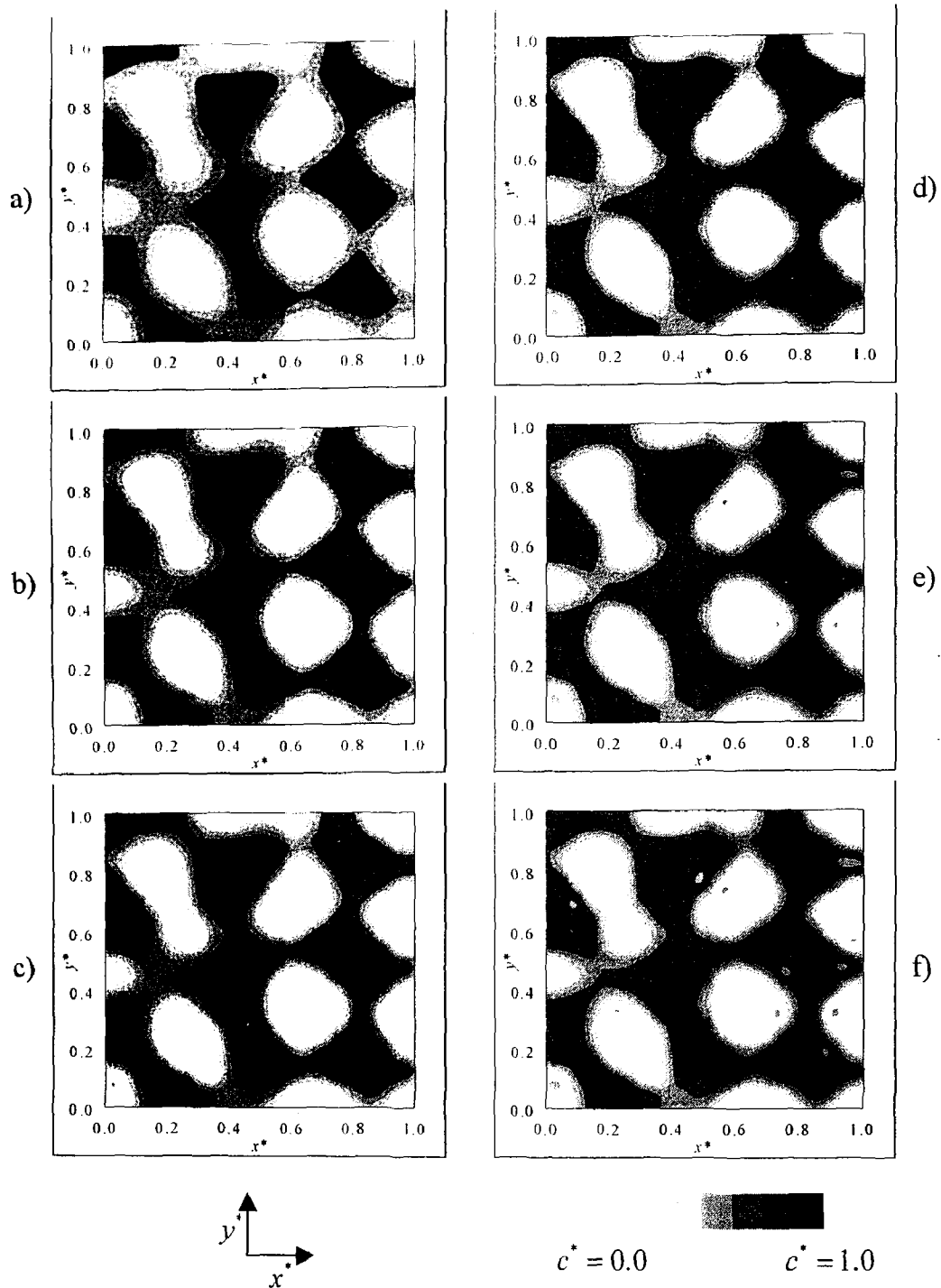


Figure 7.8: A plot of the 2-D dimensionless spatial concentration profiles, $c^*(x^*, y^*)$, showing the evolution of structure development for a double off-critical ($c_o^* = 0.6$) quench from $T_1^* = 0.25$ to $T_1^* = 0.1$ with $D^* = 200\ 000$. The following dimensionless times correspond to profiles made after the second jump at $t^* = 5.292$: (a) $t^* = 5.294$, (b) $t^* = 5.307$, (c) $t^* = 5.313$, and (d) $t^* = 5.315$ (e) $t^* = 5.317$ and (f) 5.320. The first sign of secondary phase separation occurs in (c) at $t^* = 5.313$. The grey scale represents the compositions of the phase separating blend on the bottom right.

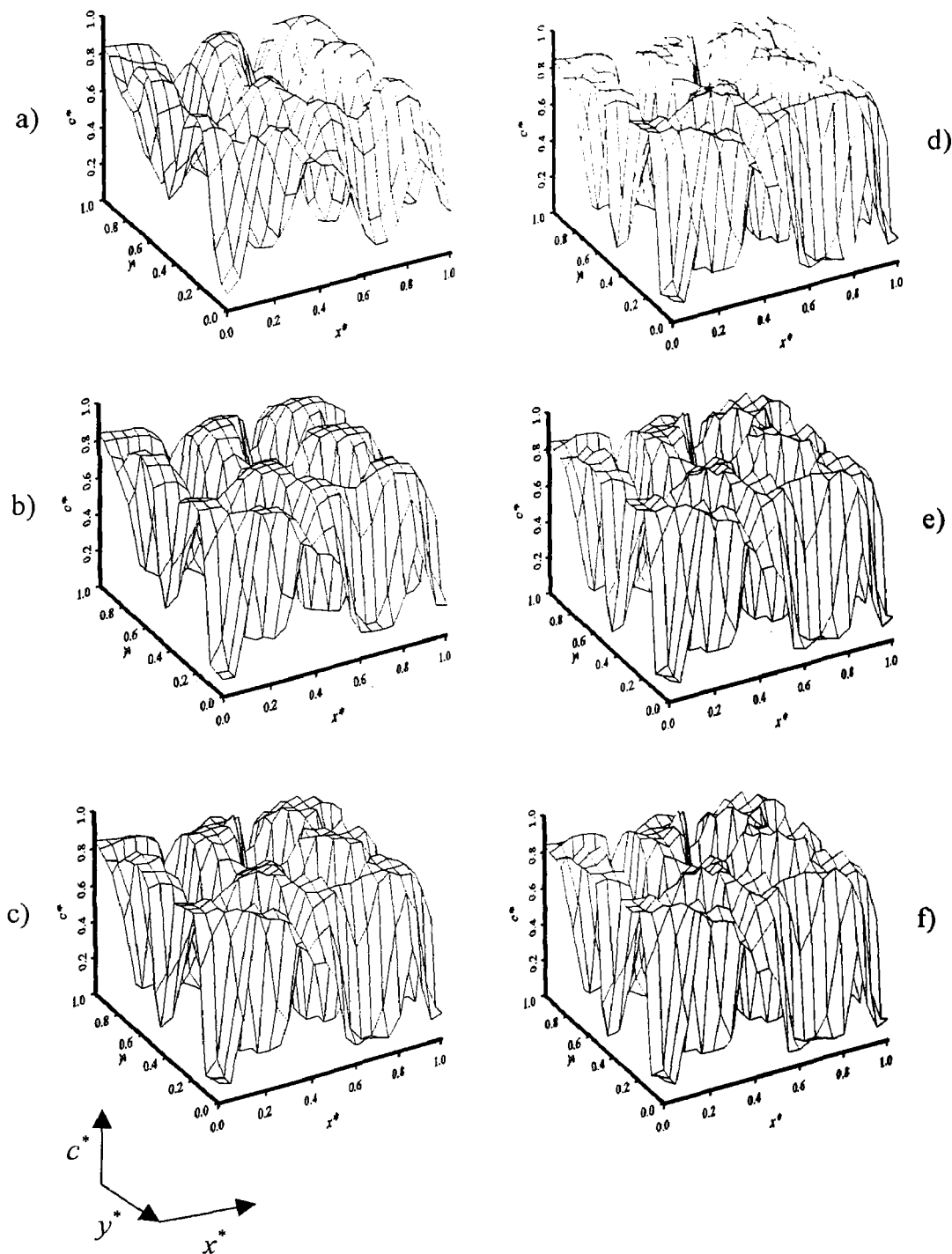


Figure 7.9: A plot of the 3-D dimensionless spatial concentration profiles, $c^*(x^*, y^*)$, showing the evolution of concentration fluctuations for a double off-critical ($c_o^* = 0.6$) quench from $T_l^* = 0.25$ to $T_l^* = 0.1$ with $D^* = 200\,000$. The following dimensionless times correspond to profiles made after the second jump at $t^* = 5.292$: (a) $t^* = 5.294$, (b) $t^* = 5.307$, (c) $t^* = 5.313$, and (d) $t^* = 5.315$ (e) $t^* = 5.317$ and (f) 5.320. The first sign of secondary phase separation occurs in c) at $t^* = 5.313$.

Chapter 8

Conclusions

A mathematical model and computer simulations were used to describe the dynamics of phase separation by spinodal decomposition for the TIPS method (single quench and a double quench) using the nonlinear Cahn-Hilliard theory and the Flory-Huggins-de Gennes free energy. The composition dependent mobility was treated using the slow mode theory and the reptation theory was used to describe the self-diffusion coefficient of the individual polymers in the blend. The composition dependent energy gradient coefficient was treated with the introduction of an additional entropic term into the F-H free energy, due to the connectivity of monomer units, to take into account changes in energy due to the creation of interfaces upon phase separation.

In the first part of this thesis, for the single critical and off-critical quench case, the numerical results in one and two dimensions replicated frequently observed trends of phase separation by spinodal decomposition in published experimental and numerical work.

In the one-dimensional model, in the early stages of phase separation by SD, the composition fluctuations grew with time at fixed wavelength and the evolution of the structure factor was exponential. In the beginning of the intermediate stages, the composition fluctuations were still increasing and nonlinear effects started to take place. This was evident in the evolution of the structure factor. It was found that in the critical quench, phase separation occurred earlier than that for the off-critical quench case at a fixed temperature, and this was due to the location of the quench within the spinodal. The further away (inward) the quench was from the spinodal curve, the more unstable the mixture was with a faster the occurrence of phase separation. In the investigation of the quench depth, from a shallower to a deeper quench, the degree of phase separation observed in the spatial composition profiles increased due to the increase in the driving force for phase separation. The time it took to observe the first sign of phase separation decreased with an increase in quench depth. The dimensionless diffusion coefficient showed an increase in the rate as well as the degree of phase separation in the range of $D^* = 200\ 000$ to $800\ 000$. Also, the increase dimensionless diffusion coefficient showed a decrease in the characteristic length (domain size), which was calculated from the plots of the structure factor using the maximum values of the wave number. From a thermodynamic point of view, the plots of the change in the spatial chemical potential, the driving force for phase separation, showed how equilibrium conditions were approached. The second derivative of the free energy with respect to composition showed the relative steepness in the curvature of the change in free energy (stability, instability and meta-stability) and the

increase in the value of D^* showed and increasing steepness. This reflects the increasing rate of phase separation observed in the spatial concentration profiles with increasing D^* .

In the two-dimensional study, the interest was in observing the pattern formation for the critical and off-critical quench was examined. The patterns formed are typical patterns observed in experimental and numerical work. The critical quench case showed the interconnected type structure, while the off-critical quench case showed the droplet type structure.

In the second part of this thesis, for the two-step quenching with an initial critical and an initial off-critical quench case, the numerical results in one and two dimensions replicated the observed trends of double phase separation by spinodal decomposition in recently published experimental and numerical work.

In the one-dimensional model, the evolution of the spatial concentration profiles showed two different trends depending on the quench depth. For the shallower second quench to $T_2^* = 0.2$, the original composition fluctuations from $T_1^* = 0.25$ continued to increase to the new equilibrium compositions with time and no sign of secondary phase-separated regions occurred. At a deeper second quench to $T_2^* = 0.1$, the original composition fluctuations from $T_1^* = 0.25$ continued to increase to the new equilibrium compositions with time. However, the composition fluctuations started to show the appearance of constructive and destructive interference as time increased. Therefore, between the two quench depths

investigated, it was suggested that there existed a critical quench depth in order for double phase separation to occur where secondary structures are formed. Furthermore, the structure factor for the shallower quench case showed a continuous increase from the original plot of the structure factor at $T_1^* = 0.25$ with no evidence of a secondary peak forming and for a deeper second quench, the evolution of the structure factor showed an increase in the original peak observed in the initial quench with the introduction of a secondary peak that continued to increase with time. The effect of the increase in the dimensionless diffusion coefficient showed an increase the rate as well as the amount of phase separation for both the shallower and deeper quench. A lag time was observed before the occurrence of secondary phase separation and it decreased with increase dimensionless diffusion coefficient. It was found that the growth rate of the secondary structures was faster with lower D^* . This was considered to be due to the larger domain size formed at lower D^* of the primary structure providing a larger confinement for the growth of the secondary structures. The growth of the primary and secondary structures after, the second temperature jump, for a shallow quench case was similar to the growth rate of the single quench case. The growth of the primary and secondary structures after, the second temperature jump, for the initial critical and initial off-critical quench case showed different growth dynamics. The growth rates of the primary and secondary peaks were broken down into three stages. The difference in the time at which the first sign of phase separation occurs and the growth dynamics was determined to be dependent on the location of the first and second quench within the spinodal and the value of

D^* . For the initial critical quench, phase separation occurs at earlier and the formation of secondary structures is faster than for the initial off-critical quench case. In terms of evolution of the secondary structures and the linear C-H theory, it was found that the early stages of the formation of the secondary structures followed the linear C-H theory shown through plots of the natural log of the structure factor with time similar to the single quench profiles. From a thermodynamic point of view, the shallower second quench showed similar results in the change in chemical potential and second derivative as for a single quench case. The only difference being at an increased rate. For the second deeper quench case, the change in the chemical potential showed a plateau when double phase separation was observed. This fattening of the change in chemical potential was thought to be due to the reorganizing of the composition in the mixture as subjected to the new imposed conditions. In the plot of the second derivative with respect to composition for the second deeper quench, evidence of the formation and evolution of a new instability was observed shortly after the second deeper jump where the local maximum between the two local minimums further divided into a double well shape. This new double well within already existing double well became more defined as D^* was increased.

In the two-dimensional study, the interest was in observing the pattern formation for a double quench with an initial critical quench to see if the model developed was able to predict the experimental work of Hashimoto and in the numerical work published by Henderson and Clarke in their study of double quenching. Therefore, the second quench was made in the late stages. The observed pattern

formation was consistent with that predicted by Hashimoto and in the numerical work of Henderson and Clarke where the second jump after the initial critical quench showed the interconnected structure with droplet type secondary structures forming. In addition to the work of Hashimoto and Henderson and Clarke, the second jump (late stages) after an initial off-critical quench was also presented where the observed pattern was droplet type for both the primary and secondary structures. This morphology is consistent with the experimental work of Tanaka.

The model using the nonlinear C-H and the F-H-deGennes free energy provided a better understanding of the formation and evolution of phase separation by SD for the single and double quench. In particular, for the formation of secondary phase-separated structures, with the limited amount of both experimental and numerical work published, the numerical work in this thesis provides a better understanding of the evolution of secondary phase separation and how the following areas are affected, the composition fluctuations, the structure factor, quench depth, dimensionless diffusion coefficient, evolution of the growth rate of primary and secondary structures, and the change in chemical potential and the second derivative of free energy.

References

Aksimentiev, A., Holyst, R., and Moorthi, K., *Macromol. Theory Simul.*, **9**, 661, (2000)

Akcasu, A., Nägele, G., and Klein, R., *Macromolecules*, **28**, 6680 (1995)

Ariyapadi, M., and Nauman, E., in: *Computer Simulation of Polymers: Spinodal Decomposition in Polymer-Polymer Systems: A Two-Dimensional Computer Simulation*: Roe, R., (Ed.). Prentice Hall Physical Life Sciences, Ch.27, (1991)

Aymard, P., Williams, M., Clark, A., and Norton, I., *Langmuir*, **16**, 7383 (2000)

Bates, F., and Wiltzius, P., *J. Chem. Phys.*, **91**, 3258, (1989)

Binder, K., *J. Chem. Phys.*, **79**, 6387, (1983)

Brochard, F., Jouffroy, J., Levinson, P., *Macromolecules*, **16**, 1638, (1983)

Brown, G., and Chakrabarti, A., *J. Chem. Phys.*, **98**, 2451, (1993a)

Brown, G., and Chakrabarti, A., *Physical Review E*, **48**, 3705, (1993b)

Brown, W. and Mortensen, K., *Scattering in Polymeric and Colloidal Systems*, Gordon and Breach Science Publishers, (2000)

Cahn, J., *J. Chem. Phys.*, **42**, 93, (1965)

Carmesin, H., Heermann, D., and Binder, K., *Z. Phys. B. Condensed Matter*, **65**, 89, (1986)

Castellano, C., and Corberi, F., *Physical Review E*, **61**, 3252, (2000)

Castellano, C., and Glotzer, S., *J. Chem. Phys.*, **103**, 9363, (1995)

Chakrabarti, A., Toral, R., Gunton, J., and Muthukumar, M., *Physical Review Letters*, **63**, 2072, (1989)

Chakrabarti, A., Toral, R., Gunton, J., Muthukumar, M., *J. Chem. Phys.*, **92**, 6899, (1990)

Chan, P., and Rey, A., *Macromol. Theory Simul.*, **4**, 873, (1995a)

Chan, P., PhD Dissertation, McGill University, Montreal, Canada, (1997)

- Chan, P.K. and Rey, A.D., *Computational Materials Science*, **3**, 337 (1995b)
- Chan, P., *Recent Res. Devel. In Macromolecul. Res.*, **3**, 439, (1998)
- Chen, W., Kobayashi, S., and Inoue, T., *Polymer*, **35**, 4015, (1994)
- Chow, T., *Journal of Materials Science*, **15**, 1873, (1980)
- Chun, Y., Park, J., Dun, J., and Kim, W., *Journal of Polymer Science: Part B: Polymer Physics*, **38**, 2072, (2000)
- Chung, T., *Finite Element Analysis in Fluid Dynamics*, McGraw-Hill, (1978)
- Clarke, N., McLeish, T., and Jenkins, S., *Macromolecules*, **28**, 4650, (1995)
- Composto, R., and Kramer, E., *Macromolecules*, **21**, 2580, (1988)
- Copetti, G., Grassi, M., Lapasin, R., and Prici, S., *Glycoconjugate Journal*, **14**, 951, (1997)
- Copetti, M. and Elliot, C., *Materials Science and Technology*, **6**, 273, (1990)
- Cowie, J., *Polymers: Chemistry, and Physics of Modern Materials*, 2nd edition, Stanley Thornes Publishers Ltd., (1998)
- Daould, M., Cotton, J., Farnoux, B., Jannink, G., Sarma, G., Benoit, H., Dulessix, R., Picot, C., and de Gennes, P., *Macromolecules*, **8**, 804, (1975)
- de Gennes, P., *J. Chem. Phys.* **55**, 572, (1971)
- de Gennes, P., *J. Chem. Phys.*, **72**, 4756, (1980)
- Doane, J., Yaniv, Z., *Liquid Crystal Chemistry, Physics and Applications*, International Society for Imaging Science and Technology, (1989)
- Doi M., and Edwards, S., *The Theory of Polymer Dynamics*, Oxford University Press, (1986)
- Elliniadis, S., Higgins, J., Clarke, N., McLeish, T., Choudhery, R., and Jenkins, S., *Polymer*, **38**, 4855, (1997)
- Elliot, C. M. and Songmu, Z., *Arch. Ration. Mech. Anal.*, **96**, 339 (1986)
- Flory, P., *Principles of Polymer Chemistry*, Cornell University Press, (1953)
- Fujita, H., Hashimoto, T., and Takenaka, M., *Macromolecules*, **22**, 4663, (1989)

- Gelles, R., and Frank, W., *Macromolecules*, **16**, 1448, (1983)
- Glotzer, S., *Annu. Rev. Comput. Phys.*, **2**, 1, (1995)
- Gorga, R., Jablonski, E., Thiyagarajan, P., Seifert, S., and Narasimhan, B., *Journal of Polymer Science: Part B: Polymer Physics*, **40**, 255, (2002)
- Graca, M., Wieczorek, S., Fialkowski, M., and Holyst, R., *Macromolecules*, **35**, 9117, (2002)
- Green, P., Palmstrom, C., Mayer, J., and Kramer, E., *Macromolecules*, **18**, 501, (1985)
- Hamley, I., *Introduction to Soft Matter: Polymers, Colloids, Amphiphiles and Liquid Crystals*, John Wiley & Sons, (2000)
- Hashimoto, T., in: *Materials Science and Technology*, Vol. 12: *Structure and Properties of Polymers*: Cahn, R., Haasen, P., and Kramer, J., (Ed.). Weinheim: VCH Publishers, Ch. 6 (1993)
- Hashimoto, T., Hayashi, M., and Jinnai, H., *J. Chem. Phys.*, **112**, 6886, (2000)
- Hashimoto, T., Jinnai, H., Hasegawa, H., and Han, C., *Physica A*, **204**, 261, (1994)
- Hashimoto, T., Itakura, M., and Hasegawa, H., *J. Chem. Phys.*, **85**, 6118, (1986a)
- Hashimoto, T., Itakura, M., and Shimidzu, N., *J. Chem. Phys.*, **85**, 6773, (1986b)
- Hashimoto, T., Kimishima, K., and Hasegawa, H., *Macromolecules*, **24**, 5704, (1991)
- Hashimoto, T., Kumaki, J., Kawai, H., *Macromolecules*, **16**, 641, (1983)
- Hashimoto, T., Sasaki, K., and Kawai, H., *Macromolecules*, **17**, 2812, (1984)
- Hashimoto, T., Takenaka, M., and Izumitani, T., *J. Chem. Phys.*, **92**, 3213, (1990)
- Hayashi, M., Jinnai, H., and Hashimoto, T., *J. Chem. Phys.*, **112**, 6897, (2000a)
- Hayashi, M., Jinnai, H., and Hashimoto, T., *J. Chem. Phys.*, **113**, 3414, (2000b)
- Henderson, I., and Clarke, N., *Macromolecules*, in press, (2004)
- Huebner, K., Thornton, E., and Byrom, T., *The Finite Element Method for Engineers*, 3rd, John Wiley and Sons, (1995)

- Inaba, N., Sato, K., Suzuki, S., and Hashimoto, T., *Macromolecules*, **19**, 1690, (1986)
- Inaba, N., Yamada, T., Suzuki, S., and Hashimoto, T., *Macromolecules*, **21**, 407, (1988)
- Izumitani, T., and Hashimoto, T., *J. Chem. Phys.*, **83**, 3694, (1985)
- Izumitani, T., and Hashimoto, T., *Macromolecules*, **27**, 1744, (1994)
- Izumitani, T., and Hashimoto, T., *J. Chem. Phys.*, **83**, 3694, (1985)
- Izumitani, T., Takenaka, M., and Hashimoto, T., *J. Chem. Phys.*, **92**, 3213, (1990)
- Jilge, W., Carmesin, I., Kremer, K., and Binder, K., *Macromolecules*, **23**, 5001 (1990)
- Jinnai, H., Hasegawa, H., Hashimoto, T., and Han, C., *Macromolecules*, **24**, 282, (1991)
- Jinnai, H., Hashimoto, T., Hasegawa, H., and Han, C., *J. Chem. Phys.*, **99**, 8154, (1993)
- Jinnai, H., Hashimoto, T., Hasegawa, H., and Han, C., *J. Chem. Phys.*, **85**, 6118, (1986)
- Jones, R., and Richards, R., *Polymers at Surfaces and Interfaces*, Cambridge University Press, (1999)
- Kalyanasundaram, S., Rajendran, S., and Chelladurai, C., *Bulletin of Electrochemistry*, **18**, 473, (2002)
- Klein, J., *Macromolecules*, **11**, 852, (1978)
- Koningsveld, R., MacKnight, W., *Polymer International*, **44**, 356, (1997)
- Kontis, M., and Muthukumar, M., *Macromolecules*, **25**, 1716, (1992)
- Kramer, E., Green, P., and Palmstrom, C., *Polymer*, **25**, 473, (1984)
- Kurata, M., *Thermodynamics of Polymer Solutions*, Vol. 1., Harwood Academic Publishers, (1982)
- Kwak, K., Okada, M., Chiba, T., and Nose, T., *Macromolecules*, **26**, 4047, (1993)
- Kyu, T., and Lim, D., *Macromolecules*, **24**, 3645, (1991)

- Kyu, T., and Saldanha, J., *Macromolecules*, **21**, 1201, (1998)
- Lacasta, A, Sancho, J., and Yeung, C., *Europhysics Letters*, **27**, 291 (1994)
- Langer, J., Bar-on, M., and Miller, H., *Physical Review A*, **11**, 1417, (1975)
- Lapidus, P. and Pinder, G., *Numerical Solution of Partial Differential Equations in Science and Engineering*, John Wiley & Sons, (1982)
- Leblond, J., *The Physics of Phase Transitions: Concepts and Applications*, Springer, (2002)
- Lee, A., and Kyu, T., *Macromolecules*, **23**, 459, (1990)
- Lee, B., Douglas, J., and Glotzer, S., *Phys. Rev. E*, **60**, 5812 (1999)
- Lee, K., Chan, P., and Feng, X., *Macromol. Theory Simul.*, **11**, 996, (2002)
- Matsuoka, T., and Yamamoto, S., *Journal of Applied Polymer Science*, **57**, 353, (1995)
- Mori, K., Tanaka, H., and Hashimoto, T., *Macromolecules*, **20**, 381, (1987)
- Mulder, M., *Basic Principles of Membrane Technology*, 2nd edition, Kluwer Academic Publishers, (1996)
- Nauman, E., and Qiwei He, D., *Chemical Engineering Science*, **56**, 1999, (2001)
- Nauman, E., and Qiwei, D., *Polymer*, **35**, 2243, (1994)
- Norton, I., and Frith, W., *Food Hydrocolloids*, **15**, 543, (2001)
- Novick-Cohen, A and Segel, L.A., *Physica D*, **10**, 277 (1984)
- Nwabunma, D., Chiu, H., Thein, K., *J. Chem. Phys.*, **113**, 6429, (2000)
- Ohnaga, T., and Inoue, T., *J. Polym. Sci. Part B, Polym. Phys.*, **27**, 1675, (1989)
- Ohnaga, T., Chen, W., and Inoue, T., *Polymer*, **35**, 3774, (1994)
- Ohnaga, T., Maruta, J., and Inoue, T., *Polymer*, **60**, 1945, (1989)
- Okada, M., Han, C., *J. Chem. Phys.*, **85**, 5317, (1986)
- Okinaka, J., and Tran-Cong, Q., *Physica D*, **84**, (1995)

- Pincus, P., *J. Chem. Phys.*, **75**, 1996, (1981)
- Ribbe, A., and Hashimoto, T., *Macromolecules*, **30**, 3999, (1997)
- Rouse, P., *J. Chem. Phys.*, **21**, 1272, (1953)
- Sato, T., Shiomi, T., Imai, K., *Polymer*, **37**, 2131, (1996)
- Schwahn, D., Hahn, K., Springer, T., *J. Chem. Phys.*, **93**, 8383, (1990)
- Schwahn, D., Mortensen, K., Springer, H., Maderia, Y., and Thomas, R., *J. Chem. Phys.*, **87**, 6078, (1987)
- Shibayama, M., Stein, R., Shimizu, N., and Hashimoto, T., *Macromolecules*, **19**, 1667, (1986)
- Skripov V., and Skripov, A., *Sov. Phys. Usp*, **22**, 389, (1979)
- Strobl, G., Bendler, J., Kambour, R., and Shultz, A., *Macromolecules*, **19**, 2683, (1986)
- Strobl, G., *Macromolecules*, **18**, 558, (1985)
- Takenaka, M., and Hashimoto, T., *J. Chem. Phys.*, **96**, 6177, (1992)
- Takenaka, M., and Hashimoto, T., *Macromolecules*, **27**, 6117, (1994)
- Takenaka, M., and Hashimoto, T., *Physical Review E*, **48**, R647, (1993)
- Takenaka, M., Izumitani, T., and Hashimoto, T., *J. Chem. Phys.*, **92**, 4566, (1990)
- Takenaka, M., Izumitani, T., and Hashimoto, T., *J. Chem. Phys.*, **97**, 6855, (1992)
- Takenaka, M., Izumitani, T., and Hashimoto, T., *Macromolecules*, **20**, 2257, (1987)
- Takenaka, M., Hashimoto, T., Kawakatsu, T., and Kawasaki, K., *Physical Review E.*, **52**, 2247, (1995)
- Takeno, H., and Hashimoto, T., *J. Chem. Phys.*, **108**, 1225, (1998)
- Tanaka, H., and Araki, T., *Phys. Rev. Lett.*, **81**, 389, (1998)
- Tanaka, H., *Journal of Physics: Condensed Matter*, **12**, R207, (2000)
- Tanaka, H., *Phys. Rev. E.*, **47**, 2946, (1993)

- Tanaka, H., *Phys. Rev. Lett.*, **72**, 3690. (1994)
- Tao, J., Okada, M., Nose, T., *Polymer*, **36**, 3909, (1995)
- Utracki, L. *Polymer Alloys and Blends*, Hanser Publishers, (1990)
- Utracki, L., *Two-Phase Polymer Systems*, Hanser Publishers, (1991)
- Vaidya, N., Dae han, C., Kim, D., Sakamoto, N., and Hashimoto, T., *Macromolecules*, **34**, 222, (2001)
- Van Dijk, M., and Wakker, A, *Concepts of Polymer Thermodynamics*, (ChemTec Publishing), (1997)
- Wen, G., Sun, Z., Yang, J., An, L., Jiang, Z., and Wu, Z., *Macromol. Theory Simul.*, **10**, 368, (2001)
- Wiltzius, P., Bates, F., and Heffner, W., *Physical Review Letters*, **60**, 1538, (1988)
- Yamada, T., Suzuki, S., and Hashimoto, T., *Macromolecules*, **21**, 407, (1988)
- Yamamura, M., Nishio, T., Kajiwara, T., and Adachi, K., *Chem. Eng. Sci.*, **57**, 2901, (2002)
- Yang, H., Shibayama, M., Stein, R., Shimizu, N., and Hashimoto, T., *Macromolecules*, **19**, 1667, (1986)
- Yang, Y., Fujiwara, H., Chiba, T., and Inoue, T., *Polymer*, **39**, 2745, (1998)
- Zhang, H., Zhang, J., and Yang, Y., *Macromol. Theory Simul.*, **4**, 1001, (1995)

Appendix A

Galerkin Finite Element Method: Hermitian Basis Functions

In the method of solution for the fourth order partial differential equation, the Galerkin Finite Element Method was employed. Hermitian basis functions were used as the interpolating functions and are listed in this appendix for the one-dimensional and two-dimensional study.

In a one-dimensional study, each element has 2 double nodes (one for the function and one for the slope) and four basis functions. The basis functions are:

$$\phi_1 = 1 - 3\xi^2 + 2\xi^3 \quad (\text{A.1})$$

$$\phi_2 = \xi - 2\xi^2 + \xi^3 \quad (\text{A.2})$$

$$\phi_3 = 3\xi^2 - 2\xi^3 \quad (\text{A.3})$$

$$\phi_4 = \xi^2 - \xi^3 \quad (\text{A.4})$$

For the two-dimensional study, each element has nodes 4 double nodes and 16 basis functions. The two-dimensional case is a product of the one-dimensional basis functions in the x and y direction. In the 2-D model, the x, y coordinates are represented by new coordinates in ξ, η space. The four nodes in ξ, η space are:

$$F_1(\xi) = (1 - 3\xi^2 + 2\xi^3) \quad (\text{A.5})$$

$$F_2(\xi) = (\xi - 2\xi^2 + \xi^3) \quad (\text{A.6})$$

$$F_3(\xi) = (3\xi^2 - 2\xi^3) \quad (\text{A.7})$$

$$F_4(\xi) = (\xi^3 - \xi^2) \quad (\text{A.8})$$

$$F_1(\eta) = (1 - 3\eta^2 + 2\eta^3) \quad (\text{A.9})$$

$$F_2(\eta) = (\eta - 2\eta^2 + \eta^3) \quad (\text{A.10})$$

$$F_3(\eta) = (3\eta^2 - 2\eta^3) \quad (\text{A.11})$$

$$F_4(\eta) = (\eta^3 - \eta^2) \quad (\text{A.12})$$

The 16 basis functions are obtained from the product of the one-dimensional basis functions ξ, η space:

$$\phi_1 = (1 - 3\xi^2 + 2\xi^3)(1 - 3\eta^2 + 2\eta^3) \quad (\text{A.13})$$

$$\phi_2 = ([\xi - 2\xi^2 + \xi^3] \Delta x)(1 - 3\eta^2 + 2\eta^3) \quad (\text{A.14})$$

$$\phi_3 = (1 - 3\xi^2 + 2\xi^3)([\eta - 2\eta^2 + \eta^3] \Delta y) \quad (\text{A.15})$$

$$\phi_4 = ([\xi - 2\xi^2 + \xi^3] \Delta x)([\eta - 2\eta^2 + \eta^3] \Delta y) \quad (\text{A.16})$$

$$\phi_5 = (1 - 3\xi^2 + 2\xi^3)(3\eta^2 - 2\eta^3) \quad (\text{A.17})$$

$$\phi_6 = ([\xi - 2\xi^2 + \xi^3] \Delta x)(3\eta^2 - 2\eta^3) \quad (\text{A.18})$$

$$\phi_7 = (1 - 3\xi^2 + 2\xi^3)([\eta^3 - \eta^2] \Delta y) \quad (\text{A.19})$$

$$\phi_8 = ([\xi - 2\xi^2 + \xi^3] \Delta x)([\eta^3 - \eta^2] \Delta y) \quad (\text{A.20})$$

$$\phi_9 = (3\xi^2 - 2\xi^3)(1 - 3\eta^2 + 2\eta^3) \quad (\text{A.21})$$

$$\phi_{10} = ([\xi^3 - \xi^2] \Delta x)(1 - 3\eta^2 + 2\eta^3) \quad (\text{A.22})$$

$$\phi_{11} = (3\xi^2 - 2\xi^3)([\eta - 2\eta^2 + \eta^3] \Delta y) \quad (\text{A.23})$$

$$\phi_{12} = ([\xi^3 - \xi^2] \Delta x)([\eta - 2\eta^2 + \eta^3] \Delta y) \quad (\text{A.24})$$

$$\phi_{13} = (3\xi^2 - 2\xi^3)(3\eta^2 - 2\eta^3) \quad (\text{A.25})$$

$$\phi_{14} = ([\xi^3 - \xi^2] \Delta x)(3\eta^2 - 2\eta^3) \quad (\text{A.26})$$

$$\phi_{15} = (3\xi^2 - 2\xi^3)([\eta^3 - \eta^2] \Delta y) \quad (\text{A.27})$$

$$\phi_{16} = ([\xi^3 - \xi^2] \Delta x)([\eta^3 - \eta^2] \Delta y) \quad (\text{A.28})$$

Appendix B

Single Quench: Dimensionless 1-D Critical and Off-Critical Quench Results

1-D Dimensionless Spatial Concentration Profiles

Figures B.1 and B.2 show the evolution of the dimensionless spatial concentration profiles for a single quench at the critical composition of $c_c = 0.5$, a dimensionless temperature of $T_l^* = 0.25$, and dimensionless diffusion coefficients of $D^* = 500\,000$ and $800\,000$, respectively. Figures B.3 and B.4 show the evolution of the dimensionless spatial concentration profiles for a single quench at an off-critical composition of $c_c = 0.6$, a dimensionless temperature of $T_l^* = 0.25$, and dimensionless diffusion coefficients of $D^* = 500\,000$ and $800\,000$, respectively. For all four figures the evolution of the one-dimensional dimensionless spatial concentration profiles show the same trends as observed in experiment. In the early stage, the initial concentration fluctuations appear due to the growth of the most dominant wavelength and are weakly nonlinear. The wavelength remains constant while the amplitude changes. In the beginning of the intermediate stage, the concentration fluctuations continue to increase and into the intermediate stage

the wavelength starts to change. The only difference in the composition fluctuations is the effect of increasing D^* . As the value of D^* (200 000, 500 000, 800 000) increases, the driving force for phase separation is larger and therefore, more phase separated regions are developed as discussed in the Chapter 5.

Evolution of the Dimensionless Structure Factor

Figures B.5 and B.6 show the evolution of the dimensionless structure factor as a function of dimensionless wave number, k^* , and dimensionless time for the critical quench case with $D^* = 500\ 000$ and $800\ 000$, respectively. Figures B.7 and B.8 show the evolution of the dimensionless structure factor as a function of dimensionless wave number, k^* , and dimensionless time for the off-critical quench case with $D^* = 500\ 000$ and $800\ 000$, respectively. In all four figures, the quench temperature is $T^* = 0.25$. The critical and off-critical quench case show that the value of the dimensionless structure factor increases exponentially with time in the early stages of phase separation by SD the wave number is constant and begins to slow down as it approaches the beginning of the intermediate stages where nonlinear effects come into play. These results are consistent with the observations made in Chapter 5.

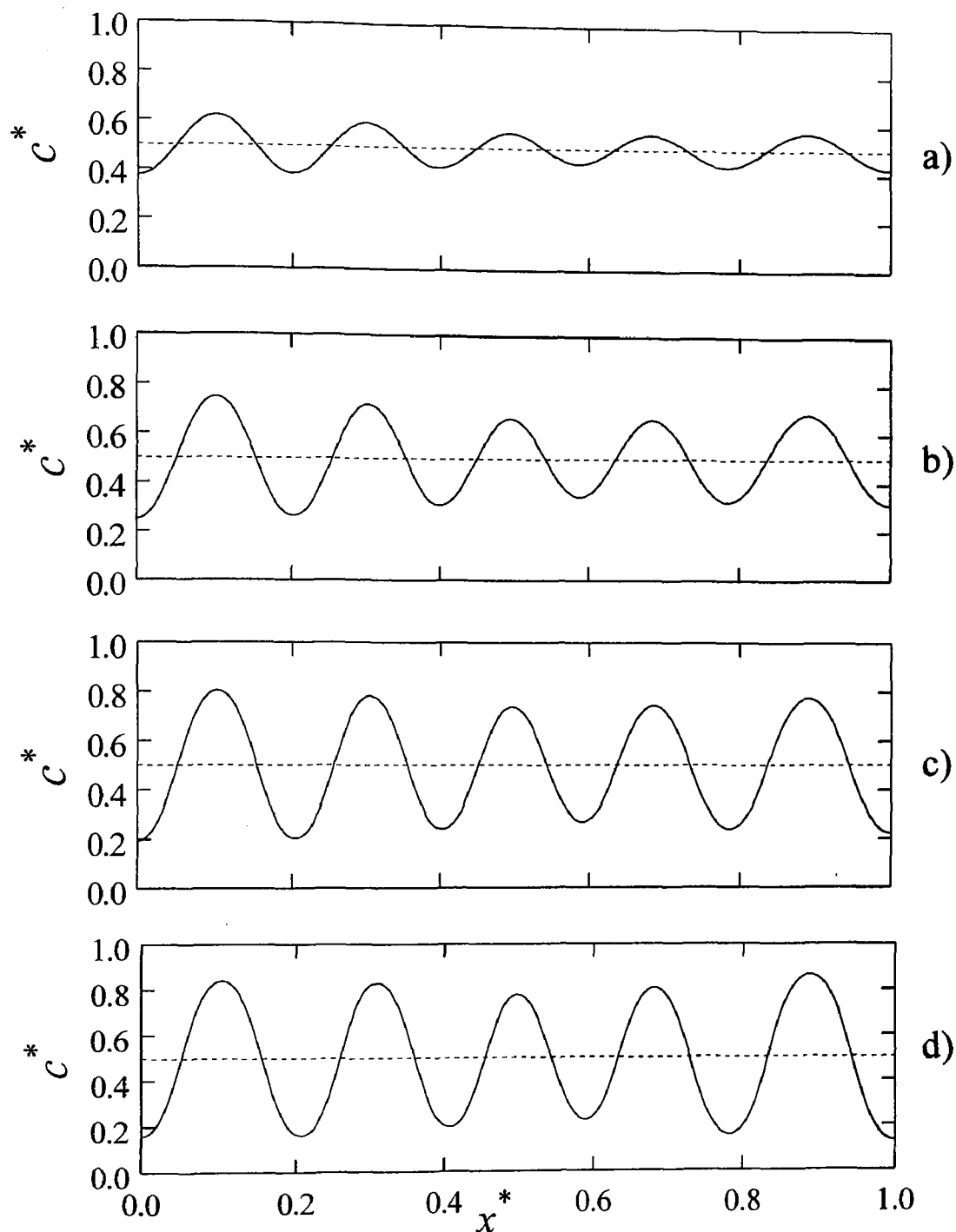


Figure B.1: The evolution of the dimensionless spatial concentration profile for a single quench into the unstable region of the phase diagram at the following dimensionless times: (a) $t^* = 0.552$, (b) $t^* = 0.5956$, (c) $t^* = 0.6252$, and (d) $t^* = 0.6946$. The dashed line through the center of the graph represents the initial average concentration $c_0^* = 0.5$. The dimensionless diffusion coefficient for this case is $D^* = 500\,000$.

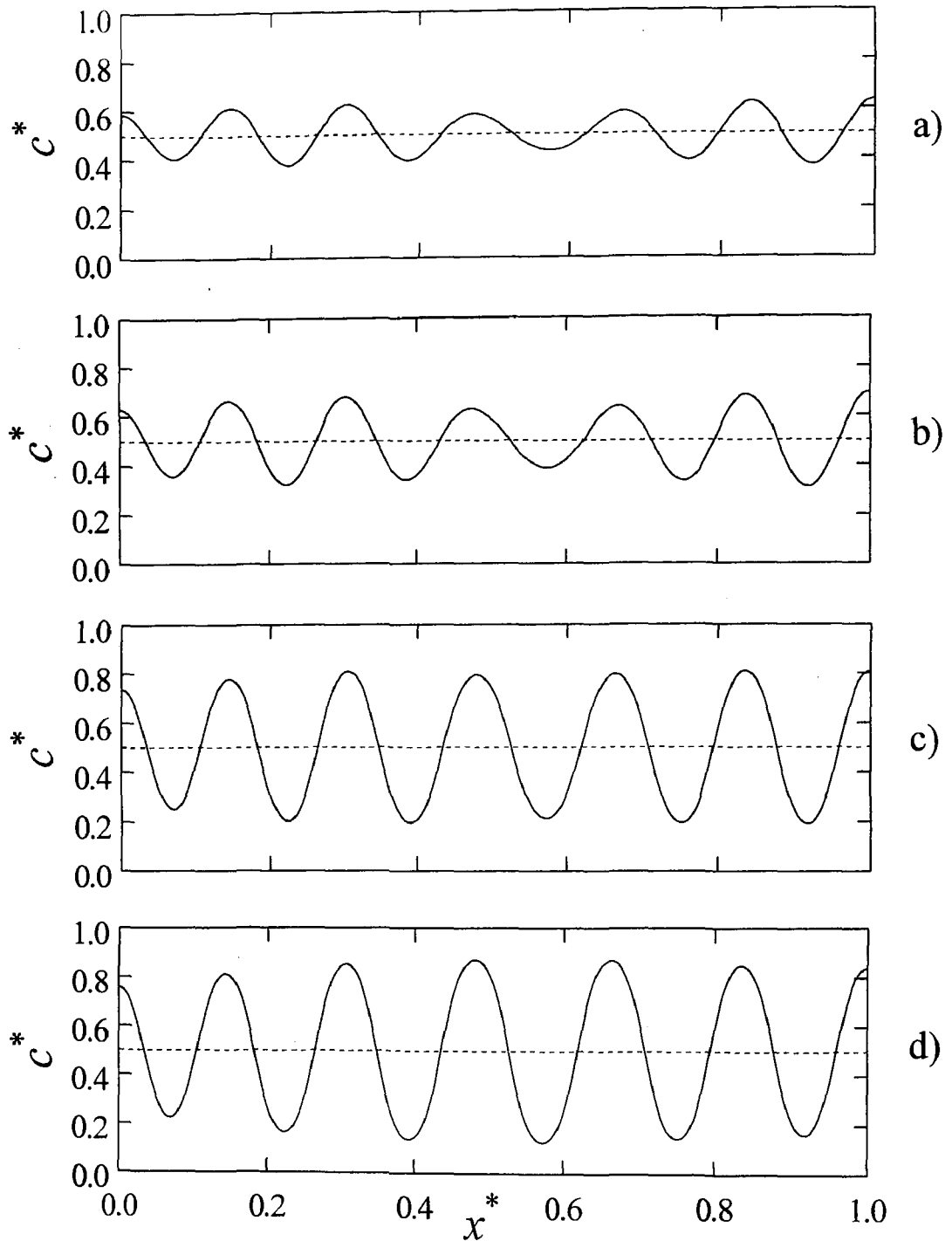


Figure B.2: The evolution of the dimensionless spatial concentration profile for a single quench into the unstable region of the phase diagram at the following dimensionless times: (a) $t^* = 0.22$, (b) $t^* = 0.2278$, (c) $t^* = 0.2479$, and (d) $t^* = 0.2733$. The dashed line through the center of the graph represents the initial average concentration $c_0^* = 0.5$. The dimensionless diffusion coefficient for this case is $D^* = 800\,000$.

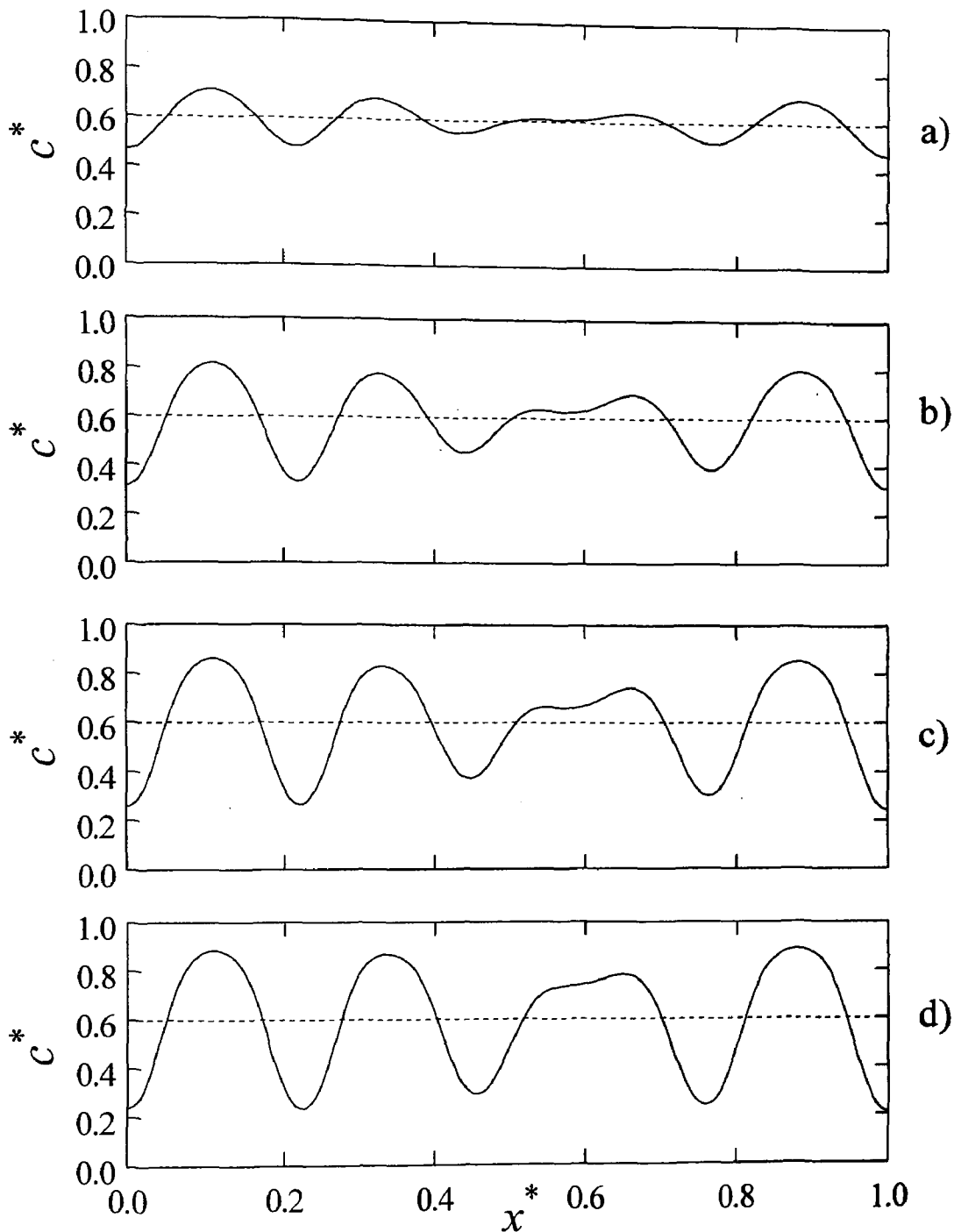


Figure B.3: The evolution of the dimensionless spatial concentration profile for a single quench into the unstable region of the phase diagram at the following dimensionless times: (a) $t^* = 0.7519$, (b) $t^* = 0.7775$, (c) $t^* = 0.842$, and (d) $t^* = 0.914$. The dashed line through the center of the graph represents the initial average concentration $c_0^* = 0.6$. The dimensionless diffusion coefficient for this case is $D^* = 500\,000$.

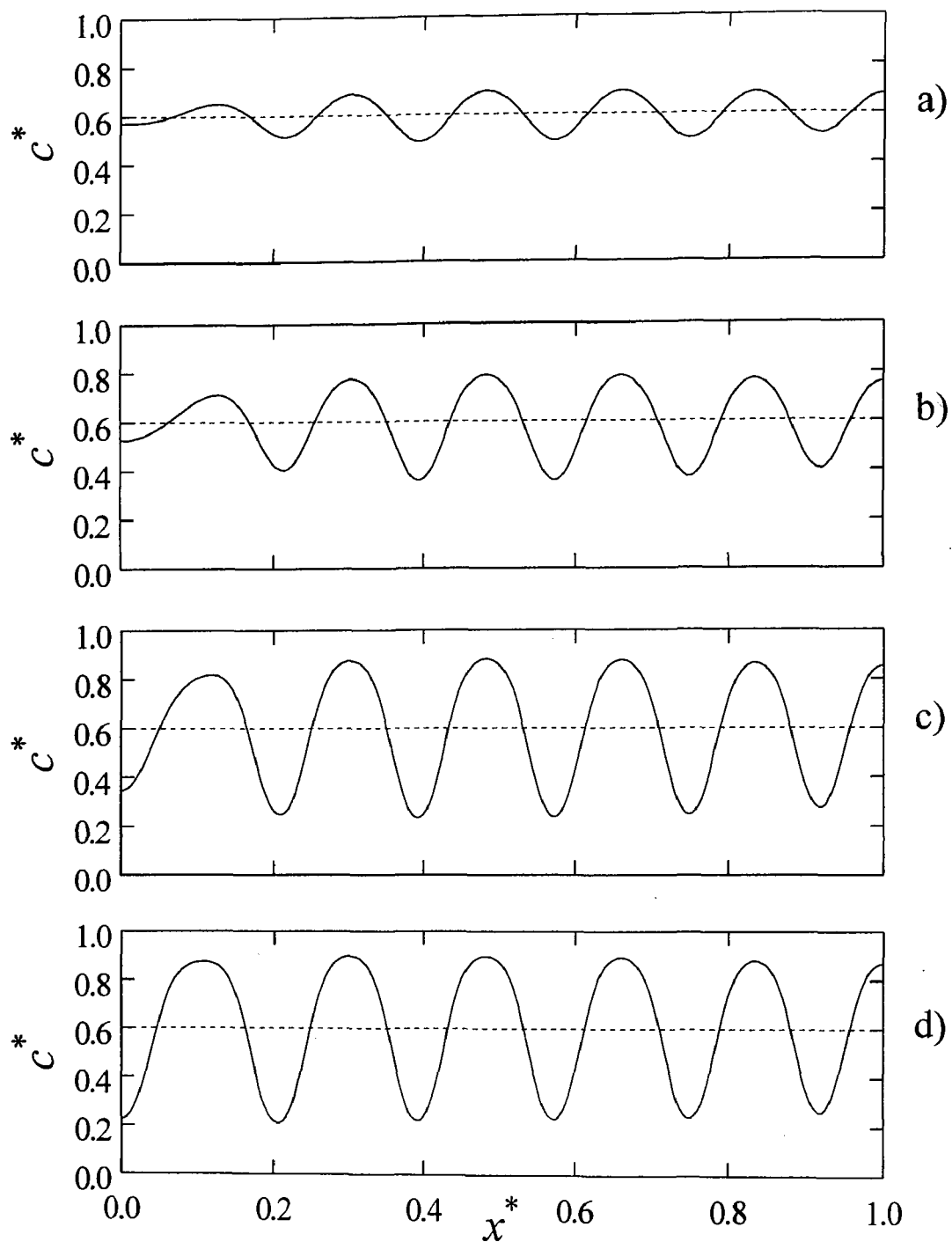


Figure B.4: The evolution of the dimensionless spatial concentration profile for a single quench into the unstable region of the phase diagram at the following dimensionless times: (a) $t^* = 0.2878$, (b) $t^* = 0.3068$, (c) $t^* = 0.3312$, and (d) $t^* = 0.3453$. The dashed line through the center of the graph represents the initial average concentration $c_0^* = 0.6$. The dimensionless diffusion coefficient for this case is $D^* = 800\,000$.

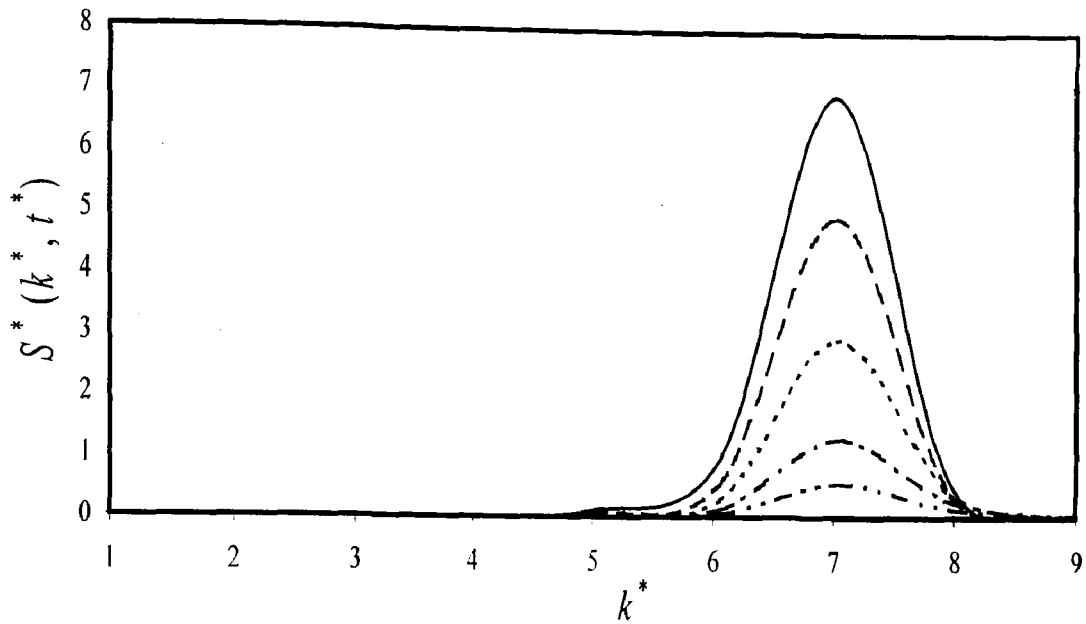


Figure B.5: The evolution of the dimensionless structure factor for a single critical quench ($c_o^* = 0.5$, $D^* = 500\,000$ and $T^* = 0.25$) into the unstable region of the phase diagram at the following dimensionless times: $t^* = 0.552$ (thick grey line), $t^* = 0.5709$ (dash with two dots), $t^* = 0.5956$ (dash-dot line), $t^* = 0.6252$ (dotted line), $t^* = 0.6548$ (long dashed line), $t^* = 0.6946$ (solid line).

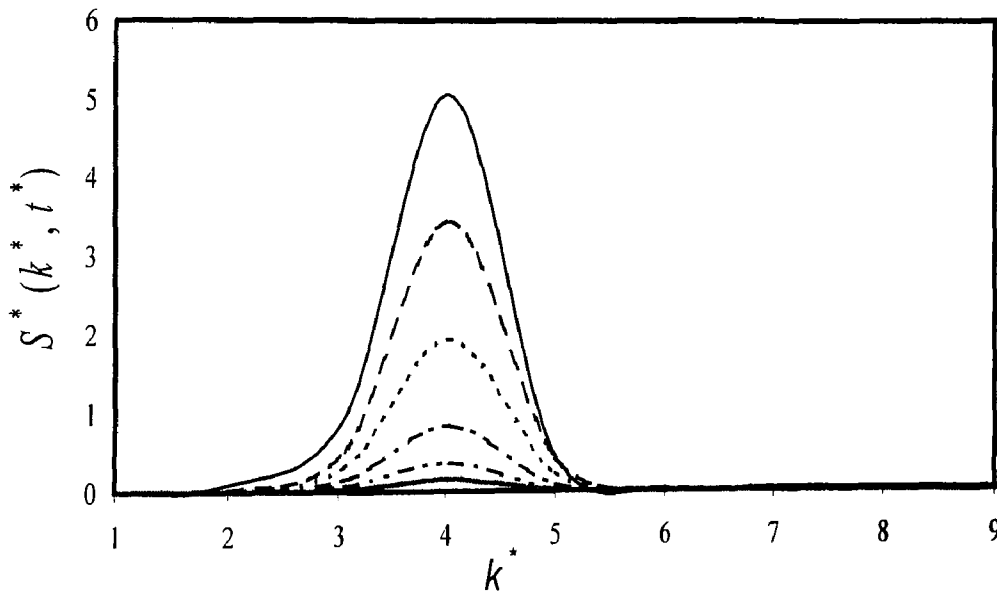


Figure B.6: The evolution of the dimensionless structure factor for a single critical quench ($c_o^* = 0.5$, $D^* = 800\,000$ and $T^* = 0.25$) into the unstable region of the phase diagram at the following dimensionless times: $t^* = 0.22$ (dash with two dots), $t^* = 0.2278$ (dash-dot line), $t^* = 0.2377$ (dotted line), $t^* = 0.2479$ (long dashed line), $t^* = 0.2733$ (solid line).

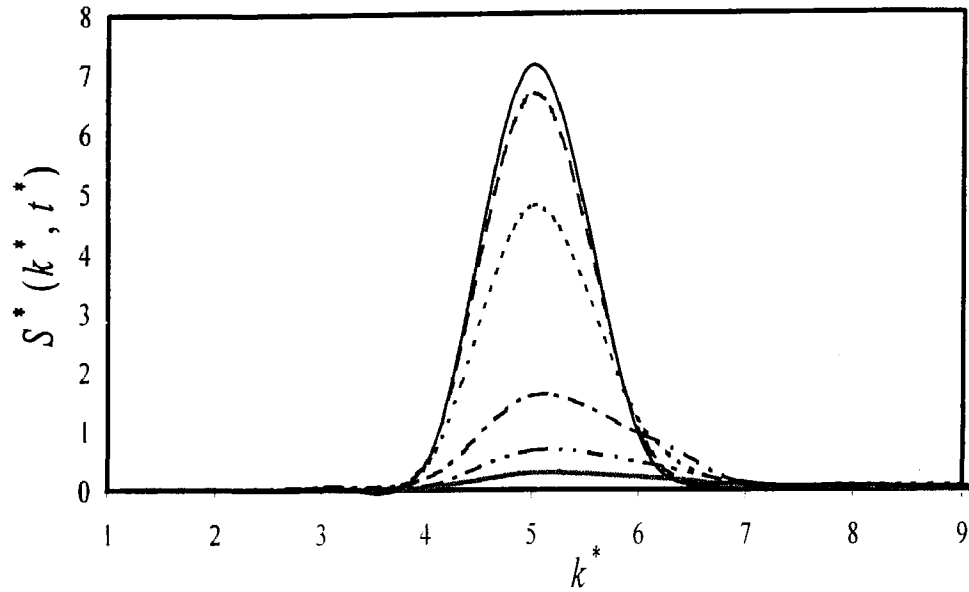


Figure B.7: The evolution of the dimensionless structure factor for a single off-critical quench ($c_o^* = 0.6$, $D^* = 500\,000$ and $T^* = 0.25$) into the unstable region of the phase diagram at the following dimensionless times: $t^* = 0.7519$ (thick grey line), $t^* = 0.7775$ (dash with two dots), $t^* = 0.842$ (dash-dot line), $t^* = 0.8748$ (dotted line), $t^* = 0.914$ (long dashed line), $t^* = 0.9292$ (solid line).

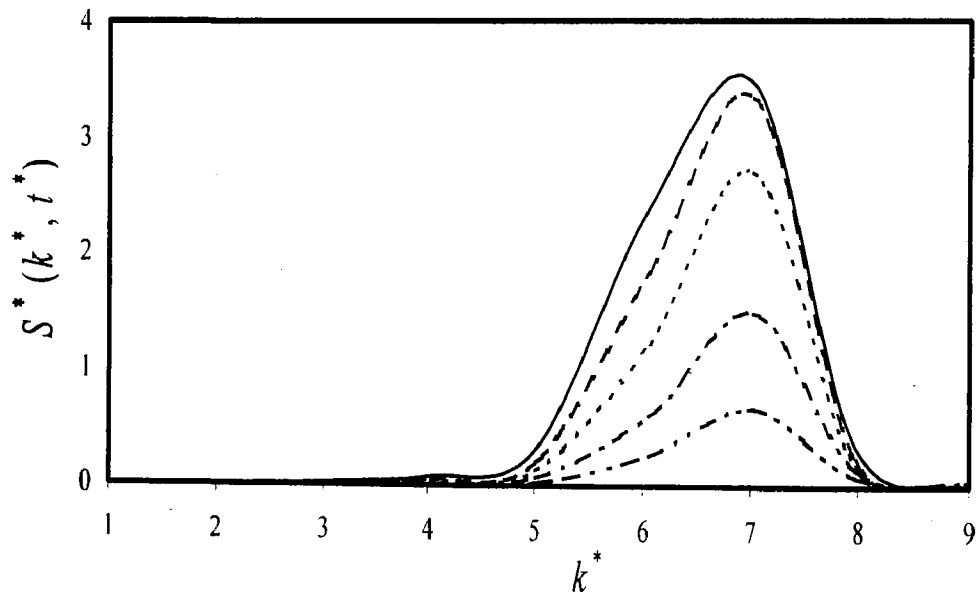


Figure B.8: The evolution of the dimensionless structure factor for a single off-critical quench ($c_o^* = 0.6$, $D^* = 800\,000$ and $T^* = 0.25$) into the unstable region of the phase diagram at the following dimensionless times: $t^* = 0.2959$ (dash with two dots), $t^* = 0.3068$ (dash-dot line), $t^* = 0.3195$ (dotted line), $t^* = 0.3312$ (long dashed line), $t^* = 0.3453$ (solid line).

The Growth of the Dimensionless Structure Factor in the Early Stages of SD

Figures B.9 to B.12 show the plots of the natural log of the maximum value of the dimensionless structure factor versus dimensionless time for the critical and off-critical quench case with $D^* = 500\,000$ and $800\,000$, respectively. For all four cases, the natural log of the dimensionless structure factor at the maximum wave number is linear for the early stages before nonlinear effects begin.

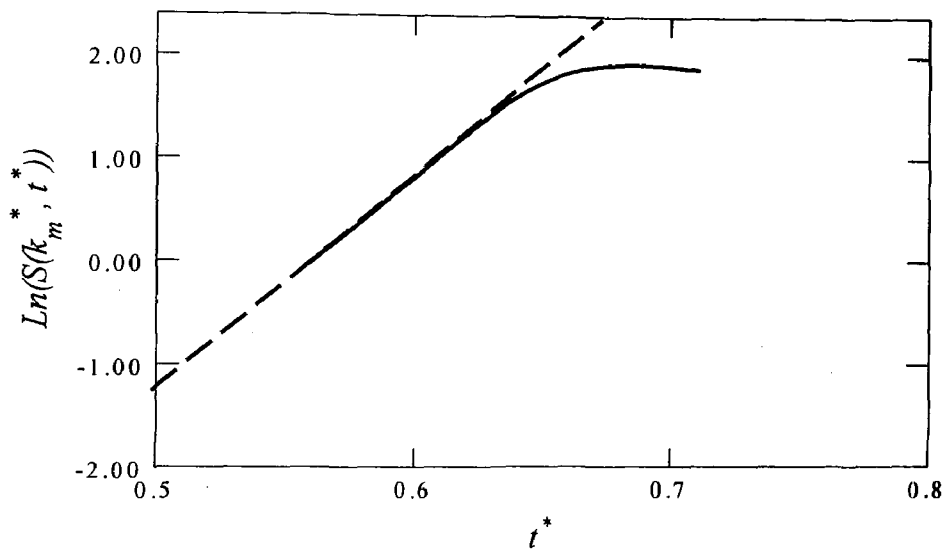


Figure B.9: The evolution of the dimensionless maximum structure factor with dimensionless time from $t^* = 0.5579$ to $t^* = 0.7104$ for a single quench ($c_0^* = 0.5$, $D^* = 500\,000$ and $T_1^* = 0.25$) into the unstable region of the phase diagram. At the early stages of phase separation by SD, the initial increase is linear and gradually slows down into the beginning of the intermediate stage where coarsening occurs. The dashed line indicates the linearity for the early stages before it deviates.

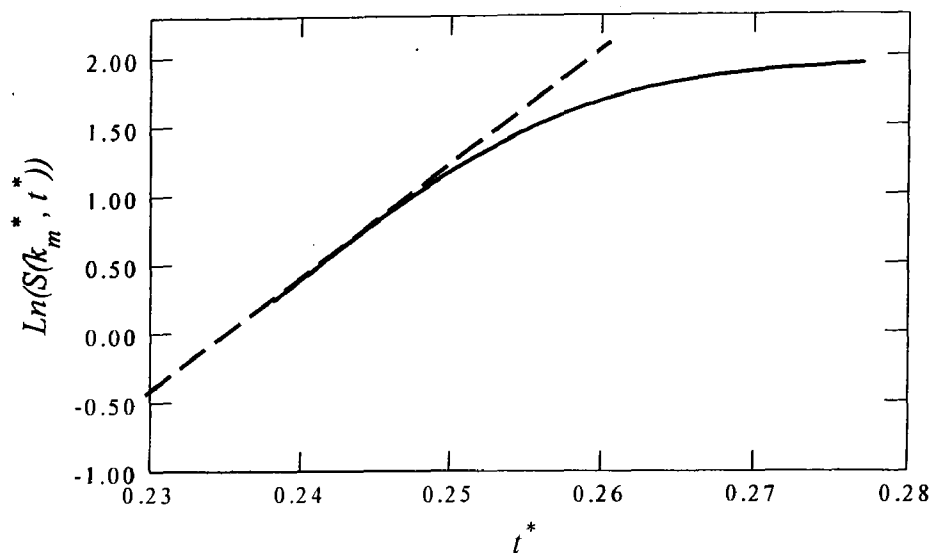


Figure B.10: The evolution of the dimensionless maximum structure factor with dimensionless time from $t^* = 0.2382$ to $t^* = 0.2771$ for a single quench ($c_o^* = 0.5$, $D^* = 800\,000$ and $T_1^* = 0.25$) into the unstable region of the phase diagram. At the early stages of phase separation by SD, the initial increase is linear and gradually slows down into the beginning of the intermediate stage where coarsening occurs. The dashed line indicates the linearity for the early stages before it deviates.

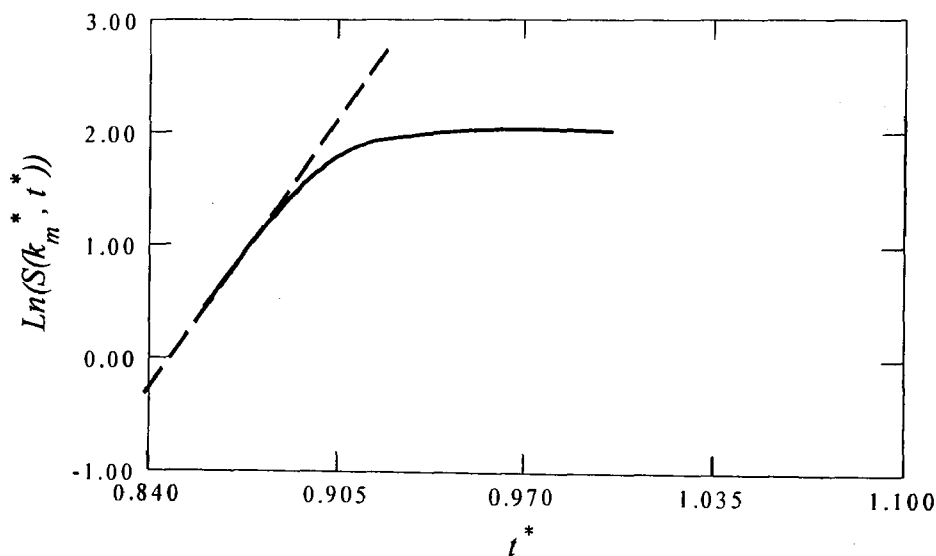


Figure B.11: The evolution of the dimensionless maximum structure factor with dimensionless time from $t^* = 0.8594$ to $t^* = 1.00$ for a single quench ($c_o^* = 0.6$, $D^* = 500\,000$ and $T_1^* = 0.25$) into the unstable region of the phase diagram. At the early stages of phase separation by SD, the initial increase is linear and gradually slows down into the beginning of the intermediate stage where coarsening occurs. The dashed line indicates the linearity for the early stages before it deviates.

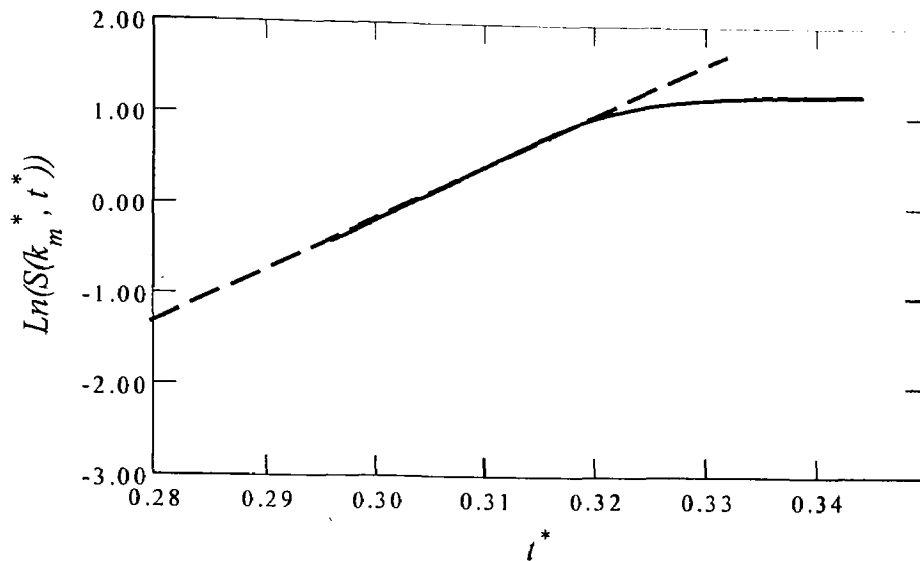


Figure B.12: The evolution of the dimensionless maximum structure factor with dimensionless time from $t^* = 0.296$ to $t^* = 0.344$ for a single quench ($c_0^* = 0.6$, $D^* = 800\,000$ and $T_1^* = 0.25$) into the unstable region of the phase diagram. At the early stages of phase separation by SD, the initial increase is linear and gradually slows down into the beginning of the intermediate stage where coarsening occurs. The dashed line indicates the linearity for the early stages before it deviates.

The Change in the Dimensionless Chemical Potential

Figures B.13 to B.16 show the plots of the evolution of the change in the dimensionless spatial chemical potential for a single critical quench and a single off-critical quench at $D^* = 500\,000$ and $800\,000$, respectively. Increasing the value of the dimensionless diffusion coefficient on the increases the rate of change in the evolution of the dimensionless spatial chemical potential for a single critical quench and a single off-critical quench. Refer back to Chapter 5 for the discussion of the observations.

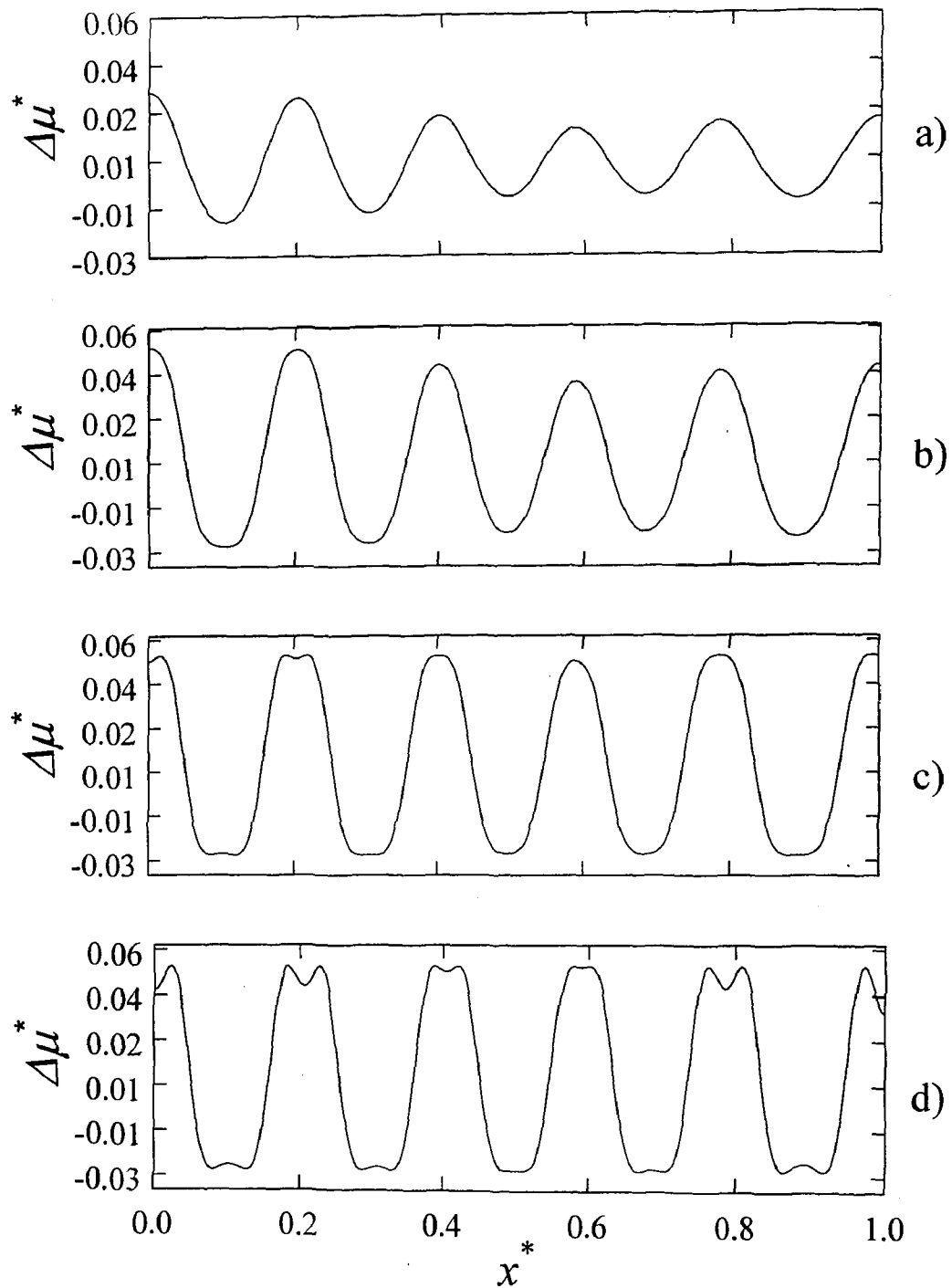


Figure B.13: The evolution of the change in the dimensionless spatial chemical potential for a single quench into the unstable region of the phase diagram at the following dimensionless times: (a) $t^* = 0.552$, (b) $t^* = 0.5956$, (c) $t^* = 0.6252$, and (d) $t^* = 0.6946$. The change in the dimensionless chemical potential is defined as the difference between the chemical potential polymer 1 in the mixture to that of its pure phase. The dimensionless initial concentration is $c_0^* = 0.5$ and the dimensionless diffusion coefficient is $D^* = 500\,000$.

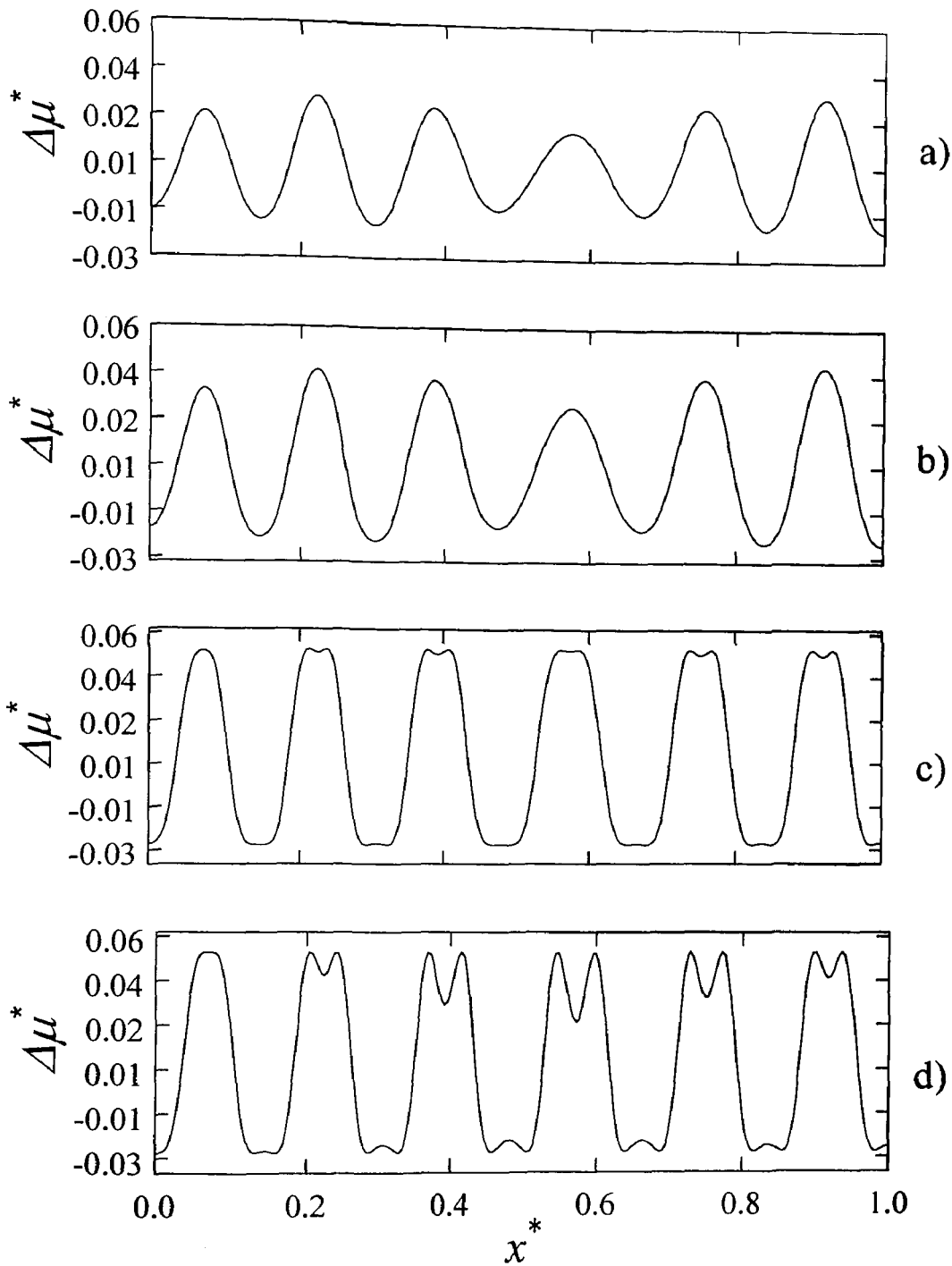


Figure B.14: The evolution of the change in the dimensionless spatial chemical potential for a single quench into the unstable region of the phase diagram at the following dimensionless times: (a) $t^* = 0.22$, (b) $t^* = 0.2278$, (c) $t^* = 0.2479$, and (d) $t^* = 0.2733$. The change in the dimensionless chemical potential is defined as the difference between the chemical potential polymer 1 in the mixture to that of its pure phase. The dimensionless initial concentration is $c_0^* = 0.5$ and the dimensionless diffusion coefficient is $D^* = 800\,000$.

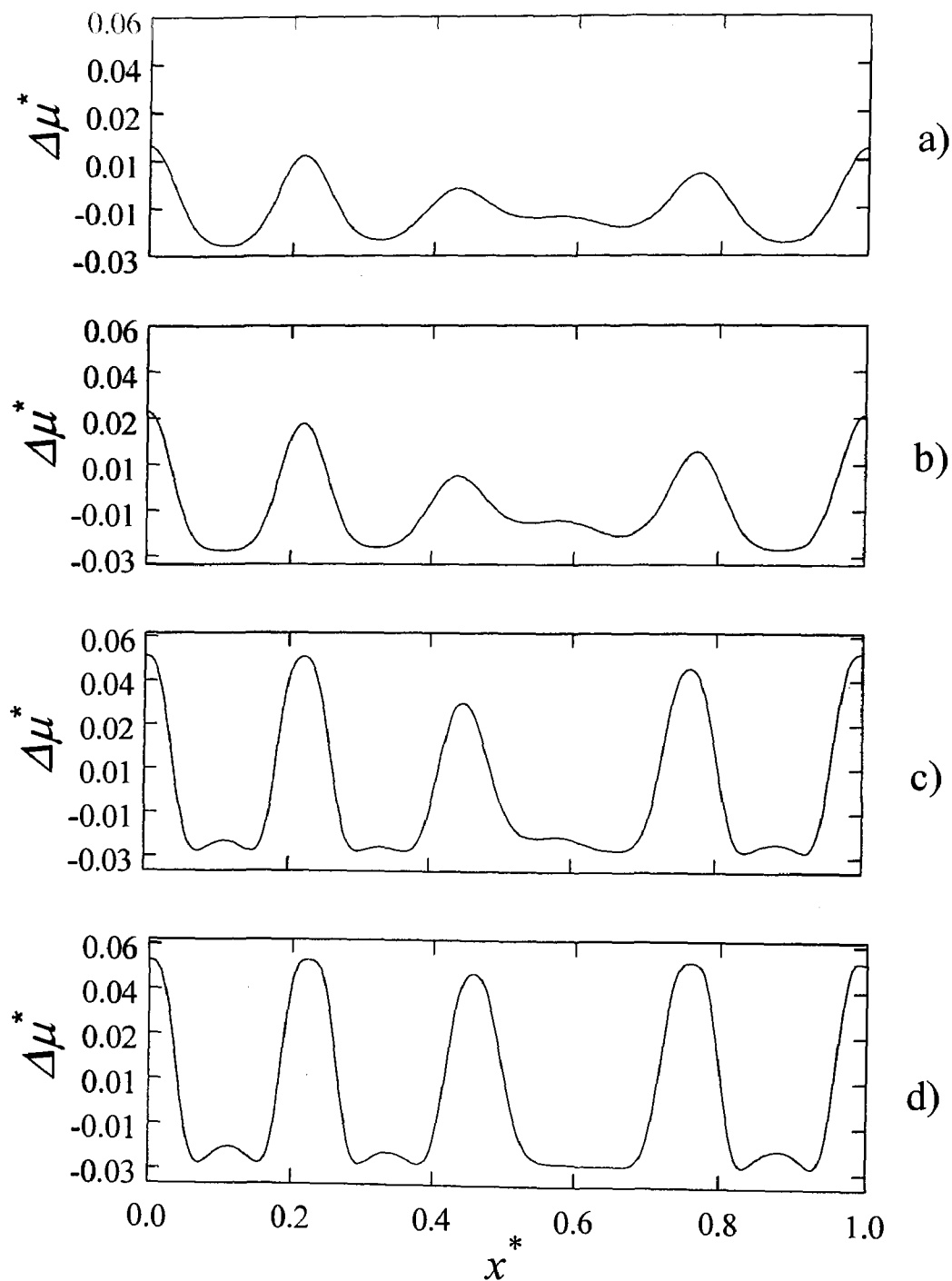


Figure B.15: The evolution of the change in the dimensionless spatial chemical potential for a single quench into the unstable region of the phase diagram at the following dimensionless times: (a) $t^* = 0.7519$, (b) $t^* = 0.7775$, (c) $t^* = 0.842$, and (d) $t^* = 0.914$. The change in the dimensionless chemical potential is defined as the difference between the chemical potential polymer 1 in the mixture to that of its pure phase. The dimensionless initial concentration is $c_0^* = 0.6$ and the dimensionless diffusion coefficient is $D^* = 500\,000$.

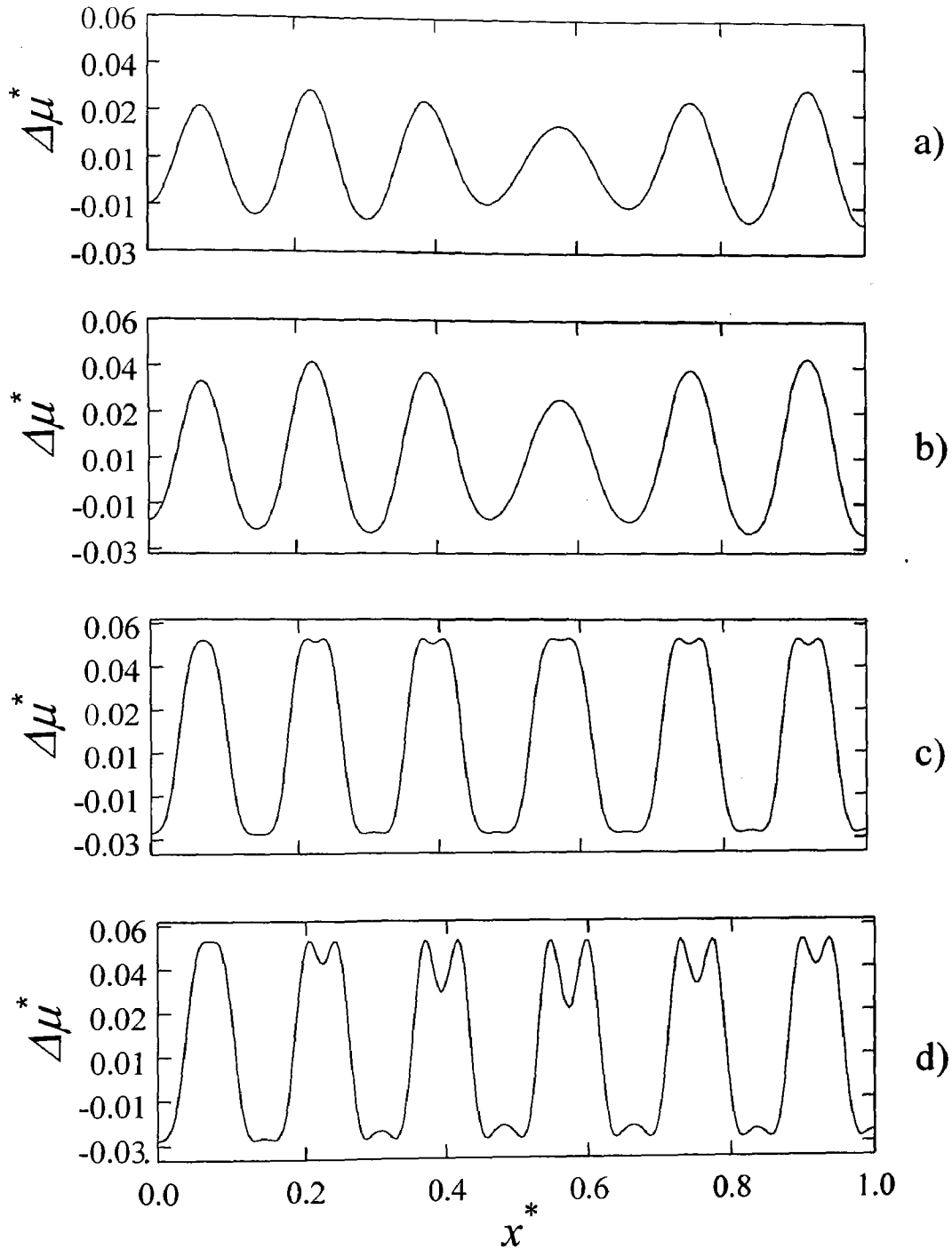


Figure B.16: The evolution of the change in the dimensionless spatial chemical potential for a single quench into the unstable region of the phase diagram at the following dimensionless times: (a) $t^* = 0.2878$, (b) $t^* = 0.3068$, (c) $t^* = 0.3312$, and (d) $t^* = 0.3453$. The change in the dimensionless chemical potential is defined as the difference between the chemical potential polymer 1 in the mixture to that of its pure phase. The dimensionless initial concentration is $c_0^* = 0.6$ and the dimensionless diffusion coefficient is $D^* = 800\,000$.

The Second Derivative of Free Energy with Respect to Composition

Figures B.17 to B.20 show the evolution of the second derivative of the free energy with respect to composition spatially the critical and off-critical quench $T_2^* = 0.25$ with $D^* = 500\,000$ and $800\,000$, respectively. As D^* increases, the steepness in the profiles also increases. This indicates an increase in the instability with time as the system phase separates.

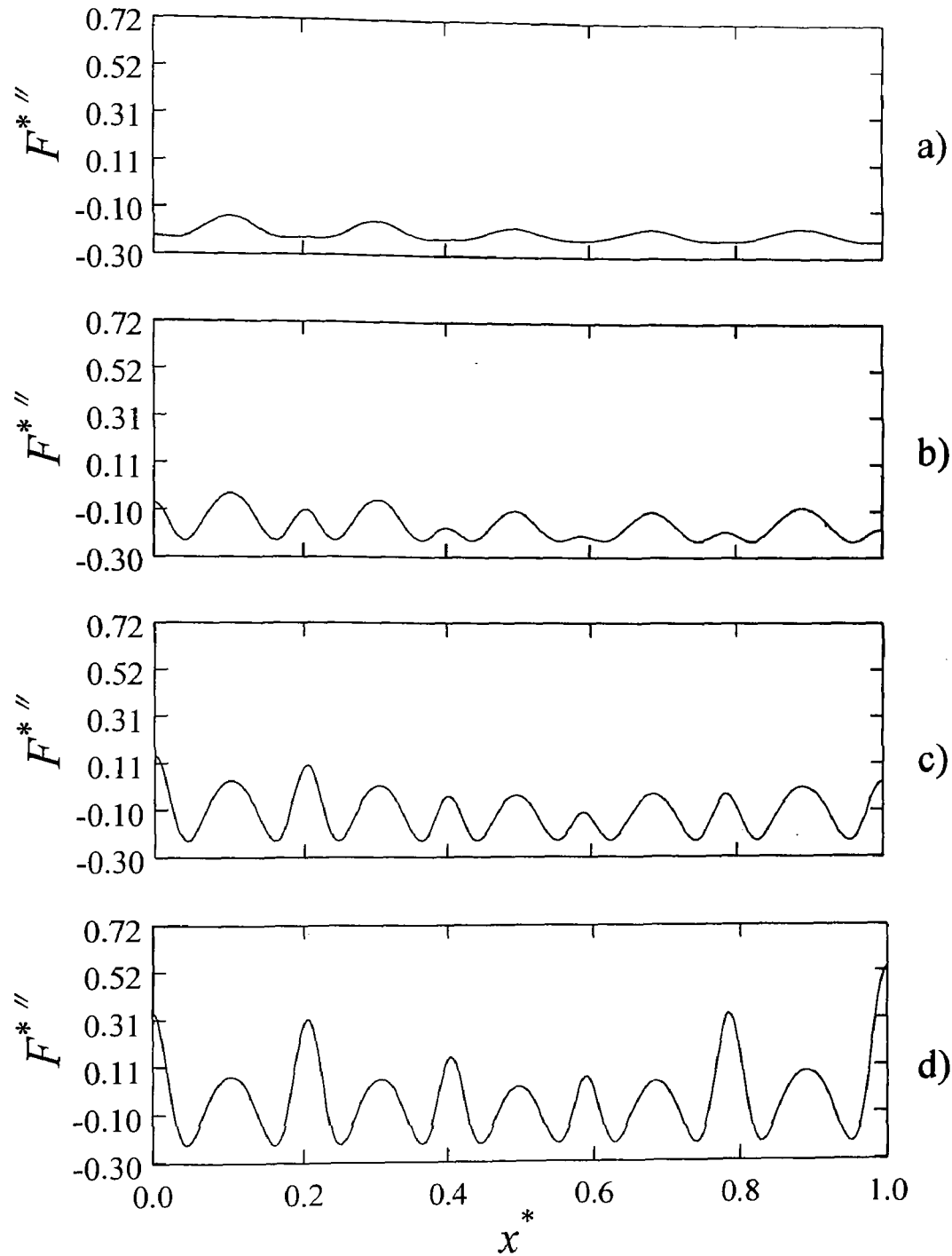


Figure B.17: The evolution of the change in the dimensionless spatial second derivative of the free energy with respect to composition of component 1 for a single quench into the unstable region of the phase diagram at the following dimensionless times: (a) $t^* = 0.5520$, (b) $t^* = 0.5956$, (c) $t^* = 0.6252$, and (d) $t^* = 0.6946$. The change in the dimensionless second derivative of free energy is used to determine the conditions of stability ($F^{*''} > 0$), meta-stability ($F^{*''} > 0$), and instability ($F^{*''} < 0$). The dimensionless initial concentration is $c_0^* = 0.5$ and the dimensionless diffusion coefficient is $D^* = 500\,000$.

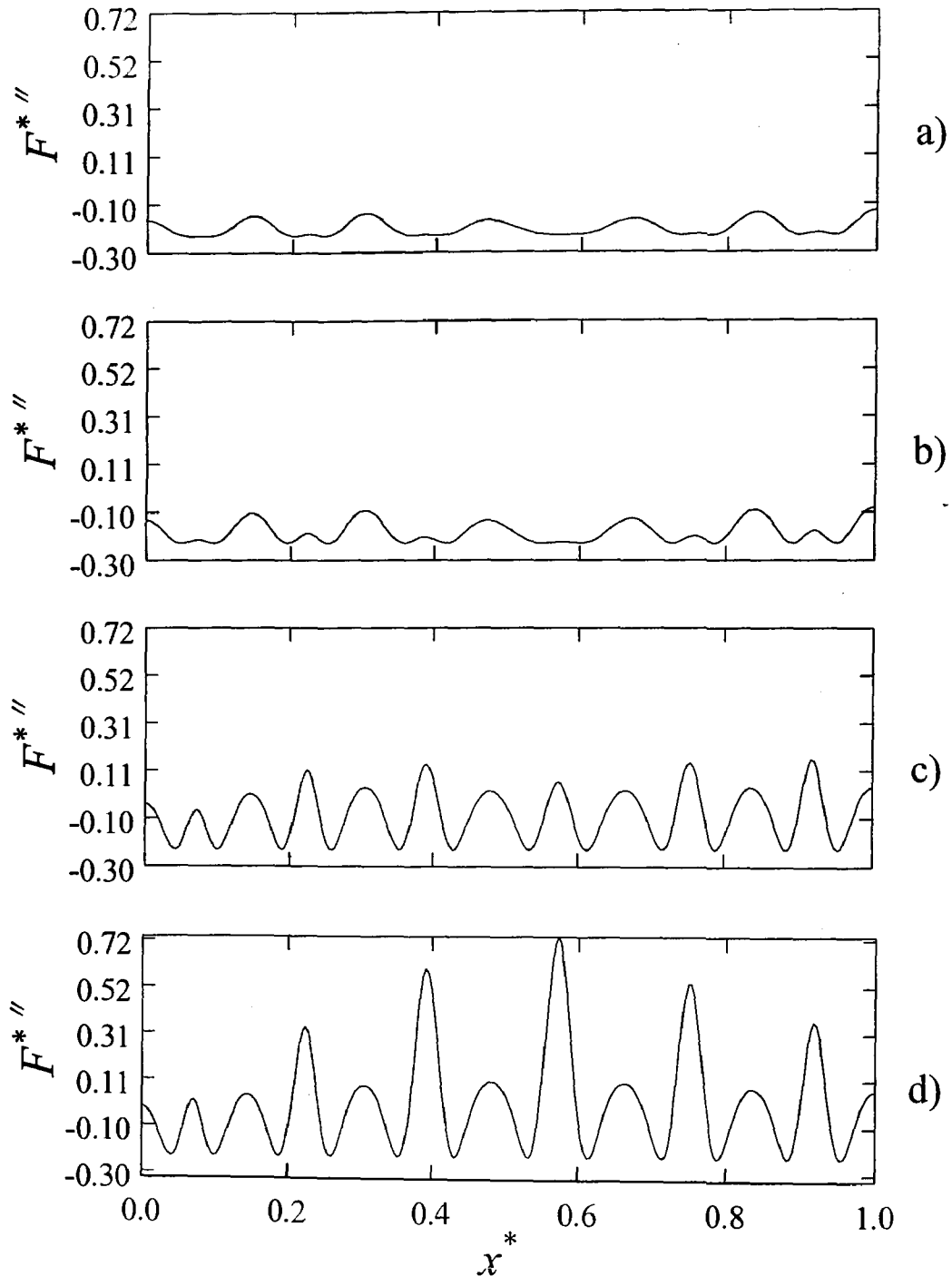


Figure B.18: The evolution of the change in the dimensionless spatial second derivative of the free energy with respect to composition of component 1 for a single quench into the unstable region of the phase diagram at the following dimensionless times: (a) $t^* = 0.22$, (b) $t^* = 0.2278$, (c) $t^* = 0.2479$, and (d) $t^* = 0.2733$. The change in the dimensionless second derivative of free energy is used to determine the conditions of stability ($F^{*''} > 0$), meta-stability ($F^{*''} > 0$), and instability ($F^{*''} < 0$). The dimensionless initial concentration is $c_0^* = 0.5$ and the dimensionless diffusion coefficient is $D^* = 800\,000$.

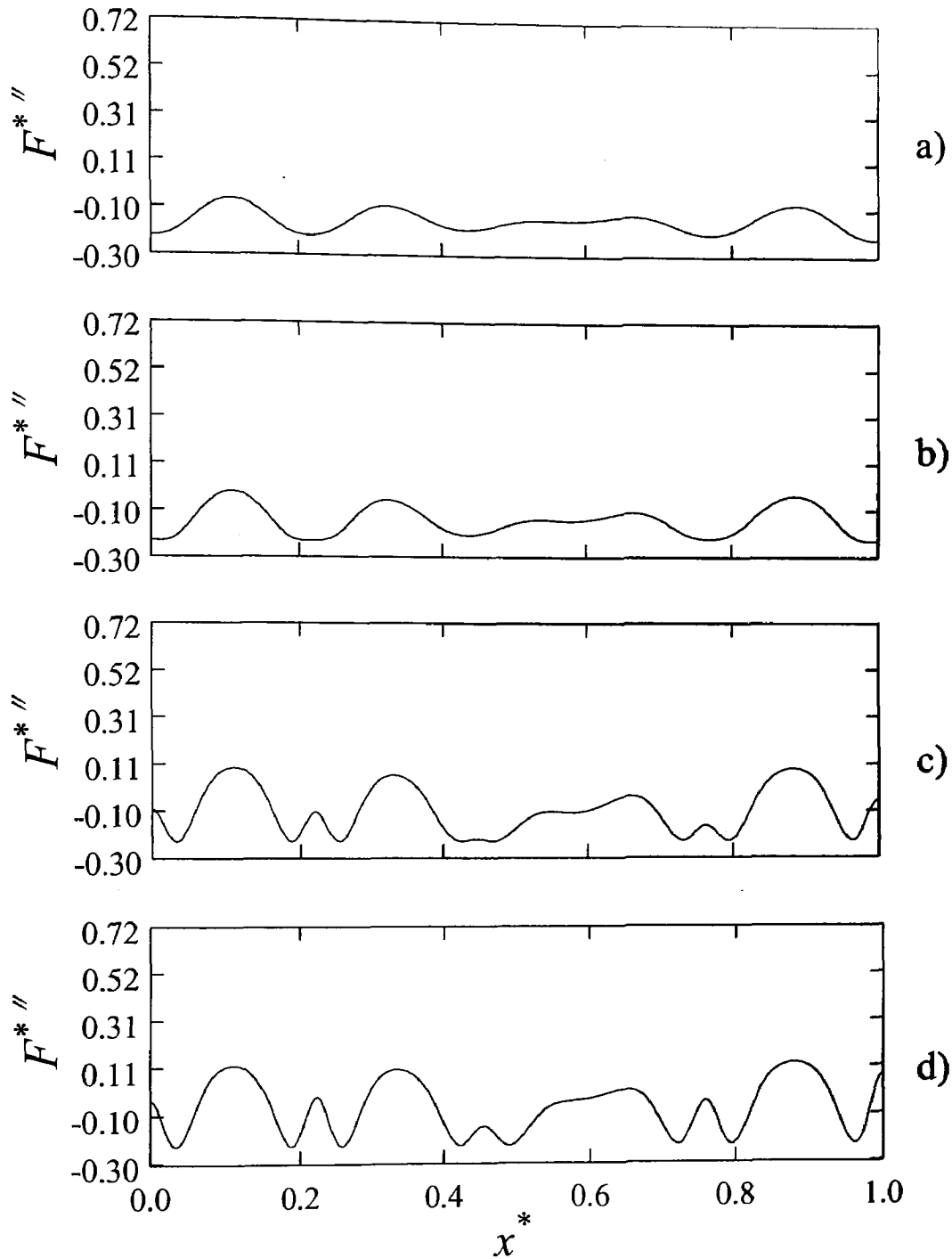


Figure B.19: The evolution of the change in the dimensionless spatial second derivative of the free energy with respect to composition of component 1 for a single quench into the unstable region of the phase diagram at the following dimensionless times: (a) $t^* = 0.7519$, (b) $t^* = 0.7775$, (c) $t^* = 0.842$, and (d) $t^* = 0.914$. The change in the dimensionless second derivative of free energy is used to determine the conditions of stability ($F^{*''} > 0$), meta-stability ($F^{*''} > 0$), and instability ($F^{*''} < 0$). The dimensionless initial concentration is $c_0^* = 0.6$ and the dimensionless diffusion coefficient is $D^* = 500\,000$.

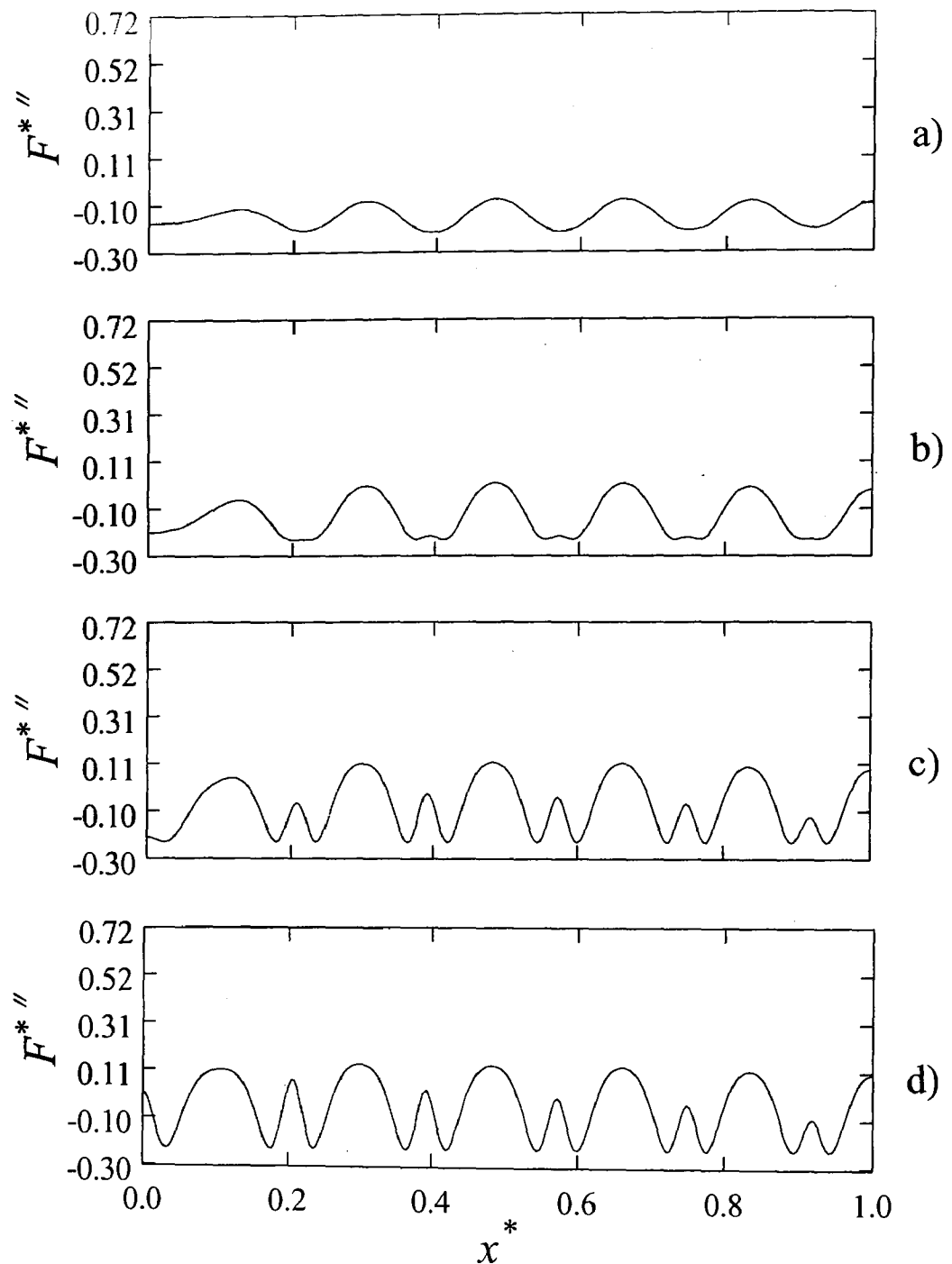


Figure B.20: The evolution of the change in the dimensionless spatial second derivative of the free energy with respect to composition of component 1 for a single quench into the unstable region of the phase diagram at the following dimensionless times: (a) $t^* = 0.2878$, (b) $t^* = 0.3068$, (c) $t^* = 0.3312$, and (d) $t^* = 0.3453$. The change in the dimensionless second derivative of free energy is used to determine the conditions of stability ($F^{*''} > 0$), meta-stability ($F^{*''} > 0$), and instability ($F^{*''} < 0$). The dimensionless initial concentration is $c_0^* = 0.6$ and the dimensionless diffusion coefficient is $D^* = 800\,000$.

Appendix C

Double Quench: Dimensionless 1-D Critical and Off-Critical Quench Results

1-D Dimensionless Spatial Concentration Profiles After the Second Quench

Figures C.1 to C.4 show the evolution of the dimensionless spatial concentration profile (for an initial critical and an initial off-critical quench) after the second temperature jump. The initial phase separation temperature is $T_1^* = 0.25$ and the second temperature jump is $T_2^* = 0.2$ at the transition time. The dimensionless diffusion coefficients are $D^* = 500\,000$ and $800\,000$. The transition times are summarized in Table 6.2. There is no sign of double phase separation in Figures C.1 to C.4. However, notice that in Figures C.3 and C.4, for the initial off-critical quench, there is slight constructive and destructive interference in peak three and peak one for $D^* = 500\,000$ and $800\,000$, respectively. Figures C.5 to C.8 show the evolution of the dimensionless spatial concentration profile (for an initial critical and an initial off-critical quench) after the second temperature jump to $T_2^* = 0.1$ at the transition times for $D^* = 500\,000$ and $800\,000$, respectively. There

are noticeable constructive and destructive interferences observed for the deeper quench attributed to the formation of secondary structures. Refer to Chapter 6 for discussion.

Evolution of the Dimensionless Structure Factor After the Second Quench

Figures C.9 and C.10 show the evolution of the dimensionless structure factor after the second quench to $T_2^* = 0.2$ from the initial critical quench at $T_1^* = 0.25$ for $D^* = 500\,000$ and $800\,000$, respectively. Figures C.11 and C.12 show the evolution of the dimensionless structure factor after the second quench to $T_2^* = 0.2$ from the initial off-critical quench at $T_1^* = 0.25$ for $D^* = 500\,000$ and $800\,000$, respectively. The box in the right hand corner of Figure C.11 and Figure C.12 shows an enlarged plot of the growth of the secondary peak. The results are different from the evolution of the dimensionless structure factor observed for the critical quench case and for the initial off-critical quench case. There was no sign of double phase separation present and for the initial critical quench case and the growth of the structure factor showed an increase in the intensity of the primary peak but no occurrence of a secondary peak forming. For the initial off-critical quench case, a slight secondary peak was observed to form with increasing D^* . However, the impact was minimal and no secondary phase separated regions formed.

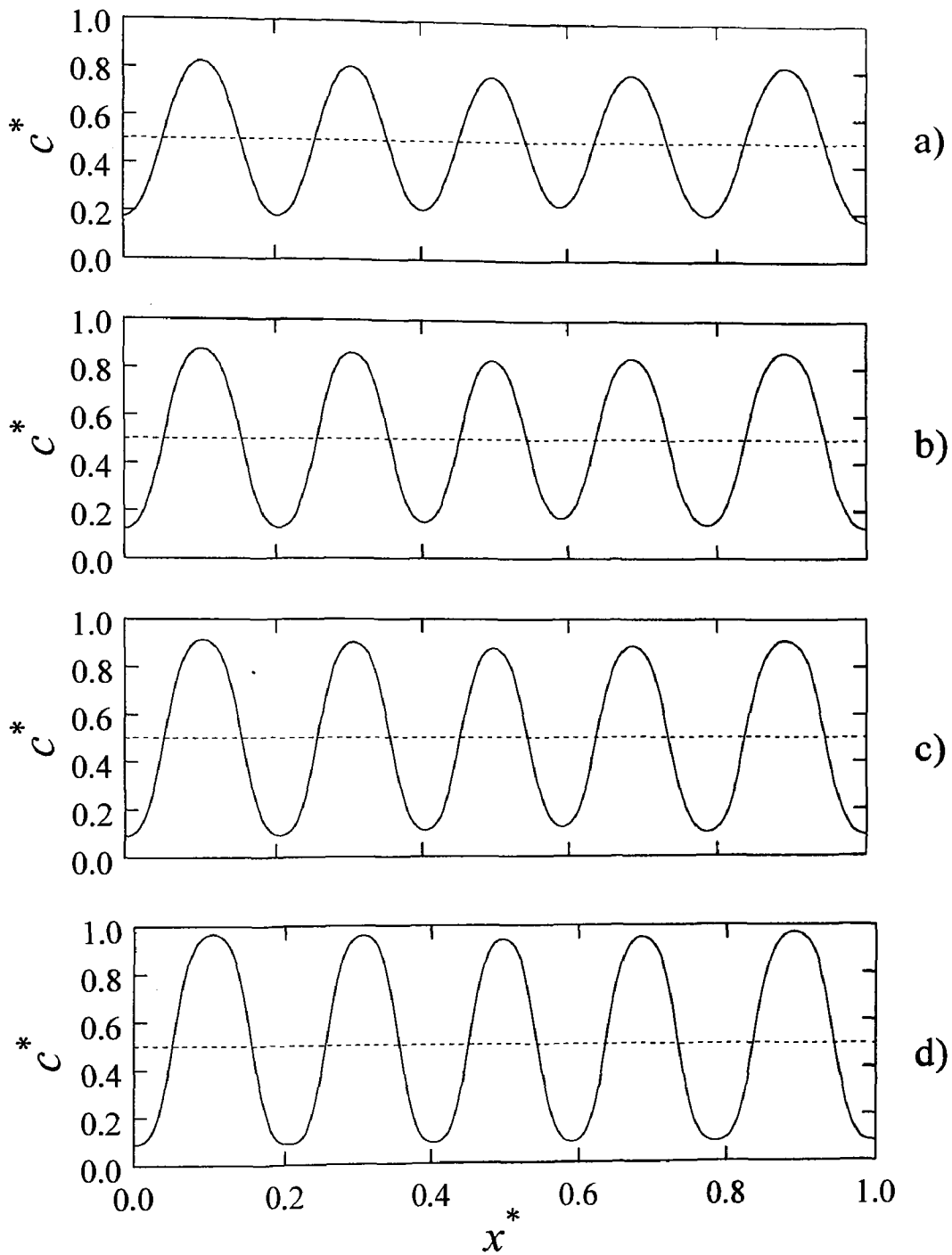


Figure C.1: The evolution of the dimensionless spatial concentration profile for a double quench from $T_1^* = 0.25$ to $T_2^* = 0.2$ at the transition time of $t_i^* = 0.650$ at the following dimensionless times: (a) $t^* = 0.6509$, (b) $t^* = 0.656$, (c) $t^* = 0.6602$, and (d) $t^* = 0.6795$. The dashed line through the center of the graph represents the initial average concentration $c_0^* = 0.5$. The dimensionless diffusion coefficient for this case is $D^* = 500\,000$.

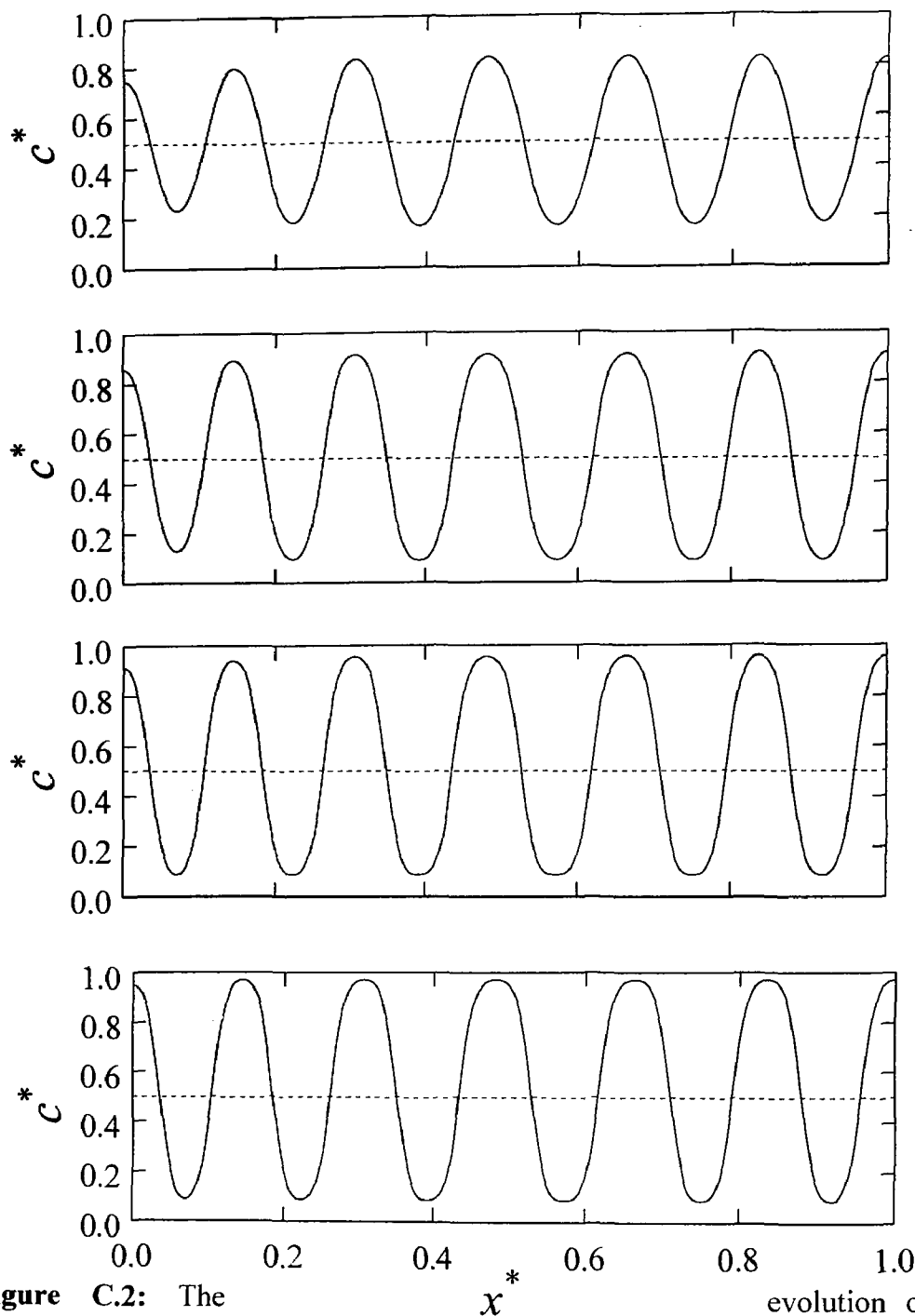


Figure C.2: The evolution of the dimensionless spatial concentration profile for a double quench from $T_1^* = 0.25$ to $T_2^* = 0.2$ at the transition time of $t_i^* = 0.256$ at the following dimensionless times: (a) $t^* = 0.2561$, (b) $t^* = 0.2596$, (c) $t^* = 0.2619$, and (d) $t^* = 0.2656$. The dashed line through the center of the graph represents the initial average concentration $c_o^* = 0.5$. The dimensionless diffusion coefficient for this case is $D^* = 800\,000$.

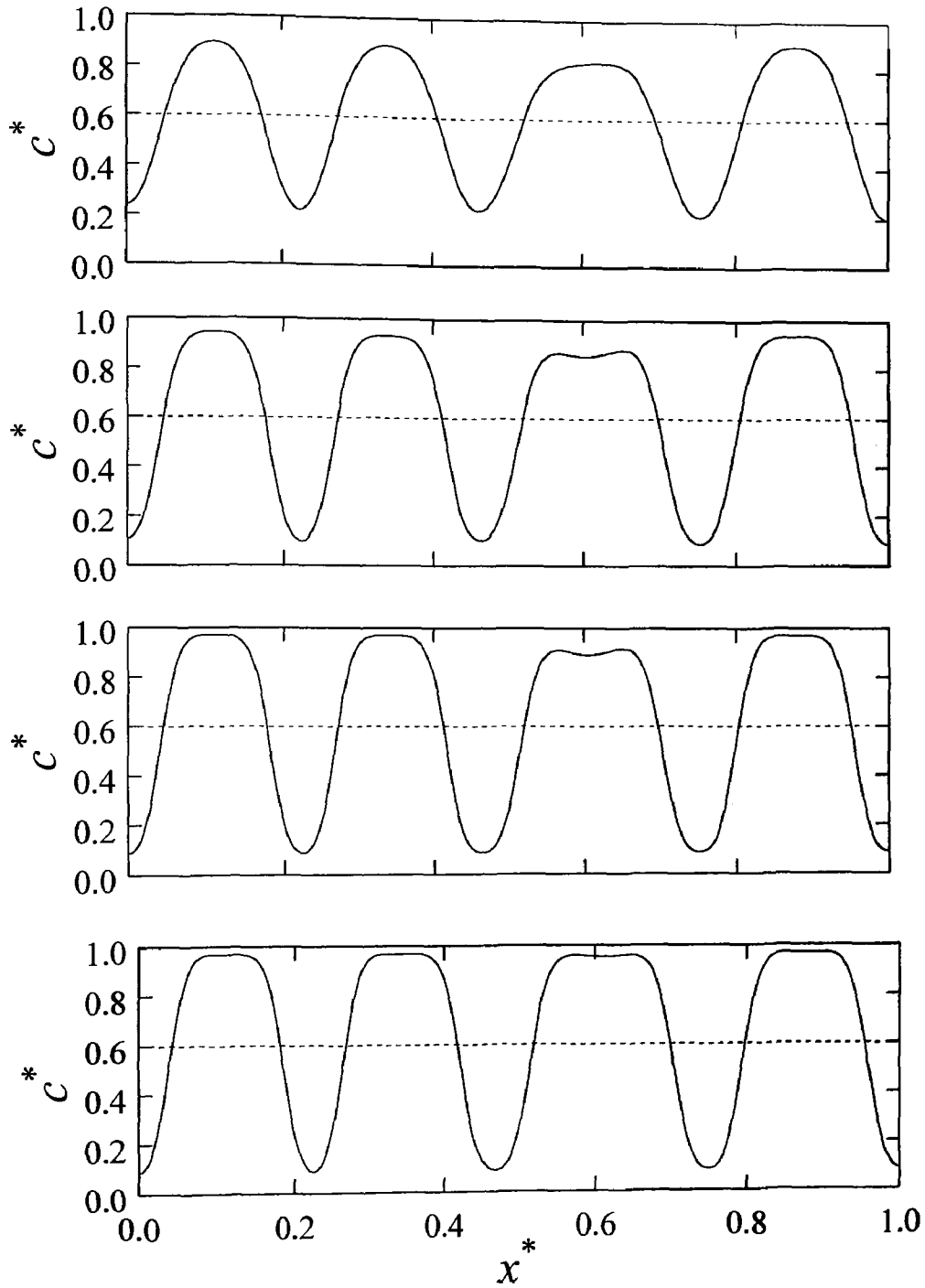


Figure C.3: The evolution of the dimensionless spatial concentration profile for a double quench from $T_1^* = 0.25$ to $T_2^* = 0.2$ at the transition time of $t_i^* = 0.903$ at the following dimensionless times: (a) $t^* = 0.9057$, (b) $t^* = 0.912$, (c) $t^* = 0.9172$, and (d) $t^* = 0.9421$. The dashed line through the center of the graph represents the initial average concentration $c_o^* = 0.6$. The dimensionless diffusion coefficient for this case is $D^* = 500\,000$.

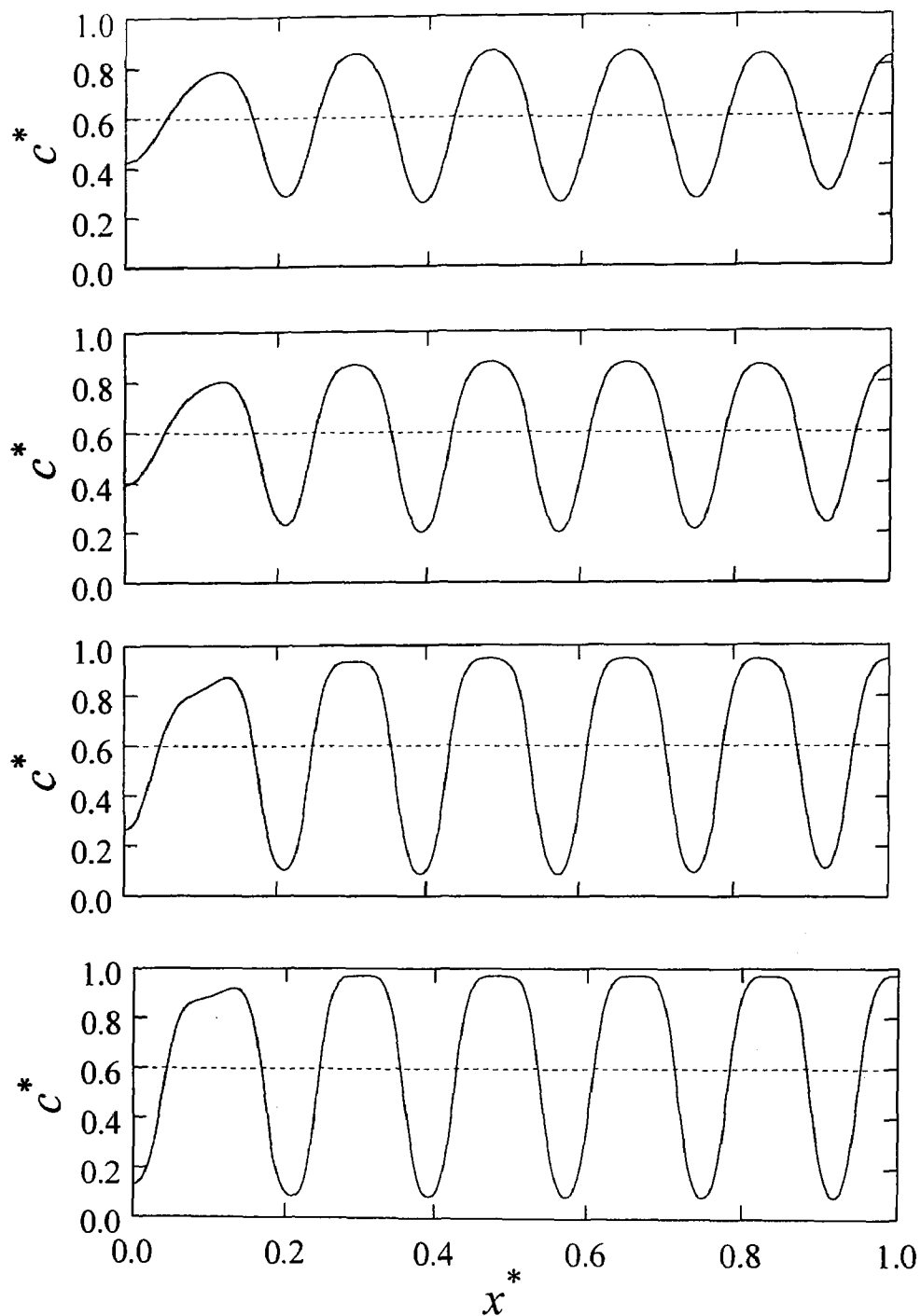


Figure C.4: The evolution of the dimensionless spatial concentration profile for a double quench from $T_1^* = 0.25$ to $T_2^* = 0.2$ at the transition time of $t_i^* = 0.323$ at the following dimensionless times: (a) $t^* = 0.3235$, (b) $t^* = 0.325$, (c) $t^* = 0.3298$, and (d) $t^* = 0.3345$. The dashed line through the center of the graph represents the initial average concentration $c_0^* = 0.6$. The dimensionless diffusion coefficient for this case is $D^* = 800\,000$.

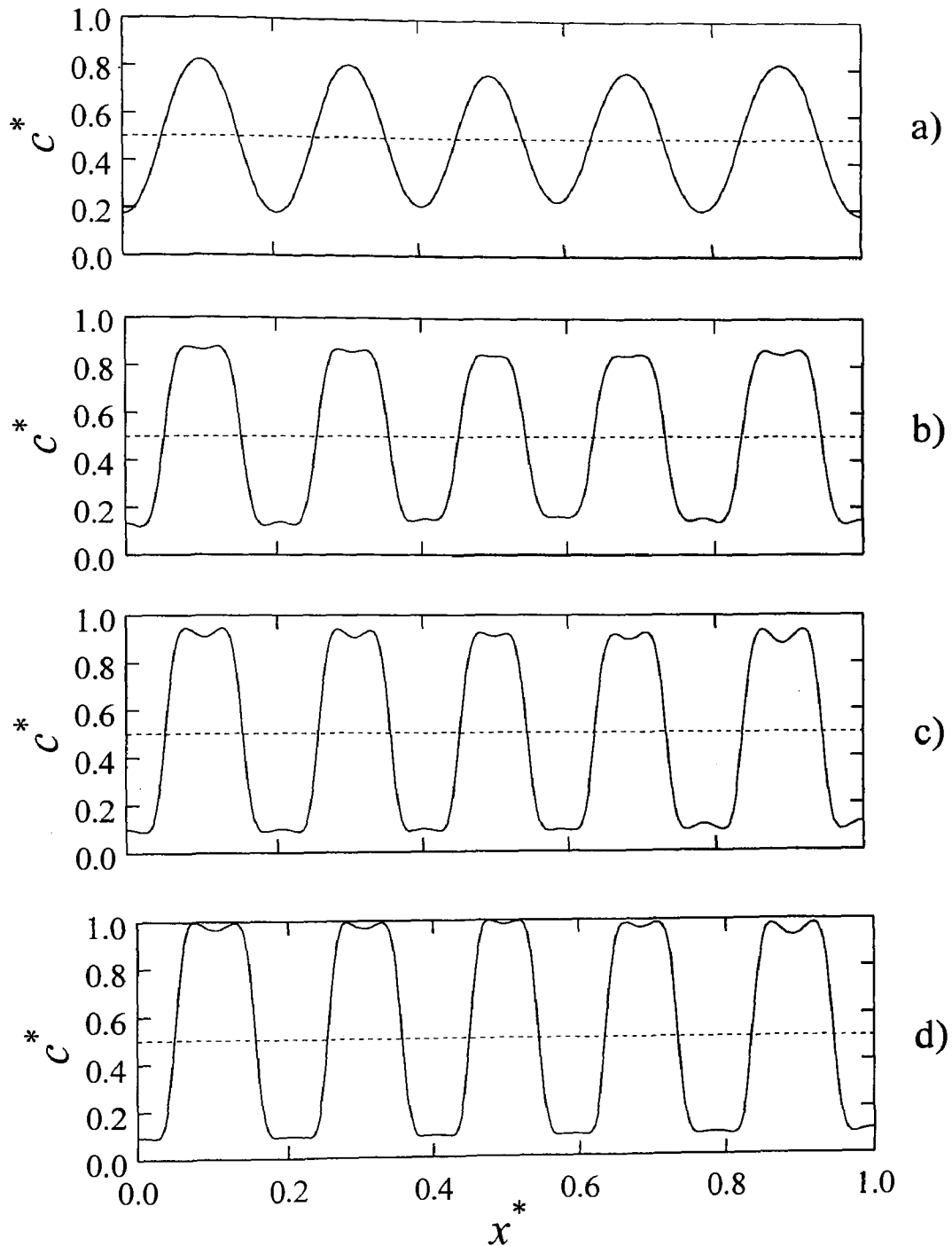


Figure C.5: The evolution of the dimensionless spatial concentration profile for a double quench from $T_1^* = 0.25$ to $T_2^* = 0.1$ at the transition time of $t_i^* = 0.650$ at the following dimensionless times: (a) $t^* = 0.6511$, (b) $t^* = 0.6541$, (c) $t^* = 0.6562$, and (d) $t^* = 0.6584$. The dashed line through the center of the graph represents the initial average concentration $c_o^* = 0.5$. The dimensionless diffusion coefficient for this case is $D^* = 500\,000$.

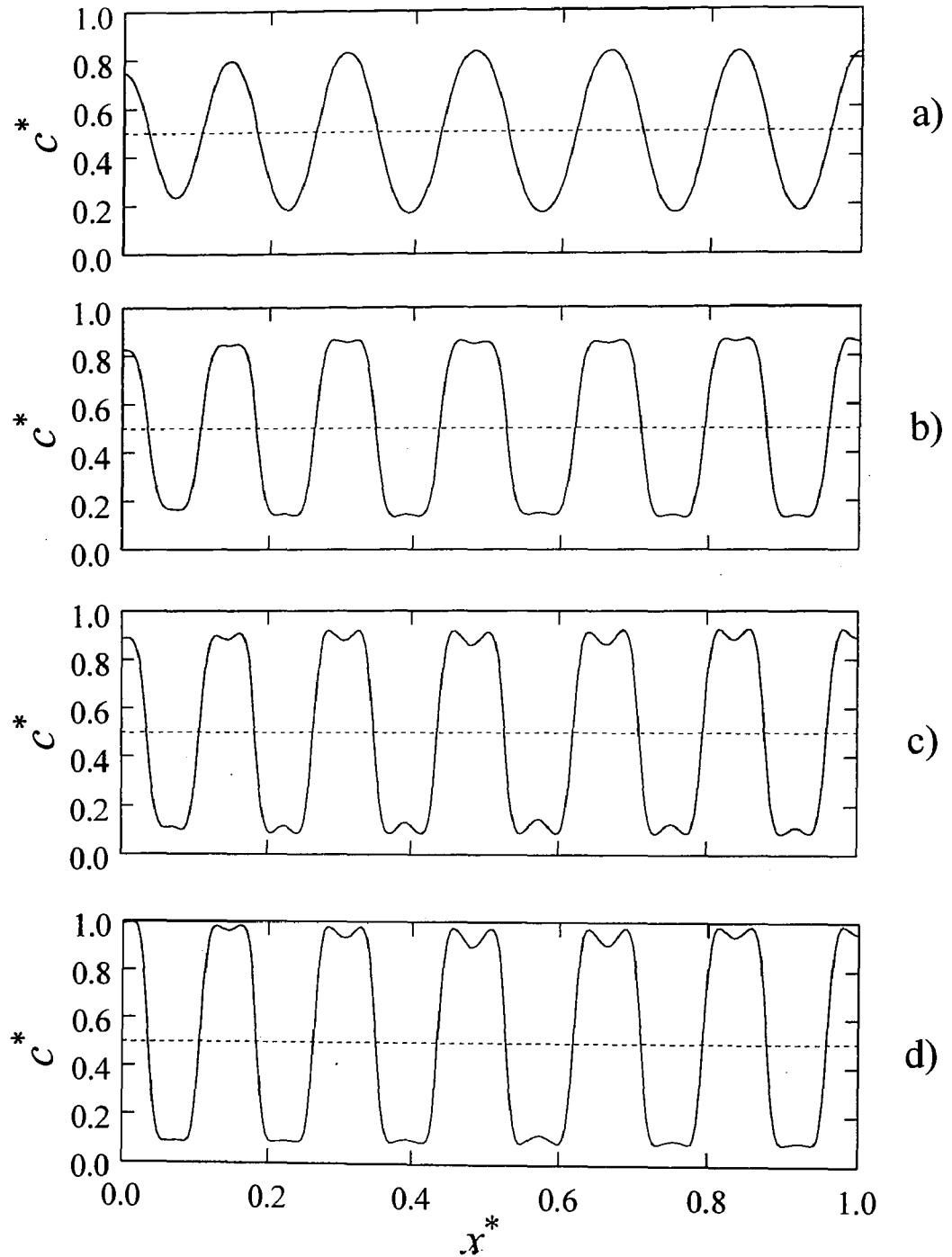


Figure C.6: The evolution of the dimensionless spatial concentration profile for a double quench from $T_1^* = 0.25$ to $T_2^* = 0.1$ at the transition time of $t_i^* = 0.256$ at the following dimensionless times: (a) $t^* = 0.256$, (b) $t^* = 0.2571$, (c) $t^* = 0.2577$, and (d) $t^* = 0.2587$. The dashed line through the center of the graph represents the initial average concentration $c_0^* = 0.5$. The dimensionless diffusion coefficient for this case is $D^* = 800\,000$.

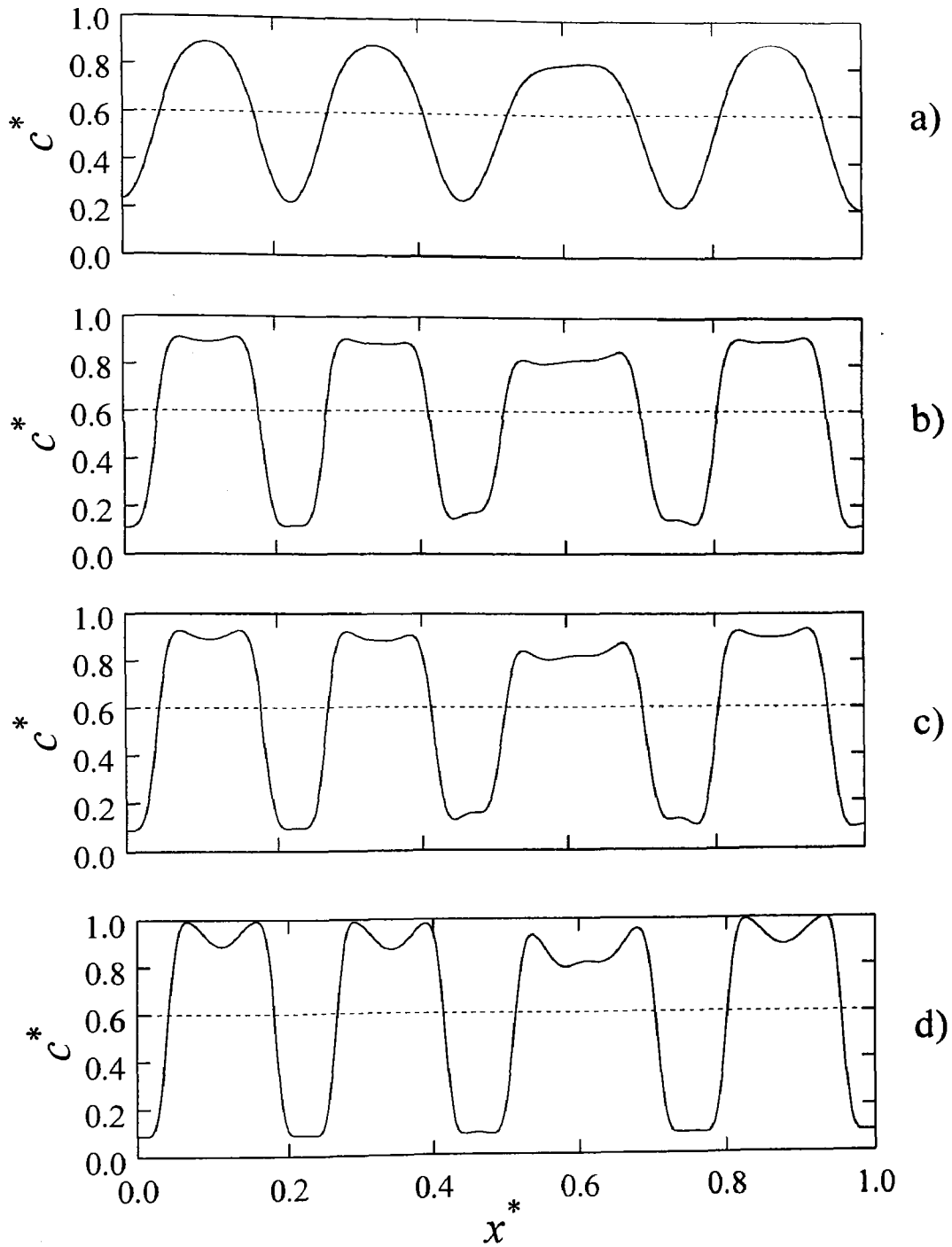


Figure C.7: The evolution of the dimensionless spatial concentration profile for a double quench from $T_1^* = 0.25$ to $T_2^* = 0.1$ at the transition time of $t_i^* = 0.903$ at the following dimensionless times: (a) $t^* = 0.9045$, (b) $t^* = 0.9077$, (c) $t^* = 0.9082$, and (d) $t^* = 0.9106$. The dashed line through the center of the graph represents the initial average concentration $c_o^* = 0.6$. The dimensionless diffusion coefficient for this case is $D^* = 500\,000$.

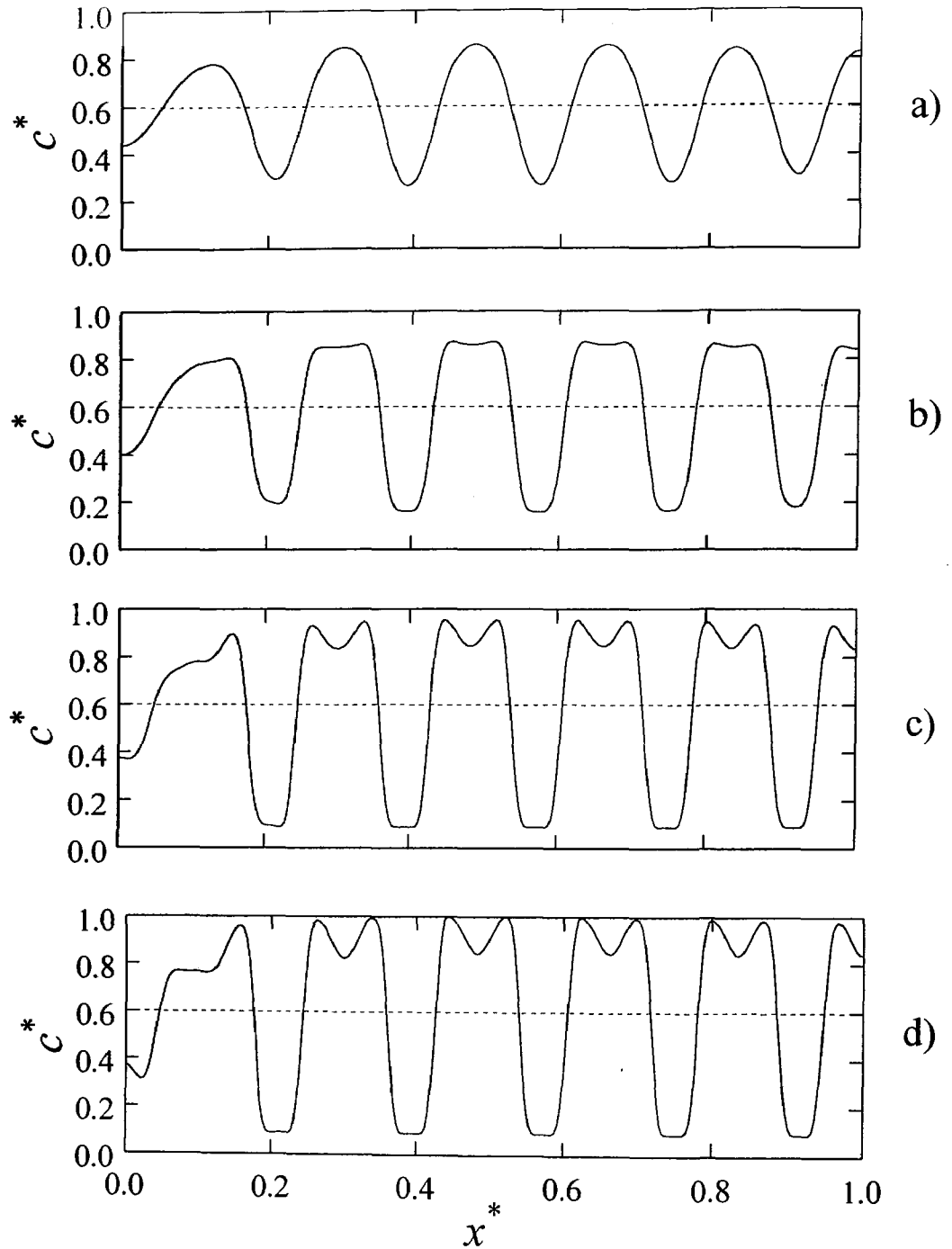


Figure C.8: The evolution of the dimensionless spatial concentration profile for a double quench from $T_1^* = 0.25$ to $T_2^* = 0.1$ at the transition time of $t_i^* = 0.323$ at the following dimensionless times: (a) $t^* = 0.3235$, (b) $t^* = 0.3247$, (c) $t^* = 0.3257$, and (d) $t^* = 0.3265$. The dashed line through the center of the graph represents the initial average concentration $c_o^* = 0.6$. The dimensionless diffusion coefficient for this case is $D^* = 800\,000$.

Figures C.13 and C.16 show the evolution of the dimensionless structure factor (initial critical and initial off critical quench) after the second quench to $T_2^* = 0.1$ from the initial critical quench at $T_1^* = 0.25$ for $D^* = 500\,000$ and $800\,000$, respectively. There are obvious secondary peaks that form right after the second quench at $T_2^* = 0.1$. In the profile, both the primary and the secondary peak grow with time. This reflects in the growth of the concentration fluctuations with time as the primary peaks and troughs start to approach the upper and lower equilibrium values and the secondary peaks and troughs start to increase in value as well at $T_2^* = 0.1$. See Chapter 6 for discussion of results.

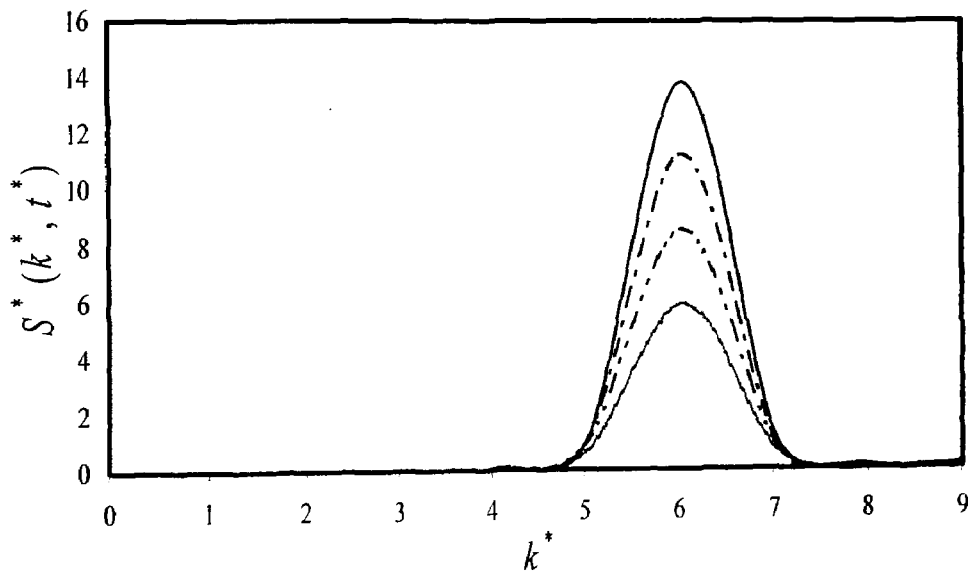


Figure C.9: The evolution of the dimensionless structure factor for a double quench from $T_1^* = 0.25$ to $T_2^* = 0.2$ (second temperature jump made at a transition time of $t_i^* = 0.650$) at the following dimensionless times: $t^* = 0.6509$ (light grey solid line), $t^* = 0.656$ (dash-two dot line), $t^* = 0.6602$ (dash-dot line), and $t^* = 0.6795$ (solid black line). The initial average concentration $c_0^* = 0.5$. The dimensionless diffusion coefficient is $D^* = 500\,000$.

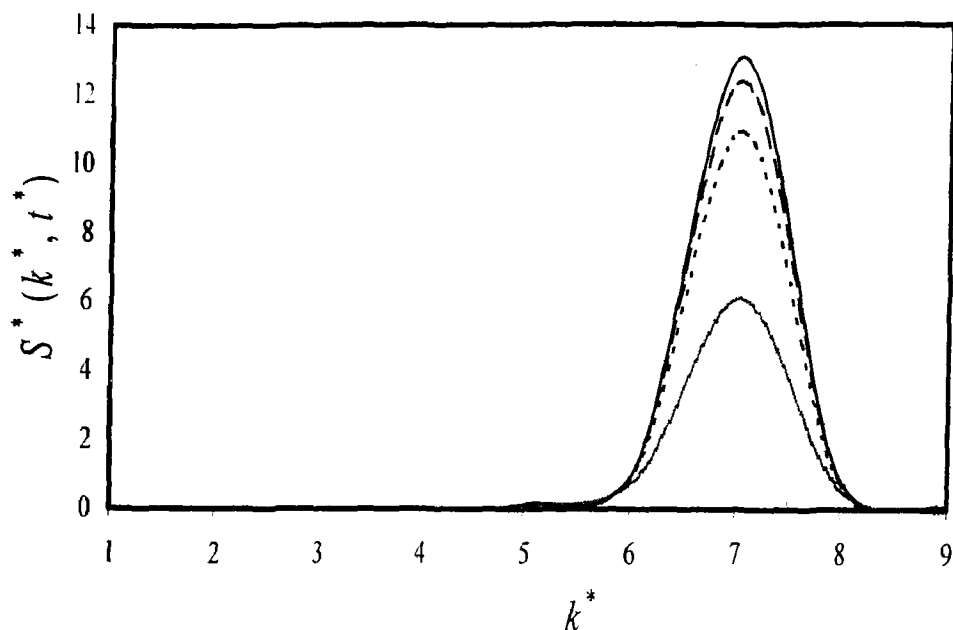


Figure C.10: The evolution of the dimensionless structure factor for a double quench from $T_1^* = 0.25$ to $T_2^* = 0.2$ (second temperature jump made at a transition time of $t_t^* = 0.256$) at the following dimensionless times: $t^* = 0.2561$ (light grey solid line), $t^* = 0.2596$ (dotted line), $t^* = 0.2619$ (dashed line), and $t^* = 0.2656$ (solid black line). The initial average concentration $c_0^* = 0.5$. The dimensionless diffusion coefficient for this case is $D^* = 800\,000$.

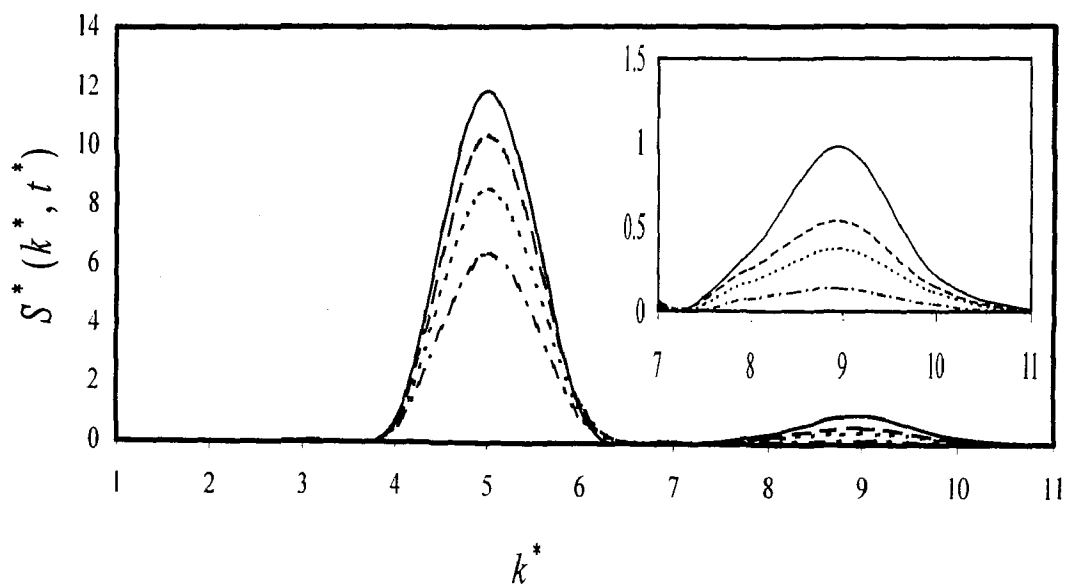


Figure C.11: The evolution of the dimensionless structure factor for a double quench from $T_1^* = 0.25$ to $T_2^* = 0.2$ (second temperature jump made at a transition time of $t_t^* = 0.903$) at the following dimensionless times: $t^* = 0.9057$ (dash-dot line), $t^* = 0.912$ (dotted line), $t^* = 0.9172$ (dashed line), and $t^* = 0.9421$ (solid black line). The initial average concentration $c_0^* = 0.6$. The dimensionless diffusion coefficient for this case is $D^* = 500\,000$.

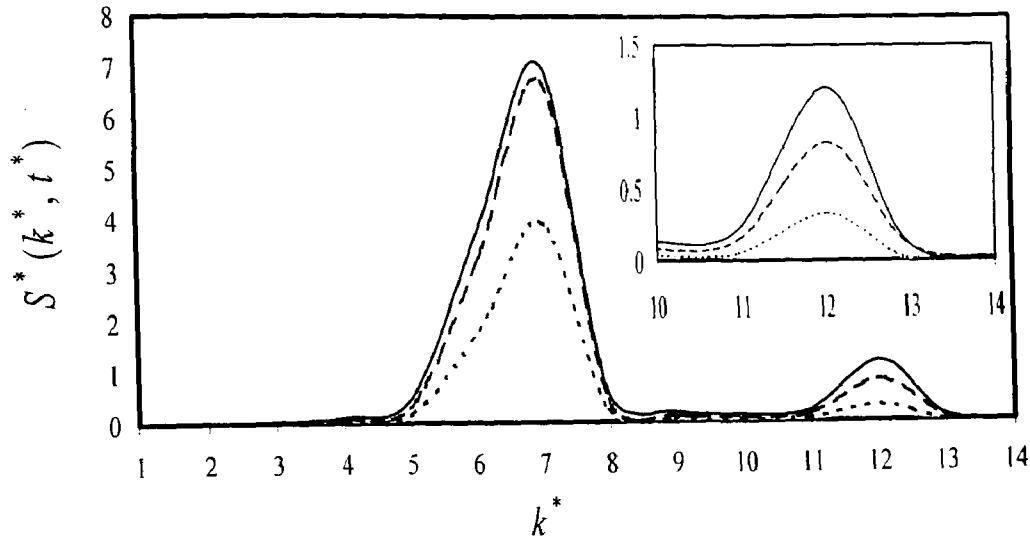


Figure C.12: The evolution of the dimensionless structure factor for a double quench from $T_1^* = 0.25$ to $T_2^* = 0.2$ (second temperature jump made at a transition time of $t_i^* = 0.323$) at the following dimensionless times: $t^* = 0.3235$ (light grey solid line), $t^* = 0.325$ (dotted line), $t^* = 0.3298$ (dashed line), and $t^* = 0.3345$ (solid black line). The initial average concentration $c_0^* = 0.6$. The dimensionless diffusion coefficient for this case is $D^* = 800\,000$.

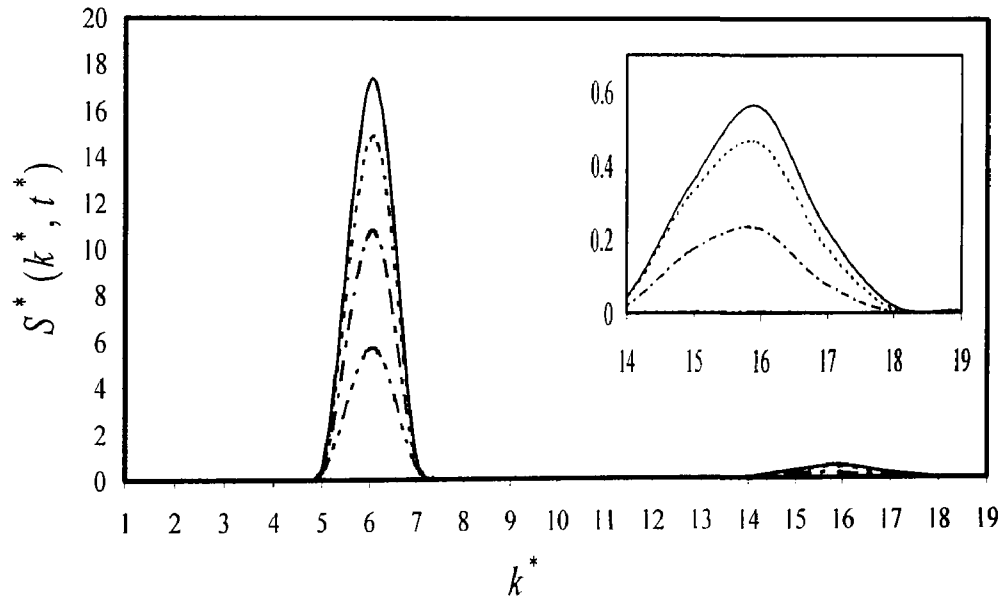


Figure C.13: The evolution of the dimensionless spatial concentration profile for a double quench from $T_1^* = 0.25$ to $T_2^* = 0.1$ (at the transition time of $t_i^* = 0.650$) at the following dimensionless times: $t^* = 0.6511$ (dash-two dots line), $t^* = 0.6541$ (dash-dot line), $t^* = 0.6562$ (dotted line), and $t^* = 0.6584$ (solid line). The initial average concentration $c_0^* = 0.5$. The dimensionless diffusion coefficient for this case is $D^* = 500\,000$.

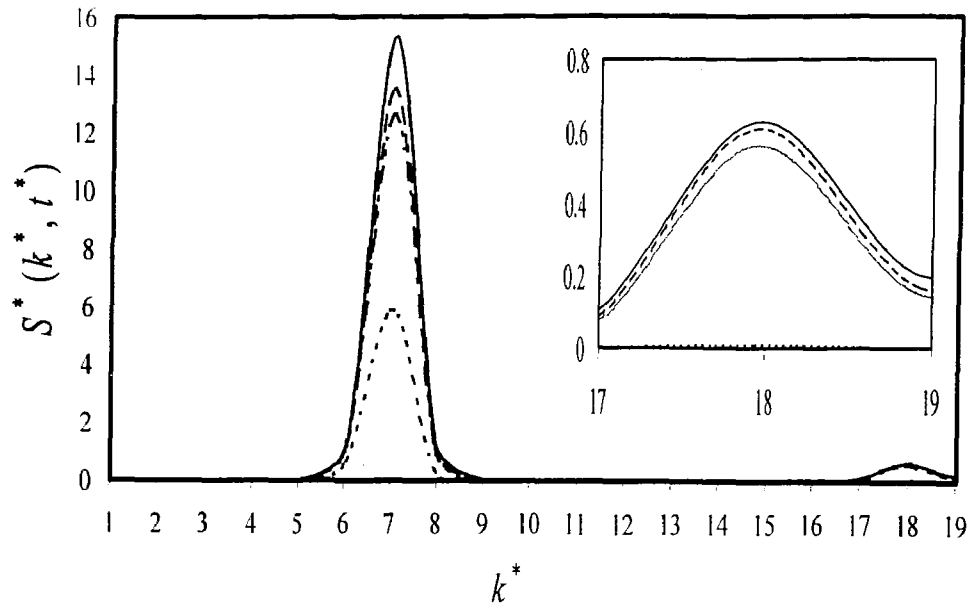


Figure C.14: The evolution of the dimensionless spatial concentration profile for a double quench from $T_1^* = 0.25$ to $T_2^* = 0.1$ (at the transition time of $t_i^* = 0.256$) at the following dimensionless times: $t^* = 0.256$ (dotted line), $t^* = 0.2571$ (dash-dot line), $t^* = 0.2577$ (dashed line), and $t^* = 0.2587$ (solid line). The initial average concentration $c_0^* = 0.5$. The dimensionless diffusion coefficient for this case is $D^* = 800\,000$.

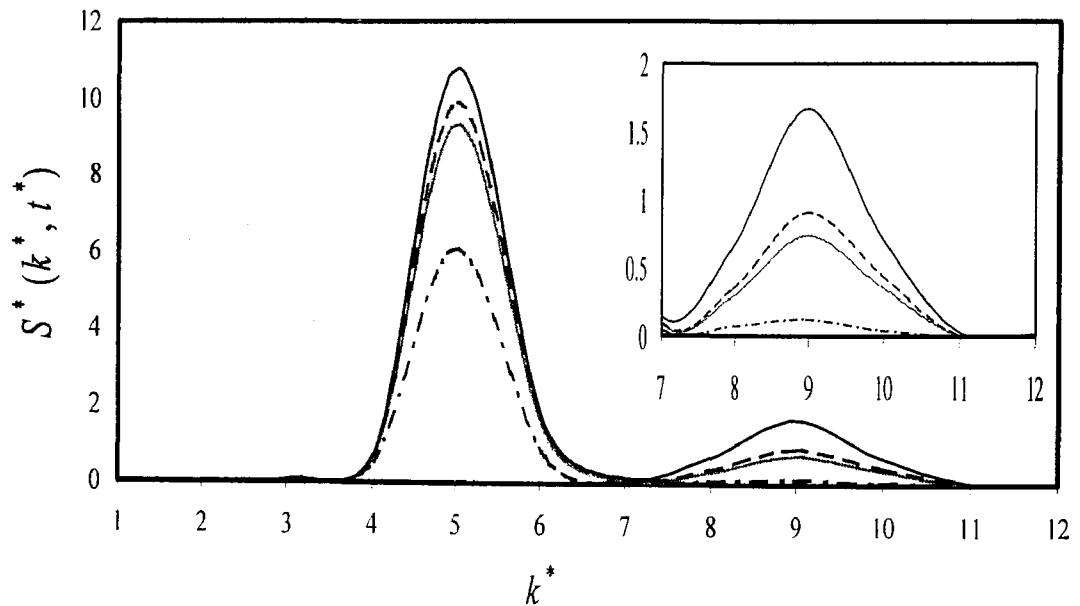


Figure C.15: The evolution of the dimensionless spatial concentration profile for a double quench from $T_1^* = 0.25$ to $T_2^* = 0.1$ (at the transition time of $t_i^* = 0.903$) at the following dimensionless times: $t^* = 0.9045$ (dash-dot line), $t^* = 0.9077$ (light grey line), $t^* = 0.9082$ (dashed line), and $t^* = 0.9106$ (solid line). The initial average concentration $c_0^* = 0.6$. The dimensionless diffusion coefficient for this case is $D^* = 500\,000$.

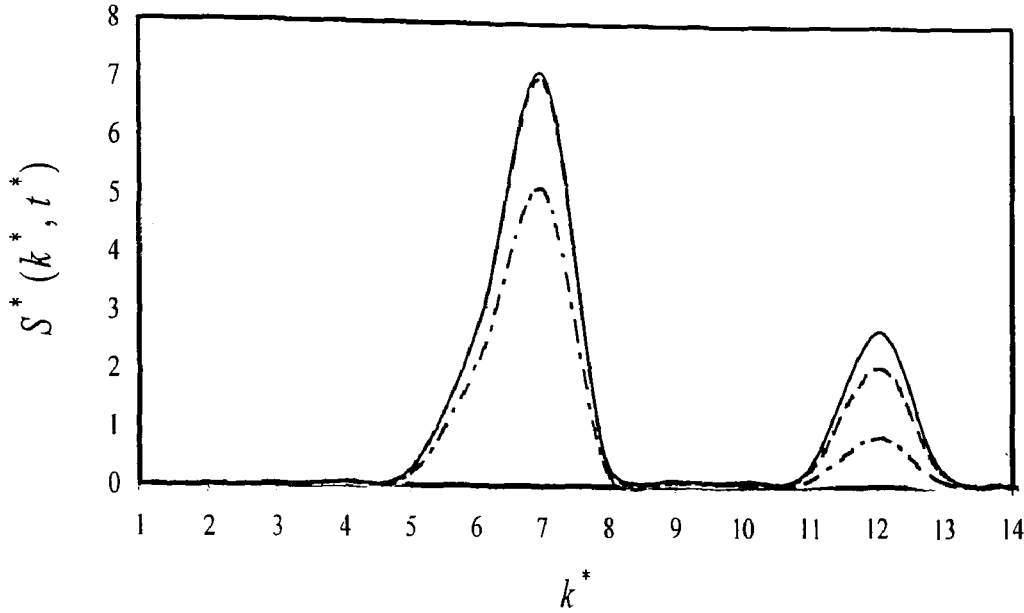


Figure C.16: The evolution of the dimensionless spatial concentration profile for a double quench from $T_1^* = 0.25$ to $T_2^* = 0.1$ (at the transition time of $t_i^* = 0.323$) at the following dimensionless times: $t^* = 0.3235$ (light grey line), $t^* = 0.3247$ (dash-dot line), $t^* = 0.3257$ (dashed line), and $t^* = 0.3265$ (solid line). The initial average concentration $c_0^* = 0.6$. The dimensionless diffusion coefficient for this case is $D^* = 800\,000$.

Change in the Dimensionless Spatial Chemical Potential

Figures C.17 to C.20 show the evolution of the dimensionless spatial chemical potential after the second quench to $T_2^* = 0.2$ at the transition time corresponding to $D^* = 500\,000$ and $800\,000$ for the initial critical and initial off-critical quench case, respectively. The evolution of the change in the dimensionless spatial chemical potential shows the same trends as for the single quench case. Figures C.21 to C.24 show the evolution of the dimensionless spatial chemical potential after the second quench to $T_2^* = 0.1$ at the transition time corresponding to $D^* = 500\,000$ and $800\,000$ for the initial critical and initial off-critical quench case, respectively. New trends are observed upon a deeper quench into the unstable region as discussed in Chapter 6. The observation of the flattening of the local

maxima and minima can be attributed to the adjusting of the blend to the change in quench conditions.

Change in the Dimensionless Spatial Second Derivative of Free Energy with Respect to Composition After the Second Quench

Figures 6.25 to C.28 show the evolution of the second derivative of the free energy with respect to composition spatially after the second quench to $T_2^* = 0.2$ from the initial critical and off-critical quench with $D^* = 500\ 000$ and $800\ 000$, respectively. The evolution of the change in the dimensionless spatial second derivative of free energy with respect to composition shows the same trends as for the single quench case. Figures 6.29 to C.32 show the evolution of the second derivative of the free energy with respect to composition spatially after the second quench to $T_2^* = 0.1$ from the initial critical and off-critical quench with $D^* = 500\ 000$ and $800\ 000$, respectively. New trends are observed upon a deeper quench into the unstable region as discussed in Chapter 6. The observation of the formation of new instabilities is observed in the form of a double well shape within the existing maxima and minima locations.

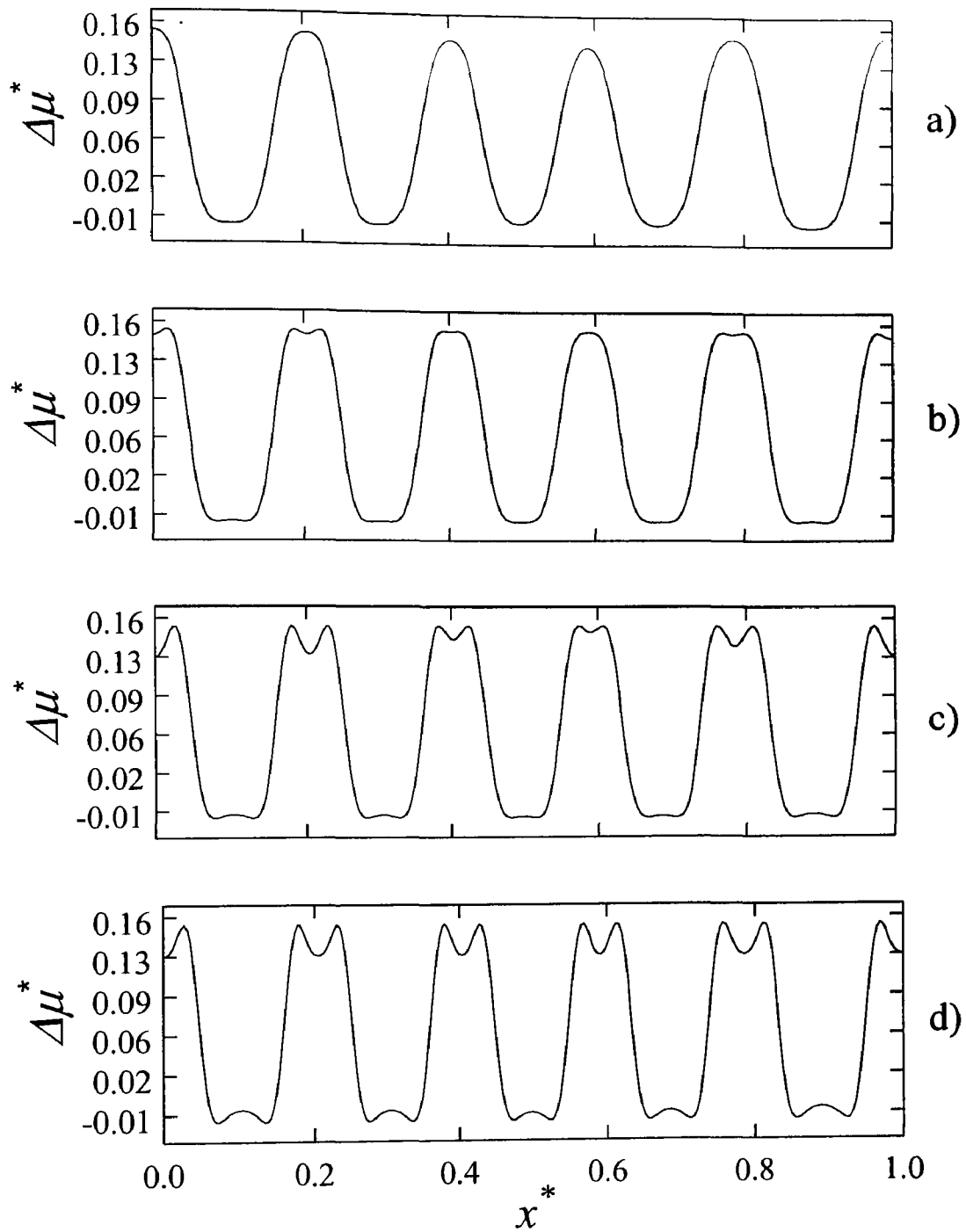


Figure C.17: The evolution of the change in the dimensionless spatial chemical potential for a double quench from $T_1^* = 0.25$ to $T_2^* = 0.2$ at the transition time of $t_i^* = 0.650$ at the following dimensionless times: (a) $t^* = 0.6509$, (b) $t^* = 0.656$, (c) $t^* = 0.6602$, and (d) $t^* = 0.6689$. The change in the dimensionless chemical potential is defined as the difference between the chemical potential polymer 1 in the mixture to that of its pure phase. The dimensionless initial concentration is $c_o^* = 0.5$ and the dimensionless diffusion coefficient is $D^* = 500\,000$.

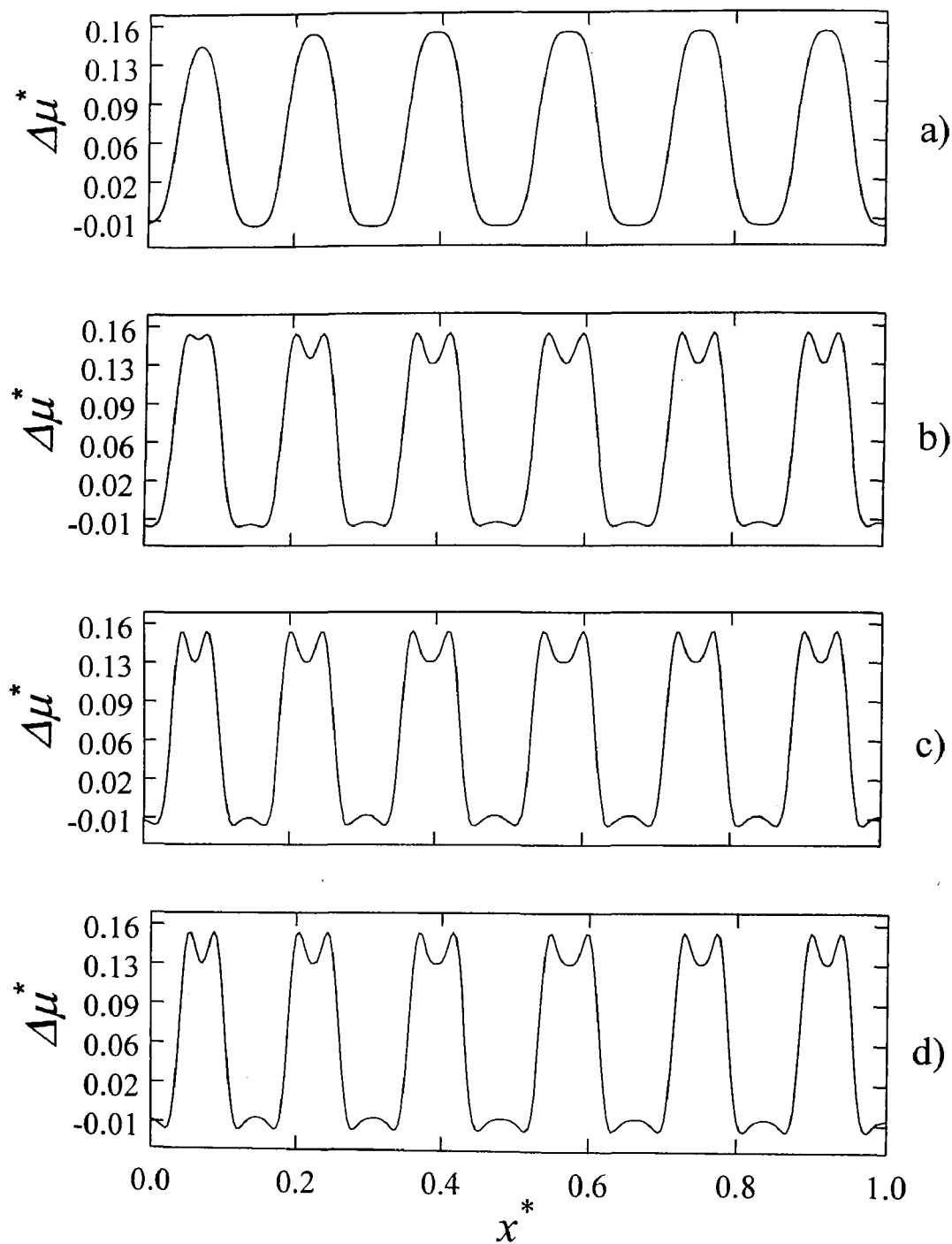


Figure C.18: The evolution of the change in the dimensionless spatial chemical potential for a double quench from $T_1^* = 0.25$ to $T_2^* = 0.2$ at the transition time of $t_i^* = 0.256$ at the following dimensionless times: (a) $t^* = 0.2561$, (b) $t^* = 0.2596$, (c) $t^* = 0.2619$, and (d) $t^* = 0.2656$. The change in the dimensionless chemical potential is defined as the difference between the chemical potential polymer 1 in the mixture to that of its pure phase. The dimensionless initial concentration is $c_0^* = 0.5$ and the dimensionless diffusion coefficient is $D^* = 800\,000$.

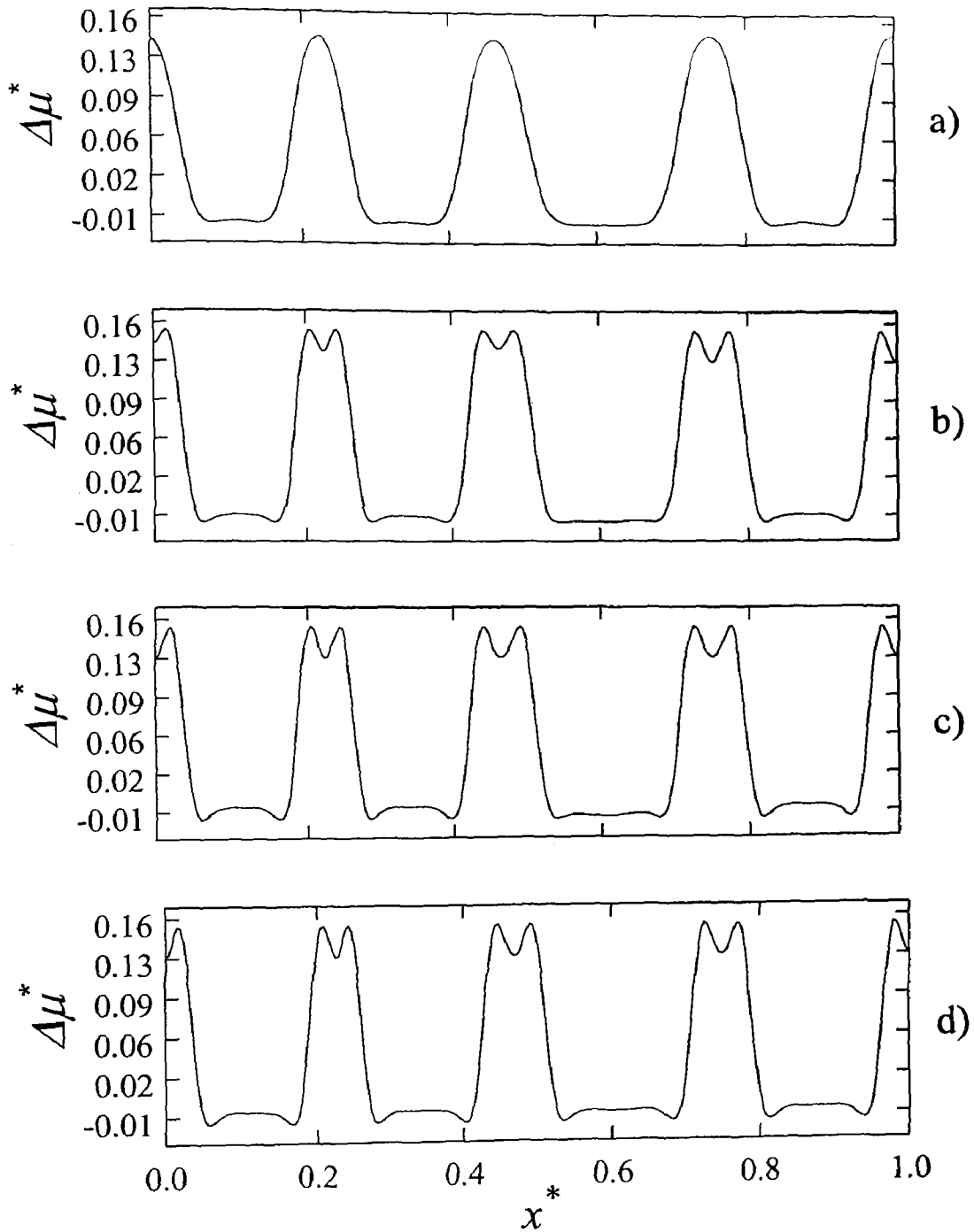


Figure C.19: The evolution of the change in the dimensionless spatial chemical potential for a double quench from $T_1^* = 0.25$ to $T_2^* = 0.2$ at the transition time of $t_i^* = 0.903$ at the following dimensionless times: (a) $t^* = 0.9057$, (b) $t^* = 0.9172$, (c) $t^* = 0.9260$, and (d) $t^* = 0.9421$. The change in the dimensionless chemical potential is defined as the difference between the chemical potential polymer 1 in the mixture to that of its pure phase. The dimensionless initial concentration is $c_0^* = 0.6$ and the dimensionless diffusion coefficient is $D^* = 500\,000$.

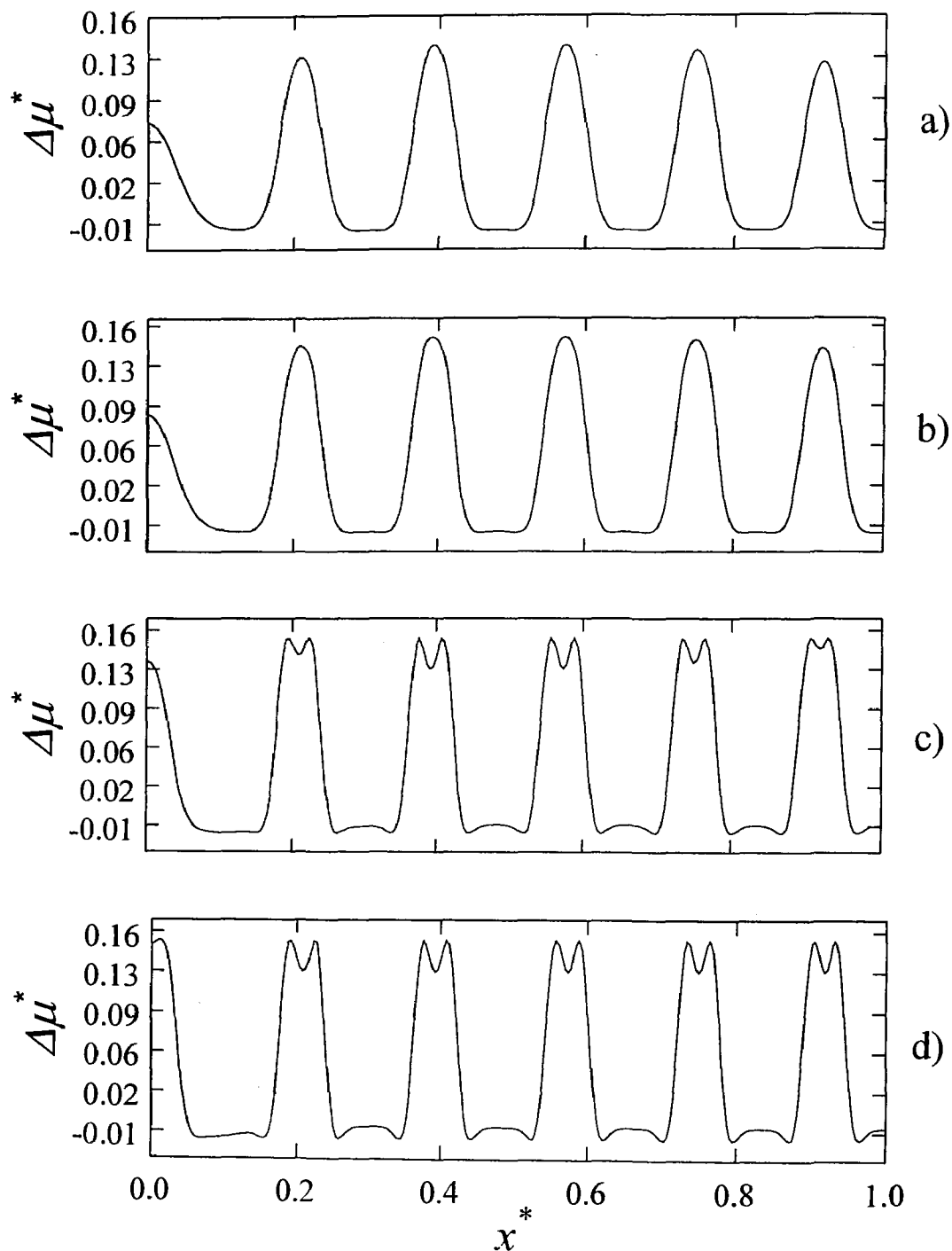


Figure C.20: The evolution of the change in the dimensionless spatial chemical potential for a double quench from $T_1^* = 0.25$ to $T_2^* = 0.2$ at the transition time of $t_i^* = 0.323$ at the following dimensionless times: (a) $t^* = 0.3235$, (b) $t^* = 0.325$, (c) $t^* = 0.3298$, and (d) $t^* = 0.3345$. The change in the dimensionless chemical potential is defined as the difference between the chemical potential polymer 1 in the mixture to that of its pure phase. The dimensionless initial concentration is $c_o^* = 0.6$ and the dimensionless diffusion coefficient is $D^* = 800\,000$.

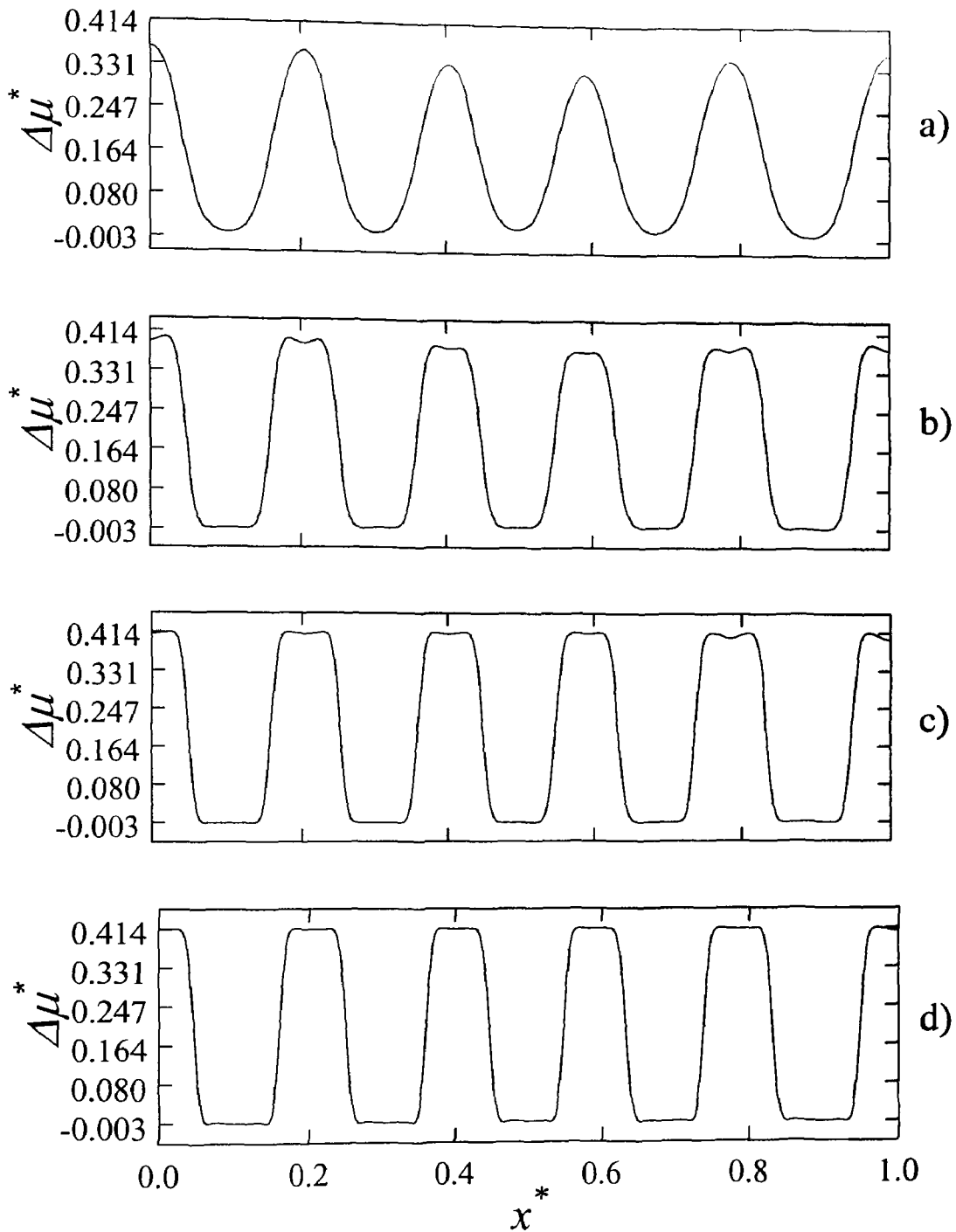


Figure C.21: The evolution of the change in the dimensionless spatial chemical potential for a double quench from $T_1^* = 0.25$ to $T_2^* = 0.1$ at the transition time of $t_i^* = 0.650$ at the following dimensionless times: (a) $t^* = 0.6511$, (b) $t^* = 0.6541$, (c) $t^* = 0.6562$, and (d) $t^* = 0.6584$. The change in the dimensionless chemical potential is defined as the difference between the chemical potential polymer 1 in the mixture to that of its pure phase. The dimensionless initial concentration is $c_0^* = 0.5$ and the dimensionless diffusion coefficient is $D^* = 500\,000$.

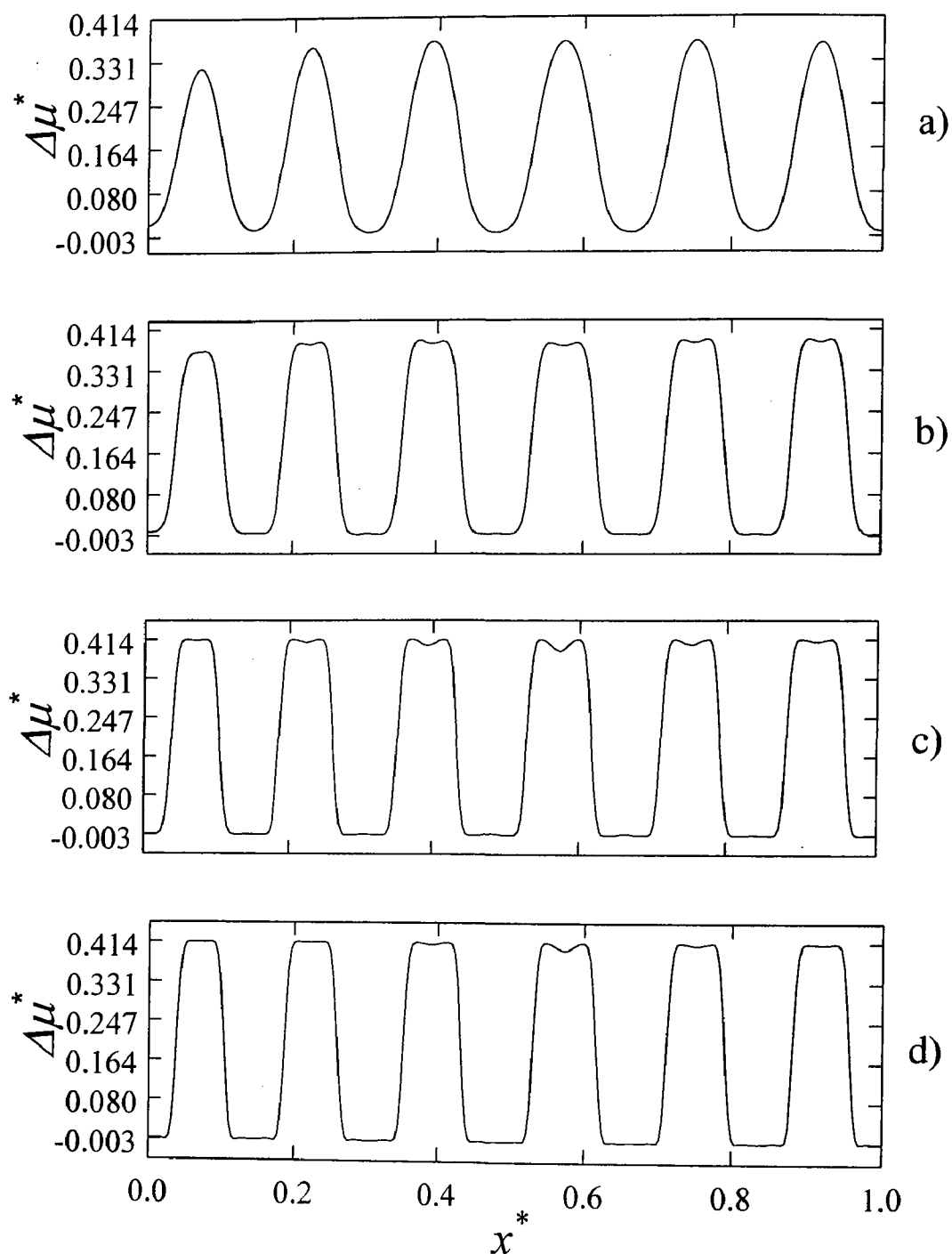


Figure C.22: The evolution of the change in the dimensionless spatial chemical potential for a double quench from $T_1^* = 0.25$ to $T_2^* = 0.1$ at the transition time of $t_i^* = 0.256$ at the following dimensionless times: (a) $t^* = 0.256$, (b) $t^* = 0.2577$, (c) $t^* = 0.2580$, and (d) $t^* = 0.2587$. The change in the dimensionless chemical potential is defined as the difference between the chemical potential polymer 1 in the mixture to that of its pure phase. The dimensionless initial concentration is $c_0^* = 0.5$ and the dimensionless diffusion coefficient is $D^* = 800\,000$.

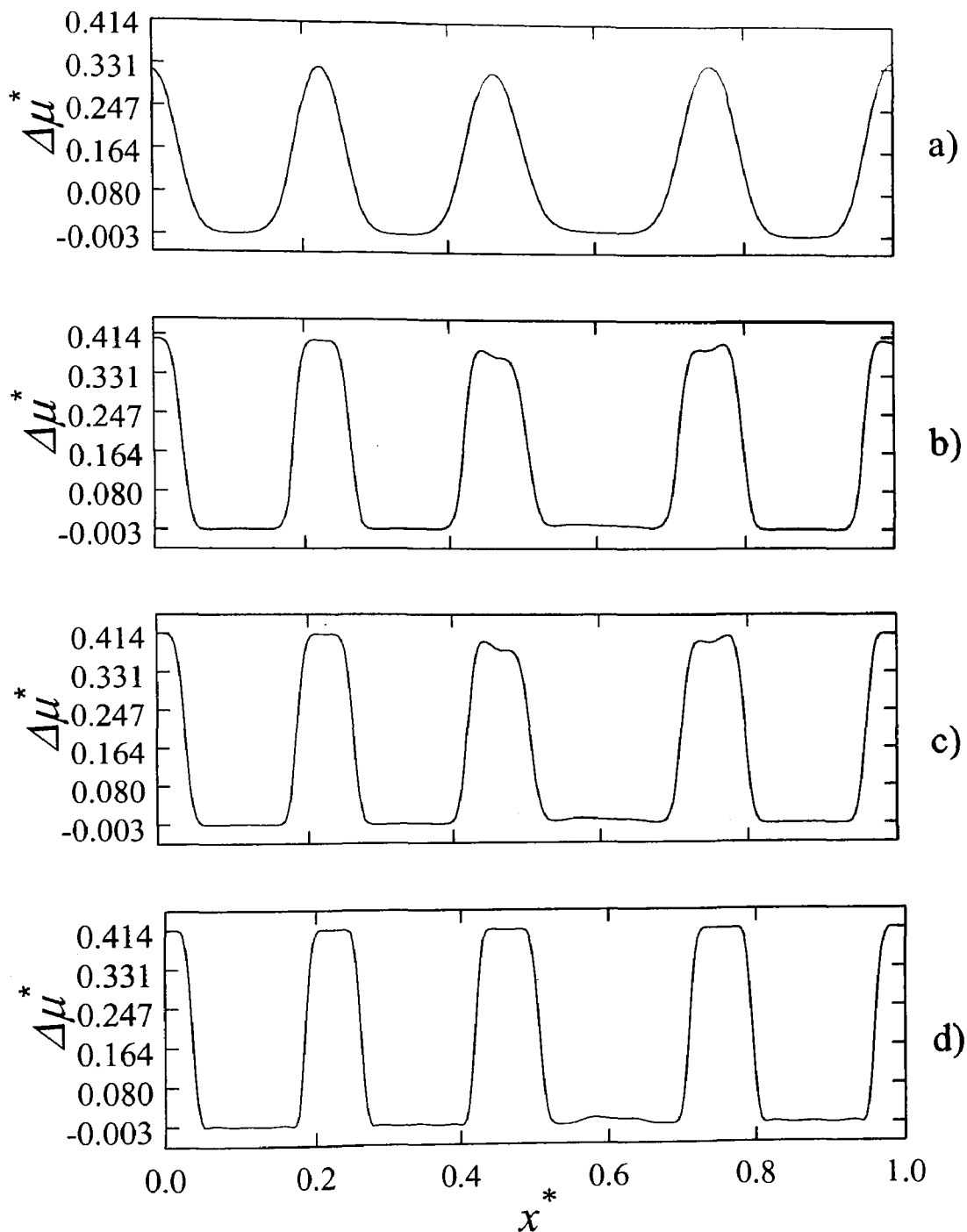


Figure C.23: The evolution of the change in the dimensionless spatial chemical potential for a double quench from $T_1^* = 0.25$ to $T_2^* = 0.1$ at the transition time of $t_i^* = 0.903$ at the following dimensionless times: (a) $t^* = 0.9045$, (b) $t^* = 0.9077$, (c) $t^* = 0.9082$, and (d) $t^* = 0.9106$. The change in the dimensionless chemical potential is defined as the difference between the chemical potential polymer 1 in the mixture to that of its pure phase. The dimensionless initial concentration is $c_o^* = 0.6$ and the dimensionless diffusion coefficient is $D^* = 500\,000$.

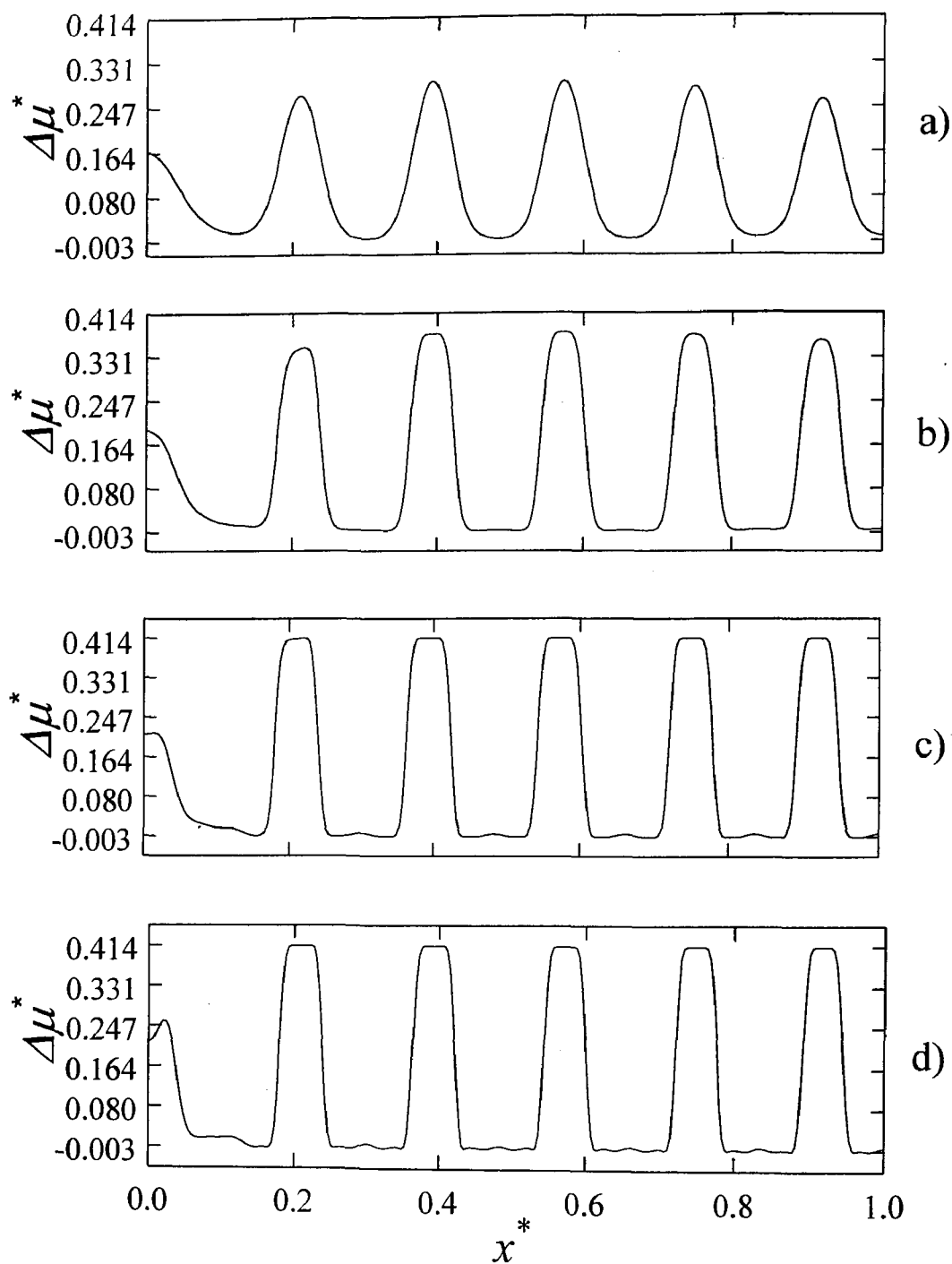


Figure C.24: The evolution of the change in the dimensionless spatial chemical potential for a double quench from $T_1^* = 0.25$ to $T_2^* = 0.1$ at the transition time of $t_r^* = 0.323$ at the following dimensionless times: (a) $t^* = 0.3235$, (b) $t^* = 0.3247$, (c) $t^* = 0.3257$, and (d) $t^* = 0.3265$. The change in the dimensionless chemical potential is defined as the difference between the chemical potential polymer 1 in the mixture to that of its pure phase. The dimensionless initial concentration is $c_0^* = 0.6$ and the dimensionless diffusion coefficient is $D^* = 800\,000$.

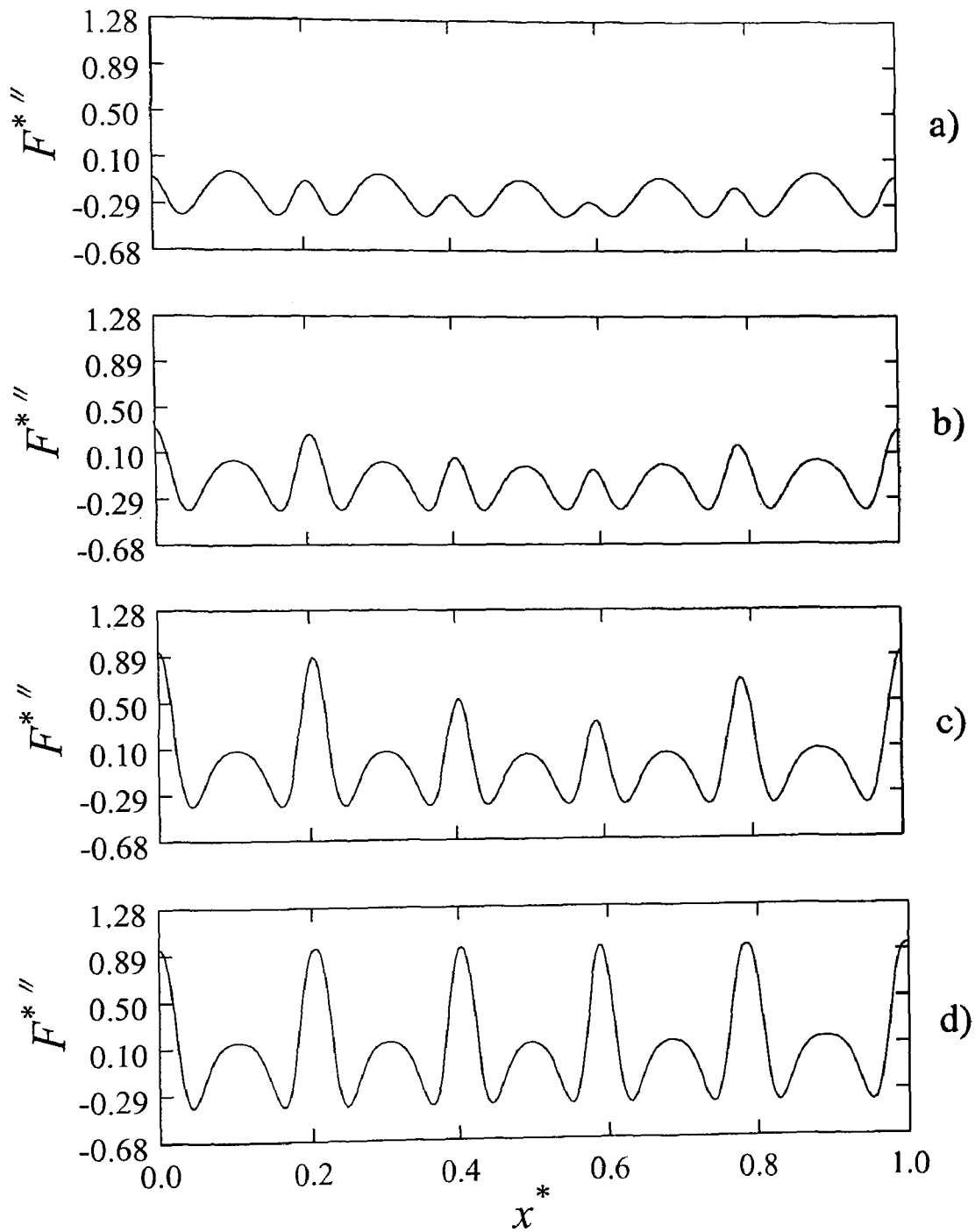


Figure C.25: The evolution of the change in the dimensionless spatial second derivative of the free energy with respect to composition of component 1 for a double quench from $T_1^* = 0.25$ to $T_2^* = 0.2$ at the transition time of $t_t^* = 0.650$ at the following dimensionless times: (a) $t^* = 0.6509$, (b) $t^* = 0.656$, (c) $t^* = 0.6602$, and (d) $t^* = 0.6689$. The change in the dimensionless second derivative of free energy is used to determine the conditions of stability ($F^{*''} > 0$), meta-stability ($F^{*''} > 0$), and instability ($F^{*''} < 0$). The dimensionless initial concentration is $c_0^* = 0.5$ and the dimensionless diffusion coefficient is $D^* = 500\,000$.

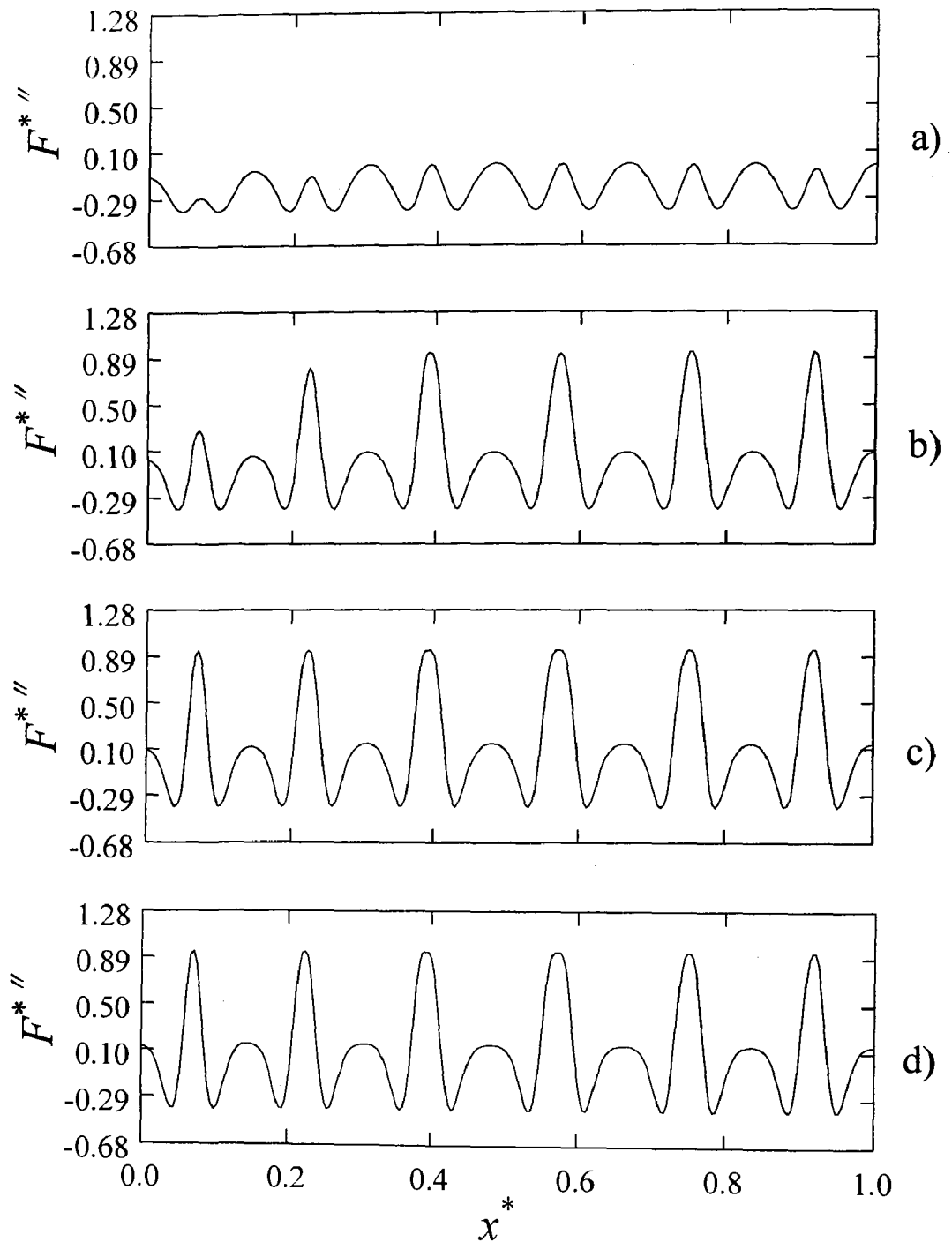


Figure C.26: The evolution of the change in the dimensionless spatial second derivative of the free energy with respect to composition of component 1 for a double quench from $T_1^* = 0.25$ to $T_2^* = 0.2$ at the transition time of $t_i^* = 0.256$ at the following dimensionless times: (a) $t^* = 0.2561$, (b) $t^* = 0.2596$, (c) $t^* = 0.2619$, and (d) $t^* = 0.2656$. The change in the dimensionless second derivative of free energy is used to determine the conditions of stability ($F^{*''} > 0$), meta-stability ($F^{*''} > 0$), and instability ($F^{*''} < 0$). The dimensionless initial concentration is $c_0^* = 0.5$ and the dimensionless diffusion coefficient is $D^* = 800\,000$.

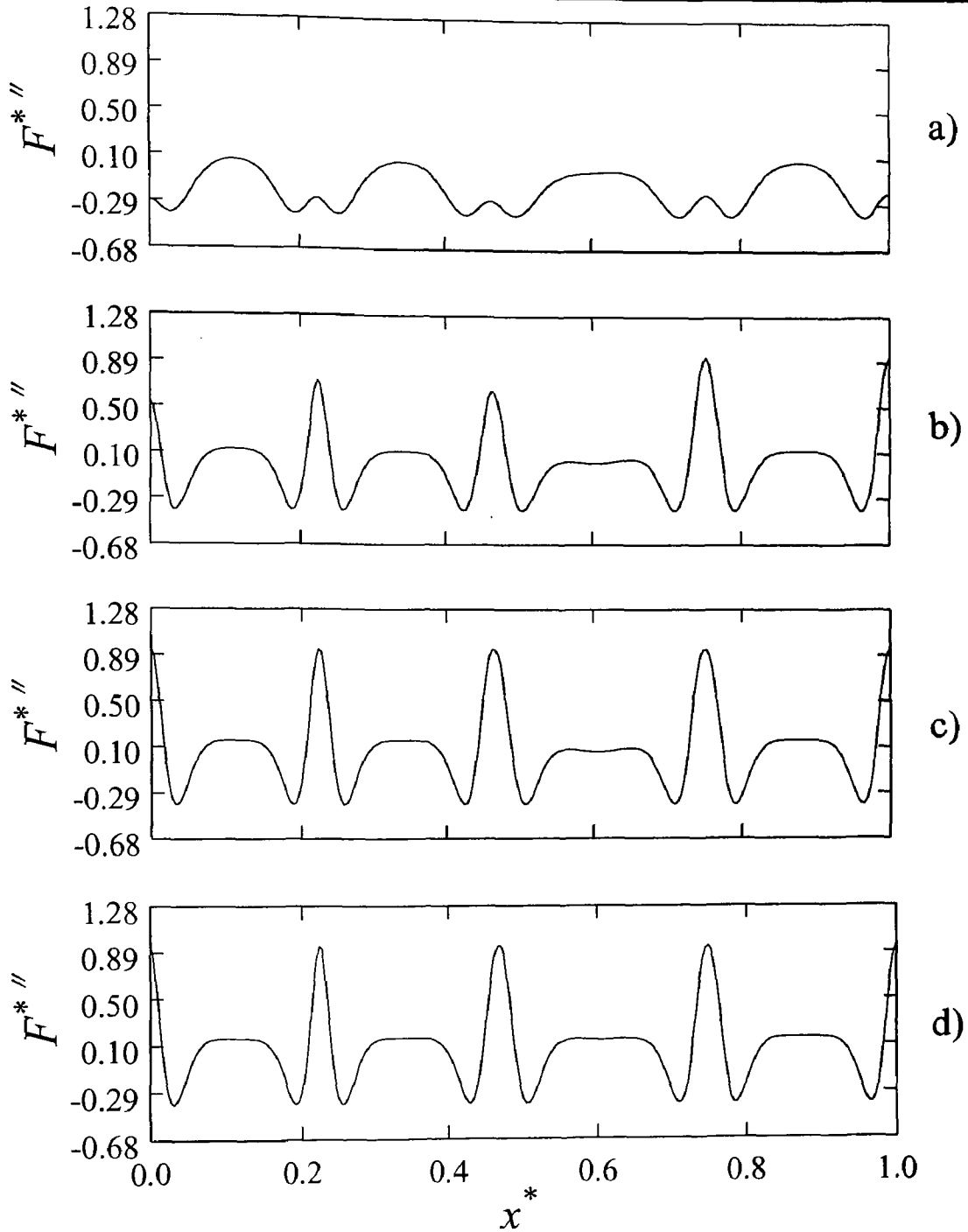


Figure C.27: The evolution of the change in the dimensionless spatial second derivative of the free energy with respect to composition of component 1 for a double quench from $T_1^* = 0.25$ to $T_2^* = 0.2$ at the transition time of $t_l^* = 0.903$ at the following dimensionless times: (a) $t^* = 0.9057$, (b) $t^* = 0.9172$, (c) $t^* = 0.9260$, and (d) $t^* = 0.9421$. The change in the dimensionless second derivative of free energy is used to determine the conditions of stability ($F^{*''} > 0$), meta-stability ($F^{*''} > 0$), and instability ($F^{*''} < 0$). The dimensionless initial concentration is $c_0^* = 0.6$ and the dimensionless diffusion coefficient is $D^* = 500\,000$.

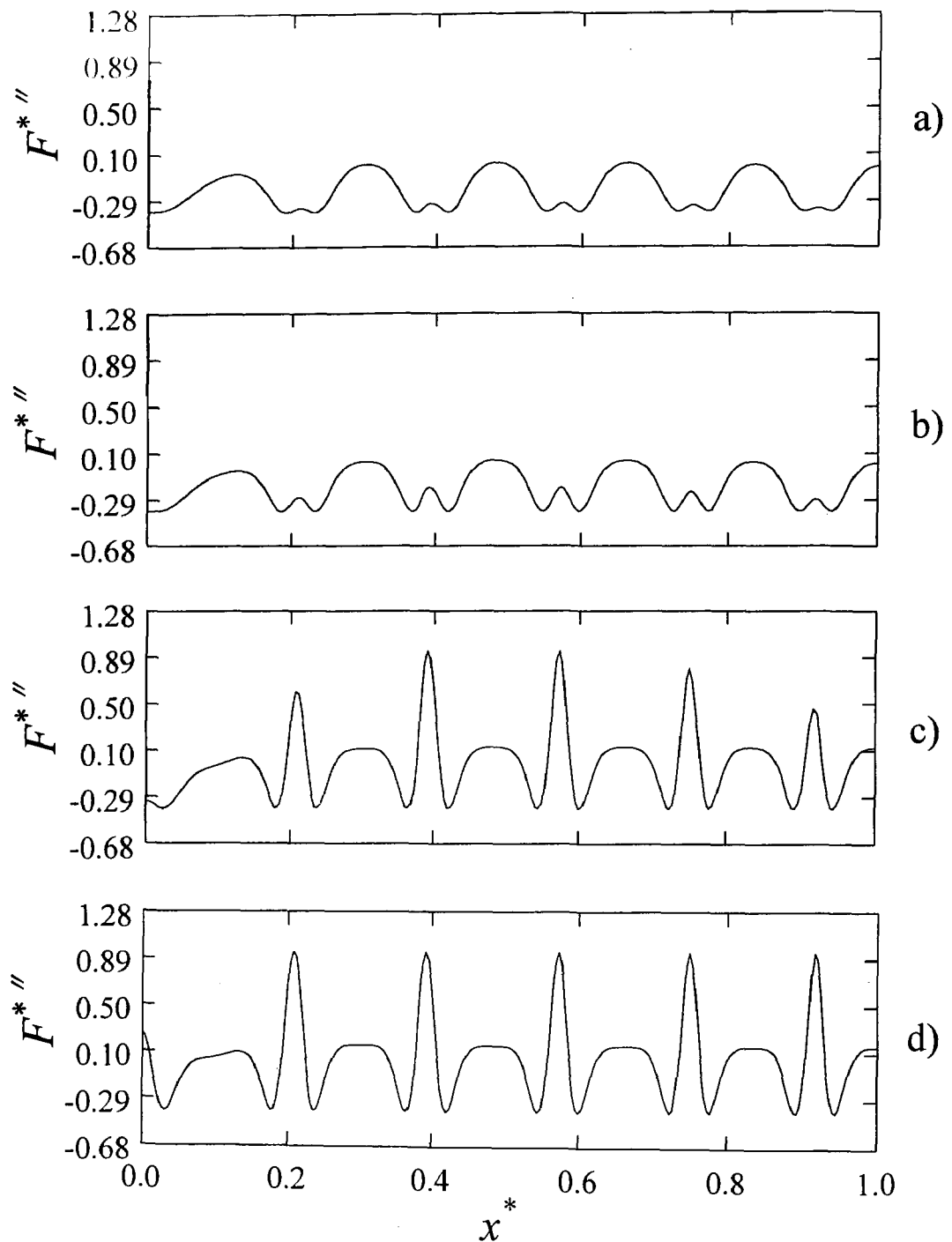


Figure C.28: The evolution of the change in the dimensionless spatial second derivative of the free energy with respect to composition of component 1 for a double quench from $T_1^* = 0.25$ to $T_2^* = 0.2$ at the transition time of $t_l^* = 0.323$ at the following dimensionless times: (a) $t^* = 0.3235$, (b) $t^* = 0.325$, (c) $t^* = 0.3298$, and (d) $t^* = 0.3345$. The change in the dimensionless second derivative of free energy is used to determine the conditions of stability ($F^{*''} > 0$), meta-stability ($F^{*''} > 0$), and instability ($F^{*''} < 0$). The dimensionless initial concentration is $c_0^* = 0.6$ and the dimensionless diffusion coefficient is $D^* = 800\,000$.

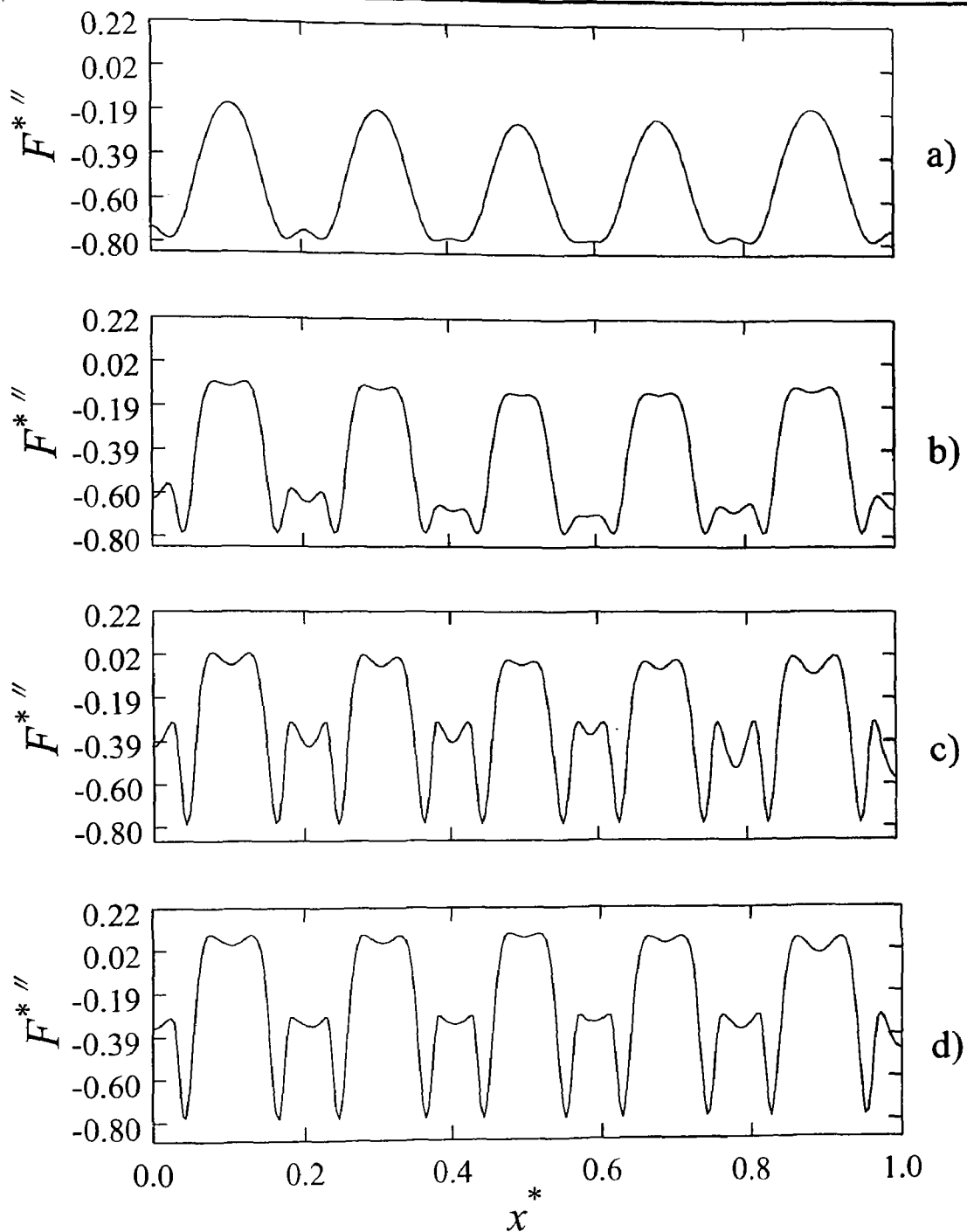


Figure C.29: The evolution of the change in the dimensionless spatial second derivative of the free energy with respect to composition of component 1 for a double quench from $T_1^* = 0.25$ to $T_2^* = 0.1$ at the transition time of $t_i^* = 0.650$ at the following dimensionless times: (a) $t^* = 0.6511$, (b) $t^* = 0.6541$, (c) $t^* = 0.6562$, and (d) $t^* = 0.6584$. The change in the dimensionless second derivative of free energy is used to determine the conditions of stability ($F^{*''} > 0$), meta-stability ($F^{*''} > 0$), and instability ($F^{*''} < 0$). The dimensionless initial concentration is $c_0^* = 0.5$ and the dimensionless diffusion coefficient is $D^* = 500\,000$.

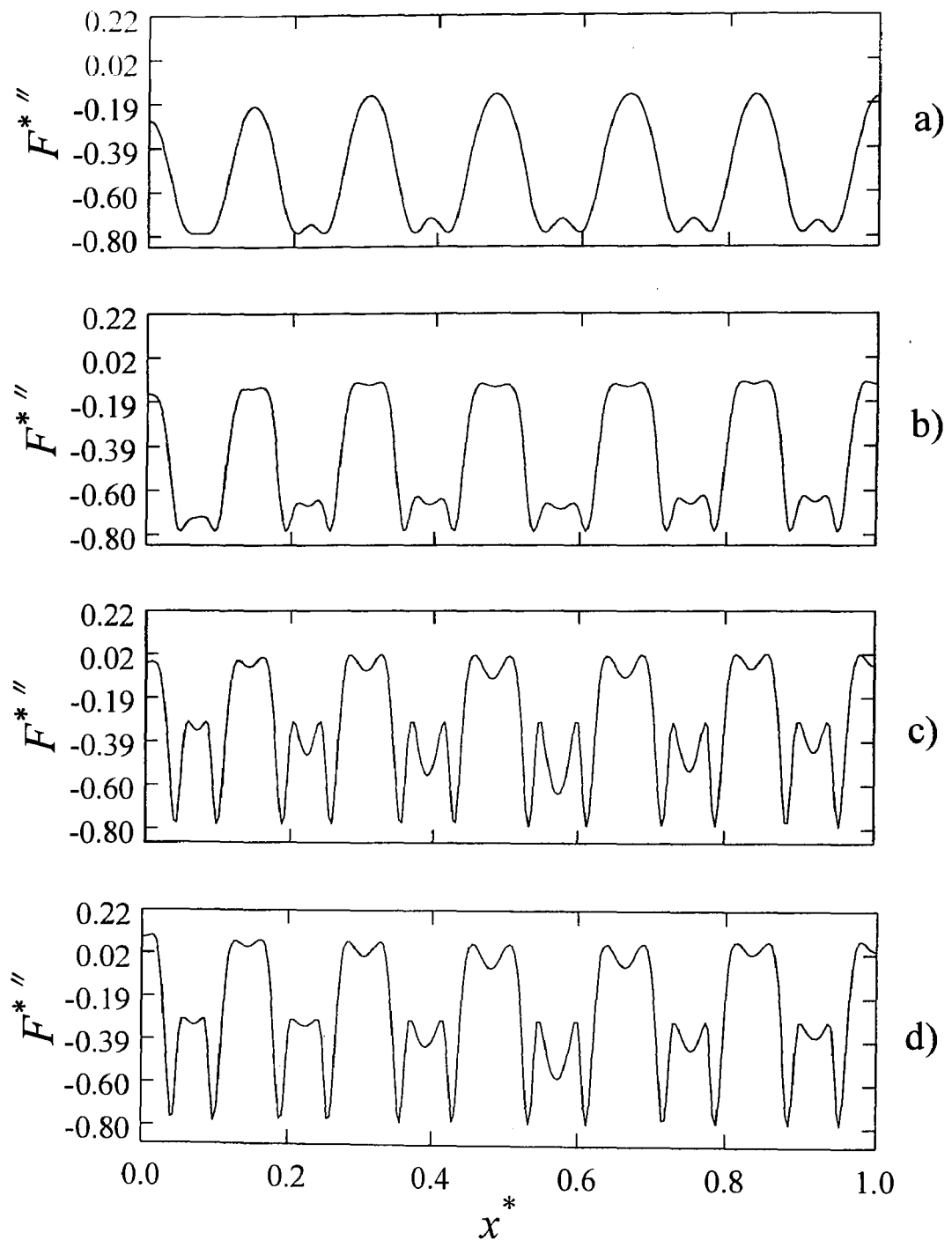


Figure C.30: The evolution of the change in the dimensionless spatial second derivative of the free energy with respect to composition of component 1 for a double quench from $T_1^* = 0.25$ to $T_2^* = 0.1$ at the transition time of $t_l^* = 0.256$ at the following dimensionless times: (a) $t^* = 0.256$, (b) $t^* = 0.2577$, (c) $t^* = 0.2580$, and (d) $t^* = 0.2587$. The change in the dimensionless second derivative of free energy is used to determine the conditions of stability ($F^{*''} > 0$), meta-stability ($F^{*''} > 0$), and instability ($F^{*''} < 0$). The dimensionless initial concentration is $c_0^* = 0.5$ and the dimensionless diffusion coefficient is $D^* = 800\,000$.

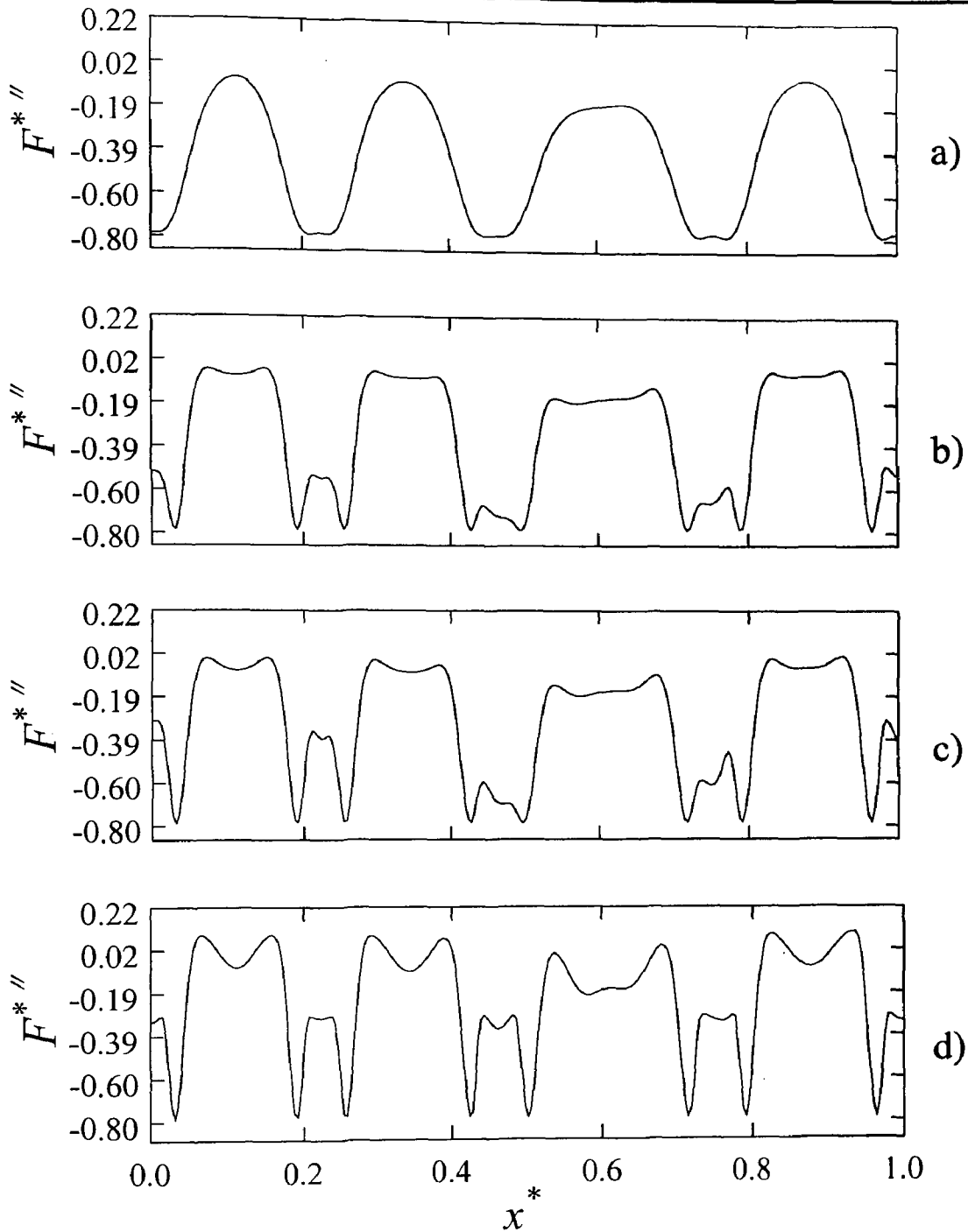


Figure C.31: The evolution of the change in the dimensionless spatial second derivative of the free energy with respect to composition of component 1 for a double quench from $T_1^* = 0.25$ to $T_2^* = 0.1$ at the transition time of $t_i^* = 0.903$ at the following dimensionless times: (a) $t^* = 0.9045$, (b) $t^* = 0.9077$, (c) $t^* = 0.9082$, and (d) $t^* = 0.9106$. The change in the dimensionless second derivative of free energy is used to determine the conditions of stability ($F^{*''} > 0$), meta-stability ($F^{*''} > 0$), and instability ($F^{*''} < 0$). The dimensionless initial concentration is $c_0^* = 0.6$ and the dimensionless diffusion coefficient is $D^* = 500\,000$.

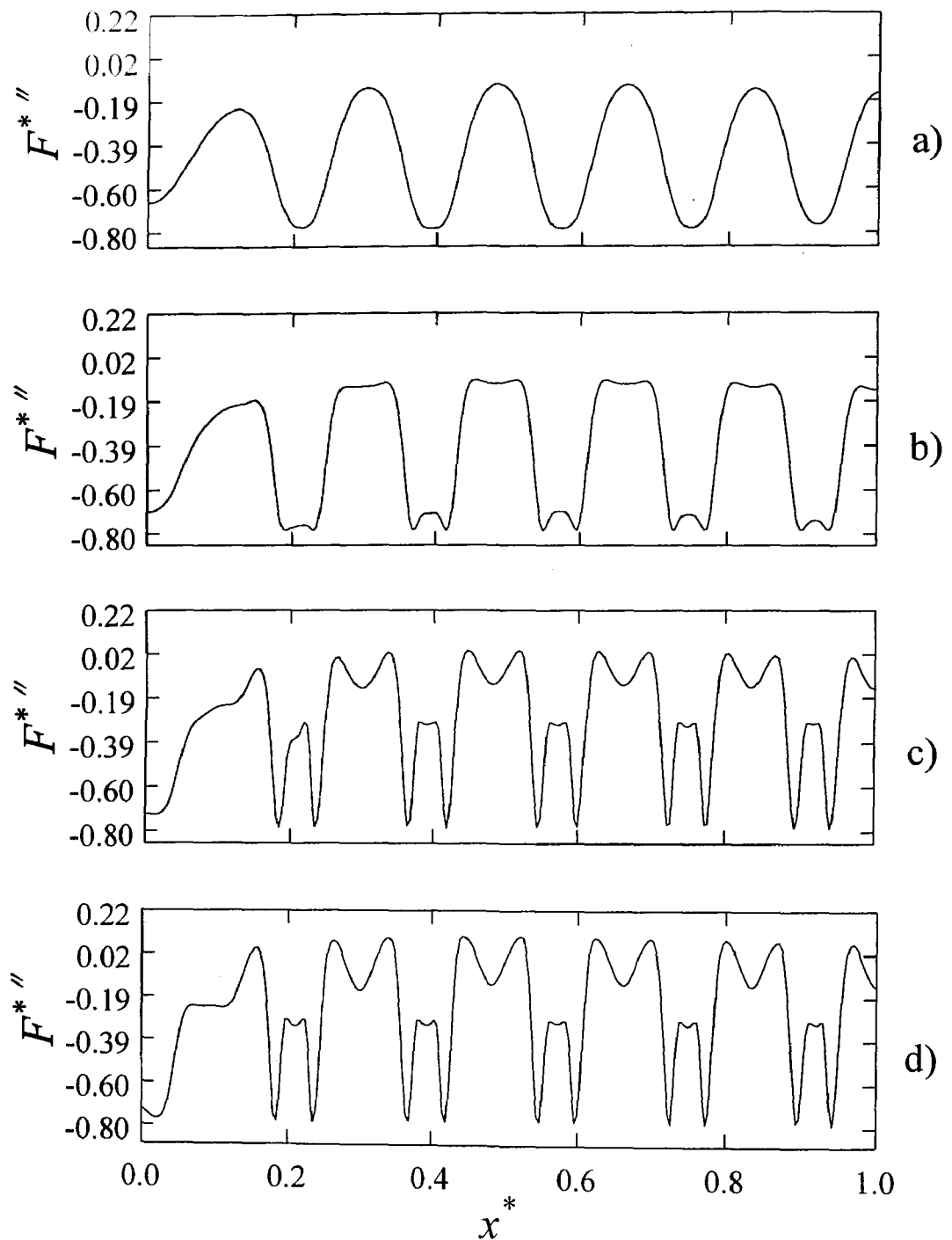


Figure C.32: The evolution of the change in the dimensionless spatial second derivative of the free energy with respect to component 1 for a double quench from $T_1^* = 0.25$ to $T_2^* = 0.1$ at the transition time of $t_i^* = 0.323$ at the following dimensionless times: (a) $t^* = 0.3235$, (b) $t^* = 0.3247$, (c) $t^* = 0.3257$, and (d) $t^* = 0.3265$. The change in the dimensionless second derivative of free energy is used to determine the conditions of stability ($F^{*''} > 0$), meta-stability ($F^{*''} > 0$), and instability ($F^{*''} < 0$). The dimensionless initial concentration is $c_0^* = 0.6$ and the dimensionless diffusion coefficient is $D^* = 800\,000$.

Growth of Primary Structures After the Second Temperature Jump to $T_2^* = 0.2$

Figure C.33 to C.36 shows the growth of the maximum value of the dimensionless structure factor with dimensionless reduced time after the second shallower quench for the initial critical quench and initial off-critical quench case for $D^* = 500\,000$ and $800\,000$, respectively. The values plotted are taken right after the second quench is made and there are three regions and discussed in Chapter 6. Figures C.35 and C.36 shows the growth rate of the primary (top) and secondary (bottom) peaks of the maximum structure factor after the second shallow quench. The difference in the profiles for the initial critical and initial off-critical quench cases were also discussed in Chapter 6.

A Comparison of the Growth of Primary and Secondary Structures After the Second Temperature Jump to $T_2^* = 0.1$

Figure C.37 to C.40 shows the growth rate of the primary (top) and secondary (bottom) peaks of the maximum structure factor after the second deeper quench at the transition times for the initial critical and initial off-critical quench case with $D^* = 50\,000$ and $80\,000$, respectively. The growth was divided into three stages. Generally, the trends are consistent for the three stages and were discussed in Chapter 6.

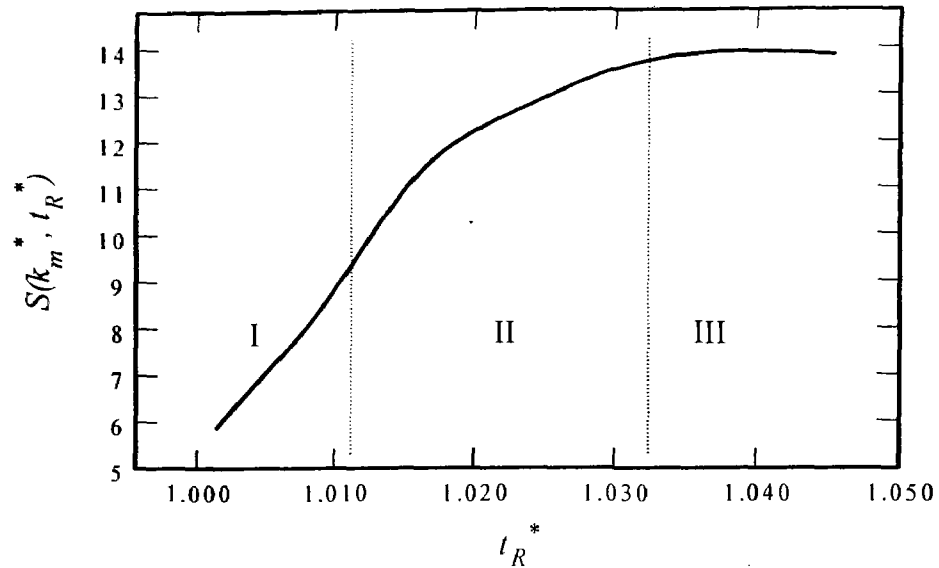


Figure C.33: The evolution of the dimensionless structure factor of the primary structure formed just after the second temperature jump to $T_2^* = 0.2$, plotted against dimensionless reduced times for a critical quench case. The second jump was made at a transition time of $t_l^* = 0.650$ with a dimensionless diffusion coefficient $D^* = 500\,000$.

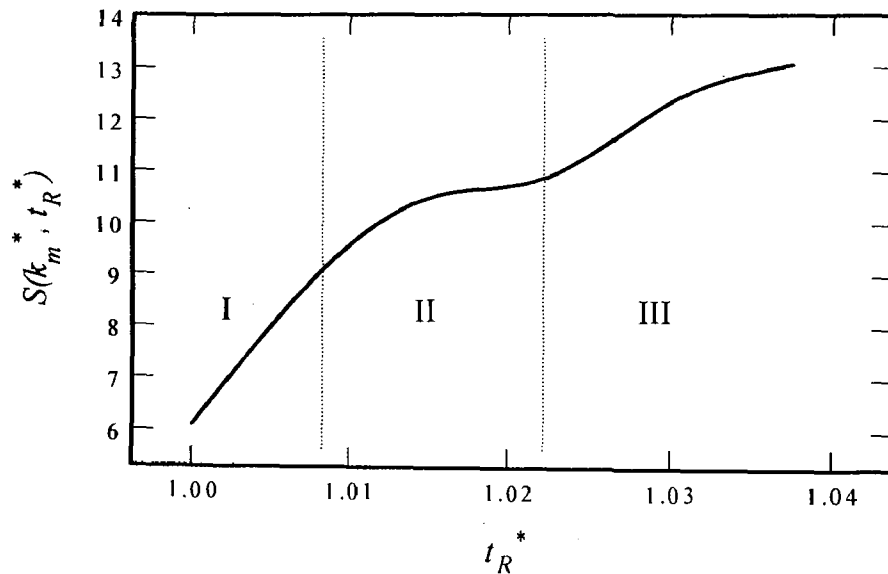


Figure C.34: The evolution of the dimensionless structure factor of the primary structure formed just after the second temperature jump to $T_2^* = 0.2$, plotted against dimensionless reduced times for a critical quench case. The second jump was made at a transition time of $t_l^* = 0.2560$ with a dimensionless diffusion coefficient $D^* = 800\,000$.

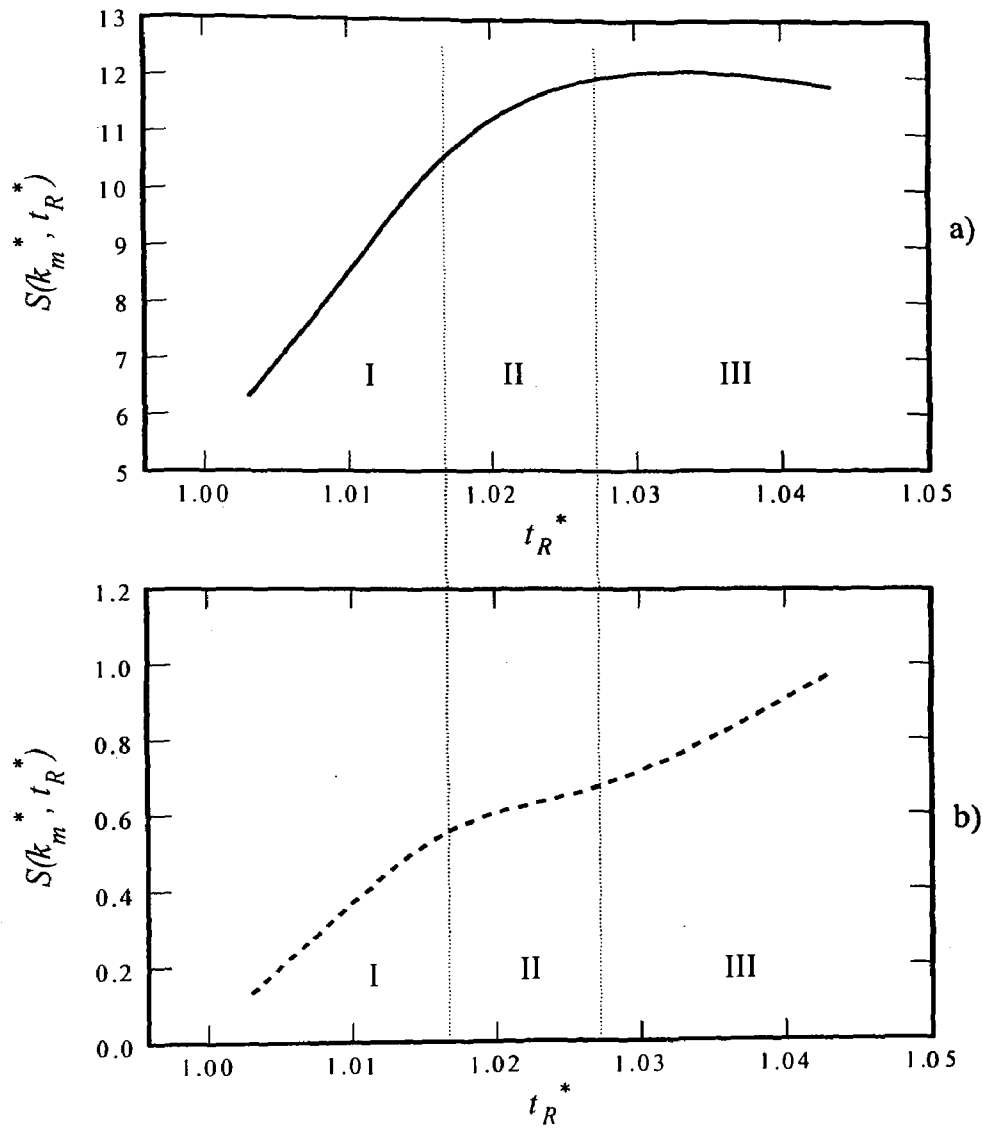


Figure C.35: The evolution of the dimensionless structure factor of the (a) primary and (b) secondary peaks formed just after the second temperature jump to $T_2^* = 0.2$ plotted against dimensionless reduced times for an off-critical quench case. The second temperature jump was made at $t_l^* = 0.903$. The dimensionless diffusion coefficient is $D^* = 500\,000$.

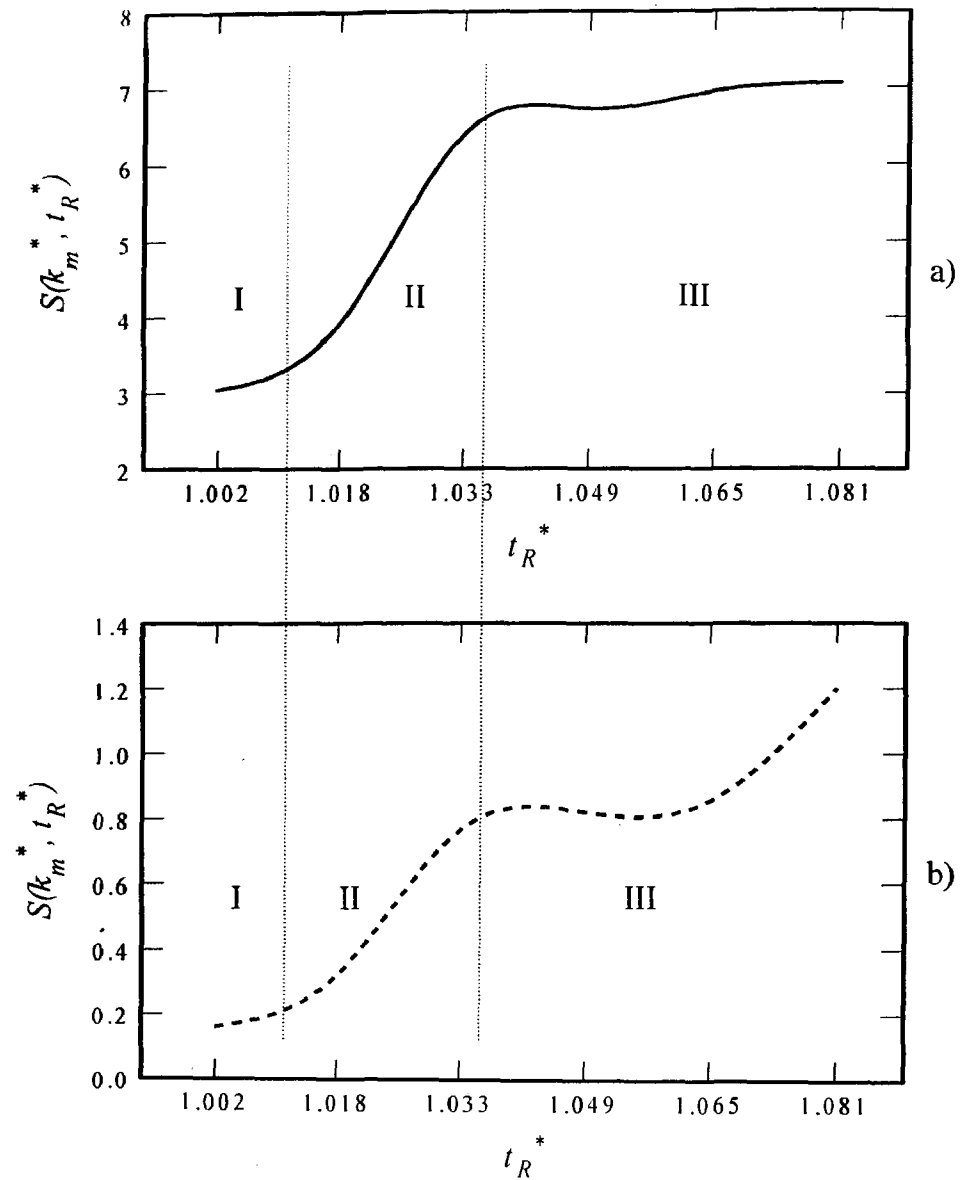


Figure C.36: The evolution of the dimensionless structure factor of the (a) primary and (b) secondary peaks formed just after the second temperature jump to $T_2^* = 0.2$ plotted against dimensionless reduced times for an off-critical quench case. The second temperature jump was made at $t_i^* = 0.323$. The dimensionless diffusion coefficient is $D^* = 800\,000$.

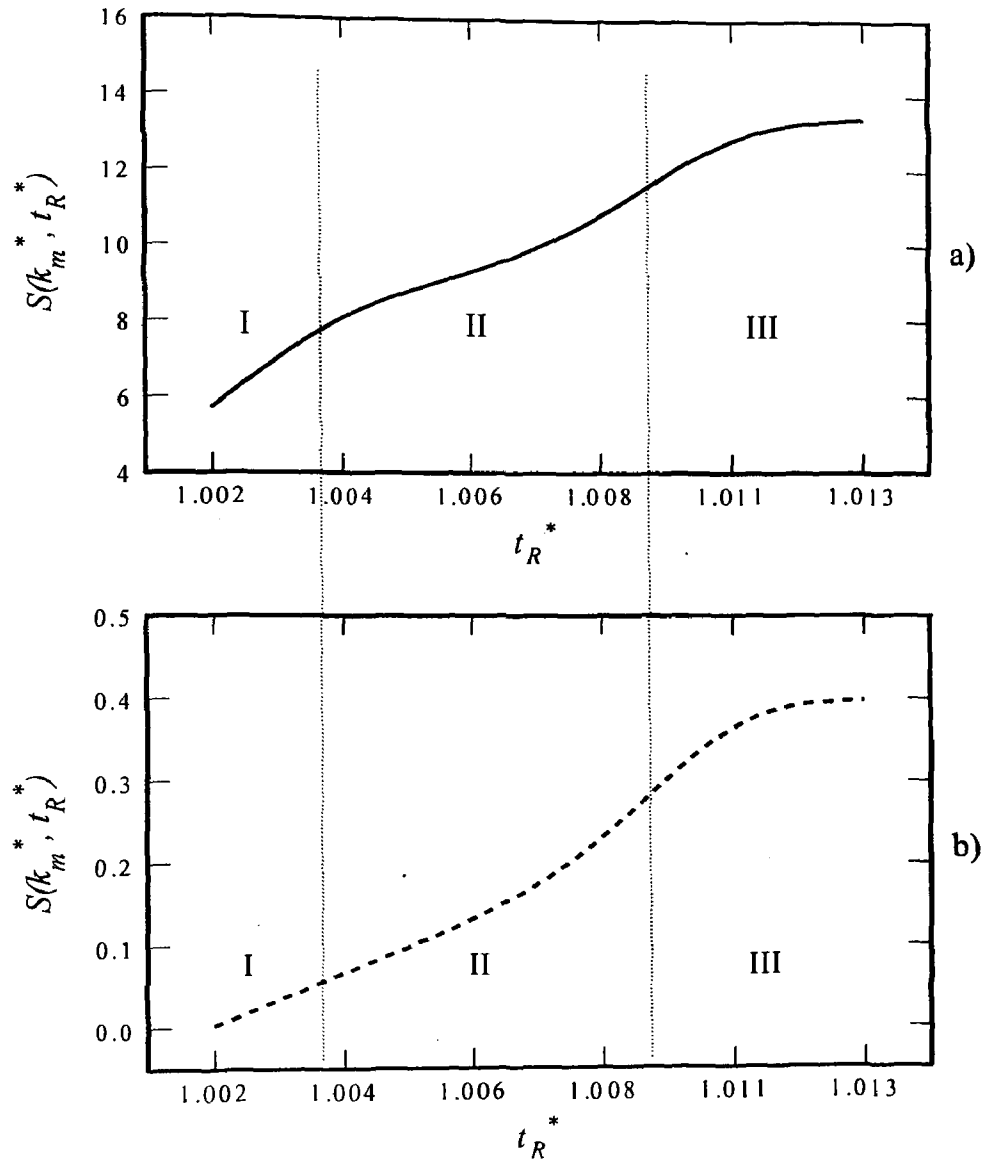


Figure C.37: The evolution of the dimensionless structure factor of the (a) primary and (b) secondary structures formed just after the second temperature jump to $T_2^* = 0.1$ plotted against dimensionless reduced times for a critical quench case. The second temperature jump was made at $t_r^* = 0.650$. The dimensionless diffusion coefficient is $D^* = 500\,000$.

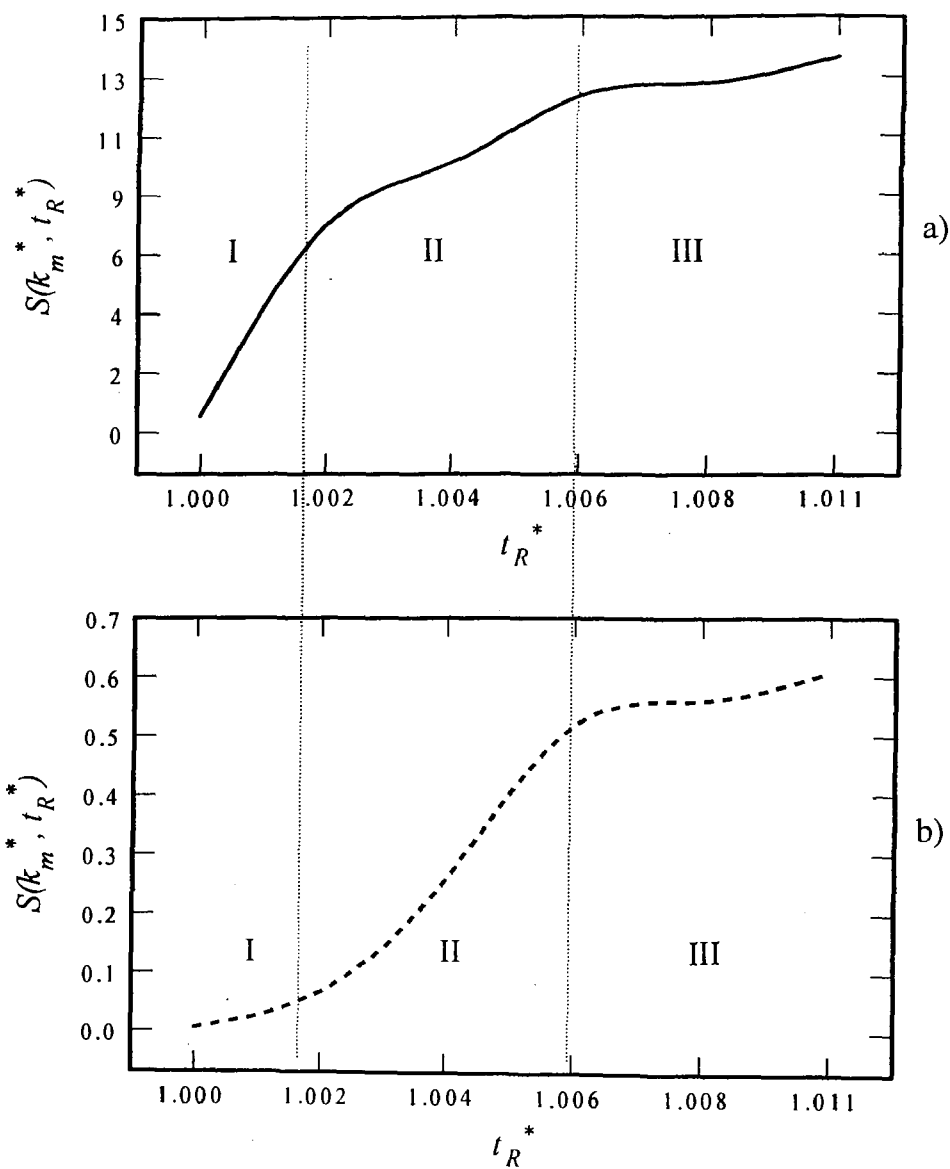


Figure C.38: The evolution of the dimensionless structure factor of the (a) primary and (b) secondary structures formed just after the second temperature jump to $T_2^* = 0.1$ plotted against dimensionless reduced times for a critical quench case. The second temperature jump was made at $t_i^* = 0.256$. The dimensionless diffusion coefficient is $D^* = 800\,000$.

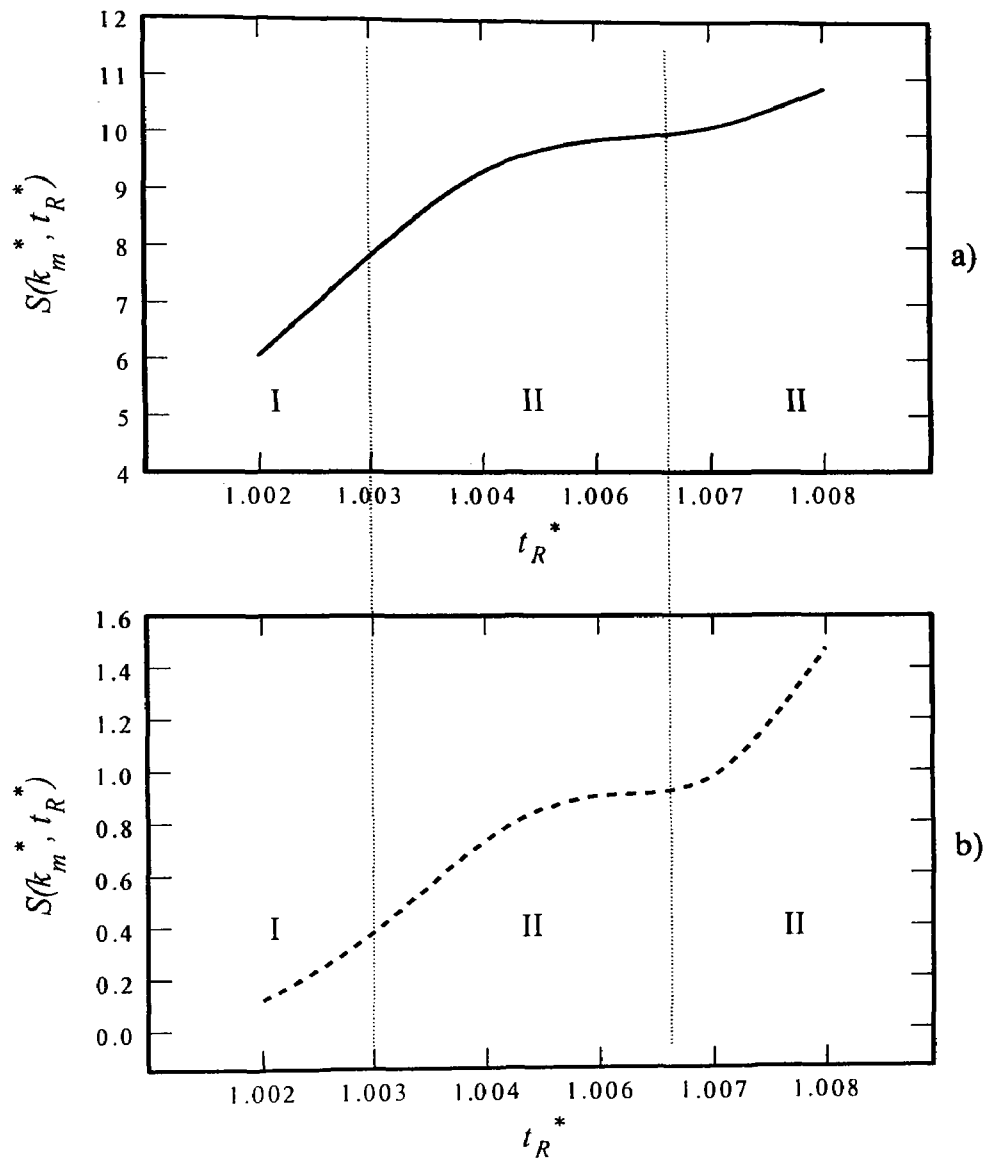


Figure C.39: The evolution of the dimensionless structure factor of the (a) primary and (b) secondary structures formed just after the second temperature jump to $T_2^* = 0.1$ plotted against dimensionless reduced times for an off-critical quench case. The second temperature jump was made at $t_i^* = 0.903$. The dimensionless diffusion coefficient is $D^* = 500\,000$.

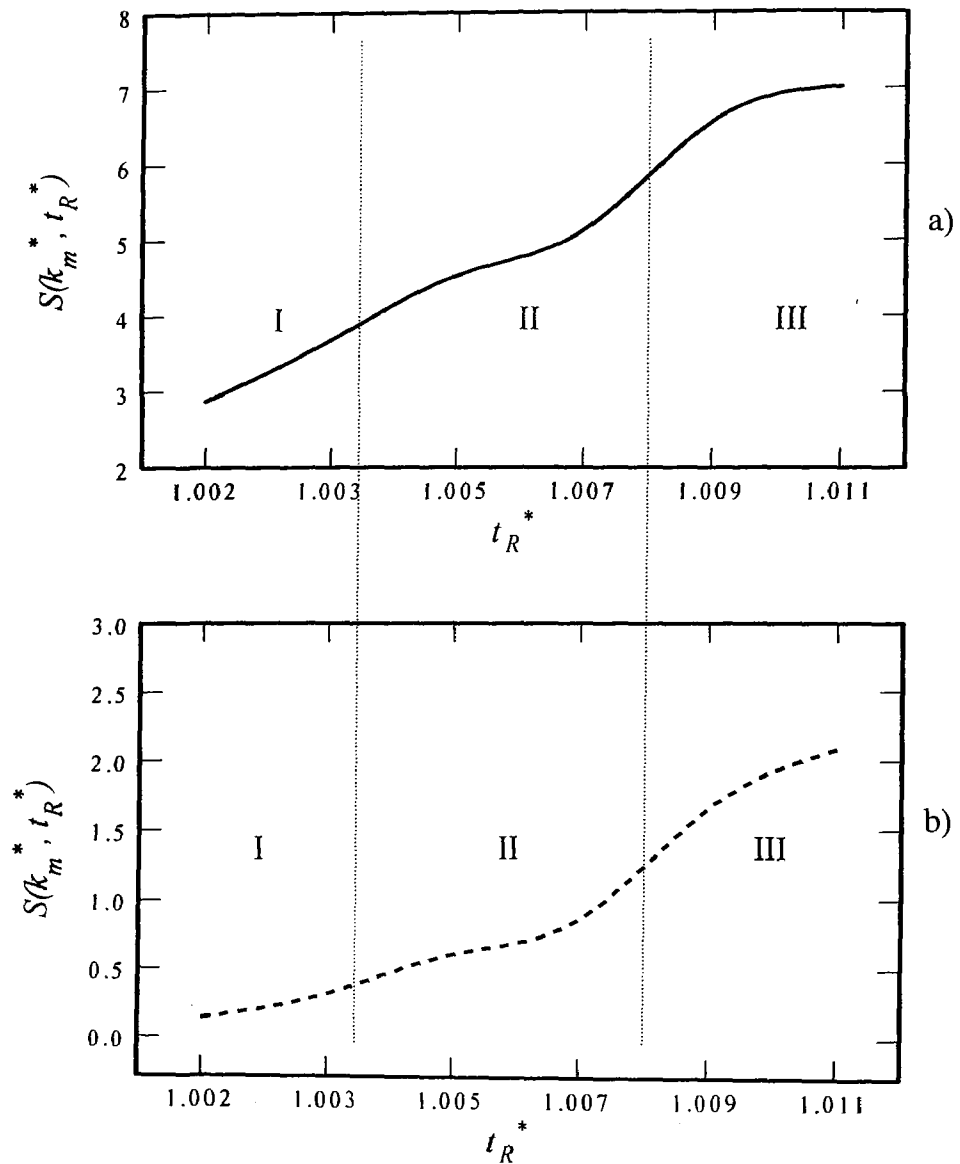


Figure C.40: The evolution of the dimensionless structure factor of the (a) primary and (b) secondary structures formed just after the second temperature jump to $T_2^* = 0.1$ plotted against dimensionless reduced times for an off-critical quench case. The second temperature jump was made at $t_i^* = 0.323$. The dimensionless diffusion coefficient is $D^* = 800\,000$.

Remarks on the Early Stages of Phase Separation After the Second Temperature Jump to $T_2^* = 0.1$ where Secondary Structures are Observed

Figures C.41 to C.44 show the plots of the natural log of the dimensionless structure factor versus dimensionless reduced time for the initial critical and initial off-critical quench case with $D^* = 500\,000$ and $800\,000$, respectively. These plots were used to determine if the numerical work presented in this section on the formation of secondary structures also follows the linear theory in the early stages right after the second quench to $T_2^* = 0.1$. All four Figures show the existence of a small linear region after the second quench when the secondary structures were forming.

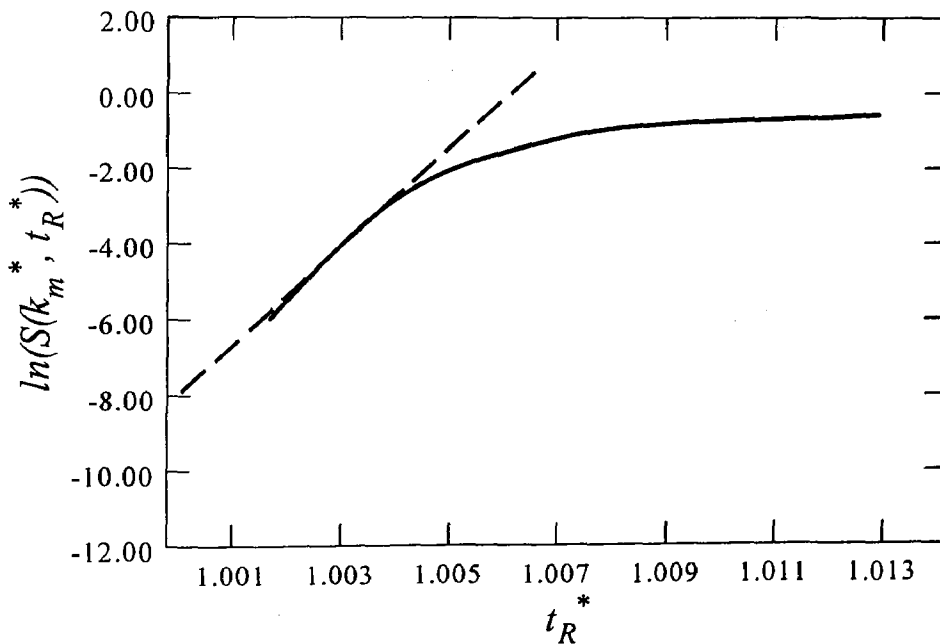


Figure C.41: The evolution of the growth of the dimensionless structure factor of the secondary structure formed at the second temperature jump, $T_2^* = 0.1$, plotted against dimensionless reduced times for a critical quench with $D^* = 500\,000$

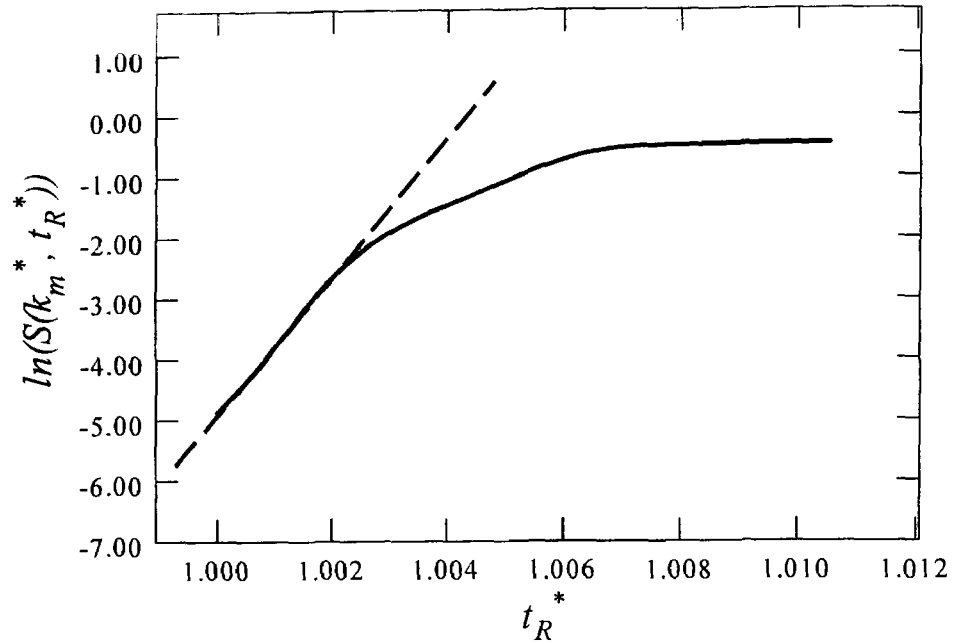


Figure C.42: The evolution of the growth of the dimensionless structure factor of the secondary structure formed at the second temperature jump, $T_2^* = 0.1$, plotted against dimensionless reduced times for a critical quench with $D^* = 800\,000$

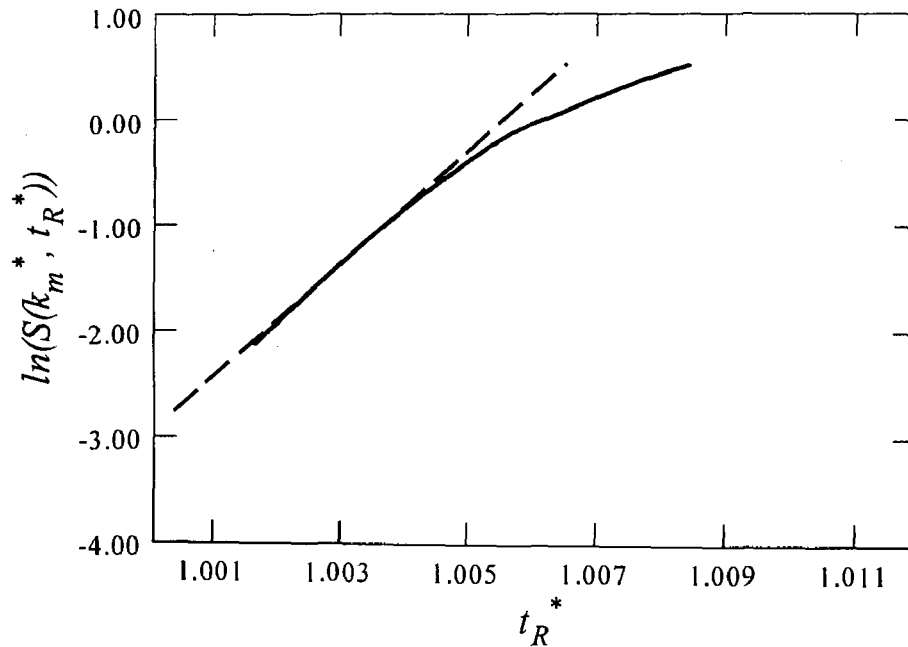


Figure C.43: The evolution of the growth of the dimensionless structure factor of the secondary structure formed at the second temperature jump, $T_2^* = 0.1$, plotted against dimensionless reduced times for an off-critical quench with $D^* = 500\,000$

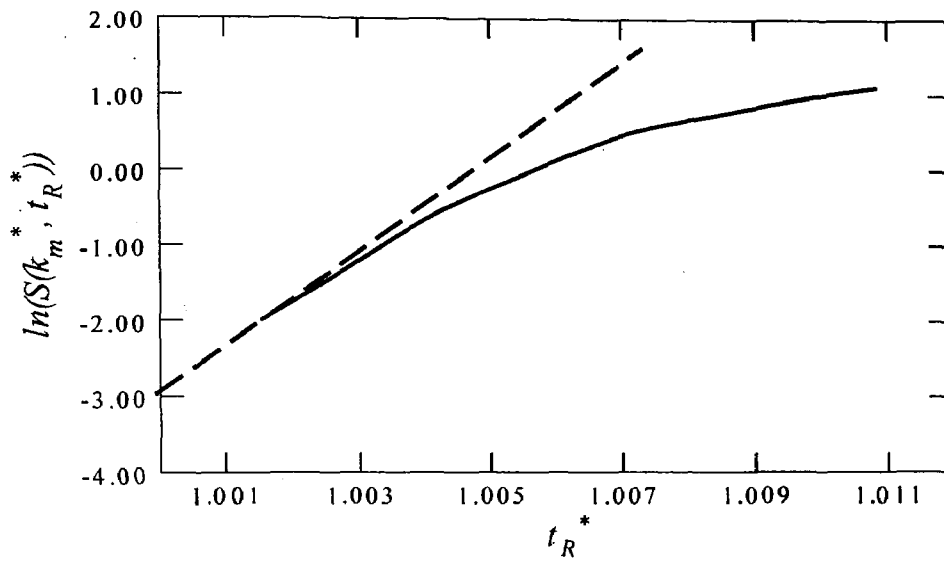


Figure C.44: The evolution of the growth of the dimensionless structure factor of the secondary structure formed at the second temperature jump, $T_2^* = 0.1$, plotted against dimensionless reduced times for an off-critical quench with $D^* = 800\,000$